





Dublin City University  
Ollscoil Chathair Bhaile Átha Cliath

---

*Analysis and Characterisation of an  
Acylphosphine Oxide Photoinitiator*

by

**Agnieszka Ciechacka B.Sc., M.Sc.**

**Thesis submitted for the Degree of Doctor of Philosophy**

**Supervisors:**

**Dr. Gillian McMahon  
Prof. Raymond Leonard  
Prof. Fiona Regan**

## Declaration

*I hereby certify that this material, which I now submit for assessment on the programme of study leading to the award of PhD is entirely my own work, that I have exercised reasonable care to ensure that the work is original, and does not to the best of my knowledge breach any law of copyright, and has not been taken from the work of others save and to the extent that such work has been cited and acknowledged within the text of my work.*

Signed: \_\_\_\_\_ (Candidate) ID No.: \_\_\_\_\_ Date: \_\_\_\_\_

*To my husband Jarek*  
*For his love, friendship, patience and support*  
*Thank you for everything*

## Acknowledgements

I would like to thank all the people who assisted me with their expertise, work or emotional support in the completion of this thesis.

First, I would like to thank my supervisor, Professor Fiona Regan for giving me the opportunity to undertake this study and for all her encouragement and assistance throughout the last three years. I am also very grateful for the chance she gave me to participate in PITTCON conference in Orlando which was a valuable experience for me. I wish to express my appreciation to my “second” supervisor, Dr. Gillian McMahon, for her support throughout the course of this research and for finding the answers to every “difficult question”. I had a special word of thanks goes to Professor Ray G. Leonard, for excellent technical information and discussion, for being a real mentor to me. He was a great source of optimism and passion of this part of chemistry. I will never forget the big white board in his office.

I would also like to thank my lab-mates: Li, Emma, Rachel, James, Tim, Lisa, Imogene, Audrey, Antoin and to my student Nicoletta, for all their support, friendship and encouragement. Thanks to Lisa, Audrey and Tim for correcting my English and to Rachel for Excel. I would like also to acknowledge other postgraduate students and staff members in Chemistry Department, my lab neighbors- Ewa, Laura, Kyriaki, Blánaid and Alex. I am very grateful to Ewa for her help, advice, and patience over the last few months of writing this thesis. You all made my time at DCU a very enjoyable experience. I have special thanks to Damian for helping me throughout some parts of my research, especially for the theoretical calculation and NMR experiments.

I would also like to thank Dr. Ian Beadham and Dr. Peter Kenny for helping me with the organic chemistry.

Thanks to all the technical staff at DCU for their support and to all research team from Henkel Loctite Technology Center, especially Paul, for his help and patience.

To my long-time friends, Czaro, Justynka, Malenstwo, Jaca, Pogi Daszka, Zakrzes for the good fun weekends, holidays (ski) and discussions, not only scientific, on Skype.

I want to express my sincere gratitude to my family without which I could have not come this far. I am grateful to my parents who gave me absolutely everything a daughter could need. Thank you so much-I love you both very much. A note of thanks goes to my little brother Adam, you are the best brother in the world. And also thanks goes to my parent's in-laws for their support, an especially to my father-in-law who gave to me a lot of energy to finish my PhD.

And finally I wish to acknowledge the Henkel Loctite Technology Center for funding this study.

## ***Table of Contents***

Title Pages.....	I
Declaration.....	II
Dedications .....	III
Acknowledgements.....	IV
Table of Contents.....	VI
Abbreviations.....	XIII
Abstract.....	XVI

## **Chapter One ..... 1**

### ***Introduction***

<b>1.1 Introduction.....</b>	<b>2</b>
<b>1.2 High-Performance Liquid Chromatography.....</b>	<b>4</b>
1.2.1 Theory of Chromatography.....	5
1.2.1.1 Separation factor and resolution .....	6
1.2.1.2 Separation efficiency .....	8
1.2.2. Modes of separations in HPLC.....	10
1.2.2.1 Normal Phase Chromatography.....	10
1.2.2.2 Reversed-Phase Chromatography.....	11
1.2.2.3 Ion-exchange.....	12
<b>1.3 Capillary Electrophoresis.....</b>	<b>13</b>
1.3.1 Electrophoresis Terminology.....	13
1.3.1.1 Electroosmotic Flow .....	14
1.3.1.2 Dispersion .....	16

1.3.1.3 Efficiency and Resolution.....	17
1.3.2 Alternative modes of CE.....	18
1.3.2.1 CEC.....	18
1.3.2.2 MEKC.....	18
<b>1.4 Mass Spectrometry .....</b>	<b>19</b>
1.4.1 Ionisation Methods used in MS .....	19
1.4.1.1 ESI.....	20
1.4.1.1.1 Introduction.....	20
1.4.1.1.2. The electrospray ionisation process .....	22
1.4.1.1.3 The multiply charged ions .....	26
1.4.2 Mass analyser.....	28
1.4.3 Tandem MS.....	29
<b>1.5 NMR.....</b>	<b>30</b>
1.5.1 <sup>31</sup> P NMR.....	31
<b>1.6 GAUSSIAN Method.....</b>	<b>36</b>
<b>1.7 Conclusions.....</b>	<b>37</b>
<b>1.8 Aims and Objectives .....</b>	<b>37</b>
<b>1.9 References.....</b>	<b>39</b>
<b>Chapter Two.....</b>	<b>45</b>
<i>Characterisation of Acylphosphine oxide Photoinitiator using HPLC and CE Methods</i>	
<b>2.1 Introduction.....</b>	<b>46</b>
2.1.1 Properties and production of Acylphosphine oxide.....	46
2.1.2 Photochemistry of Acylphosphine oxide .....	50
<b>2.2 Scope of Research .....</b>	<b>52</b>
<b>2.3 Materials and Methods.....</b>	<b>53</b>



2.3.1 HPLC-UV method .....	53
2.3.1.1 Instrumentation .....	53
2.3.1.2 Chromatographic separation conditions .....	53
2.3.2 CE methods .....	54
2.3.2.1 Instrumentation .....	54
2.3.2.2 Electrophoretic separation conditions .....	54
2.3.2.3 Preparation of CE background electrolyte .....	54
2.3.2.4 Preconditioning of the CE separation capillary .....	55
2.3.3 Preparation of standard solution .....	55
2.3.4 Chemicals .....	55
2.3.5 Experimental design .....	56
2.3.5.1 Characterisation of BAPO .....	56
<b>2.4 Results and Discussion.....</b>	<b>58</b>
2.4.2 HPLC method .....	58
2.4.2.1 Development and optimisation of HPLC method.....	58
2.4.2.2 Analysis of BAPO in ambient light and dark conditions .....	60
2.4.2.3 Comparison of strong and weak acids .....	62
2.4.2.4 Addition of stabiliser and curing additives .....	68
2.4.2.5 Addition of water .....	72
2.4.2.6 Summary of stability study of BAPO using HPLC .....	72
2.4.3 CE method .....	73
2.4.3.1. Development of CE method.....	73
2.4.3.2 MEKC .....	76
<b>2.5 Conclusion .....</b>	<b>79</b>
<b>2.6 References .....</b>	<b>80</b>

**Chapter Three ..... 82**

*Study of the Photodegradation products of BAPO using LC-MS*

<b>3.1 Introduction.....</b>	<b>83</b>
<b>3.2 Scope of Research .....</b>	<b>88</b>
<b>3.3 Materials and Methods.....</b>	<b>89</b>
3.3.1 Instrumentation .....	89
3.3.1.1 LC-MS .....	89
3.3.2 Chemicals.....	91
3.3.3 Procedures.....	91
3.3.3.1 Preparation of mobile phase.....	91
3.3.3.2 Preparation of standard solution .....	91
<b>3.4 Results and Discussion.....</b>	<b>93</b>
3.4.1 Optimisation of LC-MS parameters.....	93
3.4.2 Mass fragmentation of BAPO.....	96
3.4.3 BAPO degradation products determination by LC-MS.....	99
3.4.4 Analysis of BAPO with strong and weak acids .....	105
3.4.5 Analysis of BAPO with additives .....	112
3.4.6 Sources of contamination in LC-MS .....	118
<b>3.5 Conclusion .....</b>	<b>121</b>
<b>3.6 References.....</b>	<b>122</b>

**Chapter Four..... 125**

***Determination of the Cure Mechanism and Stability of BAPO and TPO using LC-MS, NMR and Computational Calculation***

<b>4.1 Introduction.....</b>	<b>126</b>
4.1.1 Photochemistry of photoinitiators and photosensitisers.....	126
4.1.2 Types of photoinitiators .....	127
4.1.2.1 Type I photoinitiators.....	128
4.1.2.2 Type II photoinitiators .....	129
<b>4.2 Scope of Research .....</b>	<b>131</b>
<b>4.3 Materials and Methods.....</b>	<b>132</b>
4.3.1 Instrumentation and conditions.....	132
4.3.1.1 LC-MS .....	132
4.3.1.2 NMR .....	132
4.3.1.3 Computational calculations.....	133
4.3.2 Chemicals.....	133
4.3.3 Procedures.....	134
4.3.3.1 Preparation of mobile phase.....	134
4.3.3.2 Preparation of standard solution for LC-MS .....	134
4.3.3.3 Preparation of standard solution for NMR.....	134
<b>4.4 Results and Discussion.....</b>	<b>135</b>
4.4.1 Mass fragmentation of TPO.....	135
4.4.2 TPO degradation products determination by LC-MS.....	137
4.4.3 BAPO and TPO degradation products determination by LC-MS .....	139
4.4.4 NMR analysis.....	142
4.4.4.1 <sup>1</sup> H and <sup>13</sup> C NMR study of stability of BAPO and TPO .....	142
4.4.4.2 <sup>31</sup> P NMR stability study of BAPO and TPO.....	148
4.4.5 Computational studies.....	150
<b>4.5 Conclusion .....</b>	<b>156</b>

<b>4.6</b>	<b>References .....</b>	<b>157</b>
------------	-------------------------	------------

<b>Chapter Five .....</b>	<b>158</b>
---------------------------	------------

*An Investigation of the Cure mechanism and Polymer products of Ethyl  
Cyanoacrylate samples using LC-MS*

<b>5.1</b>	<b>Introduction.....</b>	<b>159</b>
------------	--------------------------	------------

5.1.1.	Characteristics of Cyanoacrylate Adhesives.....	161
--------	---	-----

5.1.2	Chemistry of Cyanoacrylate Adhesives.....	163
-------	---	-----

<b>5.2</b>	<b>Scope of Research .....</b>	<b>167</b>
------------	--------------------------------	------------

<b>5.3</b>	<b>Results and Discussion.....</b>	<b>168</b>
------------	------------------------------------	------------

5.3.1	Instrumentation .....	168
-------	-----------------------	-----

5.3.1.1	LC-MS .....	168
---------	-------------	-----

5.3.1.2	UV Power Meter .....	168
---------	----------------------	-----

5.3.2	Chemicals.....	168
-------	----------------	-----

5.3.3	Procedures.....	169
-------	-----------------	-----

5.3.3.1	Preparation of mobile phase.....	169
---------	----------------------------------	-----

5.3.3.2	Preparation of formulation of ethyl CA .....	169
---------	--	-----

5.3.3.3	Preparation of formulation of ethyl CA for LC-MS analysis	170
---------	---	-----

<b>5.4</b>	<b>Results and Discussion.....</b>	<b>171</b>
------------	------------------------------------	------------

5.4.1	Cure mechanism of ethyl CA oligomers.....	171
-------	---	-----

5.4.2	BAPO /ethyl CA system in samples kept in dark and exposed to the light .....	179
-------	---	-----

5.4.3	TPO /ethyl CA system in samples kept in dark and exposed to light .....	193
-------	--	-----

5.4.4	Effect of photoinitiators concentration and presence of stabiliser.....	198
-------	---	-----

<b>5.5</b>	<b>Conclusion .....</b>	<b>202</b>
------------	-------------------------	------------

<b>5.6</b>	<b>References .....</b>	<b>203</b>
------------	-------------------------	------------

<b>Chapter Six .....</b>	<b>204</b>
--------------------------	------------

*Conclusions*

<b>6.1 Overall conclusions .....</b>	<b>205</b>
--------------------------------------	------------

<b>Appendix.....</b>	<b>208</b>
----------------------	------------

<b>Publications .....</b>	<b>209</b>
---------------------------	------------

<b>Oral Presentations .....</b>	<b>210</b>
---------------------------------	------------

<b>Poster Presentations.....</b>	<b>211</b>
----------------------------------	------------

## Abbreviations

ACN	acetonitrile
APCI	atmospheric pressure chemical ionisation
ATRP	atom transfer radical polymerisation
BAPO	bisacylphosphine oxide (Irgacure 819)
BDK	benzil dimethyl ketal
BF <sub>3</sub> ·2H <sub>2</sub> O	boron trifluoride dihydrate
BGE	background electrolyte
BQ	benzoquinone
CD	cyclodextrins
CE	capillary electrophoresis
CEC	capillary electrochromatography
CE-MS	capillary electrophoresis-mass spectrometry detection
CE-UV	capillary electrophoresis-ultra-violet detection
CHP	cumene hydroperoxide
CI	chemical ionisation
CIDNP	chemically induced dynamic nuclear polarisation
COSY	correlation spectroscopy
CTAB	cetyltrimethylammonium bromide
CZE	capillary zone electrophoresis
Da	dalton
DEAP	$\alpha,\alpha$ -diethoxyacetophenone
DMF	dimethylformamide
DMPA	dimethoxy-2-phenylacetophenone
DMSO	dimethyl sulfoxide
D <sub>2</sub> O	deuterium oxide
DTAB	dodecyltrimethylammoniumbromide
DTPA	diethylenetriaminepentacetic acid
EDAB	ethyl-4-dimethylaminobenzoate
EI	electron ionisation
EOF	electroosmotic flow
ESI	electrospray ionisation

FAB	fast atom bombardment
FD	field desorption
FI	field ionisation
FT	Fourier transform
GC-MS	gas chromatography –mass spectrometry
HETP	height equivalent to a theoretical plate
HMBC	heteronuclear multiple bond correlation
HMQC	heteronuclear multiple quantum correlation
HPLC	high performance liquid chromatography
HPLC-MS	high performance liquid chromatography- mass spectrometry detection
HPLC-UV	high performance liquid chromatography- ultra-violet detection
HQ	hydroquinone
I	quantum number
IC	ion chromatography
IEC	ion exchange chromatography
IR	infra-red
ITX	2-isopropylthioxanthone
LC-MS/MS	liquid-chromatography tandem mass spectrometry
LOD	limit of detection
LOQ	limit of quantification
MALDI	matrix –assisted laser desorption/ionization
MAPO	monoacylphosphine oxide
MEKC	micellar electrokinetic chromatography
MeOH	methanol
MMA	methyl methacrylate
MS	mass spectrometry
MSA	methyl sulphonic acid
m/z	mass to charge ratio
NaOH	sodium hydroxide
NMP	nitroxide mediated polymerisation
NMR	nuclear magnetic resonance
<sup>1</sup> H NMR	proton nuclear magnetic resonance

<sup>13</sup> C NMR	carbon nuclear magnetic resonance
<sup>31</sup> P NMR	phosphorous nuclear magnetic resonance
NP	normal phase
PAC	photoacoustic calorimetry
PBMA	poly( <i>n</i> -butyl methacrylate)
PIS	photoinitiating system
PLP	pulsed laser polymerisation
PMMA	poly(methyl methacrylate)
PPC	phenprocoumon
RDS	relative standard deviation
RP	reversed-phase
SDS	sodium dodecyl sulphate
THF	tetrahydrofuran
TIC	total ion chromatogram
TOF	time -of-flight
TPO	(2,4,6-trimethylbenzoyl)diphenylphosphine oxide (Darocur)
TR-ESR	time- resolved electron spin resonance
TRIR	time-resolved infra-red
UV	ultra-violet



## ABSTRACT

Photoinitiators play a key role in UV-curable systems by generating the reactive species, free radicals, ions or molecule which initiate the polymerisation of the multifunctional monomers and oligomers.

This research involves the study of the hydrolytic and photolytic stabilities of two important new photoinitiator bis (2,4,6-trimethylbenzoyl)phenylphosphine oxide (BAPO) and (2,4,6-trimethylbenzoyl)diphenyl-phosphine oxide (TPO).

BAPO is a new member in the group of well-known  $\alpha$ -cleavable photoinitiators among which monoacylphosphine oxide (MAPO) is most recognised. These  $\alpha$ -cleavable photoinitiators are characterised by low volatility and high solubility in acrylate monomers and they are very widely applied as curing agents for white and pigmented coatings including furniture coatings. Novel analytical methods were developed in order to characterise these compounds and to understand their modes of action and breakdown.

The stability of BAPO in different solvents, such as acetonitrile and a cyanoacrylate ester, was studied and the effect of storage of BAPO in light and dark conditions was evaluated. The effects of stabilisers (ferrocene, cumene hydroperoxide (CHP) and hydroquinone (HQ)), acids (methyl sulphonic acid (MSA) and boron trifluoride dihydrate ( $\text{BF}_3 \cdot 2\text{H}_2\text{O}$ )) and water present in the solvent were also investigated. These studies were monitored over time using LC-UV and CE-UV methods.

Mass spectrometry was employed for the first time to investigate the pathways and photodegradation products for both of the photoinitiators BAPO and TPO. NMR spectroscopy and computational studies were used as complementary experimental and theoretical techniques respectively for the elucidation of the photochemistry of these products.

A formulation study using the photoinitiator and ethyl cyanoacrylate monomer to ascertain the polymerisation products, and possible cure mechanism with the aid of mass spectrometry was also carried out.

## *Chapter One*

### *Introduction*

## 1.1 INTRODUCTION

Highly crosslinked polymers are readily synthesised by photoinitiated polymerisation of multifunctional monomers and polymers. The main advantage of using UV radiation to initiate the chain reaction lies in the very high polymerisation rates that can be reached under intense illumination. Another distinct feature of light-induced reactions is that the polymerisation will occur only in the illuminated areas, thus allowing complex relief patterns to be produced after solvent development.<sup>[1]</sup>

The photoinitiated polymerisation of monomer or UV radiation curing has found a large number of applications in various industrial sectors.<sup>[2, 3]</sup> This technology is now commonly utilised to perform the ultrafast drying of protective coatings, varnishes, printing inks and adhesives. Besides its great speed and spatial resolution, radiation curing presents a number of other advantages in particular ambient temperature operations, solvent-free formulations, low energy consumption and the production of polymer materials having tailor-made properties. Most of the research efforts devoted to photocuring have been centred on the development of very efficient photoinitiators and of highly reactive monomers and oligomers or polymers. This subject has been extensively covered in several books and review papers.<sup>[4-8]</sup>

Photoinitiators are a class of compounds that play a very important role in the industrial fabrication of UV-curable coating systems. They are able to generate reactive species (ions or free radicals), which initiate the polymerisation and cross-linking of such systems. Most monomers do not generate initiating species with sufficiently high yields when they are exposed to UV light; hence photoinitiators must be added to the mixture.<sup>[1]</sup> The schematic representation of photo-assisted polymerisation is shown in Figure 1.1.

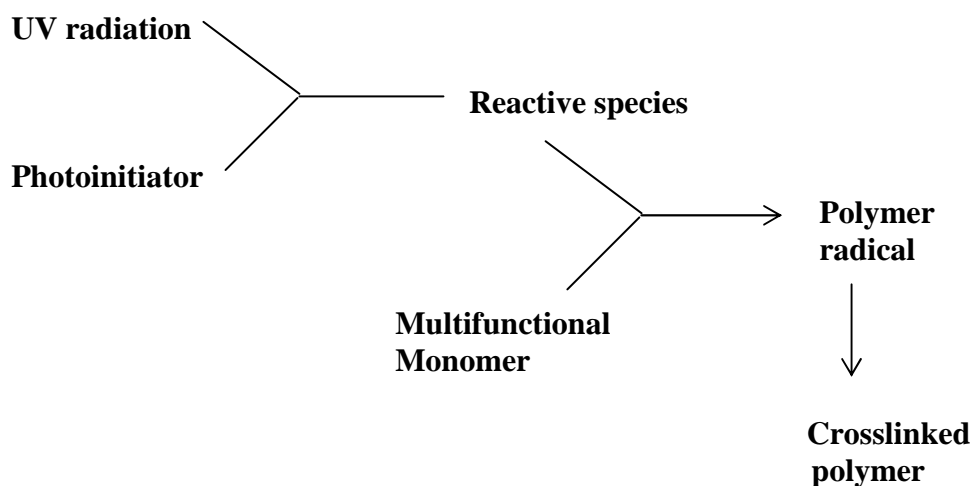


**Figure 1.1:** Schematic illustration of the UV curing process. <sup>[1]</sup>

Most efforts in research in the field of photoinitiators during the past years have therefore been dedicated to the development of more efficient materials, possessing a red-shifted absorption spectrum which can successfully compete with the pigment for the incident light. As a result, new photoinitiators, such as  $\alpha$ - amino acetophenones <sup>[9- 11]</sup> or new thioxanthone derivatives <sup>[12]</sup>, have recently been introduced as commercial photoinitiators and sensitizers.

Although these compounds show great utility in various pigmented formulations, including inks or electronic resists, they are not suitable for the curing of thick white pigmented lacquers. In the production of white furniture coatings, a high degree of whiteness is required, which can only be obtained when film thickness is in the range 50-100  $\mu\text{m}$  and high pigment content is used. No yellowing of the cured films is tolerated both immediately after the curing and later as the finished article. Both  $\alpha$ - amino acetophenone and thioxanthone derivatives impart considerable yellowness to the cured coating, unless used for the curing of very thin layers to high line speed. <sup>[10]</sup>

A satisfactory radiation curing of white pigmented lacquers was first achieved using monoacylphosphine oxide (MAPO, TPO or Darocur) photoinitiators. The compounds have been known for over a decade and have found use in a variety of applications. <sup>[13, 14]</sup> Another type of structural analogue of acylphosphine oxide is bisacylphosphine oxide (BAPO or Irgacure 819). BAPO was developed for use in

dental materials <sup>[15]</sup> but later its properties were also recognised for industrial applications, such as curing of thick sections. <sup>[10]</sup>

Acylphosphine oxides are ideal candidates to perform photoinduced polymerisation, and in this thesis the characteristics of acylphosphine oxides as alternative photoinitiators and their photochemistry are discussed. The main analytical methods used to complete this work are separation techniques such as high performance liquid chromatography (HPLC), capillary electrophoresis (CE) and liquid chromatography- mass spectrometry (LC-MS). The results obtained from separation methods are accompanied by supporting techniques such as nuclear magnetic resonance spectroscopy (NMR) and the *Gaussian* program. HPLC and CE are powerful alternative methods for analysis of acylphosphine oxide and the different modes of separation available within CE and HPLC will be discussed in the following sections.

Other analytical techniques, including MS and NMR, are also presented in this chapter. A combination of these two methods, MS and NMR, enables more conclusive identification of unknown compounds such as photodegradation products when compared to the results obtained from each of these methods separately.

## 1.2 HIGH PERFORMANCE LIQUID CHROMATOGRAPHY

High performance liquid chromatography (HPLC) is the most widely used method among all analytical separation techniques. During HPLC the components of the sample are distributed between two phases: a mobile and stationary phase. The mobile phase is flowing through and over a stationary phase bed. <sup>[16]</sup>

Chromatographic analysis includes the introduction, separation and detection of analytes in a mixture. The separation of the sample in a mixture is based on the different chemical interactions between the sample components as they interact for different lengths of time between the mobile and stationary phase. The differences in these interactions for diverse analytes will finally result in separation on the column over time.

### 1.2.1 Theory of Chromatography

The *retention time*, also called the elution time,  $t_R$ , of an analyte is measured as the elapsed time between injection of the analysed solution and the elution of the peak maximum. <sup>[17]</sup>

The *retention volume* or elution volume,  $V_R$ , is the volume of eluent passed through the column during the retention time. The relationship between  $t_R$  and  $V_R$  is given by Eqn 1.1: <sup>[18]</sup>

$$V_R = t_R F \quad \text{Eqn. 1.1}$$

where:  $t_R$  is the retention time (min)

$F$  is the flow rate ( $\text{mL min}^{-1}$ )

The chromatographic parameters are illustrated in Figure 1.2.

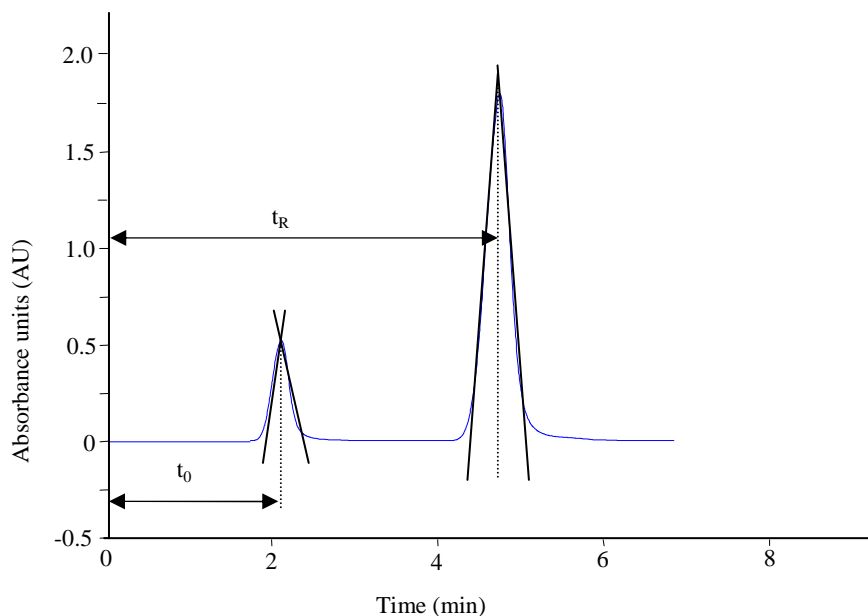


**Figure 1.2:** Representation of a typical HPLC chromatogram. <sup>[19]</sup>

The *capacity factor*,  $k'$ , also known as retention factor or partition ratio of the column, is a function of the strength of the interaction of the sample with the stationary phase and is defined by the following expression (Eqn.1.2):

$$k' = \frac{t_R - t_0}{t_0} \quad \text{Eqn. 1.2}$$

where:  $t_R$  is the time needed for a specific analyte to reach the detector,

$t_0$  is the time needed for non retained species to reach the detector.

Typically, a  $k'$  value falling between 2 and 5 represents a good balance between analysis time and separation. If  $k'$  is below 1, then elution will proceed too quickly, which will make the precise determination of retention times difficult. If the value is larger than 5, the elution will be too slow so that retention time will become excessively long. <sup>[20]</sup>

### 1.2.1.1 Separation factor and resolution

The *separation factor*,  $\alpha$ , of the chromatographic separation is a measure of the difference in retention volumes or times between two given peaks and describes how effectively a chromatographic system can separate two analytes from each other (Figure 1.2). This relationship can be expressed by Eqn.1.3:

$$\alpha = \frac{k_2'}{k_1'} = \frac{t_2 - t_0}{t_1 - t_0} = \frac{V_2 - V_0}{V_1 - V_0} \quad \text{Eqn. 1.3}$$

where:  $t_2$  is retention time of the second compound

$t_1$  is retention time of the first compound

$V_2$  is retention volume of the second compound

$V_1$  is retention volume of the first compound

*Resolution*,  $R$ , is a term used to describe the separation between adjacent peaks and can be calculated using Eqn. 1.4:

$$R = \frac{2(t_2 - t_1)}{W_1 + W_2} \quad \text{Eqn. 1.4}$$

where:  $W$  is the baseline peak width of components

Transformation of Eqn. 1.4 results in the more general formula used to express the resolution which provides a direct connection between resolution, separation factor and column efficiency (Eqn. 1.5):

$$R = \frac{\sqrt{N}}{4} \left( \frac{\alpha - 1}{\alpha} \right) \left( \frac{k_2'}{1 + k_2'} \right) \quad \text{Eqn. 1.5}$$

This equation contains three independent variables: the selectivity factor, the retention factor and plate number which ultimately control every chromatographic separation.

The first part of the equation,  $\frac{\sqrt{N}}{4}$ , describes the band broadening process and the

second part,  $\left( \frac{\alpha - 1}{\alpha} \right) \left( \frac{k_2'}{1 + k_2'} \right)$ , describes the differential migration process. <sup>[21]</sup>



### 1.2.1.2 Separation efficiency

To describe the width of a chromatographic separation, the concept of *theoretical plates*,  $N$ , is commonly used. Column efficiency can also be expressed as the theoretical plate number,  $N$ , or the height equivalent of a theoretical plate (HETP).  $N$  is determined by Eqn. 1.6:

$$N = 16 \left( \frac{t_R}{W} \right)^2 = 5.5 \left( \frac{t_R}{W_{1/2}} \right)^2 \quad \text{Eqn. 1.6}$$

where:  $W_{1/2}$  is the peak width at half height.

$N$  is directly proportional to the time the component spends on the column and inversely proportional to the peak-width of this component.

The efficiency may also be calculated experimentally using Eqn. 1.7:

$$N = \frac{L}{H} \quad \text{Eqn. 1.7}$$

where:  $L$  is the length of the column (m),

$H$  is the-plate height (HETP)

The plate theory was first proposed by Martin and Synge,<sup>[22]</sup> and it provides a simple and convenient way to measure column performance and efficiency, whereas a more realistic rate theory was developed by van Deemter.<sup>[23]</sup> This theory takes into account the diffusion effect of mass transfer and migration through a packed bed, with the resulting peak shape being affected by the rate of elution.<sup>[16]</sup> The van Deemter theory of HETP (also known as  $H$ ) is given by Eqn. 1.8:

$$H = A + B/\mu + C\mu \quad \text{Eqn.1.8}$$

where:  $\mu$  is the average velocity of the mobile phase,

$A$  is eddy diffusion,

$B$  is longitudinal diffusion,

$C$  is resistance to mass transfer.

Eddy diffusion ( $A$ ) is caused by the movement of molecules of the same analyte, which migrate through the stationary phase at random. This will cause broadening of the analyte band, because different paths are of different lengths.  $B/\mu$  is the ‘molecular diffusion’ term and is related to diffusion of analyte molecules within the mobile phase caused by local concentration gradients. Diffusion within the stationary phase also contributes to this term, which is significant only at low flow rates and increases with column length. The third parameter,  $C\mu$ , (‘mass transfer’) is dependent on the amount of the time an analyte needs in order to equilibrate between the stationary and mobile phase. If the velocity of the mobile phase is high and the analyte has a strong affinity for the stationary phase, then the analyte in the mobile phase will move ahead of the analyte in the stationary phase. The band of analyte will be broadened. In this case the higher the velocity of mobile phase, the worse the broadening observed.

The ideal situation is to have the smallest value of  $H$  as possible which yields the best efficiency. A plot of plate height against the mobile phase velocity, known as a van Deemter plot, is commonly used to determine the optimum mobile phase flow rate (where the average curve has the lowest value of  $H$ ).<sup>[24]</sup> A typical van Deemter plot is shown in Figure 1.3.

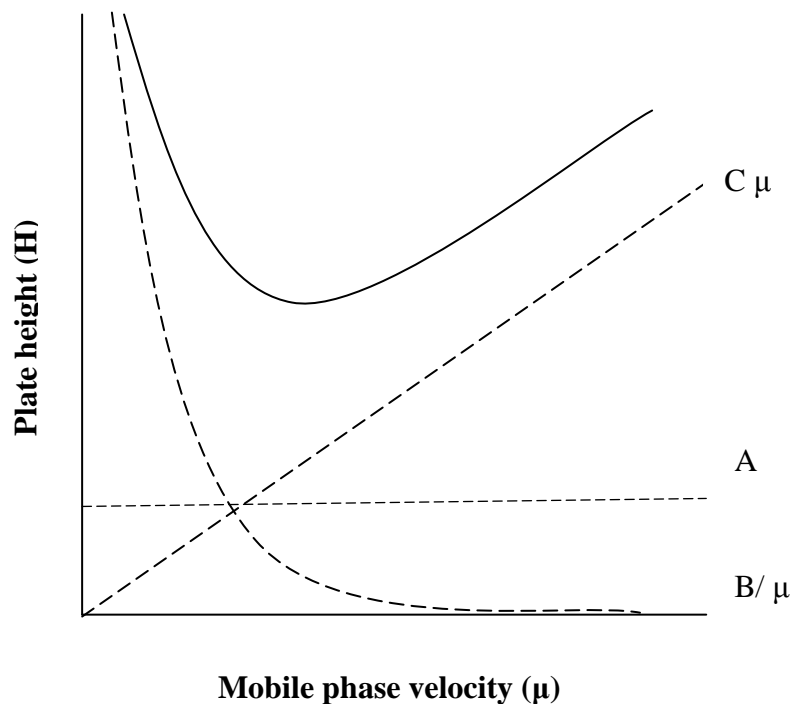


*Figure 1.3: A typical van Deemter plot. [25]*

## 1.2.2. Modes of separation in High Performance Liquid Chromatography

### 1.2.2.1 Normal Phase Chromatography

In normal phase HPLC (NP-HPLC), the stationary phase is polar whereas the mobile phase is non-polar and non-aqueous. Typically, bare silica or silica derivitised with small organic ligands, such as cyano and amino groups are used for the NP-HPLC stationary phase.<sup>[26]</sup> The mobile phase consists of a very non-polar solvent like hexane or heptane mixed with a slightly more polar solvent like isopropanol, ethyl acetate or chloroform. Analytes are separated on the basis of their polarity; the more polar the analyte, the greater is its retention on the column. Since the mobile phase is less polar than the stationary phase, increasing the polarity of the mobile phase results in decreased retention of the analyte.

NP chromatography with fluorescence detection has been used for the simultaneous determination of pharmaceuticals in human <sup>[27-29]</sup> and animal blood. The limits of quantitation in human or animal blood were 2 and 20 ng/ mL <sup>[24]</sup> respectively. However, the applications of this mode of chromatography have become limited and reversed-phase chromatography has been more widely employed separation technique and is discussed in more detail in section 1.2.2.2.

### **1.2.2.2 Reversed Phase Chromatography**

Reversed-phase HPLC (RP-HPLC), the most widely used chromatographic mode, employs a non-polar stationary phase and polar mobile phase which is opposite to that in normal phase HPLC. As a result, when the polarity of the mobile phase decreases the retention of analyte decreases as well. <sup>[25]</sup> The mobile phase used in RP-HPLC is usually a mixture of polar organic solvent(s), such as acetonitrile or methanol and an aqueous buffer or water. The most common stationary phases in RP-HPLC are those consisting of silica beads with functional groups attached to silica support- bonded phases. The most typical bonded phases are the alkyl groups, such as -CH<sub>3</sub>, -C<sub>8</sub>H<sub>17</sub>, and -C<sub>18</sub>H<sub>37</sub>, cyano [(-CH<sub>2</sub>)<sub>3</sub>CN] groups, and amino [(-CH<sub>2</sub>)<sub>3</sub>NH<sub>2</sub>] groups. Numerous RP- HPLC methods have been applied for the determination of pharmaceuticals in biological fluids (human serum and plasma) and the results are discussed in several review papers <sup>[30-32]</sup>. Also the RP-HPLC method has been useful for the study of the photodecomposition products of TMBPO photoinitiator and 2,2-dimethoxy-2-phenylacetophenone in presence or absence of amine. <sup>[33]</sup>

Three different types of reversed-phase HPLC can be recognised and they include:

- a) ion-suppression HPLC <sup>[34, 35]</sup>
- b) ion-pair HPLC <sup>[36]</sup>
- c) metal complexation.

### 1.2.2.3 Ion-Exchange Chromatography

In ion exchange chromatography (IEC) the stationary phase plays the role of exchanger. It consists of two components: the polymer matrix and attached functional groups. The functional groups used are permanently bonded ionic groups associated with counter ions of the opposite charge and retention occurs due to the exchange of analyte ions with the ions of opposite charge on the stationary phase.<sup>[17]</sup> There are two main modes of IEC:

- a) cation exchange chromatography, in which positively charged ions are retained because the stationary phase displays negatively charged functional groups;
- b) anion exchange chromatography, in which anions are retained because positively charged functional groups are present.<sup>[37]</sup>

The applications of ion-exchange chromatography range from analysis of amino acids on a cation exchanger to the simultaneous separation of inorganic anions and cations using anion and cation-exchange columns joined in tandem.<sup>[17]</sup> An alternative implement of IEC is ion chromatography, IC, which connects an ion exchange separation with suppression of mobile phase and in most cases detection is performed conductimetrically. IC has been the method of choice for the analysis of anions, and has been employed for the simultaneous separation of anions and cations using multi-column systems.<sup>[38]</sup> The trace analysis of anions in drinking water has also been performed by IC.<sup>[39, 40]</sup>

### 1.3 CAPILLARY ELECTROPHORESIS

Capillary Electrophoresis, CE, is another powerful separation method for the analysis of small charged species, such as cations and anions, <sup>[41-43]</sup> and also in the determination of pharmaceuticals in complex matrices. <sup>[44, 45]</sup> Capillary electrophoresis is the collective term which incorporates all of the electrophoretic modes, such as CEC and MEKC. These separations are facilitated by the use of high voltages, which may generate electroosmotic and electrophoretic flow of buffer solutions and ionic species, within the capillary. <sup>[46]</sup>

The following are the characteristics and advantages of CE, showing its operation ranges and general information on the technique:

- a) performed in microbore (25-75  $\mu\text{m}$ ) fused silica capillaries,
- b) utilises very high electric field strengths, often higher than 500 V/cm,
- c) high resistance of capillary leads to limited current generation and Joule heating,
- d) high efficiencies ( $N > 10^5$  to  $10^6$ ),
- e) short analysis times,
- f) small sample volume required (1 to 50 nL injected),
- g) is easily automated for precise quantitative analysis and ease of use.

The basic instrumentation for CE is very simple. All that is required is a fused-silica capillary with an optical viewing window, a controllable high voltage power supply, two electrodes and two buffer reservoirs, and usually an ultraviolet (UV) detector.

#### 1.3.1 Electrophoresis Terminology

There are few significant differences between the nomenclature of chromatography and capillary electrophoresis. The elementary term in chromatography is retention time. In electrophoresis the analogous term becomes migration time. The migration time ( $t_m$ ) is the time taken by the analyte to move from the beginning of the capillary to the detector window. Other fundamental terms are:

electrophoretic mobility ( $\mu_{ep}$ ), which can be described in terms the electrophoretic velocity ( $v_{ep}$ ), and the applied electric field, (E). The relationships between these three factors are illustrated in Eqn 1.9. <sup>[46]</sup>

$$\mu_{ep} = v_{ep} / E \quad \text{Eqn. 1.9}$$

The electric field (in volts/cm) is a function of the applied voltage and capillary length. Electrophoretic mobility depends on voltage and capillary length but is highly dependent on the nature of buffer, its pH and temperature which is expressed by Eqn 1.10

$$\mu_{ep} = q / (6\pi\eta r) \quad \text{Eqn. 1.10}$$

where:        q is charge on the ion  
                $\eta$  is buffer viscosity  
               r is ion radius

### ***1.3.1.1 Electroosmotic Flow (EOF)***

The most important parameter in CE is electroosmotic flow (EOF) which originates in the presence of an electric field when any ionic solution is in contact with a charged surface. <sup>[47]</sup> The EOF results from the dissociation of acidic silanol groups at the capillary wall that are in contact with the electrolyte buffer. <sup>[48]</sup> Hydrated cations in the electrolyte solution are attracted to the negatively charged silanol groups and become arranged into two layers as shown in Figure 1.4. One layer is tightly bound to the wall by electrostatic forces to form a compact layer, and the other one is more loosely bound and is called the diffuse layer. When an electric field is applied, the predominantly negatively charged diffuse layer breaks away and

moves towards the cathode, dragging the bulk solution of the electrolyte as the result of viscous drag.

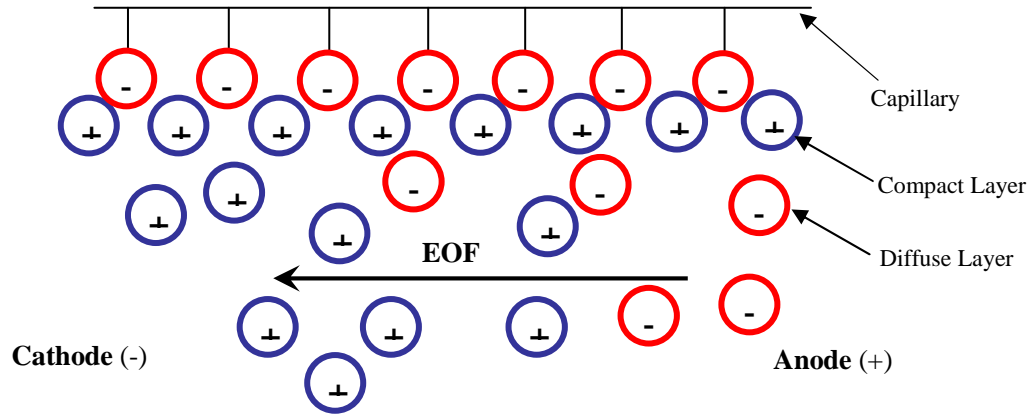


**Figure 1.4:** Representation of charged at the capillary wall. <sup>[48]</sup>

All species, regardless of charge, will move in the same net direction due to the EOF. Cations (in normal polarity) will migrate ahead of the EOF and anions migrate against the EOF and are detected last. <sup>[49]</sup> With reverse polarity, the direction of the EOF is opposite to the detector and only anions with an electrophoretic mobility greater than the EOF will be detected. Under these conditions, the capillaries are generally coated with EOF modifiers, which reverse the net charge of the inner wall and therefore reduce the EOF. <sup>[50]</sup>

The mobility of the electroosmotic flow is defined by Eqn 1.11:

$$\mu_{eo} = \frac{\varepsilon\zeta}{4\pi\eta r} E \quad \text{Eqn.1.11}$$

where:

- $\mu_{eo}$  is the mobility of the EOF
- $\varepsilon$  is the dielectric constant,
- $\eta$  is the viscosity of the buffer,
- $\zeta$  is the zeta potential,
- $r$  is the radius of the capillary.



The EOF decreases as the concentration of the background electrolyte (BGE) increases. In general, high buffer concentrations reduce the overall adsorption of analytes to the capillary wall. <sup>[51]</sup> This reduction may be caused by different factors including the charge of the ion ( $q$ ), buffer viscosity ( $\eta$ ) and the zeta potential, ( $\xi$ ). <sup>[52]</sup>

### **1.3.1.2 Dispersion**

Electrophoresis is the separation of charged species into discrete zones under the influence of an electric field. Dispersion results from differences in analyte velocity within that zone. Peak dispersion  $\sigma^2$ , can be calculated from Eqn 1.12.

$$\sigma^2 = 2 D_m t \qquad \text{Eqn.1.12}$$

where:  $D_m$ - is the diffusion coefficient of the solute in  $\text{cm}^2\text{s}^{-1}$ .

Dispersion in capillary electrophoresis can be caused by number of factors including Joule heating, injection plug length or sample adsorption on the capillary wall. These parameters may be controlled by applying a lower separation voltage or using a capillary with a small internal diameter which will reduce the effect of Joule heating. This will also aid in the dissipation of the heat already formed. <sup>[24]</sup>

### 1.3.1.3 Efficiency and Resolution

The efficiency of separation is dependent upon the high voltage applied. As the voltage is increased, the separation efficiency also increases, as shown in Eqn. 1.13.

$$N = \frac{\mu_{ep} El}{2D_m} \quad \text{Eqn. 1.13}$$

where: E is the electric field  
l is the effective capillary length

The resolution,  $R_s$ , between two species is given by the expression in Eqn 1.14.

$$R_s = \frac{1}{4} \Delta\mu_{ep} \sqrt{\frac{V}{(\mu_{ep} + \mu_{eo})D_m}} \quad \text{Eqn 1.14}$$

where:  $\Delta\mu_{ep}$  is the difference in electrophoretic mobility between the two species.

From Eqn 1.14 it is evident that the resolution of two peaks decreases with the magnitude of the EOF provided that EOF has the same direction as the electrophoretic migration.<sup>[53]</sup>

Resolution is dependent on capillary length at constant field strength and can be improved by increasing the length of the capillary and by applying reduced voltages. However, extreme magnitudes of both these variables can lead to long analysis times and Joule heating.<sup>[48]</sup>

## 1.3.2 Alternative modes of Capillary Electrophoresis

### 1.3.2.1 Capillary electrochromatography (CEC)

CEC is a hybrid of CE and HPLC, combining the separation power of reversed-phase HPLC with the high efficiency of CE.<sup>[54]</sup> The electrically driven flow transports the analytes through the capillary, which is packed with stationary phase material. For neutral analytes, separation is achieved by differential partition between the stationary and mobile phase, and they are transported through the capillary by the EOF. The separation of charged analytes is achieved by the combined effects of partitioning and electrophoresis.<sup>[55]</sup> Many of the applications of CEC are in the analysis of polymers.<sup>[56-58]</sup>

### 1.3.2.2 Micellar Electrokinetic Chromatography (MEKC)

MEKC is a combination of CE and chromatography first introduced by Shigeru Terabe in 1984.<sup>[59]</sup> MEKC is a variation of CZE, relying on the same electrophoretic mobility of analytes under an electric current. The main difference is that a surfactant is added above its critical micellar concentration, thus resulting in the formation of micelles in the background electrolyte (BGE). These micelles are generally spherical in shape with the charged head displayed on the surface and the hydrophobic tails pointing towards the centre. This arrangement causes the micelle to migrate due to its charged surface and the uncharged, neutral centre allows for the partitioning of neutral analytes between the micelle and the BGE.<sup>[60]</sup> Separation is obtained due to differences in electrophoretic mobilities and partitioning. The degree to which the separation is based on partitioning is dependent upon the type of surfactant.<sup>[61]</sup> MEKC has applications in the analysis of illicit drug compounds<sup>[62]</sup> and also in the determination of pharmaceuticals.<sup>[63]</sup> In order to improve the poor concentration sensitivity of ultraviolet (UV) detection with MEKC,

on-line preconcentration techniques have been employed. MEKC separation is also possible in the absence of EOF. This is particularly useful for acidic species which would be ionised at high pH and therefore would not interact with negatively charged sodium dodecyl sulphate (SDS) micelles.<sup>[64]</sup> Cyclodextrins (CD), have been incorporated in the buffer solution and have been successfully applied for the analysis of enantiomers, particularly neutral CDs with achiral surfactants.<sup>[65, 66]</sup>

## 1.4 MASS SPECTROMETRY

Mass spectrometry (MS) is probably the most comprehensive and flexible of all instrumental methods of analysis. Mass spectrometry is the technique that can be used to selectively detect a given analyte, determine its elemental composition and identify aspects of the molecular structure. These tasks are accomplished through the experimental measurement of the mass of gas-phase ions produced from molecules of an analyte. Unique features of MS include its capacity for direct determination of the nominal mass of an analyte, and to produce and detect fragments of the molecule that correspond to discrete groups of atoms or different elements that reveal structural features.

### 1.4.1 Ionisation Methods used in Mass Spectrometry

Mass spectrometers work by using magnetic and electric fields to exert forces on charged particles (ions) in vacuum. Therefore, a compound must be charged or ionised to be analysed by a mass spectrometer. Furthermore, the ions must be introduced in the gas phase into the vacuum system of the mass spectrometer. This is easily done for gaseous or heated volatile samples. However, many analytes decompose upon heating. These kinds of samples require either desorption or desolvation methods if they are the subject of mass spectrometry analysis. Although

ionisation and desorption/desolvation are usually two separate processes, the term ionisation is commonly used to refer to both of them.

The choice of ionisation method depends on the nature of samples as shown in Table 1.1.

**Table 1.1:** Ionisation sources and resulting ionisation events. <sup>[67]</sup>

Ionisation Source	Acronym	Event
Electrospray Ionisation Nanoelectrospray Ionisation	<b>ESI</b> <b>nanoESI</b>	Evaporation of charged droplets
Atmospheric Pressure Chemical Ionisation	<b>APCI</b>	Corona discharge and proton transfer
Matrix Assisted Laser Desorption Ionisation	<b>MALDI</b>	Photon absorption/proton transfer
Desorption/ Ionisation on silicon	<b>DIOS</b>	Photon absorption/ proton transfer
Fast Atom Bombardment	<b>FAB</b>	Ion bombardment/ proton transfer
Electron Impact	<b>EI</b>	Electron beam/electron transfer
Chemical Ionisation	<b>CI</b>	Proton transfer

#### 1.4.1.1 Electrospray Ionisation (ESI)

##### 1.4.1.1.1 Introduction

Application of electrospray ionisation, ESI, has widened significantly the applications of mass spectrometry by introducing new features not otherwise available in classical MS that relied on gas-phase analytes for ionisation. <sup>[68, 69]</sup>

Hence, it is now possible to:

- a) form ions from nonvolatile, thermally labile compounds,
- b) produce multiply-charged ions, the mass-to charge ( $m/z$ ) value of such ions are still within the range of most universally used mass spectrometers,
- c) provide the most successful interface for LC-MS; some recent applications are given in Table. 1.2,

d) directly analyse inorganic cations and anions, providing information on the valence state and molecular formulate,

e) investigate noncovalent associations of macromolecules such as proteins <sup>[70]</sup>, peptides <sup>[71, 72]</sup>, also small molecules <sup>[73, 74]</sup> and polymers <sup>[75, 76]</sup>.

Electrospray ionisation mass spectrometry (ESI-MS) has proved to be a powerful tool for analysis of polymers produced by laser initiation <sup>[77-79]</sup> and controlled radical polymerisation <sup>[80-82]</sup>. Szablan *et al.* <sup>[78]</sup> found the polymeric product generated by pulsed laser polymerisation (PLP) of methyl methacrylate (MMA) in the presence of the photoinitiators: 2,2- dimethoxy -2-phenylacetophenone (DMPA), benzoin and benzil. Termination products were identified with high accuracy.

In 2000, Kasperczyk and Li published a paper on the analysis of degradation products of copolymers using mass spectrometry (ESI-MS) together with NMR. This work confirmed that both these method can provide more detailed information on the subject of the chemical structure of copolymer chains. <sup>[83]</sup> Several papers presented results for ESI-MS together with NMR showing the importance of both methods as very potent tools for identifying structures of compounds, such as photodegradation products. <sup>[84-86]</sup> NMR spectroscopy will be discussed in section 1.5.

**Table 1.2:** ESI-MS in photoinitiator and polymerisation product analysis.

Compound	Comments	Reference
Inorganic polymers	ESI-MS used. The investigation of the polymerisation was conducted in both negative and positive mode	[75]
PPC metabolites	LC/LC-MS/MS used. An analysis of chiral PPC metabolites	[87]
Nitroxide mediated polymerisation (NMP), atom transfer radical polymerisation (ATRP)	LC-MS (MALDI-TOF and ESI-MS) used. Both methods were used to study catalytic and free radical polymerisation	[88]
Poly(butyl acrylate)	ESI-MS used. The method was used to study the product of polymerisation at different experimental conditions	[89]
2-isopropylthioxanthone (ITX), Benzophone, Irgacure 184, Ethyl-4-dimethylaminobezoate (EDAB).	Determination of ink photoinitiators in packaged beverages by ESI-MS	[90]

### 1.4.1.1.2. The electrospray ionisation process

There are three major steps in the production of the gas-phase ions from electrolyte ions in solution:

- a) production of charged droplets at the ES capillary tip;
- b) shrinkage of the charged droplets due to solvent evaporation and repeated charge-induced droplet disintegrations leading ultimately to very small highly charged droplets capable to producing gas-phase ions;
- c) the actual mechanism by which gas-phase ions are produced from these droplets.

The stages (a) and (c) occur in the atmospheric pressure region of the apparatus, refer to Figure 1.5. <sup>[91]</sup>

As shown in Figure 1.5, a voltage  $V_c$ , of 2-3 kV, is applied to the spray capillary. Typically the capillary is 1 mm o.d. and located 1-3 cm from the counterelectrode. Because the spray capillary tip is very thin, the electric field  $E_c$  at the capillary tip is very high ( $E_c = 10^6$  V/m). The value of the field at the capillary tip opposite a large and planer counterelectrode can be estimated from the approximate relationship: <sup>[92]</sup>

$$E_c = \frac{2V_c}{r_c \ln(4d/r_c)} \quad \text{Eqn. 1.15}$$

where:

$V_c$  is the applied potential,

$r_c$  is the capillary outer radius

$d$  is the distance from capillary tip to the counterelectrode.

The field can penetrate the solution and reach the highest value near the spray capillary tip. This causes a polarization of the solvent near the meniscus of the liquid. In the presence of an electrolyte the solution becomes sufficiently conducting and the positive and negative electrolyte ions in the solution will move under influence of the field. This movement leads to an enrichment of positive ions near surface of the meniscus and negative ions away from the meniscus. The downfield forces due to the

polarization cause a distortion of the meniscus into a cone pointing downfield. The increase of surface due to the cone formation is resisted by the surface tension of the liquid. The cone formed is called a Taylor cone. <sup>[93]</sup> If the applied field is sufficiently high the tip becomes unstable and fine jet emerges from the cone tip. The surface of the jet is charged by an excess of positive ions. The repulsion between the charged droplets on the jet causes the jet to break up into small charged droplets (see Figure 1.5). <sup>[91]</sup>

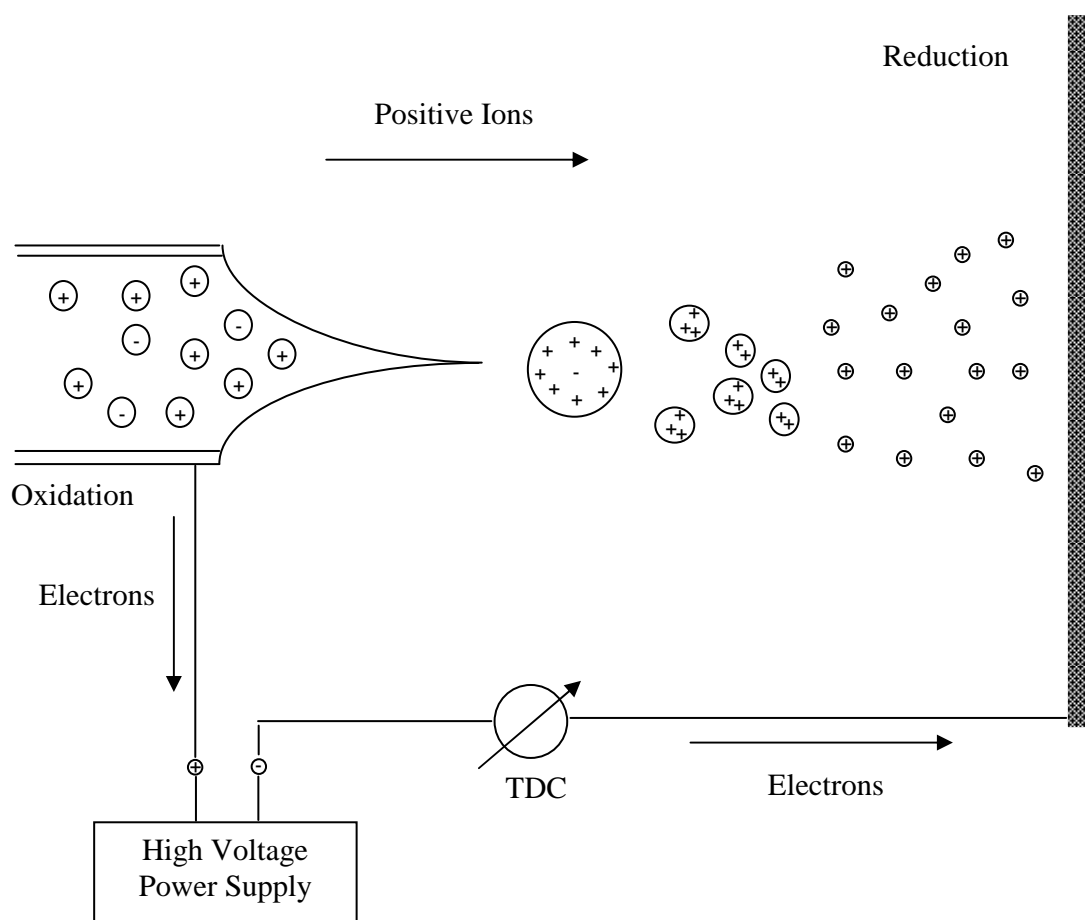


**Figure 1.5:** Illustration of major processes in the atmospheric pressure region of an ESI on source run in positive mode.

The charged droplets produced at the spray needle shrink due to solvent evaporation while the charge remains constant. The energy required for the solvent evaporation is



provided by the thermal energy of the ambient nitrogen, air at atmospheric pressure in most cases. As the droplet gets smaller the repulsion between the charges at the surface increases and at a certain droplets radius, this repulsion overcomes the cohesive force of the surface tension. An instability results and leads to fission of the droplet that typically releases a jet of small, charged progeny droplets. The condition for the instability also called Coulomb fission is given by the Rayleigh<sup>[94]</sup> equation:

$$Q_{Ry} = 8\pi(\epsilon_0\gamma R^3)^{1/2} \quad \text{Eqn. 1.16}$$

where:

$Q_{Ry}$  is the charge on droplet

$\gamma$  is the surface tension of the solvent

$R$  is the radius of the droplet

$\epsilon_0$  is the electrical permittivity

There is still no consensus on the mechanism by which analyte ions are formed from charged droplets. Two mechanisms were proposed to account for the formation of gas-phase ions from the very small and highly charged droplets. The first mechanism was proposed by Dole who was interested in analytes of high molecular mass.<sup>[95]</sup> Evaporation of the solvent from the initially formed droplet as it traverses a pressure gradient toward the analyser leads to a reduction in diameter and an increase in surface field, until the Rayleigh limit is reached. A Coulomb explosion occurs, as the magnitude of the charge is sufficient to overcome the surface tension holding the droplet together. The resulting instability disperses the droplet into a collection of smaller droplets that continue to evaporate until they too reach the Rayleigh limit and disintegrate. A continuation of this process may be envisaged to result in the formation of an ion containing a single analyte molecule. The molecule retains some of this droplet's charge to become a free ion as the last of the solvent vaporises. This assumption is now known as the Charged Residue Model (CRM).

Iribarne and Thomson<sup>[96]</sup> who worked with small ionic analytes such as  $\text{Na}^+$  and  $\text{Cl}^-$ , proposed a different mechanism called IEM (Ion Evaporation Model). This model

predicts that direct ion emission from the droplets can occur after the radii of droplets shrink to radii less than 10 nm. The ion evaporation process by removing charge, replaces Coulomb fission. Iribarne and Thomson supported their model by experimental results <sup>[96]</sup> and theoretical calculations <sup>[97]</sup>. The experimental results involved measurements of the relative abundance of the ions produced by ESI of solutions containing NaCl as the only solute. A diagram illustrating the CRM and IEM models of formation in electrospray is shown below (Figure 1.6)

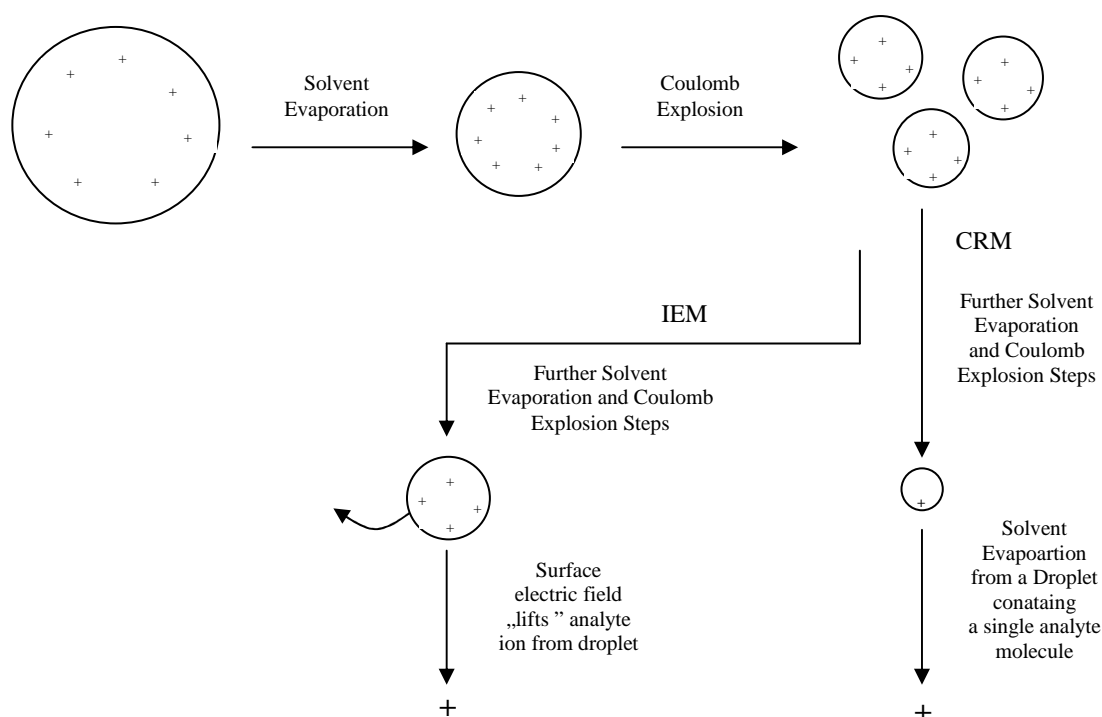


**Figure 1.6:** Electrospray ionisation processes, proposed by Dole (CRM) and by Iribarne and Thomson (IEM). <sup>[98]</sup>

In summary, the IEM is experimentally well supported for small (in)organic ions. However, the theoretical derivation of the model does not apply for very large ions such as proteins. For these macromolecular species, the CRM is much more plausible.

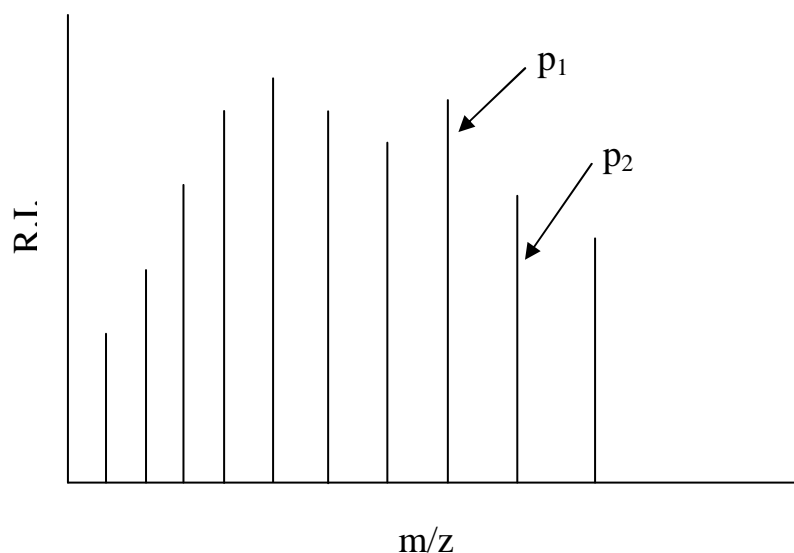
## 1.4.1.1.3 The multiply charged ions

ESI can produce singly or multiply charged ions. The number of charges retained by a particular analyte depends on several factors such as the size, chemical composition, and higher order structure of the analyte molecule, the solvent composition and the instrument parameters. For small molecules (< 2000 Da) ESI typically generates singly, doubly, or triply charged ions, while for large molecules (> 2000 Da) ESI can produce a series of multiply charged ions. Because mass spectrometers measure the mass-to-charge ( $m/z$ ) ratio, the ESI mass spectrum for a large molecule typically contains multiple peaks corresponding to the different charge states.<sup>[99]</sup> In these cases a series of peaks in the ESI mass spectrum represents multiple-charged variants<sup>[89]</sup> of the analyte but sometimes these multiple-charges include species such as Na or K, which have replaced hydrogen. Some possible clusters formed during ESI are represented in Table 1.3.

**Table 1.3:** Some of the possible combination of clusters of the analyte molecule (M).<sup>[100]</sup>

$[M+H]^+$	$[M+nH]^{+n}$
$[M+Na]^+$	$[M+nNa]^{+n}$
$[M+K]^+$	$[M+nK]^{+n}$
$[M-H]^-$	$[M-nH]^{-n}$
$[M+nH + xNa + yK]^{+(n+x+y)}$	
$[nM+H]^+$	

Because of the multiple-charge species, several algorithms<sup>[101, 102]</sup> have been developed to calculate the mass of the analyte and a related algorithm has also been developed to process LC- MS data<sup>[103]</sup>. In Figure 1.7 a general scheme is presented where the  $m/z$  values of the peaks in the spectrum are represented by  $p_1$  and  $p_2$ .



$p$  is a peak in the mass spectrum; ( $p=m/z$ ),  $p_2 > p_1$

$M$  is the molecular weight of analyte;

$H^+ = 1 \text{ Da}$  (1.0078 Da)

$n$  is the number of charges,  $n_1 > n_2$

Adjacent peaks represent ions differing by 1 charge state

$$p_1 = (M + (n_2 + 1)H^+) / (n_2 + 1) \quad \text{Eqn. 1.17}$$

$$p_2 = (M + n_2 H^+) / n_2 \quad \text{Eqn. 1.18}$$

When the value for  $M$  is known and substituted into Eqn 1.15, it can be solved for  $n_2$

$$n_2 = (p_1 - H^+) / (p_2 - p_1) \quad \text{Eqn. 1.19}$$

If peaks  $p_1$  and  $p_2$  are measured from the spectrum,  $n_2$  can be calculated from Eqn 1.19 and  $M$  from Eqn 1.17 or 1.18.

**Figure 1.7:** Scheme for mathematical relationship between charge state and mass of analyte and charge carrier (adduct) in rationalising the  $m/z$  value of peaks observed in the ESI mass spectrum. <sup>[100]</sup>

The triply charged ions of small molecules were reported by Morvay and Cormides.<sup>[104]</sup> In their paper, mass spectrometric evidence for the existence of two triatomic ( $\text{CS}_2^{3+}$  and  $\text{CSe}_2^{3+}$ ) and one diatomic ( $\text{S}_2^{3+}$ ) triply charged species was presented. In 2006, Bai and co-workers published a paper on doubly charged cluster ions, besides singly charged cluster ions, from sodium and potassium nitrates in both positive and negative ion electrospray ionisation ion trap mass spectrometry. The fragmentation pathways for doubly charged cluster ions were studied in detail using ESI tandem mass and two pathways were observed depending on the cluster sizes of alkali metal nitrates.<sup>[105]</sup> It is also found that doubly charged cluster ions could be produced from ESI and collision induced dissociation (CID) was employed to determine their fragmentation patterns<sup>[106]</sup>. However, the doubly charged cluster ions were mostly generated in positive ion mode.

#### 1.4.2 Mass analyser

The mass analyser, known also as a  $m/z$  analyser is used to separate ions according to their mass to charge ratios ( $m/z$ ) where the charge is produced by the addition or loss of proton(s), cation (s), anion (s) or electrons. The addition of charge allows the molecule to be affected by the electric field thus allowing its mass measurement. However, not all analysers operate in the same way, some separate ions in space while others separates ions by time.

The first mass analysers, made in the early 1900s, used a magnetic field to separate ions according to their radius of curvature through the magnetic fields. The design of modern analysers has changed significantly in the last five years, now offering much higher accuracy, increased sensitivity and broader mass range. Typical mass analysers and some of their applications are presented in Table 1.4

**Table 1.4:** The typical mass analysers.

Mass Analysers	Event	Comments and References
Quadrupole and triple Quadrupole	Scan radio frequency field	Analysis of peptides using ESI <sup>[107]</sup> , Analysis of carbosulfan and seven of its main metabolites using LC-MS/MS <sup>[108]</sup>
Quadrupole Ion Trap	Scan radio frequency field	Comparison of LC using triple quadrupole and quadrupole ion trap mass analyser to pesticides <sup>[109]</sup>
Time -of -Flight TOF	time-of -flight correlated directly to ions $m/z$	Analysis of quaternary ammonium herbicides in drinking water <sup>[110]</sup> , TOF combination with the ICP source <sup>[111]</sup>
Time-of-Flight Reflectron	time-of-flight correlated directly to ions $m/z$	Characteristic of time -of flight mass reflectron <sup>[112]</sup>
Quad-TOF	Radio frequency field scanning and time of flight	Analysis of multi-class polar pesticides and transformation products <sup>[113]</sup>
Magnetic Sector	magnetic field affects radius of curvature of ions	Sensitive detection of proteins <sup>[114]</sup>

### 1.4.3 Tandem Mass Spectrometry

In the tandem mass spectrometry, MS/MS method the analyser allows the ion separate of different ions, create of product ions from the ion selected and then measurement of the mass of the product ions (see Figure 1.8). The fragmented ions are used for structural determination of original molecular ions. Typically, tandem MS experiments are performed by collision of a selected ion with inert gas molecules such as argon, helium, and the masses of resulting product ions are analysed.

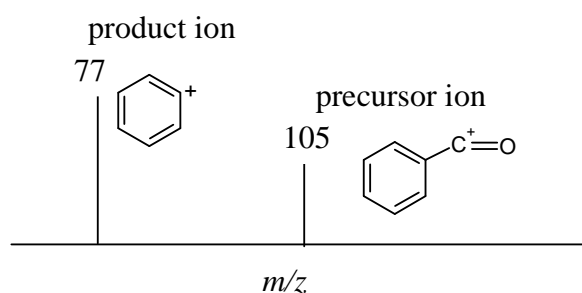
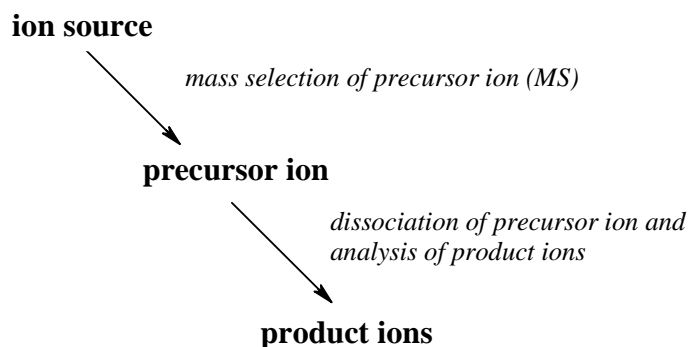


**Figure 1.8:** Tandem mass spectrometry analysis. In this case ions of  $m/z$  77 are selected to be precursor ions by the first mass spectrometer. <sup>[100]</sup>

Tandem mass analysis is used to determine the sequence of peptides and structurally characterise carbohydrates and small- oligo-nucleotides. Also MS/MS has been employed to generate further structural information about polymers <sup>[115, 116]</sup> for example PMMA (poly(methyl methacrylate)) and PBMA (poly(*n*-butyl methacrylate)). <sup>[117]</sup>

## 1.5 NUCLEAR MAGNETIC RESONANCE SPECTROSCOPY (NMR)

Nuclear magnetic resonance spectroscopy, commonly referred to as NMR, has become a powerful tool for organic chemists since the instruments became easily available in the late 1950s, and developments in instrumentation in the last fifty years have extended the usefulness of the technique <sup>[118-120]</sup>. NMR spectroscopy has developed into a very important tool for chemists, biochemists, physicists, and more

recently medical scientists. The main field of application of NMR is that of determining the structures of molecules. The necessary information for this is obtained by measuring, analysing and interpreting the high-resolution NMR spectrum recorded in liquids of low viscosity.

The techniques are only applicable to those nuclei that possess a spin quantum number ( $I$ ) greater than zero. The most important of such nuclei as far the organic chemists are concerned include  $^1\text{H}$  and  $^{13}\text{C}$ , both of which have a spin quantum number of  $\frac{1}{2}$ . Other nuclei with non zero spin quantum numbers are  $^{19}\text{F}$  and  $^{31}\text{P}$ , with  $I = \frac{1}{2}$ ; or  $^{14}\text{N}$  and  $^2\text{D}$ , with  $I = 1$ .

### 1.5.1 $^{31}\text{P}$ NMR

The phosphorus atom plays a central role in the chemistry of most compounds that contain this atom in their structure. It is of great importance to recognise and understand the changes in bonding and stereochemistry that occur at the phosphorus atom in such compounds. After 1950, chemists interested in phosphorus compounds began to utilise the ideas and techniques of polymer science and advanced organic chemistry. Since many phosphorus compounds are relatively labile compared to the compounds of classical organic chemistry, they simply undergo rearrangements and other reactions. The  $^{31}\text{P}$  nucleus, with spin  $\frac{1}{2}$ , exhibits a relatively high NMR sensitivity, due to 100% natural abundance, quite large magnetogyric ratio, and large chemical shift range. Shortly it became the method of choice for rapid molecular assays for phosphorus chemists who could afford a multinuclear NMR spectrometer. By 1960, the use of NMR based on  $^{31}\text{P}$  and other nuclei (particularly proton NMR) for the determination and characterisation of phosphorus compounds was well established and effort was directed to the study of rapid reactions using NMR line broadening. In 1967 massive progress was made because of the introduction of Fourier transform (FT) techniques for acquiring  $^{31}\text{P}$  NMR data. By 1970, phosphorus NMR had become a primary experimental technique in many areas for analysis of organic compounds, in coordination chemistry and biological systems. By 1983, instrumental and relaxation aids available to enhance sensitivity made it possible to



estimate phosphorus containing compounds at the 200 ppm- level down to even the 5 ppm level. <sup>[121]</sup>

Phosphorus chemical shifts extend over a range exceeding 1000 ppm. The presence of a lone pair of electrons on the phosphorus tends to widen the chemical shift range. <sup>31</sup>P chemical shift is usually reported relative to the signal for 85% phosphoric acid. <sup>[122]</sup> The acid is invariably used as an external reference due to its reactivity. A number of secondary standards are in use that give much sharper signals than 85% phosphoric acid. A 0.2 M solution of crystalline phosphoric acid in 14% aqueous perchloric acid (tetrahydroxyphosphonium perchlorate) gives a very sharp signal at – 0.06678 ppm. An aqueous solution (D<sub>2</sub>O) of disodium ethylene diphosphonate (16.72 ppm) is most useful as a secondary standard for aqueous samples because it gives no further correction for the type of the spectrometer employed. There was a change in sign convention in the mid 1970s so that positive chemical shifts were deshielded of the standard (this convention has again been reversed). Although modern NMR spectrometry can provide extremely accurate data for compounds studied under a given set of conditions, this advantage is offset for many organophosphorus compounds by the dependence of their <sup>31</sup>P NMR chemical shifts on concentration, solvent, and the presence of other compounds. <sup>31</sup>P NMR spectroscopy can also provide a very convenient method for determining the optical purity of chiral phosphorus compounds. Thus when an enantiomer that forms an adduct with a phosphorus compound is added, different chemical shifts are often observed for the diastereometric products.

The NMR chemical shifts of some phosphorus compounds are reported in Table 1.5 by class of compounds so that the relationships between chemical shifts and the substituent groups can be recognised. <sup>[123, 124]</sup>

**Table 1.5:** Nuclear Magnetic Resonance Spectra of Phosphorus Compounds. <sup>[121]</sup>

Compound	Solvent	$\delta$ (ppm)	Multiplicity	J (Hz)
$(C_6H_5P)_n=2 \text{ or } 4$	benzene	4.6	...	...
$(C_6H_5CH_2O)_2P(O)H$	neat	-7.9	d	713
$C_6H_5OP(O)Cl_2$	neat	-1.8	...	...
$(C_6H_5O)_2P(O)Cl$	neat	6.1	...	...
$(C_2H_5O)_2P(O)OH$	aqueous	0	...	...
$C_6H_5OP(O)(OH)_2$	aqueous	4.8	...	...
$(C_6H_5O)_2P(O)OH$	methanol	12.7	...	...
$(C_6H_5CH_2O)_2P(O)OH$	dioxane	1.1	...	...
$(C_2H_5)_2P(O)OP(O)(OC_2H_5)_2$	neat	13.4	...	...
$(C_6H_5)_2P(O)OP(O)(OC_6H_5)_2$	neat	23.9	...	...
$(C_2H_5)_2P_\alpha(O)OP_\beta(O)-$ $(OC_6H_5)OP(O)(OC_2H_5)_2$	neat	+26.6( $\alpha$ )	d	16
$(C_6H_5)_2P_\alpha(O)OP_\beta(O)-$ $(OC_6H_5)OP(O)(OC_6H_5)_2$	neat	+35.6( $\beta$ )	t	16
$C_6H_5OP(O)NHC_6H_4NH_2$	ethanol	-18.1	t	15
$(C_6H_5)_2P(O)NH_2$	methanol	-25.5		

In 1995, Kolczak published the first paper about application of  $^{31}P$  NMR-CIDNP spectroscopy to investigate the formation and decay of phosphorus-centered radicals formed upon cleavage of photoinitiators.<sup>[125]</sup> In these studies monoacylphosphine oxides and bisacylphosphine oxides were used. All products were shown to undergo a photoinduced cleavage of the C-P bond from a triplet state precursor. The primary radicals can undergo various reactions. Since the phosphinoyl radicals possess adequate spin density, both at the phosphorus and oxygen atoms (Figure 1.9), reactions at both centres occur, given by the superposition of two structures with the unpaired electron located on the oxygen or phosphorus.

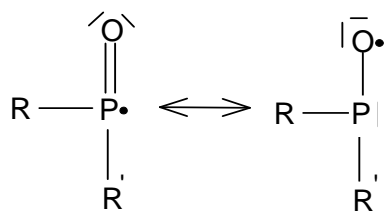


**Figure 1.9:** Resonance structures of phosphinoyl radicals.

The spin density distribution in the phosphinoyl radicals indicates that three possible types of escape product may be obtained by recombination of these radicals (Figure 1.10).

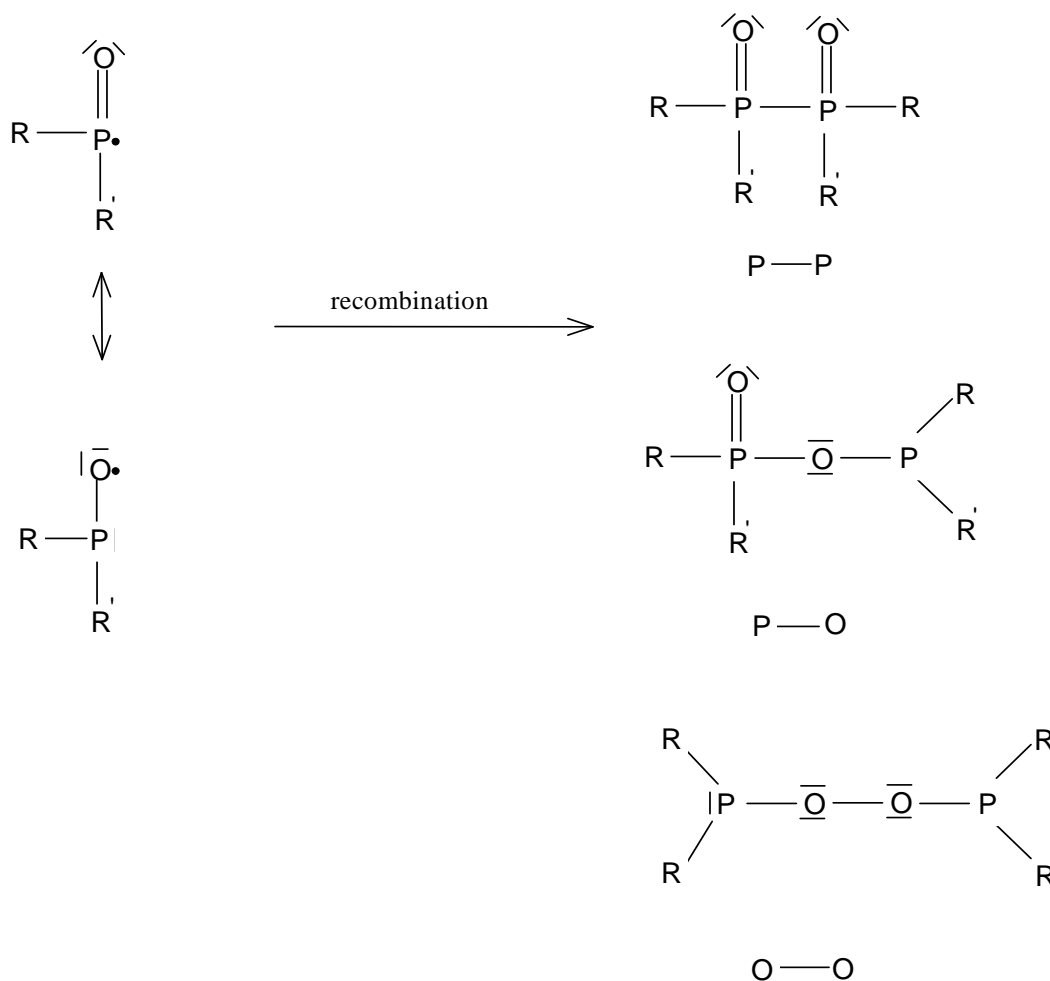


**Figure 1.10:** Escape products from the recombination of phosphinoyl radicals. <sup>[125]</sup>

The formation of the dimer with a P-P bond and the one with a P-O bond was observed with <sup>31</sup>P –CIDNP spectrum but there was no evidence for the formation of O-O recombination products. Chemically induced dynamic nuclear polarisation (CIDNP) spectroscopy is a powerful tool for the elucidation of the radical reactions. <sup>1</sup>H and <sup>13</sup>C-NMR –CIDNP techniques have been successfully used for the determination of species responsible for the initiation of polymerisation by various types of photoinitiators <sup>[126]</sup> including Irgacure 369 <sup>[127]</sup> or Irgacure 907. <sup>[9]</sup> <sup>31</sup>P NMR has been also used to identify the chemical reactions between a sol-gel matrix and two different types of photoinitiators (Irgacure 819 and 1800). <sup>[128]</sup>

## 1.6 GAUSSIAN Method

*Gaussian* is a modelling program used to elucidate electronic structure by chemists<sup>[129]</sup>, chemical engineers, biochemists<sup>[130]</sup>, physicists and others for research in established and emerging areas of chemical interest.

Starting from the basic laws of quantum mechanics, *Gaussian* predicts the energies<sup>[131, 132]</sup>, molecular structures, and vibrational frequencies of molecular systems, along with several molecular properties derived from these basic computation types. It can be used to study molecules and reactions<sup>[133, 134]</sup> under a wide range of conditions, including both stable species and compounds which are difficult or impossible to observe experimentally, for example short-lived intermediates<sup>[135]</sup> and transition structures.

With the development of quantum mechanical methods such as *Gaussian* a new approach based on both experiments and molecular modelling techniques started to be used in the field of PIS, (photoinitiating system). In 2003, Allonas et al. published a paper which combined laser induced photoacoustic calorimetry (PAC) and molecular modelling for investigation of the cleavage process in radical photoinitiating systems.<sup>[136]</sup> Another paper was published by Zhao et al. on the new photoinitiating system of acetone/water (acetone functioning as a high efficient photoinitiator) for photografting polymerisation.<sup>[137]</sup> For both above papers calculations were made with usage of *Gaussian*. Also the joint use of MS, NMR and computational techniques demonstrated by Silva et al. confirmed this to be a powerful combination of tools for the complete elucidation of metal-DTPA (DTPA-diethylenetriaminepentacetic acid) complex structure.<sup>[138]</sup>

## 1.7 CONCLUSIONS

In this introduction, the underlying theories of the instrumental techniques used in this thesis have been discussed. They include separation techniques such as high performance liquid chromatography and capillary electrophoresis, spectroscopic techniques such as mass spectrometry, and NMR and molecular modelling program (*Gaussian*).

## 1.8 AIMS AND OBJECTIVES

The aim of this work was to determine the chemical pathways of photoinitiators and study how these pathways affect the curing mechanism.

The objectives of the research were:

- The development and optimisation of chromatographic and electrophoretic separation methods for the analysis of photoinitiator bis(2,4,6-trimethylbenzoyl)phenylphosphine oxide, BAPO or Irgacure 819.
- The study of samples under light and dark conditions to determine the stability and chemical pathways of photoinitiators.
- The study of the curing mechanism and degradation products using complementary methods: LC-MS and NMR spectroscopy.
- The theoretical calculation approach used to support the experimental parts of investigations of the cure mechanism of photoinitiators.

**1.9 REFERENCES**

- [1] Decker, C., *Prog. Polym. Sci.*, **1996**, *21*, 593.
- [2] Pappas, S.P., *Radiation Curing Science and Technology*, Plenum, New York, **1992**.
- [3] Fouassier, J.P., Rabek, J.F., *Radiation Curing in Polymer Science and Technology*, Vols, I-IV, Elsevier Applied Science, London, **1993**.
- [4] Kronganz, V.V., Trifunac, A.D., *Processes in Photoreactive Polymers*, Chapman and Hall, New York, **1995**.
- [5] Crivello, J.V., *Adv. Polym. Sci.*, **1984**, *62*, 2.
- [6] Decker, C., *Handbook of Polymer Science and Technology 3*, (N.P. Cheremisinoff Ed.), p 541, Marcel Dekker, New York, **1989**.
- [7] Decker, C., *J. Coat. Technol.*, **1993**, *65*, 49.
- [8] Decker, C., *Acta Polym.*, **1994**, *45*, 333.
- [9] Rutsch, W., Berner, G., Kirchmayr, R., Hüsler, R., Rist, G., Bühler, N., *Organic Coatings- Science and Technology*, Vol 8, Marcel Dekker, New York, **1996**.
- [11] Rutsch, W., Angerer, H., Desobry, V., Dietliker, K., Hüsler, R., *Proc. XVI Conf. Organic Coatings- Science and Technology*, Athens, Greece, **1990**.
- [12] Köhler, M., Misev, L., Desobry, V., Dietliker, K., Bussian, B.M., Karfunkel, H., *Radiation Curing of Polymer II*, Cambridge, **1991**.
- [13] Jacobi, M., Henne, A., *J. Radiat Curing*, **1983**, *19*, 16.
- [14] Jacobi, M., Henne, A., Böettcher, A., *Polym. Paint. Colour, J.*, **1985**, *175*, 636.
- [15] Ellrich, K., Herzig, C., *Eur. Patent.Applic., No. 184095*, **1984**.
- [16] Szepesi, G., *How To Use Reverse Phase HPLC*, VCH Publishers, New York, **1992**.
- [17] Willard, H.H., Mairitt, L. L., Dean, J.A., Settle F.A., *Instrumental Methods of Analysis*, 6 th Edition, Wadsworth Publishing Company, California, **1981**.
- [18] Knox, J.H., *High Performance Liquid Chromatography*, Wiley-VCH Verlag GmbH, Edinburgh, **1978**.
- [19] [www.chem.neu.edu](http://www.chem.neu.edu).

- [20] Gavenda, A., Sevick, J., Psotova, J., Bednar, P., Bartak, P., Adams, P., Simanek, V., *Electrophoresis*, **2001**, 22, 2782.
- [21] Snyder, R., Dolan, W., Jupille, H., *Advanced HPLC Method Development, LC Resources*, 2 nd Edition, John Wiley & Sons, New York, **2005**.
- [22] Martin, A.J.P., Synge, R.L.M., *J Biochem.*, **1941**, 35, 1358.
- [23] Van Deemter, J.J., Zuiderweg, F.J., Klinkenberg, A., *A. Chem. Eng. Soc.*, **1956**, 5, 271.
- [24] [www.shu.ac.uk](http://www.shu.ac.uk)
- [25] Witkiewicz, Z., *Podstawy Chromatografii*, Wydawnictwa Naukowo-Techniczne, Warszawa, **2005**.
- [26] Pesek, J.J., Matyska M.T., *LC GC*, **2006**, 24, 296.
- [27] Liu S-Y., Liu, K-S, Kuei, Ch-H, Tzeng, J-I., Ho,S-T., Wang, J-J., *J. Chromatogr. B*, **2005**, 818, 233.
- [28] Zhu, H-J., Wang, J-S., Patrick, S.K., Donovan, J.L., Lindsay De Vane, C., Markowitz, J.S., *J. Chromatogr. B*, **2007**, 858, 91.
- [29] Srinivasu, M.K., Mallikarajana Rao, B., Sridhar, G., Rejender Kumar, P., Chandrasekhar, K.B., Islam, A., *J. Pharm. Biomed. Anal.*, **2005**, 37, 453.
- [30] Bharami, G., Mohammadi, B., *J. Chromatogr. B.*, **2006**, 837, 24.
- [31] Fahmy, O.T., Korany, M.A., Maher, M.H., *J. Pharm. Biomed. Anal.*, **2004**, 34, 1099.
- [32] Bharami, G., Kiani, A., *J. Chromatogr. B*, **2006**, 835,123.
- [33] Baxter, J.E., Davidson, R.S., Hageman, H.J., Hakvoort, G.T.M., Overeem, T., *Polymer*, **1988**, 29, 1575.
- [34] Haddad P.R., Jackson, P.E., *J. Chromatogr. Libr.*, **1990**, 46, 230.
- [35] Bidlingmeyer, J., *J. Chromatogr. Sci.*, **1980**, 18, 525.
- [36] Abbott, S.R., *J. Chromatogr. Sci.*, **1980**, 18, 540.
- [37] Small, H., *Ion Chromatography*, Springer, New York, **1989**.
- [38] Nesterenko, P.N., *Trends in Anal. Chem.*, **2001**, 20, 311.
- [39] Kaniansky, D. Masar, M., Marak, J., Bodor, R., *J Chromatogr. A*, **1999**, 834,133.
- [40] Jackson, P.E., *Trends in Anal. Chem.*, **2001**, 20, 320.
- [41] Barron, L., Nesterenko, P.N., Paull,B., *J. Chromatogr. A*, **2005**, 1072, 207.
- [42] Kuban, P., Kuban, V., *J. Chromatogr. A*, **1999**, 836, 75.



- [43] Fung, Y.S., Lau, K.M., *Electrophoresis*, **2003**, 24, 3224.
- [44] Lloyd, D.K., *J. Chromatogr. A*, **1996**, 735, 29.
- [45] Taga, A., Du, Y., Suzuki, S., Honda, S., *J. Pharm. Biomed. Anal.* **2003**, 30, 1587.
- [46] [www.beckmancoulter.com/literature/](http://www.beckmancoulter.com/literature/)
- [47] Tagliaro, F., Manetto, G., Crivellente, F., Smith, F.P., *Forensic Science International*, **1998**, 92, 75.
- [48] Weston, A., Brown, P., *HPLC and CE, Principles and Practice*, Saunders Company, California, **1997**.
- [49] Altria, K.D., *Capillary Electrophoresis Guidebook- Principles, Operations and Applications*, Human Press, Totowa, **1995**.
- [50] Landers, J.P., *Handbook of Capillary Electrophoresis*, CRC Press, Boca Raton, **1997**.
- [51] Cikalo, M.G., Bartle, K.D., Robson, M.M., Myers, P., Euerby, M.R., *Analyst*, **1988**, 123, 87R.
- [52] St. Claire, R.L., *Anal. Chem.*, **1996**, 68, 569.
- [53] Kuhn, R., *Capillary Electrophoresis; Principles and Practice*, Springer Verlag Telos, **1993**.
- [54] McMahon, G., *Analytical Instrumentation*, John Wiley & Sons, Ltd, West Sussex, **2007**.
- [55] Dermaux, A., Sandra, P., *Electrophoresis*, **1999**, 20, 3027.
- [56] Cifuentes, A., Canalejas, P., Diez-Masa, J.C., *J. Chromatogr. A.*, **1999**, 830, 423.
- [57] *Encyclopedia of Polymer Science and Technology*, Vol.1, Wiley, New York, **1985**.
- [58] Odian, G., *Principles of Polymerisation*, Wiley, New York, **1991**.
- [59] Terabe, S., Otsuka, K., Ando, T., *Anal. Chem.*, **1985**, 57, 834.
- [60] Ewing, A.G., Wallingford, T.M., Olefirowicz, *Anal. Chem.*, **1989**, 61, 292.
- [61] Harakuwe, A. H., Haddad, P.R., *Trends in Anal. Chem.*, **2001**, 20, 375.
- [62] Gomes, P., Sippel, J., Jablonski, A., Steppe, M., *J. Pharm. Biomed. Anal.*, **2004**, 36, 909.
- [63] Öztekin, N., Baskan, S., Erim, F.B., *J. Chromatogr. B.*, **2007**, 850, 488.
- [64] Altria, K.D. *J. Chromatogr.A.* ,**1999**, 856, 443.

- [65] Terabe, S., *Anal. Chem.* **2004**, *76*, 240A.
- [66] Razak, J.L., Doyen, H.J. Lunte, C.E., *Electrophoresis*, **2003**, *24*, 1764.
- [67] Siuzdak, G., *The Expanding Role of Mass Spectrometry*, MCC Press, NY, **2006**.
- [68] Kebarle, P., *J. Mass Spectrom.* **2000**, *35*, 804.
- [69] Kabarle, P., *Int. J Mass Spectrom.*, **2000**, *200*, 313.
- [70] Wang, H, Hu, G., Zang, Y., Yuan, Z., Zhao, X., Zhu, Y., Li, Y., Shengyinan, X., Deng, Y., *J Chromatogr. B*, **2010**, *878*, 1946.
- [71] Tucholska, M., Florentinus, A., Williams, D., Marsall, J. G., *J. of Proteomics*, **2010**, *73*, 1254.
- [72] Wang, H., Dass, Ch., *Peptides*, **2002**, *23*, 2143.
- [73] Henriksen, T., Juhler, K.R., *J. Am. Soc. Mass Spectrom*, **2005**, *16*, 446.
- [74] Yu, Yonghao, Sweeney, M., D., Saad, O..M., Leary, A., J., *J. Am. Soc, Mass Spectrom.*, **2006**, *17*, 524.
- [75] Simonsen, M.E., Søggaard, E.G, *Inter. J. of Mass Spectr.*, **2009**, *285*, 78.
- [76] Hart-Smith, G., Baner-Kowalik, Ch., *Polymer*, **2009**, *50*, 5175.
- [77] Vana, P., Davis, T.P., Barner-Kowalik, C., *Aust. J. Chem.*, **2002**, *55*, 315.
- [78] Szablan, Z., Lovestead, T.M., Davis, T.P., Stenzel, M.H., Barner-Kowalik, C., *Macromolecules*, **2007**, *40*, 26.
- [79] Barner-Kowalik, C., Vana, P., Davis, T.P., *J. Polym. Sci. Part A*, **2002**, *40*, 675.
- [80] Vana, P., Albertin, L., Barner, L., Davis, T.P., Barner-Kowalik, C., *J. Polym., Sci., Part A*, **2002**, *40*, 4032.
- [81] Nguyen, D.H., Vana, P., *Aust. J. Chem.*, **2006**, *59*, 549.
- [82] Stenzel, M.H., Cummins, L., Roberts, G.E., Davis, T.R., Vana, P, Barner-Kowalik, C., *Macromol. Chem. Phys.*, **2003**, *204*, 1160.
- [83] Kasperczyk, J., Li, S., Jaworska, J., Dobrzynski, P., Vert, M., *Polym. Degrad. Stabil.*, **2008**, *93*, 990.
- [84] Wu, L., Hong, T.Y., Vogot, F.G., *J. Pharm. Biomed. Anal.*, **2007**, *44*, 763.
- [85] Kamel, A.M., Zandi, K.S., Masefski, W.M., *J. Pharm., Biomed. Anal.*, **2003**, *31*, 1211.
- [86] Ding, L., Wang, X., Yang, Z., Chen, Y., *J. Pharm., Biomed. Anal*, **2008**, *46*, 282.

- [87] Kammerer, B., Kahlich, R., Ufer, M., Laufer, S., Gleiter, Ch.H., *Anal. Biochem.*, **2005**, 339, 297.
- [88] Barner-Kowalik, Ch., Davis, T.P., Stenzel, M.H., *Polymer*, **2004**, 45, 7791.
- [89] Koo, S.P.S., Junkers, T., Barner-Kowalik, Ch., *Macromolecules*, **2009**, 42, 62.
- [90] Sagratini, G., Caprioli, G., Cristalli, G., Giardiná, D., Ricciutelli, M., Volpini, R., Zuo, Y., Sauro, V., *J. Chromatogr. A*, **2008**, 1194, 213.
- [91] Kebarle, P., Verkerk, U.H., *Mass Spectr. Rev.*, **2009**, 28, 898.
- [92] Loeb, L., Kip, A.F., Hudson, G.C., Bennet, W.H., *Phys. Rev.*, **1941**, 60, 714.
- [93] Fernandez de la Mora, J., *J. Annu. Rev. Fluid Mech.*, **2007**, 39, 217.
- [94] Rayleigh, L., *Phil. Mag., Ser.*, **1882**, 5(14), 184.
- [95] Dole, M., Meck., L.L., Hines, R.L., Mobley, R.C., Ferguson, L.D., *J. Chem. Phys.*, **1968**, 49, 2240.
- [96] Iribarne J.V., Thomson, B.A., *J. Chem. Phys.*, **1976**, 64, 2287.
- [97] Thomson, B.A., Iribarne, J.V., *J. Chem. Phys.*, **1979**, 71, 4451.
- [98] Bottrill, A.R. *PhD Thesis*, University of Warwick, **2000**.
- [99] [www.qb3.berkeley.edu](http://www.qb3.berkeley.edu).
- [100] Watson, J.T., Sparkman, O.D., *Introduction to Mass Spectrometry*, 4th Edition, John Wiley & Sons, West Sussex, **2007**.
- [101] Mann, M., Meng, C., Fann, J., *Anal., Chem.*, **1989**, 61, 1702.
- [102] Williams, J.D., Weinr, B.E., Ormand, J.R., Brunner, J., Thornquest, A.D., Burinsky, D.J., *Rapid Commun Mass Spectrom.*, **2001**, 15 (24), 2446.
- [103] Percy, J.O., Lee, T.D., *J. Am. Soc., Mass Spectrom.*, **2001**, 12, 599.
- [104] Morvay, L., Cornides, J., *Int. J. Mass Spectrom and Ion Processes*, **1984**, 62, 263.
- [105] Bai, J., Liu, Z., Shi, L., Liu, S., *Int. J. Mass Spectrom.*, **2007**, 260, 75.
- [106] Zhang, D., Cooks, R.G., *Int. J. Mass Spectrom.*, **2000**, 667, 195.
- [107] Bunner, A.E., Trauger, S.A. Siuzdak, G., Willameson, J.R., *Anal. Chem.*, **2008**, 80, 9379.
- [108] Soler, C., Hamilton, B., Furey, A., James, K.J., Mañes, J., Picó, Y., *Anal. Chem., Acta*, **2006**, 571, 1.
- [109] Solar, C., Mañes, J., Picó, Y., *J. Chromatogr. A*, **2005**, 1067, 115.
- [110] Núñez, O., Moyano, E., Galceran, M.T., *Anal. Chem., Acta*, **2004**, 525, 183.

- [111] Benlchedda, K., Infante, H.G., Adams, F.C., *Trens in Anal. Chem.*, **2002**, 21, 5.
- [112] Bandura, D.R., Makarov, A.A., *Int. J. Mass Spectrom. and Ion Processes*, **1993**, 127, 45.
- [113] Hermández, F., Pozo, Ó.J., Sancho, J.V., López, F.J., Marin, J.M., Ibáñez, *Trends in Anal. Chem.*, **2005**, 24, 7.
- [114] Jakubowski, N., Mocns, L., Vanhacckc, F., *Spectrochim. Acta, Part B*, **1998**, 53, 1739.
- [115] Scrivens, J.H., Jackson. A.T., Yates, H.T. Green, M.R., Critcheley, G., Brown, J., Bateman, R.H., Bowers, M.T, Gidden, J., *J Mass Spectrom.*, **1997**, 165, 363.
- [116] Laine, O., Trimpin, S., Rader, H.J., Mullen, K., *Eur. J. Mass Spectrom.*, **2003**, 9, 195.
- [117] Jackson, A.T., Slade, S.E., Scrivens, J.H., *Inter. J. Mass Spectrom.*, **2004**, 238, 265.
- [118] Field, L.D., Sternhell, S., *Analytical NMR*, John, Wiley& Sons, New York, **1989**.
- [119] Friebolin, H., *Basic One- and Two-Dimensional NMR Spectroscopy*, Wiley-Vch, Heidelberg, **2008**.
- [120] Akitt, J.W., Mann, B.E., *NMR and Chemistry, An introduction to modern NMR spectroscopy*, 4 th Edition, Stanley Thornes, Cheltenham, **2000**.
- [121] Verkade, J.G., Quin, L.D., *Phosphorus-31 NMR spectroscopy in Stereochemical Analysis*, VCH Publishers Inc., Florida, **1987**.
- [122] Lipok, J., Owsiak, T., Młynarz, P., Forlani, G., Kafarski, P., *Enzyme and Microb Tech.*, **2007**, 41, 286.
- [123] Timbrell, J.A., *Principles of Bichemical Toxicology*, 2 nd Edition, Taylor & Francis, London, **1991**.
- [124] Zieliński W., Rajcy, A. *Metody Spectroskopowe i ich zastosowanie do identyfikacji związków organicznych*, WNT, Warszawa, **2000**.
- [125] Kolczak, U., Rist, G., Dietliker, K., Wirz,J., *J. Am. Chem. Soc.*, **1996**, 118, 6477.
- [126] Seguroła, J., Allen, N.S., Edge, M., McMahon, A., Wilson, S., **1999**, 64, 39.

- [127] Desobry, V., Dietliker, K., Misev, L., Rembold, M., Rist, G., Rutsch, W., *Radiation curing of polymeric materials*, American Chemical Society, Washington, **1990**.
- [128] Versace, D.L., Oubaha, M., Copperwhite, R., Croutxe-Barghorn, C., MacCraith, B.D., *Thin Solid Films*, **2008**, *516*, 6448.
- [129] Zandler, M.E., Smith, P.M., Fujitsuka, M., Ito, O., D'Souza, F., *J. Org. Chem.*, **2002**, *67*, 9122.
- [130] da Silva, C.H.T.P., Del Ponte, G., Neto, A.F., Taft, C.A., *Bioorganic Chemistry*, **2005**, *33*, 274.
- [131] Bjørsvik, H.R., Gambarotti, C., Jensen, V.R., González, R., *J. Org. Chem.*, **2005**, *70*, 3218.
- [132] Vila, A., Mosquera, R.A., *Chem. Phys. Lett.*, **2003**, *371*, 540.
- [133] Kemikawa, K., Tachibana, A., Shimizu, Y., Uchida, K., Furusyo, M., Uemura, M., *Tetrahedron*, **2006**, *62*, 922.
- [134] Plazuk, D., Warkentin, J., Werstiuk, N.H., *Tetrahedron*, **2005**, *61*, 5788.
- [135] Radziwicz, P., Doltsinis, L.N., *J. Phys. Chem. A*, **2009**, *113*, 6266.
- [136] Allonas, X., Lalevée, J., Fouassier, J-P., *J. Photoch. Photobio. A.*, **2003**, *159*, 127.
- [137] Zhao, A., Li, Z., Wang, H., *Polymer*, **2010**, *51*, 2099.
- [138] Silva, V.L., Carvalho, R., Freitas, M.P., Tormena, C.F., Melo, W. C., *Spectrochim. Acta*, **2007**, *68*, 1197.



*Chapter Two*

*Characterisation of Acylphosphine oxide Photoinitiator  
using HPLC and CE Methods*

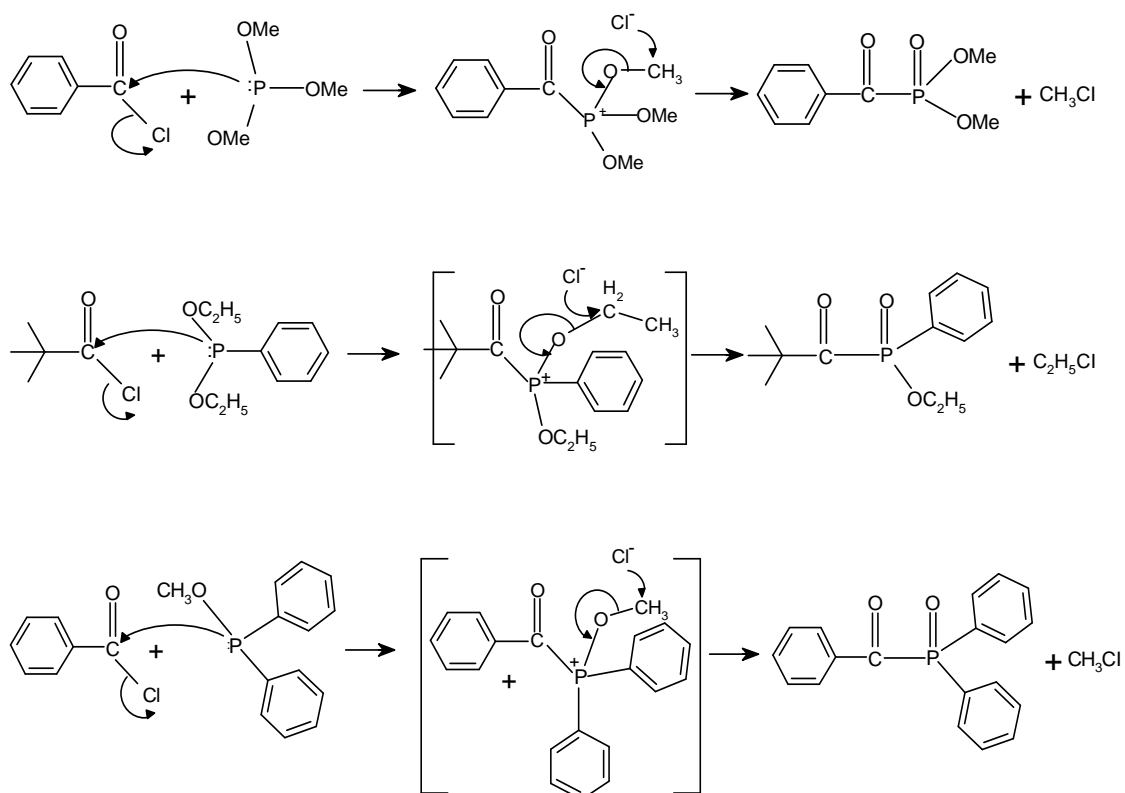
## 2.1 INTRODUCTION

This work describes the development of high performance liquid chromatography (HPLC) and capillary electrophoresis (CE) as alternative methods for the analysis of bis(2,4,6-trimethylbenzoyl)phenylphosphine oxide (BAPO) stability.

### 2.1.1 Properties and production of Acylphosphine oxide (APO)

Acylphosphine oxides are a class of  $\alpha$ -cleavage photoinitiators which are widely studied for their industrial applications. APO derivatives are prepared quite easily by the Michealis-Arbuzov reaction.<sup>[1]</sup> A schematic illustration of the synthesis mechanism is shown in Figure 2.1.



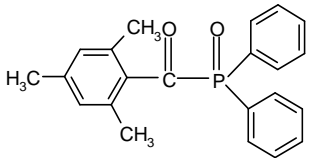
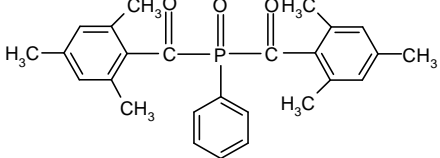
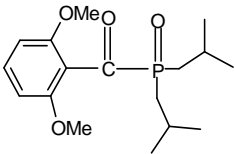
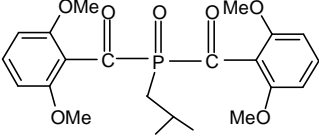
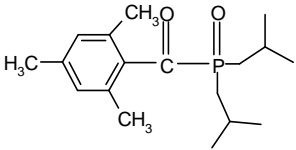
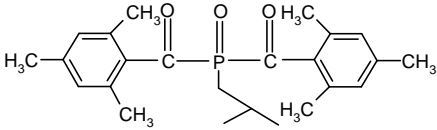
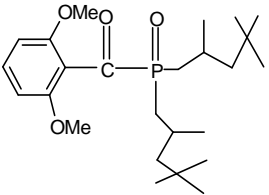
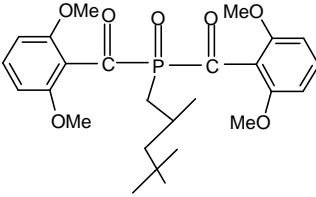


**Figure 2.1:** Schematic illustration of the synthesis of acylphosphine oxide derivatives by the Michealis- Arbuzov reaction. <sup>[1]</sup>

Acylphosphine oxides possess a low volatility and high solubility in the acrylate monomer, in particular the monoacylphosphine oxide (MAPO). The range of their applications is wide <sup>[1, 2]</sup> but they are most suitable for the fabrication of white lacquers used as furniture coatings <sup>[3]</sup>.

Another interesting type of  $\alpha$ -cleavage photoinitiator is the bisacylphosphine oxide (BAPO) group that has been shown to be particularly effective in the photopolymerisation of pigmented coatings and composite materials <sup>[4, 5]</sup>. BAPO contains two acyl substituents attached to the phosphine oxide unit. The structures of some acylphosphine oxides are shown in Table 2.1. <sup>[5]</sup>

**Table 2.1:** Structures of acylphosphine oxide.

Monoacylphosphine oxide photoinitiator	Bisacylphosphine oxide photoinitiator
 <p data-bbox="384 562 740 622">(2,4,6-trimethylbenzoyl)diphenylphosphine oxide</p>	 <p data-bbox="975 551 1289 611">bis(2,4,6-trimethylbenzoyl)-phenylphosphine oxide</p>
 <p data-bbox="384 880 778 940">bis(2-methylpropyl)(2,6-dimethoxybenzoyl)phosphine oxide</p>	 <p data-bbox="975 846 1315 936">bis(2,6-dimethoxybenzoyl)-(2-methylpropyl)phosphine oxide</p>
 <p data-bbox="384 1223 783 1283">bis(2-methylpropyl)(2,4,6-trimethylbenzoyl)phosphine oxide</p>	 <p data-bbox="959 1182 1299 1272">bis(2,4,6-trimethylbenzoyl)-(2-methylpropyl)phosphine oxide</p>
 <p data-bbox="403 1588 810 1648">bis(2,4,4-trimethylpentyl)(2,6-dimethoxybenzoyl)phosphine oxide</p>	 <p data-bbox="975 1588 1286 1677">bis(2,6-dimethoxybenzoyl)-(2,4,4-trimethylpentyl)-phosphine oxide</p>

Both photoinitiators (MAPO and BAPO) undergo fast photolysis leading to the formation of free radicals: benzoyl, phosphinoyl and phosphinoyl diradical <sup>[6]</sup>. (see Figure 2.2). These radicals show very good reactivity <sup>[7]</sup> and the capability to initiate the polymerisation of such monomers as styrene and acrylates <sup>[4]</sup>.

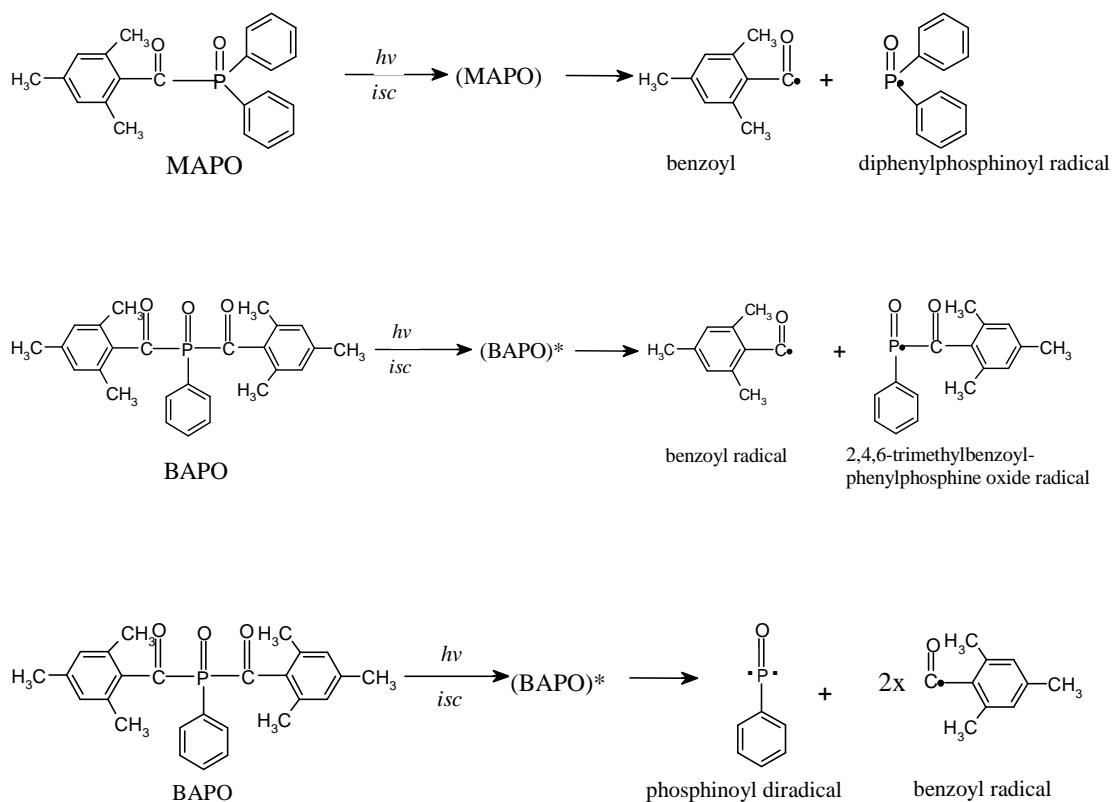


**Figure 2.2:**  $\alpha$ -cleavage of MAPO and BAPO. <sup>[6]</sup>

Although the number of reactive species formed from these two photoinitiators is different, their photochemistry is very similar. However, BAPO photoinitiators are superior to MAPO and are extremely effective as they can generate four radicals from the  $\alpha$ -cleavage of the triplet excited state <sup>[8, 9]</sup>. The investigation of the photochemistry of BAPO and MAPO is discussed in detail in section 2.1.2

### 2.1.2 Photochemistry of Acylphosphine oxide

The photochemistry of acylphosphine oxide has been investigated using a wide range of analytical techniques such as UV-Vis spectroscopy <sup>[10-13]</sup>, gas chromatography-mass spectrometry <sup>[12]</sup> and time – resolved spectroscopy <sup>[14, 15]</sup> which are discussed in this section as well as chemically induced dynamic nuclear polarisation (CIDNP) <sup>[5]</sup> <sup>31</sup>P-NMR which was discussed in section 1.5.1.

Photochemistry is a process that can promote the crosslink between specific bonds. Furthermore, light-induced polymerisation is the basis of important advanced technologies, since it is among the most efficient methods capable of achieving fast and extensive curing of multifunctional oligomers. High reactivity systems are cured within a fraction of time upon exposure to UV radiation.

Jacobi and Henne first reported on development of photoinitiators, such as acylphosphine oxide, and demonstrated their effectiveness in the curing of some coatings, <sup>[16]</sup> such as white lacquers. Results of this work have shown that the absorption of APO compounds extends well into the range of wavelengths above 380 nm, in which the pigment does not absorb all of the light.

Baxter et al. also investigated the efficiency of acylphosphine oxide with respect to alternative photoinitiators-acylphosphonates. Results of this work have shown that acylphosphine oxides are more efficient photoinitiators than acylphosphonates for the curing of acrylates. This curing efficiency was shown to be further increased by the addition of amines. The performance of these initiators was compared with two common photoinitiators: 2,2-dimethoxy-2- phenylacetophenone and benzoin methylether. <sup>[13]</sup>

The role of the amine on acylphosphine oxide photoinitiator was investigated by high performance liquid chromatography (HPLC) and GC-MS. <sup>[12]</sup> From these investigations it was concluded that the curing efficiency is significantly decreased in the absence of amines. The experimental evidence showed that the role of the amine in the UV-curable formulation is predominantly that of an oxygen scavenger. Also, the presence of the amine may reduce the shelf life of the pigmented resin.

Time resolved spectroscopy is another method which provides information on the photochemistry of acylphosphine oxide. Time resolved spectroscopy provides information on the excited state of materials. The technique, which follows the time expansion of radicals is electron spin resonance (ESR).

ESR is a similar technique to NMR, the fundamental difference being that ESR describes the magnetically induced splitting of electronic spin while NMR involves transition between the spin states of nuclei. Nuclei possess mechanical spins which, in conjunction with the charge of the nuclei, produce magnetic fields whose axes are directed along the spin axes of the nuclei. The possible spin states of the nucleus are indicated as  $-I$ ,  $(-I+1)$ , ...  $+I$ ; where  $I$  is the spin quantum number of the nucleus. For example, with spin  $I= 1/2$ , spin states of  $-1/2$  and  $+1/2$  are possible, and with  $I= 1$ , spin state of  $-1$ ,  $0$  and  $+1$  are possible. Spin transitions occur only between adjacent spin states. Nuclei having  $I= 0$  have only one spin state and cannot undergo spin excitation. <sup>[17]</sup>

ESR has been used as an investigative tool for the study of radicals formed in solid materials, since the radicals typically produce an unpaired spin on the molecule from which an electron is removed. Particularly fruitful has been the study of the ESR spectra of radicals produced by radiation damage from ionisation radiation. <sup>[18]</sup>

Time resolved spectroscopy provides concise information on the radicals. It was determined that the reactivity of the different phosphorus radicals was correlated with the degree of radical localisation and s- character on the phosphorus atom. It was shown that typical radical reactions correlate well with the  $^{31}\text{P}$  hyperfine coupling. <sup>[19]</sup> TR-ESR has also been employed in conjunction with time-resolved infra-red (TRIR) and UV spectroscopy to determine further the photochemistry of acylphosphine oxide and also the reactivity of the radicals produced <sup>[15]</sup>.

## **2.2 SCOPE OF RESEARCH**

In this chapter, the characterisation of BAPO photoinitiator, bis(2,4,6-trimethylbenzoyl)phenylphosphine oxide, was carried out using HPLC and CE. The solubility of the BAPO was investigated using different organic solvents, such as tetrahydrofuran (THF), chloroform, methanol and acetonitrile. A time stability study was performed with various analytes added such as stabilising agent, Lewis and protonic acids, using HPLC-UV, and comparison of its stability was determined in samples which were maintained in dark and ambient light conditions.

## 2.3 MATERIALS AND METHODS

### 2.3.1 HPLC-UV method

#### 2.3.1.1 Instrumentation

The Agilent HPLC system used throughout this work consisted of an 1100 pump, a 1200 detector module and a 1050 autosampler. The HPLC system was equipped with an Ascentis™ C<sub>18</sub> (Supelco, Bellefonte, PA USA) column (250 mm x 4.6 mm, I.D., 5 µm).

#### 2.3.1.2 Chromatographic separation conditions

The mobile phase for HPLC-UV was a mixture of acetonitrile- water [90/10, v/v] and was filtered (47 mm Nylon 66 membranes with 0.45 µm pore size) under vacuum and sonicated for 20 to 30 min to remove dissolved gases.

The applied flow rate was 1 mL min<sup>-1</sup> and, depending on the measurement, 10 µL of biphenyl standard or BAPO sample solution was injected onto the column. All sample analyses were carried out using UV detection at 270 nm with a deuterium lamp.

## 2.3.2 CE method

### 2.3.2.1 Instrumentation

CE separations were performed using Agilent (Agilent Technologies Ireland) and Beckman P/ACE MDQ (Fullerton, CA) CE systems.

*For Agilent CE:* the PDA detector range was 200-280 nm. The CE instrument was operated using Agilent ChemStation software.

*For the Beckman CE:* the instrument was equipped with a UV absorbance detector. All sample analyses were carried out using direct UV detection at 280 nm with a deuterium lamp. Data analysis was performed using Beckman (version 3.4) software. The fused- silica capillaries (Composite Metal Services, the Chase, Hallow, Worcs. WR2 6LD) were 64 cm long (56 cm to the detector) with 50  $\mu\text{m}$  id unless otherwise stated.

### 2.3.2.2 Electrophoretic separation conditions

Hydrodynamic sample injection was performed at 50 mbr for 5 s. A constant voltage of 20 kV was employed and the capillary temperature was maintained at 25°C. All experiments were carried out by applying positive mode.

### 2.3.2.3 Preparation of CE background electrolyte (BGE)

Electrolytes were prepared using deionised water. The BGE solution was prepared which consisted of a boric acid solution. A stock solution of 500 mM boric acid was prepared, from which 250 mM and 50 mM borate solutions were obtained by dilution of stock solution with deionised water. The pH of the electrolytes was



adjusted to 9.0 using 1M NaOH solution. All electrolyte solution was filtered with a 0.45  $\mu\text{m}$  swinny filter (Gelman Nylon Acrodisc) prior to use.

#### **2.3.2.4 Preconditioning of the CE separation capillary**

The capillary was rinsed each day with ACN or MeOH for 10 min, H<sub>2</sub>O for 5 min, HCl for 10 min, H<sub>2</sub>O for 5 min, 0.1 M NaOH for 10 min, H<sub>2</sub>O for 5 min and 20 min buffer. Between each analysis, the capillary was rinsed with ACN or MeOH, 0.1 NaOH and buffer for 1, 1 and 2 min respectively. When the capillary or buffer was changed, the capillary was conditioned with a 5 min. rinse with MeOH or ACN, 10 min. rinse with H<sub>2</sub>O and 5 min rinse with buffer.

#### **2.3.3 Preparation of standard solution**

A 0.5 g sample of BAPO was dissolved in 100 mL acetonitrile (0.01% of water) and 0.005 g of biphenyl (internal standard) was added. One set of samples was prepared in amber volumetric flasks and stored in a dark room, while the other set was prepared in clear volumetric flasks and was exposed to the ambient light at room temperature. The samples were injected directly into the HPLC. The stability of the samples was determined over one year.

#### **2.3.4 Chemicals**

MeOH, ACN, (LC-MS Chromasolv) Na<sub>2</sub>HPO<sub>4</sub>, NaH<sub>2</sub>PO<sub>4</sub>, NaOH, HCL, biphenyl and SDS were purchased from Sigma - Aldrich (Dublin, Ireland). Water free (0.01%)/ predried acetonitrile was obtained from Biotech Quality, Sigma-Aldrich Chemie GmbH (Germany). Boric acid was from Riedel-de Haën, (Seelze, Germany).

Chloroform, toluene, THF, ethyl acetate, acetone, was purchased from Labscan Ltd. (Dublin, Ireland). Bis(2,4,6-trimethylbenzoyl)phenylphosphine oxide (Irgacure 819 or BAPO) photoinitiator, ferrocene, methyl sulphonic acid (MSA), boran trifluoride dihydrate ( $\text{BF}_3 \cdot 2\text{H}_2\text{O}$ ), cumene hydroperoxide (CHP) and hydroquinone (HQ) samples were all obtained from Henkel Technologies Ltd (Dublin, Ireland). Deionised water was treated with a Hydro Nanopure system to specific resistance  $> 18 \text{ M}\Omega \text{ cm}$  (Millipore, Bedford, MA, USA).

### 2.3.5 Experimental design

#### 2.3.5.1 Characterisation of BAPO

The typical physical properties of BAPO were reported in the Ciba company products guide, as shown in Table 2.2.

**Table 2.2:** *The physical properties of BAPO.*<sup>[20]</sup>

Typical physical properties photoinitiator	Chemical class	Chemical identity	Appearance	Melting point (MP, °C)	Specific gravity (water=1)	UV/VIS absorption peaks (nm) in ACN
IRGACURE 819	Bis Acyl Phosphine (BAPO)	Bis (2,4,6-trimethylbenzoyl) phenylphosphine oxide	light yellow powder	MP 127-133° C	1.2	280, 370

For research purposes the solubility of BAPO with several solvents of different polarities was established. Results are illustrated in Table 2.3.

**Table 2.3:** Solubility of BAPO (0,5%) in the different solvents.

Solvent	Polarity	Solubility of BAPO
toluene	2.3	Fully dissolved
chloroform	3.4	Fully dissolved
THF	4.2	Fully dissolved
ethyl acetate	4.3	Fully dissolved
acetone	5.4	Fully dissolved
acetonitrile	6.2	Fully dissolved
methanol	6.6	Fully dissolved
water	9.0	Not dissolved

Table 2.4 shows all the compositions of BAPO samples with addition of acids, stabiliser and curing additives for samples kept in dark and exposed to the ambient light analysed using HPLC method.

**Table 2.4:** Compositions of samples for ambient light and dark conditions.

Compositions of samples
BAPO
BAPO/ MSA
BAPO/ $\text{BF}_3 \cdot 2\text{H}_2\text{O}$
BAPO/ Ferrocene
BAPO/ Ferrocene/ MSA
BAPO/ Ferrocene/ $\text{BF}_3 \cdot 2\text{H}_2\text{O}$
BAPO/ Ferrocene/ HQ
BAPO/ Ferrocene/ CHP
BAPO/ $\text{H}_2\text{O}$

## 2.4 RESULTS AND DISCUSSION

### 2.4.2 HPLC method

#### 2.4.2.1 Development and optimisation of HPLC method

Reversed- phase stationary phases are the most popular in chromatography for the analysis of food, pharmaceutical and environmental samples <sup>[21, 22]</sup>. Reversed-phase chromatography, for the analysis of BAPO, was chosen due to two main factors: solubility and molecular weight. A schematic of a guide to developing a HPLC method is shown in Figure 2.3.

The bis(2,4,6-trimethylbenzoyl)phenylphosphine oxide has a molecular weight of less than 2000 and is also soluble only in organic solvents. Therefore, following the scheme highlighted in red in Figure 2.3, the mode of HPLC employed for this research was reversed-phase chromatography. Acetonitrile was selected as an appropriate organic solvent because of its ability to dissolve the photoinitiators (it also resembled the monomer used in the adhesive formulations insofar that it contained a nitrile function) its compatibility with electrospray ionisation MS and its miscibility with water. It was also possible to source anhydrous ACN for the experiments involving the addition of water.

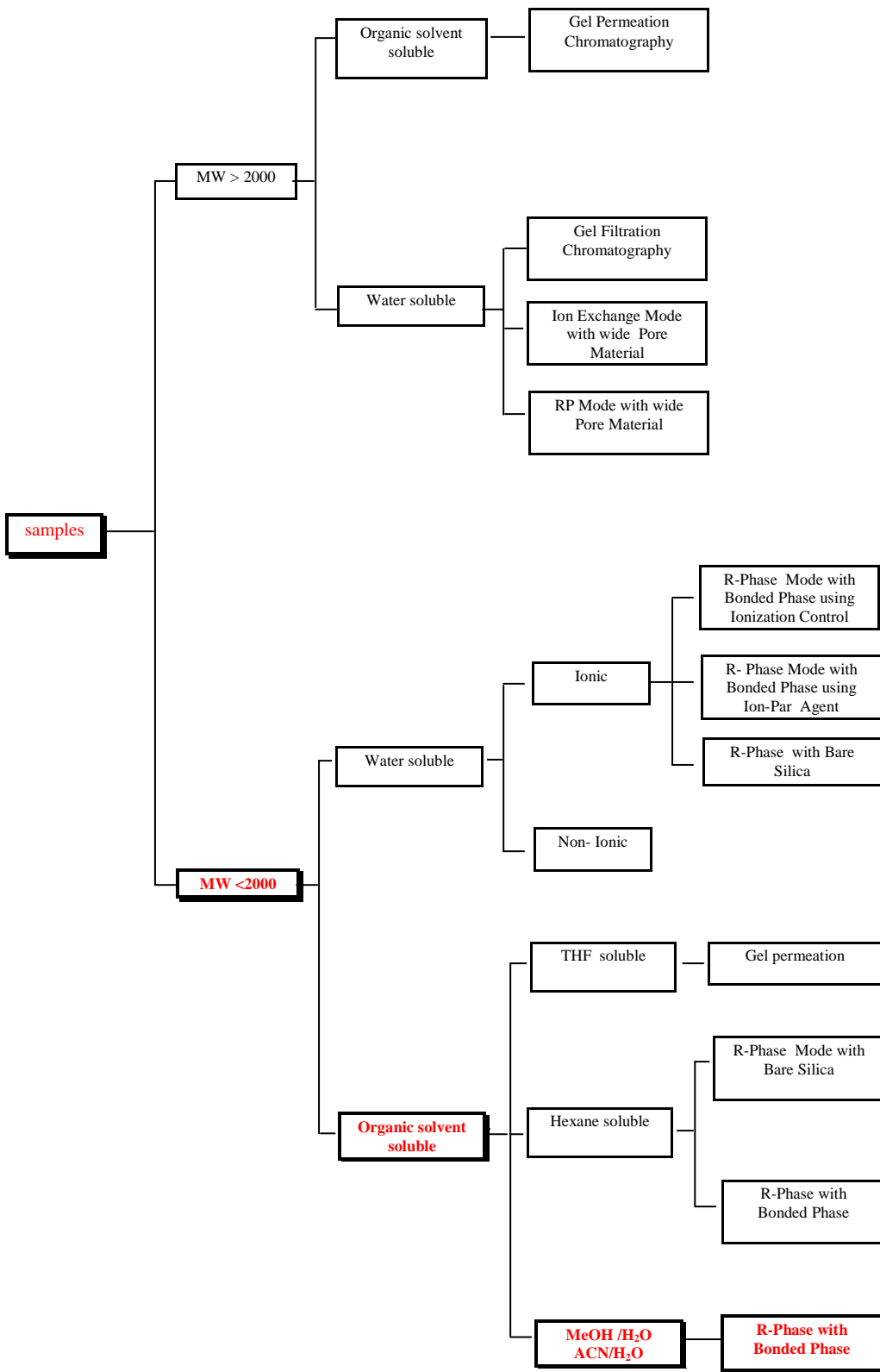
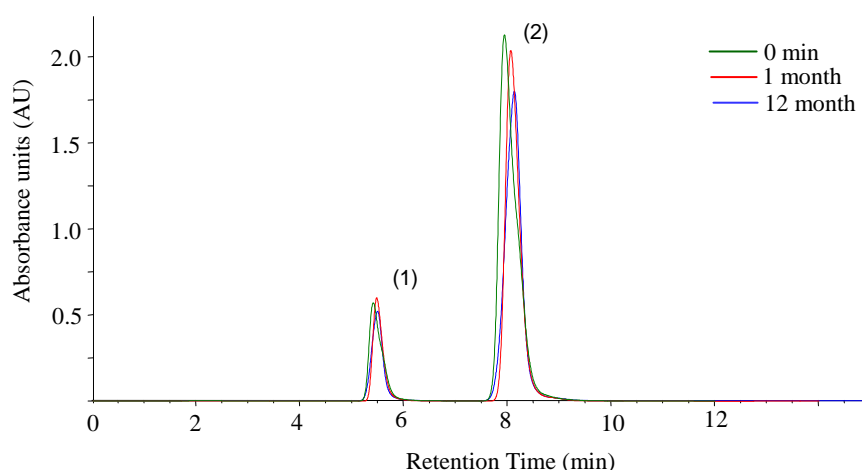


Figure 2.3: Schematic of a guide to selecting a HPLC method. [23]

Initially, the separation of BAPO was performed using an isocratic method and a mobile phase composed of acetonitrile-water [85/15, v/v]. The internal standard, biphenyl, was more polar than the BAPO and was therefore expected to elute first. With the 85% ACN mobile phase, the BAPO was retained on the column for approximately 11 min and its peak shape was asymmetrical, with fronting of the peak evident. This indicated that the BAPO required a higher proportion of organic modifier in the mobile phase. Also at 14 min the overall run time was excessively long. It was found that increasing the ACN content by 5 % improved the peak shape of BAPO and also reduced the retention time from 14 min to 10 min. The resolution (R) between the two analytes was also very good, determined to be 1.74<sup>[24, 25]</sup>. The final mobile phase composition was a mixture of acetonitrile-water [90/10, v/v]. The flow rate through the analytical column was 1 mL min<sup>-1</sup>. UV detection was at 270 nm<sup>[20]</sup> although a number of other wavelengths were investigated i.e. 220, 250 nm.

#### ***2.4.2.2 Analysis of BAPO in ambient light and dark conditions***

The stability of BAPO in anhydrous acetonitrile was investigated over 12 months and a comparison was made between samples stored under dark and light conditions. Figure 2.4 illustrates the separation of biphenyl (internal standard) and BAPO after t= 0, one month and one year in the dark. Analysis of the results showed that after 12 months the peak area of BAPO stored in the dark was reduced by only 1.2% when compared to the results obtained after t= 0, in effect, the compound was found not to degrade under dark conditions.



**Figure 2.4:** HPLC separation of (1) biphenyl ( $500 \mu\text{g mL}^{-1}$ ) and (2) BAPO (0.5%). Experimental conditions: mobile phase 90/10 acetonitrile and water; flow rate  $1 \text{ mL min}^{-1}$ , UV detection at 270 nm, pressure 52-55 bar. Samples maintained in the dark over 12 months.

On the other hand, for the samples exposed to light, significant degradation of BAPO occurred. Degradation started after only 48 h, and the sample was completely broken down after only one month. The colour of the solution also changed completely from yellow to colourless. This breakdown was confirmed by the appearance of a new peak on the HPLC chromatogram at 4.5 min, as illustrated in Figure 2.5, and corresponded to a degradation product of the BAPO. It was therefore determined that the BAPO was photosensitive, upon exposure to ambient light.

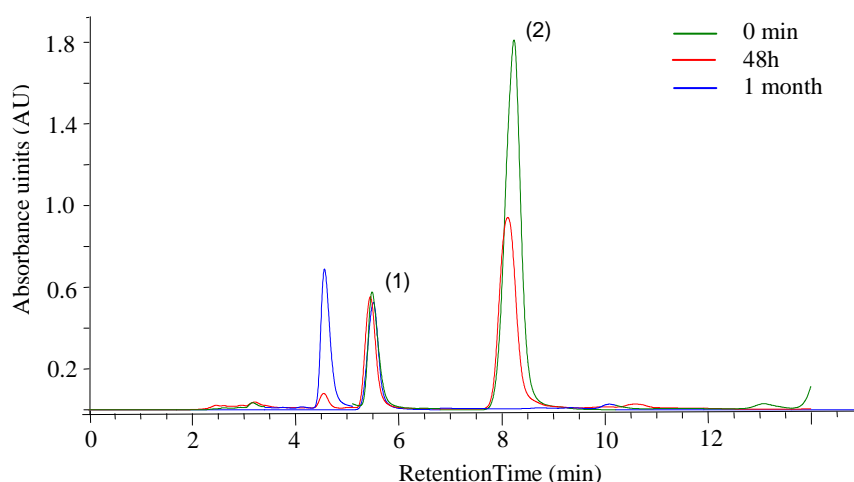


**Figure 2.5:** HPLC separation of (1) biphenyl ( $500 \mu\text{g mL}^{-1}$ ) and (2) BAPO (0.5%). Experimental conditions: mobile phase 90/10 acetonitrile and water; flow rate  $1 \text{ mL min}^{-1}$ , UV detection at 270 nm, pressure 52-55 bar. Samples exposed to the ambient light.

#### 2.4.2.3 Comparison of strong and weak acids

In this part of the experimental work, the stability of the BAPO in presence of protonic acid, methyl sulphonic acid (MSA) and a Lewis acid, boron trifluoride dihydrate ( $\text{BF}_3 \cdot 2\text{H}_2\text{O}$ ) were investigated.

Acids were of particular interest because the cyanoacrylate esters used in the adhesive technology are very labile towards anionic initiation. The presence of acids, either protonic or Lewis, stabilises them against premature gellation.

Different concentrations of both acids (30-50  $\mu\text{g/g}$ ) were mixed with BAPO under both light and dark conditions for one week.

The lowest degradation of BAPO was observed for concentration MSA 40  $\mu\text{g/g}$ , as shown Table 2.4. For this reason concentration of MSA was used in subsequent separation studies.



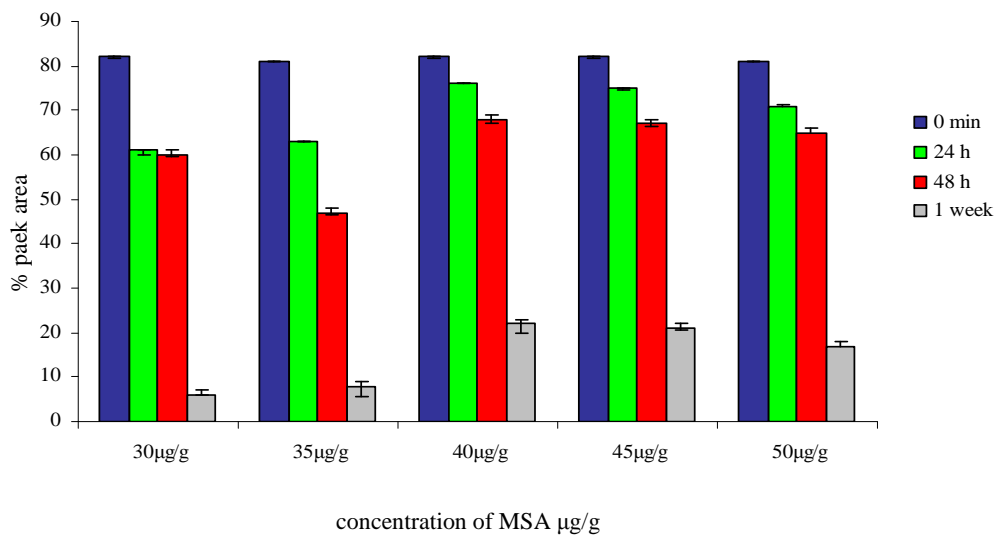
**Table 2.4:** Presentation of peak area for MSA samples exposed to ambient light and kept in dark from  $t=0$ , 24h, 48h and 1 week. Shows also average values of 3 repeat HPLC injections,  $\sigma$  and % RSD for the results.

	Light exposure			Dark exposure		
	average peak area $n=3$	std dev	%RSD $n=3$	average peak area $n=3$	std dev	%RSD $n=3$
<b>30 <math>\mu\text{g/g}</math></b>						
0 hr	82,46	0,152753	0,18	81,90	0	0
24 hr	61,06	0,152753	0,25	80,53	0,57735	0,07
48 hr	60,73	1,011599	1,66	80,76	0,57735	0,71
1 week	5,73	0,981495	17,11	78,70	0,866025	1,10
<b>35 <math>\mu\text{g/g}</math></b>						
0 hr	81,43	0,057735	0,07	82,46	0,057735	0,07
24 hr	63,96	0,321455	0,67	80,50	0,1	0,12
48 hr	47,53	0,416333	0,65	80,63	0,057735	0,07
1 week	8,36	0,11547	1,38	75,26	0,750555	0,99
<b>40 <math>\mu\text{g/g}</math></b>						
0 hr	82,10	0	0	81,70	0	0
24 hr	76,63	0,11547	0,15	80,86	0,57735	0,07
48 hr	68,30	0,43589	0,63	80,30	0,264575	0,32
1 week	21,66	2,369247	10,93	76,83	1,24231	1,61
<b>45 <math>\mu\text{g/g}</math></b>						
0 hr	82,70	0	0	82,53	0,23094	0,28
24 hr	75,20	0	0	81,43	0,057735	0,07
48 hr	67,00	0,781025	1,16	77,76	0,83865	1,08
1 week	23,43	2,362908	10,08	72,23	0,503322	0,70
<b>50 <math>\mu\text{g/g}</math></b>						
0 hr	81,50	0,173205	0,21	82,90	0	0
24 hr	71,83	0,321455	0,44	81,30	0	0
48 hr	64,83	0,665833	1,02	78,66	0,750555	0,95
1 week	17,20	0,52915	3,07	72,33	0,450925	0,62

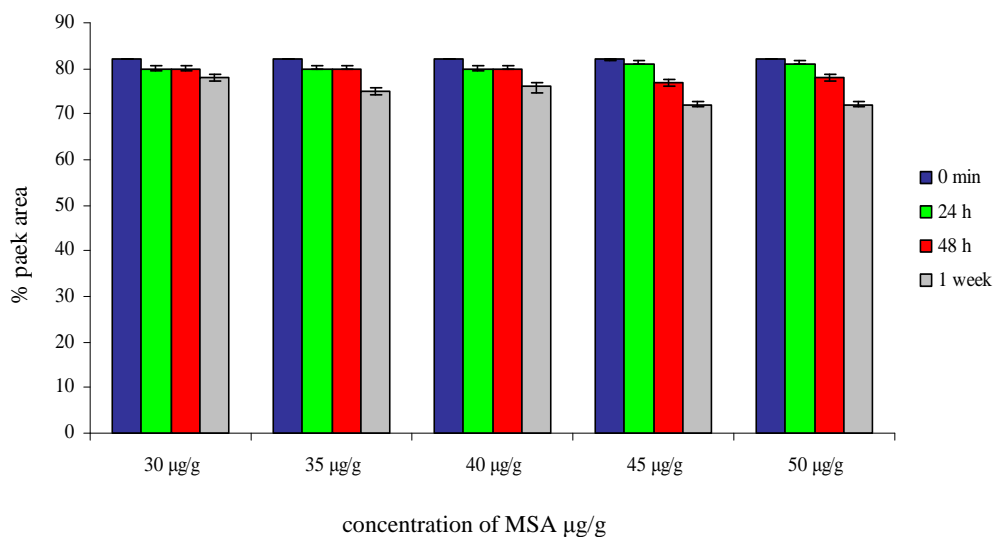
The results illustrated in Table 2.4 show the excellent performance of the HPLC method used. Evaluation of the method was by precision analysis shown here as % RSD values of repeat injections ( $n=3$ ). Typically values of precision were  $< 1\%$ ; however, in some cases where samples were exposed for 1 week % RSD values were as high as 17%. The latter is only the case for samples exposed to the ambient light for 1 week.

Figure 2.6 illustrates the significant decrease in the BAPO peak area over the time frame when the sample was also exposed to ambient light for all concentrations of MSA. A much smaller decrease in peak area was observed when the sample was maintained in the dark (Figure 2.7). Because further degradation of all samples was

observed up to one week, the study of this sample is continuing over a 12-month period.



**Figure 2.6:** Graphic presentation of the effect of addition of different concentrations of MSA on BAPO peak area degradation for samples exposed to ambient light ( $n=3$ ).



**Figure 2.7:** Graphic presentation of the effect of addition of different concentrations of MSA on BAPO peak area degradation for samples stored in the dark ( $n=3$ ).

The study was reported with boron trifluoride dihydrate ( $\text{BF}_3 \cdot 2\text{H}_2\text{O}$ ). The lowest degradation of BAPO was observed for a concentration of  $\text{BF}_3 \cdot 2\text{H}_2\text{O}$  of 30  $\mu\text{g/g}$ . Figure 2.8 illustrates the significant decrease in BAPO peak area over the time frame when the samples were exposed to ambient light for all concentrations, 30 to 50  $\mu\text{g/g}$  of weak acid.

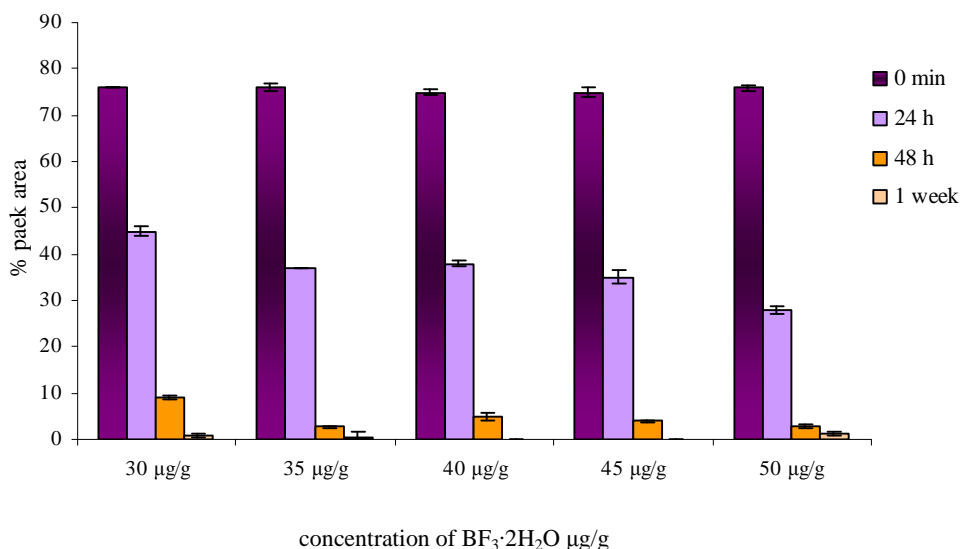


**Figure 2.8:** Graphic presentation of the effect of addition of different concentrations of  $\text{BF}_3 \cdot 2\text{H}_2\text{O}$  on BAPO peak area degradation for samples exposed to ambient light ( $n=3$ ).

A much smaller decrease in peak area was observed for samples maintained in the dark, (Figure 2.9). The average decrease in the peak area of BAPO with  $\text{BF}_3 \cdot 2\text{H}_2\text{O}$  (30  $\mu\text{g/g}$ ) after 1 week was 54% when compared to the same samples at  $t=0$ .

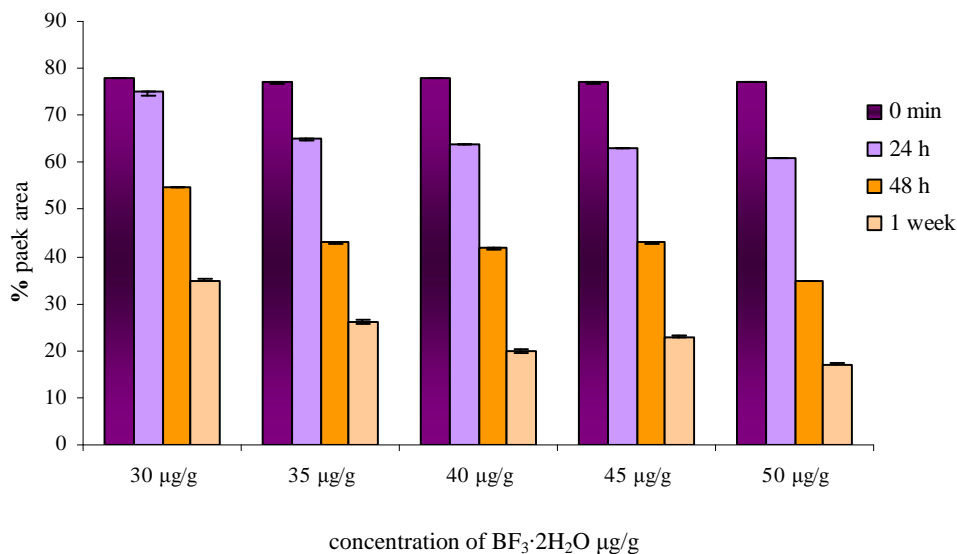


**Figure 2.9:** Graphic presentation of the effect of addition of different concentrations of  $\text{BF}_3 \cdot 2\text{H}_2\text{O}$  on BAPO peak area degradation for samples stored in the dark ( $n=3$ ).

For this part of the stability study of BAPO it was found that the lowest degree of degradation of BAPO was observed at a concentration of 40  $\mu\text{g/g}$  MSA and 30  $\mu\text{g/g}$  of Lewis acid. For the reason stated (for future separation studies) this concentration of MSA and  $\text{BF}_3 \cdot 2\text{H}_2\text{O}$  was selected for implementation.

Generally, for the samples containing protonic and Lewis acid stored in dark, the rate of degradation was slower than for samples exposed to ambient light, as shown in Figure 2.10.

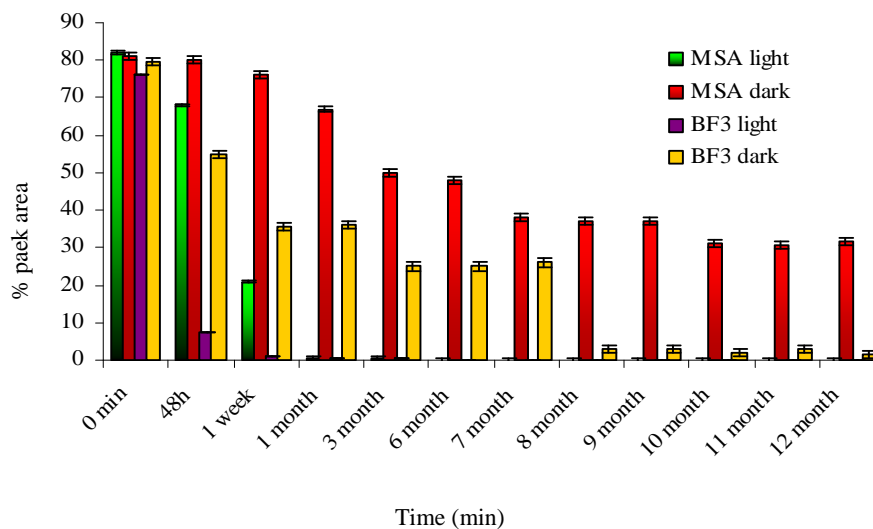


**Figure 2.10:** Graphic presentation a stability comparison of BAPO-MSA and BAPO- $\text{BF}_3 \cdot 2\text{H}_2\text{O}$  for samples kept in the ambient light and the dark ( $n=3$ ).

MSA was found as significantly slowing down rate of degradation of BAPO samples stored in the dark but only for the first month. After this time the presence of MSA in the BAPO samples stored in the dark caused an increase in the rate of degradation. It was determined that over 12 months the peak area of BAPO/MSA was reduced by 62% when compared to the results after  $t=0$  for the same samples. It also decreased by 64% when compared to the stability of neat BAPO after the same time period. MSA was not found to have an inhibiting effect on the degradation of BAPO when samples were exposed to the light over one week. The data shows the significant decrease of the BAPO peak area over the one week period for all concentrations of MSA.

Figure 2.10 also illustrates the effect of  $\text{BF}_3 \cdot 2\text{H}_2\text{O}$  on the degradation of BAPO. It was found that a much larger decrease in the peak area was observed for BAPO with Lewis acid maintained in the dark than for BAPO-MSA. After 10 months it decreased to 96% of the value obtained after  $t=0$ , which means that in the presence of weak acid BAPO had almost completely degraded after 10 months.

Another observation made when analysing the results was that after eight months the stability of BAPO/MSA and BAPO/ $\text{BF}_3 \cdot 2\text{H}_2\text{O}$  stored in the dark did not significantly change with regard to the % peak area.

This suggests that after 8 months BAPO in the presence of protonic or Lewis acid does not degrade anymore and thus was not further investigated.

For this part of the stability study of BAPO it was found that even though different acids were used (MSA is a protonic acid, which generally exists as a salt and as a result is very acidic, while  $\text{BF}_3 \cdot 2\text{H}_2\text{O}$  is a Lewis acid), after 12 months the results were almost the same. The above results show that the both acids significantly affecting the stability of BAPO increasing the rate of degradation of the photoinitiator. However the Lewis acid is the more reactive compared with the protonic acid.

#### 2.4.2.4 Addition of stabiliser and curing additives

Ferrocene, which acts as a stabiliser, protects BAPO from undergoing further hydrolysis, (ferrocene is also added to increase the rate of photopolymerisation of cyanoacrylate ester and is discussed in Chapter 5). The effect of ferrocene itself on the stability of BAPO was determined and it was found that for the samples stored in the dark, degradation after 12 months was comparable with that of neat BAPO. Also for samples exposed to the ambient light, the addition of ferrocene in the BAPO samples reduced the degradation of BAPO. Thus, as shown in Figure 2.11, degradation of BAPO was not complete by one month, (degraded completely after 3 months) as had previously been observed. A very small peak was observed at 7.7 min; therefore, the presence of ferrocene resulted in a decrease in the rate of degradation of BAPO.



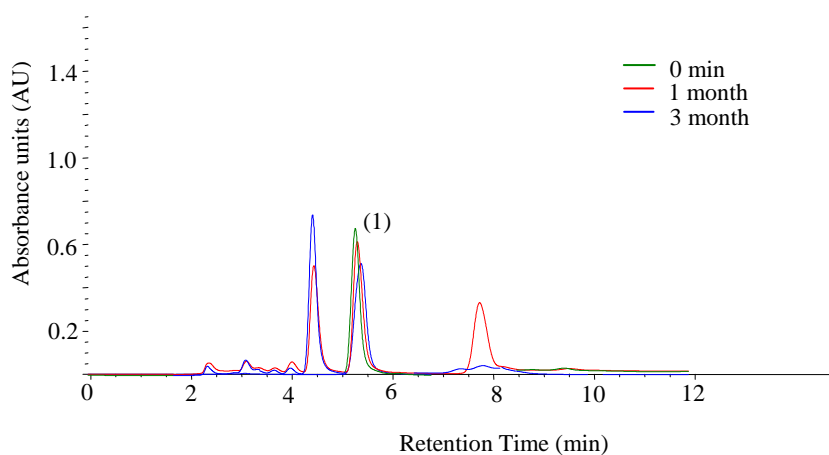


**Figure 2.11:** HPLC separation of (1) biphenyl ( $500\mu\text{g ml}^{-1}$ ) and (2) BAPO (0.5%) with UV detection at 270 nm for samples exposed to the ambient light with ferrocene.

When the Ferrocene/ $\text{BF}_3 \cdot 2\text{H}_2\text{O}$  was added to the samples exposed to ambient light, the rate of degradation was affected in a different way. All the samples of BAPO degraded completely after 6 months and further analysis was not carried out after that point.

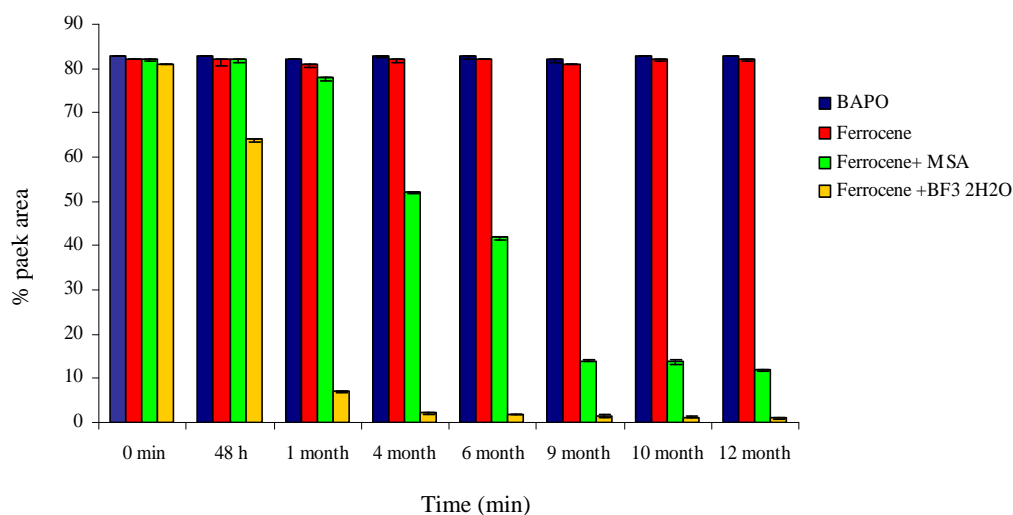


**Figure 2.12:** Graphical illustration of peak area degradation for BAPO, BAPO with ferrocene, ferrocene/MSA and ferrocene/BF<sub>3</sub>·2H<sub>2</sub>O. Samples kept in the dark (n=3.)

The addition of ferrocene/BF<sub>3</sub>·2H<sub>2</sub>O and ferrocene/MSA to the samples stored in the dark was investigated. It was found that these two acids caused an increase in the rate of BAPO degradation and the results are presented in Figure 2.12. It was determined that over 12 months the peak area of BAPO was reduced by 83% and 98% for ferrocene/MSA and ferrocene/BF<sub>3</sub>·2H<sub>2</sub>O, respectively, when compared to the neat samples after the same time.

As both MSA and BF<sub>3</sub>·2H<sub>2</sub>O affected the rate of degradation for samples exposed to the ambient light when added in conjunction with ferrocene, a number of other additives were also analysed. BAPO samples exposed to the light with ferrocene and either (CHP) or (HQ) added, were analysed by the optimised HPLC-UV method. It was found that the BAPO samples exposed to ambient light in the presence of ferrocene/CHP degraded almost completely after one month. The degradation time is identical to that for neat BAPO and ferrocene/HQ samples exposed to the ambient light.

The BAPO samples in the presence of additives and kept in the dark showed no significant difference in the peak area or peak height of the BAPO samples after 12 months and therefore there is no significant difference in the rate of its degradation.



The addition of ferrocene to the BAPO sample reduced the degradation to a similar level to the BAPO sample with no additions, however, the addition of CHP and HQ to the samples caused a slight increase to the rate of degradation as illustrated in Figure 2.13.

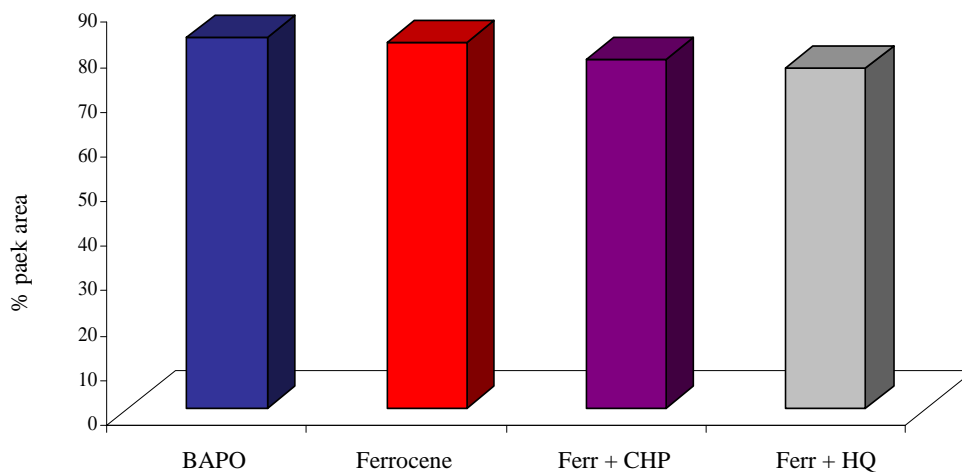


**Figure 2.13:** Graphical illustration of peak area degradation for BAPO, BAPO with ferrocene, ferrocene+CHP and ferrocene+ HQ. Samples stored in the dark.

The HQ was added to the BAPO sample with ferrocene, and this again decreased the rate of degradation.

Therefore, it can be concluded that for samples kept in the dark the addition of both HQ and CHP in conjunction with ferrocene slightly increase the rate of BAPO degradation, whereas, the addition of ferrocene with MSA and  $\text{BF}_3$  resulted in a considerable increase in the rate of BAPO degradation.

### 2.4.2.5 Addition of water

The analysis of the stability the BAPO was performed through the addition of deionised water at a concentration of 0.5% v/v. The addition of water to the anhydrous ACN did not affect the rate of degradation of BAPO samples stored in the dark and only slightly (only 1.1% after one week) decreased the rate of degradation of BAPO for samples exposed to ambient light.

### 2.4.2.6 Summary of stability study of BAPO using HPLC

The overall results of stability study of BAPO in dark and ambient light conditions are given in Table 2.5

**Table 2.5:** Summary of results of BAPO stability study.

Compositions of samples	Ambient Light	Dark
BAPO	Completely degrades after 1 month	Stable over 12 months
BAPO/ MSA	Completely degrades after 1 month	Slightly slowed down degradation
BAPO/ BF <sub>3</sub> ·2H <sub>2</sub> O	Almost completely degrades after 1 week	Almost completely degrades after 10 month
BAPO/ Ferrocene	Completely degrades after 3 month	Stable over 12 months
BAPO/ Ferr/MSA	Completely degrades after 1 month	Slightly slowed down degradation
BAPO/ Ferr/ BF <sub>3</sub> ·2 H <sub>2</sub> O	Completely degrades after 1 month	Completely degrades after 12 month
BAPO/ Ferr/ HQ	Completely degrades after 1 month	Slowed down degradation
BAPO/ Ferr/ CHP	Completely degrades after 1 month	Slowed down degradation
BAPO/ H <sub>2</sub> O	Slightly slowed down degradation after 1 month	Stable over 12 months

### 2.4.3 CE method

A CE method was developed for analysis of the BAPO and was compared with the HPLC-UV method.

#### 2.4.3.1. Development of CE method

The CE analysis of BAPO was performed using a borate buffer which has a  $pK_a$  value of 9.24. <sup>[26]</sup>

Two borate buffer systems were investigated: 50mM and 250 mM, in the working range between pH 8-10. Electropherograms showed that longer migration times resulted at high pH. In order to determine the optimum separation voltage for the analysis of BAPO an Ohm's plot was obtained, as described by Nelson et al., <sup>[27]</sup> and plotted in Figures 2.14 and 2.15.

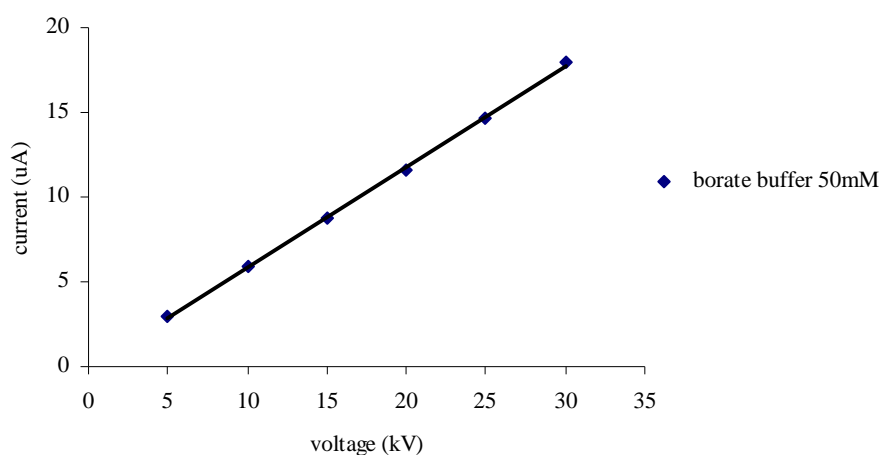


**Figure 2.14:** Ohm's Law plot for 50 mM borate buffer, pH 9.0. Effective capillary length 64 cm.

From this Ohm's Law plot in Figure 2.14, it is evident that a linear relationship exists between current and voltage. The analysis could be performed at separation voltages as high as 30 kV for the 50 mM borate buffer.

Increase of borate buffer concentration from 50 to 250 mM again showed a longer migration time, (a similar effect was observed for the highest pH), and decreased the magnitude of the EOF. This effect has been correlated to a decrease in zeta potential of colloidal silica <sup>[27]</sup> and increase in the currents generated, as shown in Figure 2.15, and Joule heating resulted.

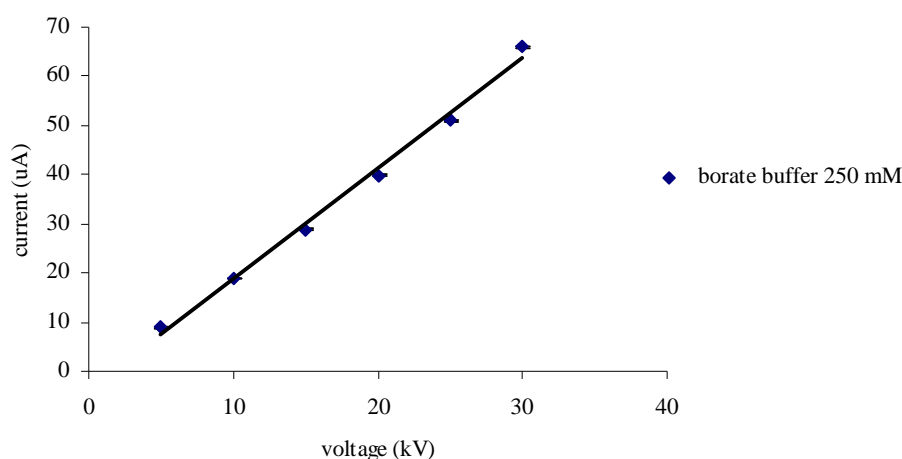


**Figure 2.15:** Ohm's Law plot for 250 mM borate buffer, pH 9.0. Effective capillary length 64 cm.

From Figure 2.15, it was determined that a linear relationship between current and voltage existed from 5 to 25 kV, after which Joule heating was evident.

Figure 2.16 illustrates a separation of BAPO from an ACN matrix using 50 mM borate buffer. It was found, see Figure 2.16, that using the separation voltage of 25 kV, the separation was complete by 4 min, this was a reduction of 4 min from the analysis time achieved by HPLC. Also, increased separation efficiencies of 112785.9 plates  $m^{-1}$  were obtained. However, BAPO is a neutral compound and migrates with electroosmotic flow (EOF). As a result, an alternative mode of CE more relevant to

the analysis of neutrals should be employed for further study, such as micellar electrokinetic chromatography (MEKC).

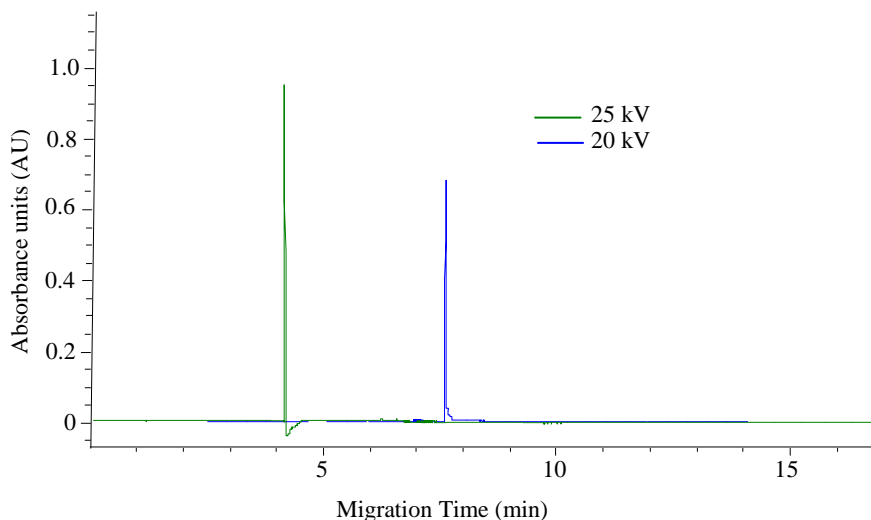


**Figure 2.16:** Effect of separation voltage for CE analysis of BAPO.

Separation voltage 20 and 25 kV employed with direct UV detection at 270nm, pressure injection 50 mbar/5s. BGE: 50 mM borate buffer, pH 9. Effective capillary length 64 cm (Agilent system).

Due to the increased total analysis time with lowest voltages for 50 mM of borate and the higher concentration of borate, a buffer of 50 mM borate at pH 9 and separation voltage at 25 kV was employed for further analysis. The use of pH 9 over pH 10 reduced the migration times and was closer to the pKa of the borate which made preparation and control of the resultant pH easier. Also, borate buffer at pH 9 was used for the first study of CE with BAPO photoinitiator. <sup>[26]</sup>

### 2.4.3.2 Micellar electrokinetic chromatography (MEKC)

MEKC is now a widely employed CE mode in pharmaceutical analysis with an increasing role in food, environmental and clinical analysis. <sup>[27]</sup> MEKC was originally developed for the separation of neutral analyte, including BAPO, by the used of surfactants in the running buffer. The most common surfactants for this method are anionic surfactants-sodium dodecyl sulfate (SDS), which have a net negative charge. Typical surfactant systems used for this method are shown in Table 2.6.

**Table 2.6:** Typical surfactants used in MEKC. <sup>[27]</sup>

	Biological detergents	*CMC (mM)	Aggregation number
Anionic	SDS	8.2	62
Cationic	DTAB	14	50
	CTAB	1.3	78
Non ionic	Octylglucoside	-	-
	n-Dodecyl- $\beta$ -D-maltoside	0.16	-
	Triton X-100	0.24	140
Zwitterionic	CHAPS	8	10
	CHAPSO	8	11
Bile salt	Cholic acid	14	2-4
	Deoxycholic acid	5	4-10
	Taurocholic acid	10-15	4

\*CMC-critical micelle concentration.

A stability study of BAPO was performed, over a 1 month time frame, using the CE and MEKC methods, for samples exposed to the ambient light and maintained in the dark. For the micellar electrokinetic chromatography the most common anionic surfactant-20 mM SDS was used.

The results obtained for both of these methods were similar, with the degradation of the photoinitiator going the same way in both. For the samples maintained in the dark no degradation of BAPO was observed after 1 month. For samples exposed to the

ambient light it was found that complete photodegradation of BAPO had occurred by 1 month, which validated the results obtained in the HPLC method. After 1 month, three new peaks were clearly observed, the separation times for these peaks were: 7.3; 7.6; 7.8 min. The new degradation products were possibly less hydrophobic than BAPO and have no interaction with the (SDS), therefore, all the products moved in the same direction as the EOF, as illustrated in Figure 2.17. Also the chromatogram in Figure 2.17 presented the peak of fresh BAPO samples ( $t=0$ ). The front slope of this peak suggested the BAPO samples could be impure. However, the purity of BAPO samples was not reported by Henkel Company.

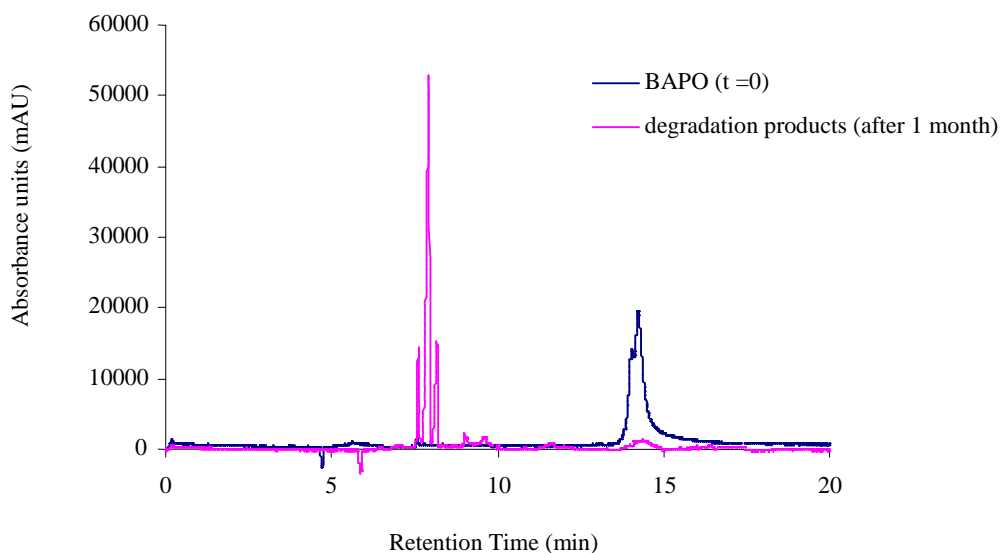


**Figure 2.17:** MEKC separations for the analysis of BAPO sample exposed to the ambient light for  $t=0$  min and after 1 month. Separation voltage 25 kV employed with direct UV detection at 270nm, pressure injection 50 mbar/5s. BGE: 50 mM borate buffer, 20 mM (SDS), pH 9 (CE Beckman P/ACE system).

The suitability of the CE method as an alternative mode of analysis of degradation products of BAPO was demonstrated. Also the CE method had a lower consumption of reagents. The operation costs in CE are also lower than for the HPLC method. The typical volume of buffer used per day was of the order 10-15 mL. With

the HPLC method, sometimes litres of waste organic solvent were “produced” per day. However, some disadvantages of the capillary electrophoresis methods were also found. The first problem was the fused-silica capillaries, which broke very often when acetonitrile was used a solvent. To combat this, the acetonitrile was replaced with MeOH. Another major limitation of the CE was the poor reproducibility of migration times for BAPO which made peak identification and quantitation difficult.



## 2.5 CONCLUSION

A HPLC method was developed and was successfully applied to the analysis of the  $\alpha$ -cleavable photoinitiator, bis(2,4,6-trimethylbenzoyl)phenylphosphine oxide (BAPO). A comparison of its stability was determined in samples, which were kept in the dark and samples exposed to the ambient light, over a 12 months time frame for HPLC method. From this study it was determined that the degradation of BAPO had almost completely occurred by 1 month (started after 24h) for samples exposed to the ambient light. For the samples maintained in the dark, only 1.2% reduction in the BAPO peak height was observed, when compared to the results obtained after  $t = 0$  min. In effect, the compound was found not to degrade under dark conditions. It was also found that the compound had completely degraded by 1 month for samples exposed to the ambient light when the protonic and Lewis acids were added and ferrocene/CHP and ferrocene/HQ. BAPO was more stable when only ferrocene was added. The degradation of BAPO for samples exposed to the light was not complete after one month and for samples kept in the dark degradation after 12 months was comparable with neat BAPO. The presence of water slightly decreased the rate of degradation of BAPO for samples exposed to the ambient light but did not affect samples kept in the dark. The application of CE to the analysis of BAPO was shown. The CE method is an alternative mode of analysis with increased the separation efficiencies obtained, 3120.5 plates  $m^{-1}$  with HPLC and 112 785.9 plates  $m^{-1}$  with CE, and also a reduction of total analysis time by 4 min was achieved.

The results from the HPLC method yielded important information about the stability and conditions of BAPO. The investigation of the products of photodegradation and the curing mechanism of BAPO with LC-MS is discussed in detail in Chapter 3.

**2.6 REFERENCES**

- [1] Jacobi, Henne, A., M., *J. of Radiation Curing*, **1983**, 19, 16.
- [2] Jacobi, M., Henne, A., *J. of Radiation Curing*, **1985**, 175, 636.
- [3] Rutsch, W., Dietliker, K., Leppard, D., Kohler, M., Misev, L., Kolczak, U., Rist, G., *Prog. Org. Coatings*, **1996**, 27, 227.
- [4] Decker, C., Zahouly, K., Decker, D., Nguyen, T., Thi Viet, *Polymer*, **2001**, 42, 7551.
- [5] Kolczak, U., Rist, G., Dietliker, K., Wirz, J., *J. Am. Chem. Soc.*, **1996**, 118, 6477.
- [6] Keskin, S., Jockusch, S., Turro, J.N., Arsu, N., *Macromolecules*, **2008**, 41, 4631.
- [7] Baxter, J.B., Davidson R. ,S., Hageman H.,J, Overeem, T., *Makrom.Chem.*, **1988**, 189, 2769.
- [8] Jockusch, S., Turro, N.J., *J. Am. Chem. Soc.*, **1998**, 120, 11773.
- [9] Jockusch, S., Koptug, I.V., Mc Garry, P. F., Sluggett, G.W., Turro, N. J., Watkins, D. M., *J. Am. Chem. Soc.*, **1997**, 119, 11495.
- [10] Baxter, J. E., Davidson, R.S., Hageman, H.J., *Eur. Polym. J.*, **1988**, 24, 419.
- [11] Baxter, J.E., Davidson, R.S., Hageman, H.J., *Eur. Polym. J.*, **1988**, 24, 551.
- [12] Baxter, J.E., Davidson, R.S., Hageman, H.J., Hakvoort, G.T.M., Overeem, T., *Polymer*, **1988**, 177, 1575.
- [13] Baxter, J.E., Davidson, R.S., Hageman, H.J., *Polymer*, **1988**, 29, 1569.
- [14] Gatlik, I., Rzadek, P., Gescheidt, G., Rist, G., Hellrung, B., Wirz, J., Dietliker, K., Hug, G., Kunz, M., Wolf, J-P., *J. Am., Chem., Soc.*, **1999**, 121, 8332.
- [15] Sluggett, G.W., Turro, C., George, M. W., Koptug, I.V., Turro, N. J., *J. Am. Chem. Soc.*, **1995**, 117, 5148.
- [16] Jacobi, M., Henne, A., *Polymers Paint Colour J.*, **1985**, 175, 4150.
- [17] Pasto, D., Johnson, C., Miller, M., *Experiments and Techniques in Organic Chemistry*, Prentice-Hall, New Jersey, **1992**.
- [18] Beiser, A., *Concepts of Modern Physics*, 5th Ed., McGraw-Hill, **1995**.
- [19] Jockusch, S., Turro, N., J., *J. Am. Chem. Soc.*, **1998**, 120, 11773.

- [20] Ciba Specialty Chemicals Inc, *Photoinitiator for UV Curing*, **2003**.
- [21] Barba Olives, A.I., Camara Hrtado, M., Sanchez Mata, M.C., Fernandez Ruiz, V., Lopez Saenz de Tejada, M., *Food Chemistry*, **2006**, 95, 328.
- [22] Gosetti, F., Mazzucco, E., Gianotti, V., Polati, S., Gennaro, M.C., *J. Chromatogr. A*, **2007**, 1149, 151.
- [23] Agilent Technologies, *Agilent HPLC Column Selection Guide*, **2009**.
- [24] Weston A., Phyllis R. Brown, *HPLC and CE principles and Practice*, Andrea, New York, W.B. Saunders Company, **1997**.
- [25] Witkiewicz Z., *Podstawy Chromatografii*, Warszawa, Wydawnictwa Naukowo-Techniczne, **2005**.
- [26] Whitaker, G., *PhD Thesis*, Dublin City University, **2006**.
- [27] Agilent Technologies, *High performance Capillary Electrophoresis*, **2009**.

*Chapter Three*

*Study of the Photodegradation products of  
BAPO using LC-MS*

### 3.1 INTRODUCTION

Mass spectrometry is recognised as a powerful analytical technique especially for its: sensitivity, detection limits, speed and diversity of its applications.

In analytical chemistry, the most recent applications are biological or pharmaceutical in nature such as characterisation of proteins <sup>[1, 2]</sup>, peptides <sup>[3, 4]</sup>, oligonucleotides, and high throughput analysis in drug discovery and metabolism <sup>[5-10]</sup>. Other analytical applications are in the environmental field <sup>[11]</sup> (such as water quality), food contamination, clinical *e.g.* neonatal screening, hemoglobin analysis and food control <sup>[12]</sup> such as natural products or process monitoring. Other, less prevalent applications include atomic physics, reaction physics and kinetics, geochronology, ion-molecule reactions, determination of thermodynamic parameters ( $\Delta G^\circ_f$ ,  $K_a$ , etc.) and many more. <sup>[13]</sup>

Mass spectrometry has progressed extremely rapidly during the last decade and this has led to the continuing development of more advanced instruments. Historically, a large number of mass spectrometers have been developed according to the fundamental scheme developed in Thomson's experiments in 1897. Listed here are some highlights of this development, as shown in Table 3.1.

**Table 3.1:** Some highlights of development in mass spectrometry. <sup>[14]</sup>

Year	Name	Highlights
1886	E. Goldstein	discovers anode rays (positive gas phase ions) in gas discharge
1897	J.J. Thomson	discovers the electron and determines its mass to charge ratio. <b>Nobel Prize in 1906</b>
1974	P.J. Arpino, M.A. Baldwin, F.W. McLafferty	first spectrometers coupled with a high – performance liquid chromatography
1974	M.D. Comisarov, A.G. Marshall	develop Fourier transformed ICR (FTICR) mass spectrometry
1978	R.A.Yost, C.G.Enke	build the first quadrupole mass spectrometer, one of the most popular types of tandem instrument
1983	C.R. Blakney, M.L.Vestal	describe the thermospray (TSP)
1983	G.C Stafford, P.E. Kelly, J.E Syka, W.E. Reynolds, J.F.J. Todd	describe the development of gas chromatography detectors based on an ion trap and commercialized by Finnigan under the name Ion Trap
1987	T. Tanaka, M. Karas, D. Bachmann, U. Bahar, F. Hillenkamp	discover matrix-assisted laser desorption/ionization (MALDI), TANAKA receives the <b>Nobel Prize in 2002</b>
1987	R.D. Smith	describes the coupling of capillary electrophoresis (CE) with mass spectrometry.
1988	J Fenn	develops electrospray (ESI). First spectra of proteins above 20.000Da. He demonstrated the electrospray's potential as a mass spectrometric technique for small molecules in 1984. The concept of this source was proposed in 1968 by M.DOLE. FENN receives the <b>Noble Prize in 2002</b> .
1991	B.Spengler, D. Kirsch, R. Kaufmann	obtain structural information with reflectron TOF mass spectrometry (MALDI- post-source decay).
1994	M. Wilm, M. Mann	describe the nanoelectrospray source
1999	A.A. Makrov	describes a new type of mass analyzer: the orbitrap. The orbitrap is a high-performance ion trap using an electrostatic quadro-logarithmic field

The progress of experimental methods and the refinements in instruments led to improvements in resolution, sensitivity, mass range and accuracy.

The achieved resolutions ( $m/\delta m$ ) are shown in Table 3.2:

**Table 3.2:** Resolution developments in mass spectrometry.

Year	Resolution ( $m/\delta m$ )	Name	Reference
1913	13	J.J. Thomson	[14]
1918	100	A.J. Demster	[14]
1919	130	F.W. Aston	[14]
1937	2000	F.W. Aston	[15]
1998	8000000	A.G. Marshall	[16]

Mass spectrometry is also an extremely powerful technique to investigate the degradation of products, for example drugs. A wide number of drugs are affected by degradation when exposed to light. Light induced decomposition of pharmaceuticals might result in the loss of potency or lead to unwanted effects due to the formation of a toxic photodegradation product. Stability testing of drugs in different conditions such as various temperatures especially light stress tests is now on the list of requirements by the European Agency for the Evaluation of Medicinal Products (EMA) [17] to identify and characterise products of degradation and to check the stability of active substances. However, as degradation products generated during storage in light may be at very low levels, stress studies have suggested using the higher volumes of investigated drugs.

In some instances due to their low amounts, it is difficult to isolate these products from the stress mixture and to analyse them for structural information. Therefore, LC-MS, with its excellent sensitivity, is currently the method of choice used for this particular kind of study.

Maquille and Habib Jiwan [18] reported the photodegradation of the antiemetic drug, metoclopramide. The photolytic degradation of metoclopramide aqueous solutions was analysed by high performance liquid chromatography-ion trap mass spectrometry equipped with an atmospheric pressure chemical ionisation (APCI)

source in order to characterise the photodegradation products. From the mass spectra and dissociation obtained 18 photolysis products of metoclopramide were identified. Dissociation of the chloride was the major photodegradation pathway of this drug and was accompanied by reaction coupling of the products to generate high molecular weight compounds.

In 2008, Bansal and Singh <sup>[19]</sup> published a paper related to the degradation products of glimepiride in accordance with the ICH guidelines. Five degradation products of glimepiride formed under different conditions, such as hydrolysis, oxidation, dry heat and photolysis. All the degradation products were characterised by LC-UV and LC-MS methods. The MS and LC-MS studies were carried out using positive or negative electrospray ionisation ((+)ESI and (-)ESI). The degradation pathway of the drug to the products was also proposed in this paper.

Analyses of drugs were carried out by Fiori and Bertucci <sup>[20]</sup> using the HPLC-MS/MS system to characterise the photostability of lercanidipine. The analysis by HPLC coupled with ESI mass spectrometry provided information on the molecular weight of the analytes. The tandem mass analyses characterised the main photodegradation products of lercanidipine.

ESI-MS was also used to investigate the effect of the solvent on the photostability and degradation kinetic of the drugs.

Another application of electrospray ionisation for the study of photodegradation products was reported by Gosetti and Gennaro <sup>[21]</sup>. The photodegradation products were found in “diffused commercial red aperitif that contains a mixture of the yellow E110 dye (about 43 mg L<sup>-1</sup>) and the red Chromotrope E122 (about 34 mg L<sup>-1</sup>) in the presence of aromas and glucose-fructose syrup” <sup>[21]</sup>. HPLC–diode array-MS/MS analysis clearly showed some impurities with naphthalene–based structures in the aperitif.

The ESI-MS approach has also helped in study of the photochemical degradation of pesticides and one such study was published by Chen in 2009. <sup>[22]</sup> This paper focused on the suitability of using liquid chromatography ion trap mass spectrometry (LC-IT-MS) for determination of pirimicarb pesticide and identification of degradation products. The mass spectrometer was equipped with an ESI source and operated in positive polarity. This paper reported photodegradation products not only under UV light irradiation but also with visible light irradiation. The different



degradation products were obtained by both photodegradation of pirimicarb in aqueous solution and microbiological degradation in soil.

As was described in more detail in Chapters 1 & 2, the majority of research papers published for BAPO report the use of UV-Vis <sup>[23-26]</sup>, time resolved spectroscopy <sup>[27, 28]</sup> or CIDNP <sup>[29]</sup> to monitor the degradation of this important photoinitiator and to characterise the final products of such processes. The use of LC-MS, which appears to be a very powerful and suitable method for such studies, has not yet been reported in literature. We are the first research group that has taken this approach and in this chapter we present our results for the characterisation of BAPO and the identification of its degradation products using LC-MS technique.

### **3.2 SCOPE OF RESEARCH**

The short literature review presented in the previous section of this chapter, focusing on the determination of degradation products of drugs, has already proven the usefulness of LC and LC-MS for such analysis. However, to date no research has been done on the characterisation of BAPO and identification of its decomposition products using LC-MS. In this chapter the outcomes of the investigation of fragmentation pathways and photodegradation products of the BAPO (Irgacure 819) photoinitiator, bis(2,4,6-triethylbenzoyl)phenylphosphine oxide are presented. The work was done using LC coupled with mass spectrometry detection (LC-MS), with electrospray ionisation (ESI) as the source. All degradation products are identified based on the molecular weight and dissociation products.

### 3.3 MATERIALS AND METHODS

#### 3.3.1 Instrumentation

##### 3.3.1.1 *Liquid chromatography-Mass spectrometry*

The HPLC system for LC-UV analysis consisted of a binary pump, a photodiode array (PDA) detector and an autosampler (Agilent Technologies, Ireland). The separations were carried out on a Zorbax C<sub>18</sub> (150 mm × 2.1 mm I.D., 5µm) analytical column (Agilent Technologies) using a mobile phase composed of a mixture of acetonitrile and water (90/ 10, v/v) with a flow rate of 0.2 mL min<sup>-1</sup>. The injection volume was 10 µL and eluent was detected and monitored at 270 nm.<sup>[30]</sup>

The MS and LC-MS studies were carried out using positive as well as negative electrospray ionisation ((+)ESI and (-)ESI) modes on a Bruker Daltonics instrument (Bruker Daltonics Esquire 3000 LC-MS, ion trap, GmbH, Germany). The operating conditions for the MS scan of BAPO and its degradation products in (+) ESI mode were optimised as shown in Table 3.3:

**Table 3.3:** Parameters for ESI-MS.

	(+) ESI	(-) ESI
<b><u>Mode :</u></b>		
Mass Range mode	Std/Normal	Std/Normal
Ion Polarity	Positive	Negative
Ion Source Type	ESI	ESI
Current Alternating Ion Polarity	N/A	N/A
Alternating Ion Polarity	N/A	N/A
<b><u>Tune Source:</u></b>		
Trap Drive	37.2	33.3
Octopole RF Amplitude	150.00 Vpp	-110.00 Vpp
Lens 2	-60 Volt	+65 Volt
Capillary Exit	116.1 Volt	-109.0 Volt
Lens 1	-5.0 Volt	-9.0 Volt
Dry Temp (Set)	365°C	325°C
Nebulizer (Set)	30.08 psi	30.08 psi
Dry Gas (Set)	8.01 L/min	8.01 L/min
HV Capillary	4402 V	-4402 V
HV End Plate Offset	-500 V	-500 V
Skim1	40.4 Volt	-35.08 Volt
<b><u>Tune SPS*:</u></b>		
Target Mass	441 m/z	
Compound Stability	100%	
Optimise	Normal	
Smart Parameter Setting	active	
<b><u>Trap:</u></b>		
Rolling	Off	Off
Scan Begin	50.00 m/z	50.00 m/z
Scan End	800 m/z	800 m/z
Averages	5 Spectra	5 spectra
Max. Acc Time	50000µs	50000 µs
ICC Target	20000	20000
Charge Control	On	On
Accumulation Time	1066µs	1046 µs

\*SPS- Smart Parameter Setting

The operating conditions for MS scan of BAPO in (-) ESI mode were the same as in (+) ESI mode (nebuliser pressure 30.08 psi and dry gas 8.01 L min<sup>-1</sup>), except that the drying temperature was set to 325°C.

### 3.3.2 Chemicals

All chemicals were of reagent grade described in Chapter 2 in section 2.3.4.

### 3.3.3 Procedures

#### *3.3.3.1 Preparation of mobile phase*

The mobile phase for HPLC-UV was a mixture of water-acetonitrile [90/10, v/v] and was filtered (47 mm Nylon 66 membranes with 0.45  $\mu\text{m}$  and PTFE filter) under vacuum and sonicated for 20 to 30 min to remove dissolved gases.

#### *3.3.3.2 Preparation of standard solution*

A stock (0.5% BAPO) solution of each analyte was prepared in acetonitrile. Standards of known concentration were prepared by dilution of the stock with acetonitrile and making the volume to 100 mL in volumetric flask. Table 3.4 shows the standard solution of each analyte.

**Table 3.4:** Standard solution compositions and corresponding concentrations of the preparations.

Standard Solution	Concentration (%)
BAPO	0.5
BAPO/MSA	0.5/ 0.004
BAPO/ BF <sub>3</sub> ·2H <sub>2</sub> O	0.5/ 0.003
BAPO/Ferrocene	0.5/ 0.01
BAPO/ Ferrocene/MSA	0.5/ 0.01/ 0.004
BAPO/Ferrocene/BF <sub>3</sub> ·2H <sub>2</sub> O	0.5/ 0.01/ 0.003
BAPO/HQ	0.5/ 0.1
BAPO/CHP	0.5/ 0.1

One set of samples was prepared in amber volumetric flasks and stored in a dark room; the other set was prepared in clear volumetric flasks and was exposed to the ambient light at room temperature. The samples were injected directly into the LC-MS.

## 3.4 RESULTS AND DISCUSSION

### 3.4.1 Optimisation of LC-MS parameters

The analysis of BAPO samples was performed using LC-ESI-MS. The photolysis of BAPO can proceed through three hypothetical cure mechanisms:

- a) a free radical mechanism with the generation of phosphinoyl and benzoyl radicals taking place,
- b) a nucleophilic mechanism, due to the presence of a source of hydrogen atoms,
- c) an anionic mechanism.

The ESI was the preferred ionisation techniques due to the low molecular weight and the polarity properties of the BAPO (see section 1.4.1.1.1).

From the previous study it was found that either ACN water or MeOH water were preferred mobile phases for the analysis of the BAPO, as illustrated in Figure 2.3. Many typical HPLC solvents are compatible with ESI and the common solvents that are used with ESI-LC techniques are shown in Table 3.5

A good electrospray solvent will easily support ions in solution and this generally requires such solvent to have some dipole moment *i.e.* polarity.<sup>[31]</sup> For this reason solvents such as toluene, which are non-polar and do not easily support ions in solution cannot be employed for the ESI experiments.

**Table 3.5:** Common solvents for the ESI-LC techniques. <sup>[31]</sup>

	Surface tension (dyn/ cm)	Dipole	Dielectric constant (@20°C)	Viscosity (cp)
methanol	22.55	2.87	32.7	0.59
ethanol	22.32	1.66	24.55	1.10
propanol	23.70	3.09	20.33	2.30
isopropanol	21.79	1.69	19.92	2.40
butanol	22.98	1.75	17.51	2.98
acetonitrile	19.10	3.44	37.50	0.38
water	72.80	1.87	80.10	1.00
DMF (1)	36.76	3.86	36.71	0.92
DMSO (1)		4.10	46.68	2.24
acetic acid	13.63		8.55	0.93
acetone	23.22	2.69	20.70	0.36
toluene	28.53	0.31	2.38	0.59
hexane	17.91	0.08	1.88	0.31
chloroform	28.12	1.15	4.81	0.57
cyclohexane	24.98	0.0	2.02	1.00

The LC column determines the choice of flow rate for chromatography. For the larger columns higher flow rates are used and each column will have an optimum flow rate as illustrated in Table 3.6.

**Table 3.6:** LC columns and corresponding to the flow rates. <sup>[31]</sup>

Column i.d.	Typical flow
4.6 mm	1.0 mL min <sup>-1</sup>
3.9 mm	0.5 mL min <sup>-1</sup>
2.1 mm	0.2 mL min <sup>-1</sup>
1.0 mm	40-50 µL min <sup>-1</sup>
capillary	< 10 µL min <sup>-1</sup>



For many analytes the best responses were obtained with flow rates are in the range 150-200  $\mu\text{L min}^{-1}$ . However, the optimum value is strongly related to the physiochemical properties of the compound and the mobile phase used.

The analytical conditions that must be taken into consideration when performing ESI-MS analyses are the flow rate of the nebulising gas and the solvent flow. Good nebuliser performance can be realised with the flow rates from 1  $\mu\text{L min}^{-1}$  up to over 1  $\text{mL min}^{-1}$ . The optimum nebuliser pressure depends on the flow rate. At low flow rates 10 psi is generally sufficient, while at higher flow rate pressures up to 40 psi are required. Pneumatic nebulisation by pressurised gas (at 10 to 40 psi) helps create droplets, but often when a sample is introduced at a high flow ( $> 20$  to  $50 \mu\text{L min}^{-1}$ ) droplets are still not small enough to produce ions before reaching the sample cone. The high flow source also consists of the heated gas stream (desolvation gas) that helps to reduce droplet size further by accelerating solvent evaporation from the droplets. The typical ESI-MS conditions as shown in Table 3.7.

**Table 3.7:** Typical ESI Source Conditions. <sup>[32]</sup>

HPLC flow rate ( $\mu\text{L min}^{-1}$ )	Nebuliser pressure (psi)	Drying gas flow ( $\text{L min}^{-1}$ )	Dry gas temp. ( $^{\circ}\text{C}$ )
1-10	10-15	4	300
10-50	15-20	5	325
50-200	20-40	6-9	325-365
200-500	30-50	8-10	365
500-1000	50-70	9-12	365

The optimised ESI-MS method (based on the maximum signal intensity) parameters as shown in this table was used: conditions are shown in section 3.3.1.1.

### 3.4.2 Mass fragmentation of BAPO

To optimise the parameters for ESI-MS analysis, a BAPO sample, containing neither an internal standard nor additives, was injected directly into the ESI source. Figure 3.1 illustrates a  $MS^2$  spectrum of a BAPO sample.

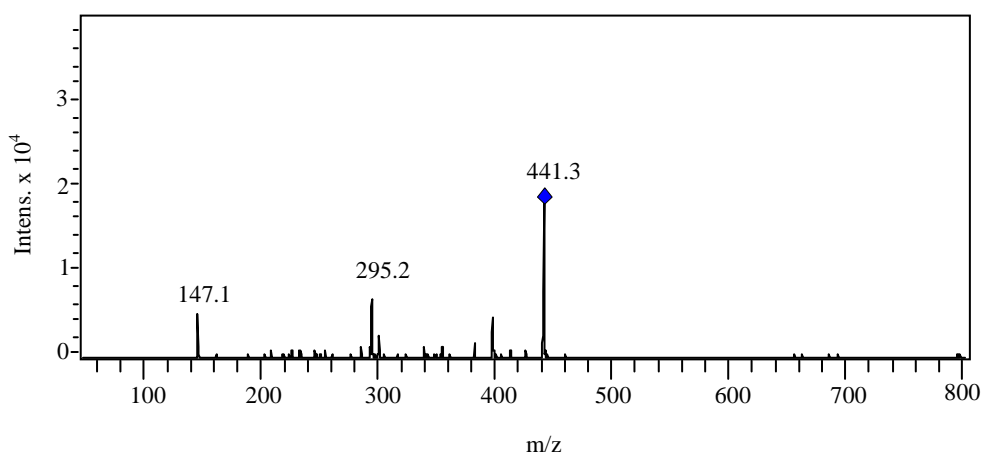
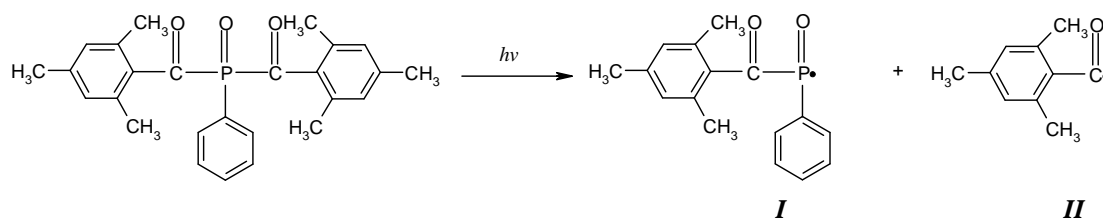


**Figure 3.1:** (+)  $MS^2$  spectrum of BAPO from  $m/z$  441.

The parent ion of BAPO (MW= 418) provided a signal at  $m/z$  441.3 which was the sodium adduct  $[M+ Na]^+$  (owing to the presence of sodium in the acetonitrile solution employed as the mobile phase) in full scan MS in positive ion mode.

Upon UV irradiation the BAPO undergoes  $\alpha$ -cleavage of the carbonyl-phosphorous bond which leads to formation of benzoyl and phosphinoyl radicals or 2,4,6 -trimethylbenzoylphenylphosphine oxide radical as shown in Figure 3.2 a) <sup>[33]</sup> and b) <sup>[29]</sup>

a)



b)

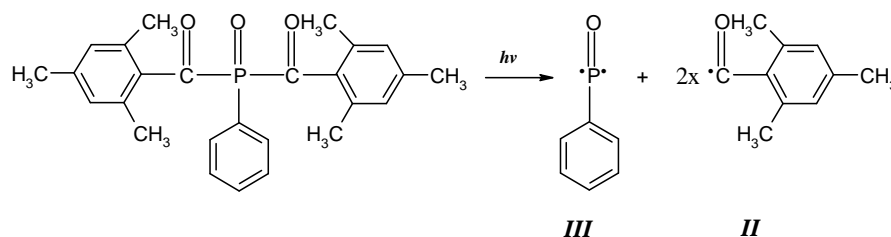
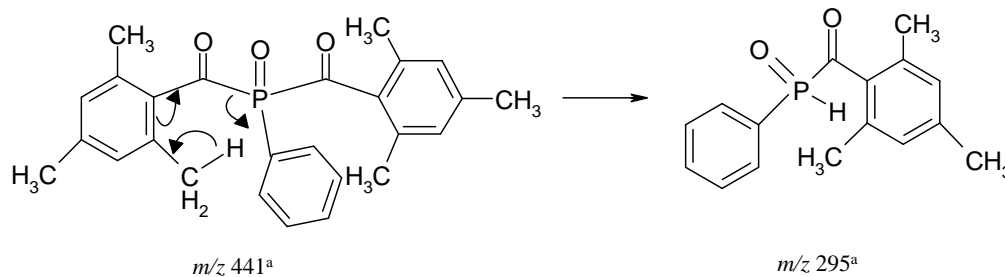


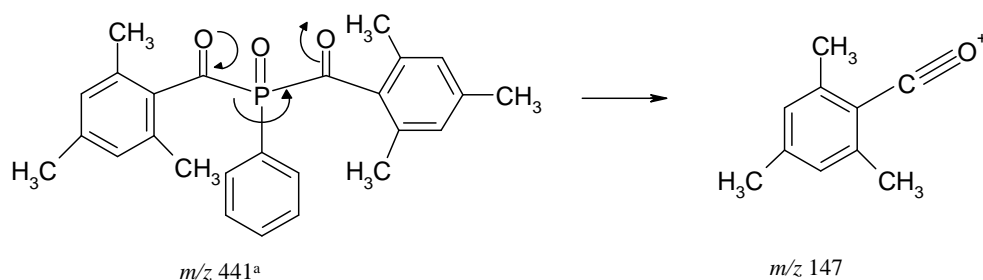
**Figure 3.2:**  $\alpha$ -cleavage of BAPO, a) to produce I- 2,4,6-trimethylbenzoylphenylphosphine oxide radical and II- benzoyl radical <sup>[29]</sup>, b) to produce III- phosphinoyl diradical and II-benzoyl radical. <sup>[33]</sup>

The LC-MS<sup>2</sup> spectrum of BAPO (see Figure 3.1) reveals product ions at  $m/z$  147 and  $m/z$  295. Based on both ions observed and their proposed reaction schemes, the following mechanisms could occur to yield the same product ions, as illustrated in Figure 3.3.

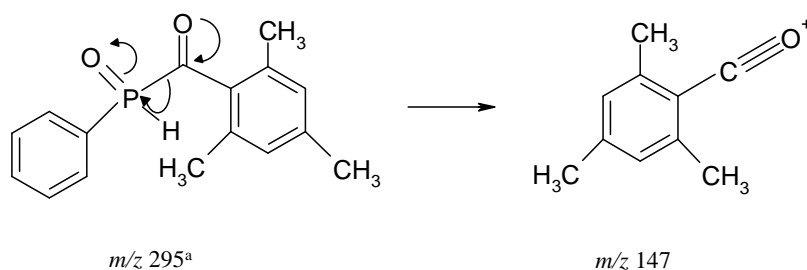
a)



b)

<sup>a</sup>[M+Na]<sup>+</sup>**Figure 3.3:** Mechanisms of BAPO fragmentation.

The  $m/z$  295 product ion may possibly be the result of a rearrangement processes. This is one example of the “*ortho effect*” noted when the substituents can be in a six-membered transition state to make possible loss of a neutral molecule, 2,4,6-trimethylbenzoylphenylphosphine oxide sodium adduct. Dole and co-workers<sup>[36-38]</sup> in their pioneering work on ESI, first recognised the possibility of sodium attachment to neutral organic molecules. MS<sup>2</sup> analysis of ion  $m/z$  295 revealed a fragment ion at  $m/z$  147 (see Figure 3.4). The possible mechanism as shown in Figure 3.3b could easily generate the 2,4,6 trimethylbenzoyl ion (which is characteristic ion for the cleavage of aryl ketones)<sup>[39]</sup>. Loss of CO from this fragment gives the product ion at  $m/z$  119, as illustrated in Figure 3.5.

<sup>a</sup>[M+Na]<sup>+</sup>**Figure 3.4:** Mechanism of BAPO MS<sup>3</sup> fragmentation.

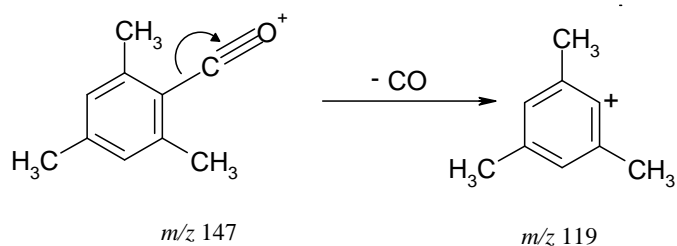


**Figure 3.5:** Mechanism of BAPO MS<sup>3</sup> fragmentation.

### 3.4.3 BAPO degradation products determination by LC-MS

A stability study and analysis of photodegradation products of BAPO was performed from  $t=0$  to 24 h and a comparison between samples maintained in the dark and ambient light was obtained (see Figure 3.6). It was determined from LC-UV investigation that photodegradation of BAPO did not occur for samples kept in the dark as shown in Figure in 2.4.

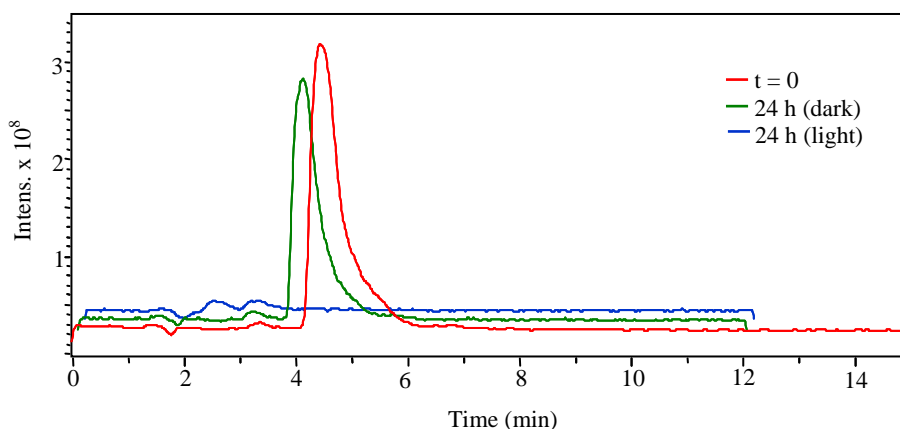


**Figure 3.6:** Total ion chromatogram (TIC) of BAPO ( $t=0$  and 24 h) for samples exposed to ambient light and kept in the dark.

When BAPO was exposed to ambient light for 24 h, two new peaks at retention time 2.4 and 3.4 minutes were clearly observed and the corresponding mass spectrum is shown in Figure 3.7 b).

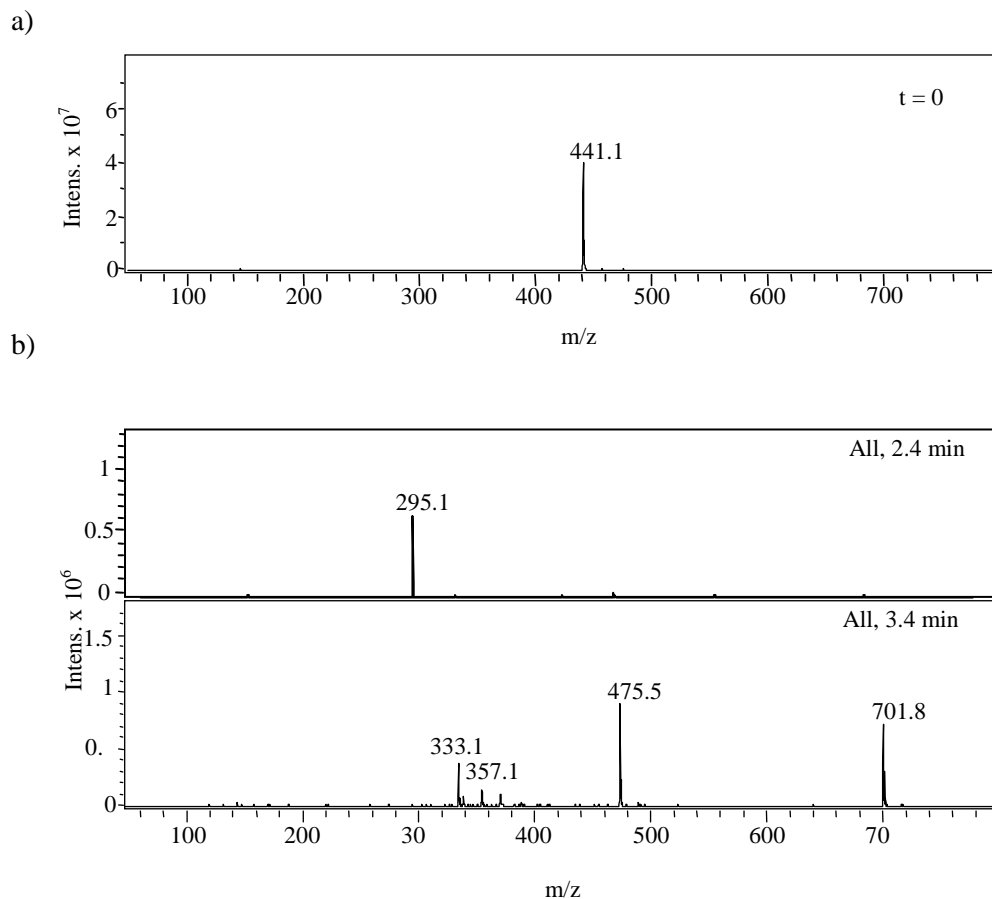
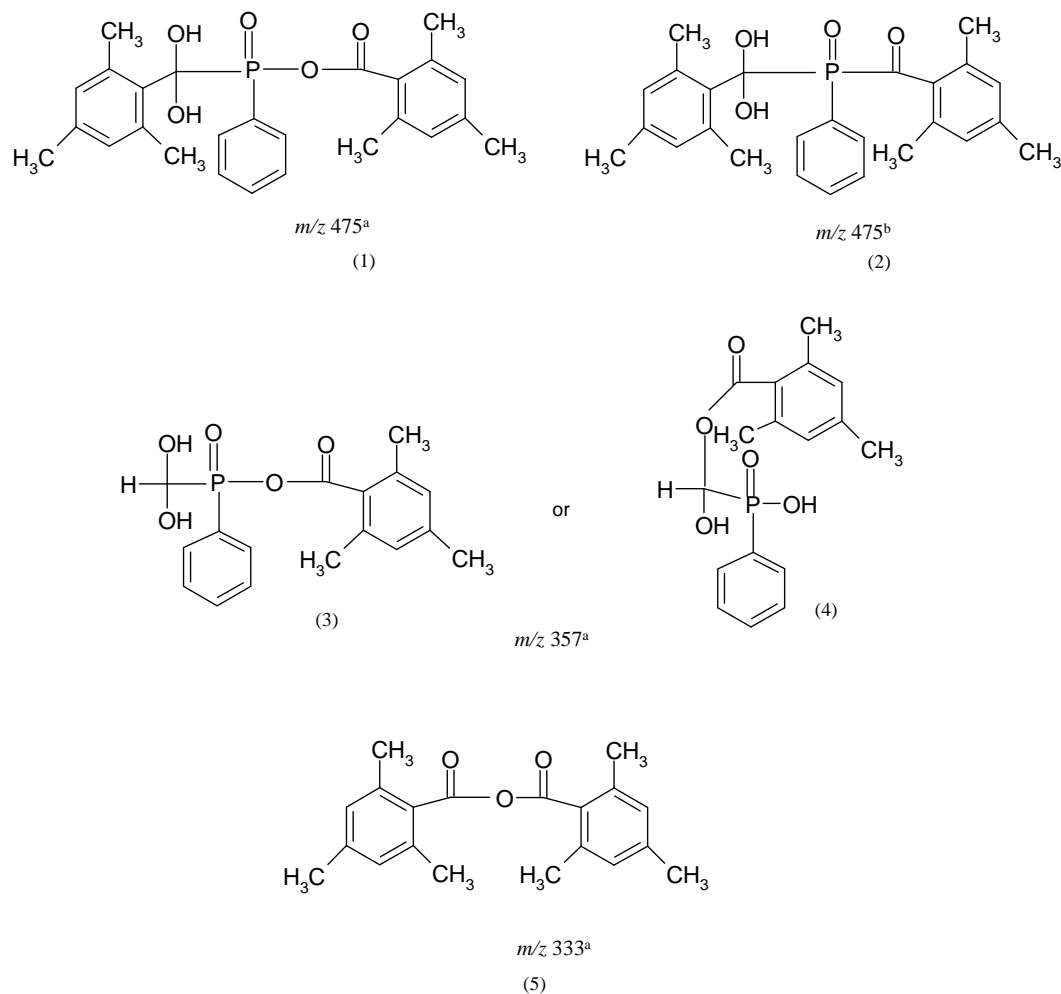


**Figure 3.7:** (+) ESI-MS mass spectra of BAPO: a) BAPO spectrum ( $t = 0$ ) and b) spectrum of degradation products (after 24 h) for samples exposed to ambient light.

The (+) ESI-MS identification of these BAPO photodegradation products suggested that these four products might be compounds of  $m/z$  295 and  $m/z$  475,  $[M + Na]^+$  (1) or  $[M + K]^+$  (2), 357,  $[M + Na]^+$  (3) or (4), 333,  $[M + Na]^+$  (5), see Figure 3.8. The ion at  $m/z$  702 is likely to be the cyclic nylon trimer<sup>[49]</sup> sodium adduct discussed in section 3.4.6.



<sup>a</sup>[M+Na]<sup>+</sup>

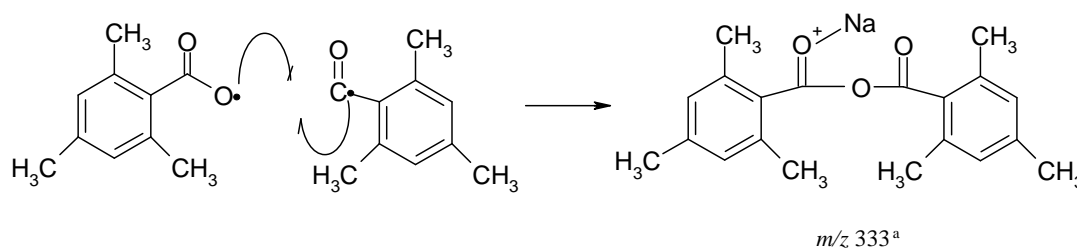
<sup>b</sup>[M+K]<sup>+</sup>

**Figure 3.8:** Proposed structure for degradation products of BAPO when samples were exposed to ambient light.

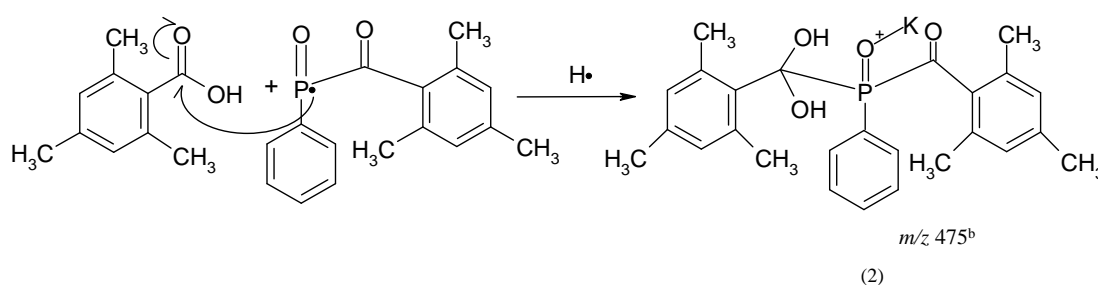
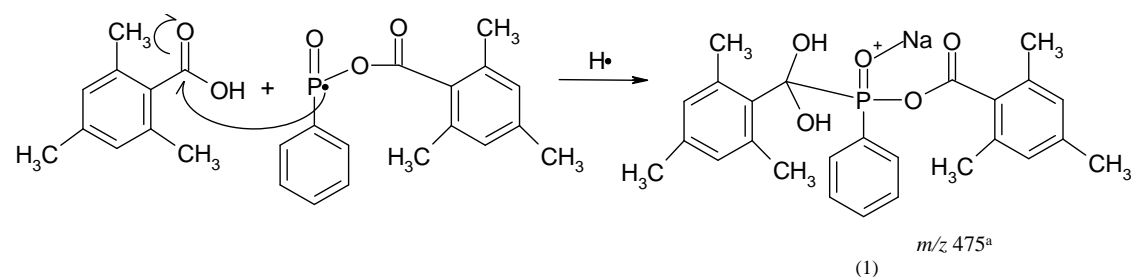
The degradation pathway of BAPO to three characteristic photodegradation products is outlined in Figure 3.9. It could be postulated that BAPO degraded to the product at  $m/z$  333 through reaction by combination of benzoyl radical with 2,4,6-trimethylphenylcarboxy radical, as illustrated Figure 3.9a. A similar mechanism for the degradation product of BAPO was reported in previous literature by Kolczak and co-workers.<sup>[29]</sup> Another photodegradation product at  $m/z$  475 suggested that two possible types of adducts (sodium (1) or potassium (2)) could be obtained by reaction

of 2,4,6-trimethylbenzoyl acid with phosphinoyl or phosphinoxy radical (see Figure 3.9b). The product ion at  $m/z$  357 (4) can be formed by loss of  $C_9H_{10}$  (via five-membered transition state) from the photodegradation product at  $m/z$  475, (see Figure 3.9c). Again, a similar structure of the degradation of BAPO product was reported by Kolczak and co-workers. [29] It was reported that, this product (with a P-C bond) is expected to be less stable than other photoproducts possessing the P-P or P-O bond.

a)

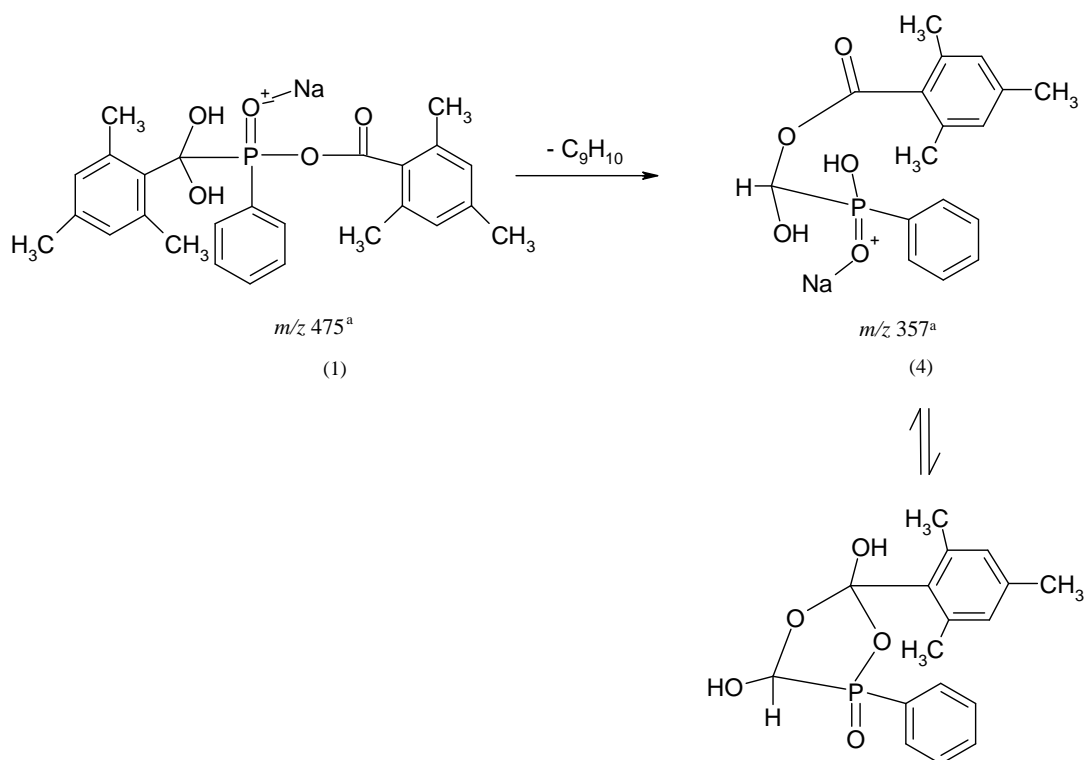


b)





c)

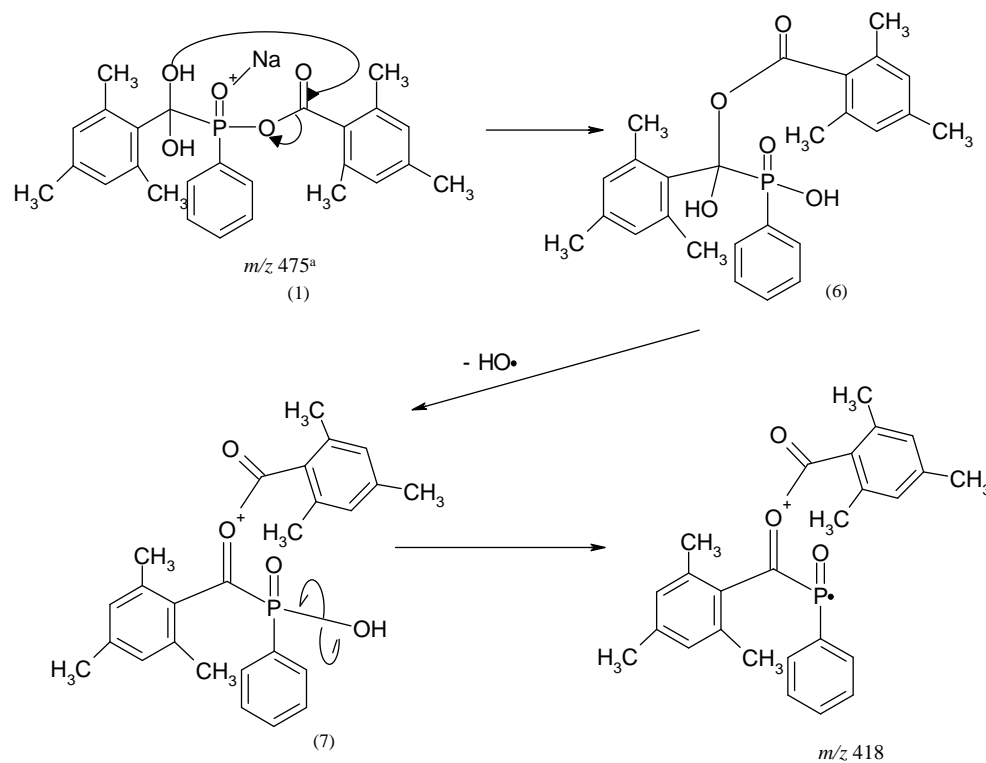
<sup>a</sup>[M+Na]<sup>+</sup><sup>b</sup>[M+K]<sup>+</sup>

**Figure 3.9:** Proposed photodegradation pathway of degradation products of BAPO, a)  $m/z$  333; b)  $m/z$  475; c)  $m/z$  357.

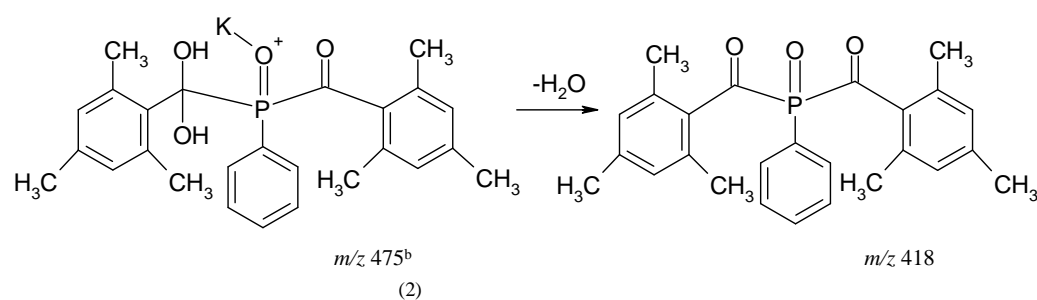
The MS<sup>2</sup> of the ion  $m/z$  475 yielded the product ions at  $m/z$  418,  $m/z$  337 and  $m/z$  362. The most likely mechanism involves a five-membered transition state proposed in Figure 3.10a, via fragmentation occurring by proton transfer from the OH<sup>-</sup> group to the phosphinate group to give intermediate product (6), which then may lose OH<sup>-</sup> to produce the intermediate product (7). The fragment ion  $m/z$  418 might be formed from the intermediate product (7) by losing OH<sup>-</sup> group. The alternative mechanism for the ion  $m/z$  418 could be from a possible loss of H<sub>2</sub>O from the product ion  $m/z$  475 [M+K]<sup>+</sup> (see Figure 3.10b). The product ion at  $m/z$  337 might be formed by losing of C<sub>9</sub>H<sub>10</sub> (via five-membered transition state) from the product ion at  $m/z$  475 [M+Na]<sup>+</sup> (see Figure 3.10c) or might be explained by recombination of two

phosphinoxy radicals<sup>[29]</sup> (see Figure 3.10d). The product ion at  $m/z$  337,  $[M+K]^+$  was reported in a previous study by Ciba-Geigy.<sup>[40]</sup> The product ion  $m/z$  362 could not be rationalised.

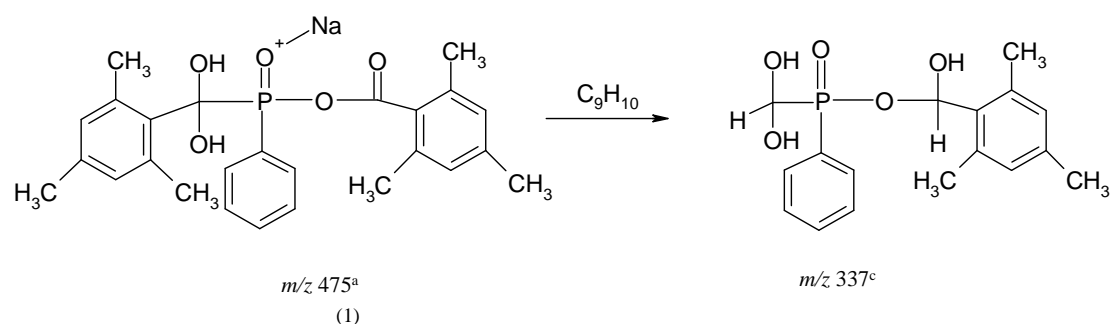
a)



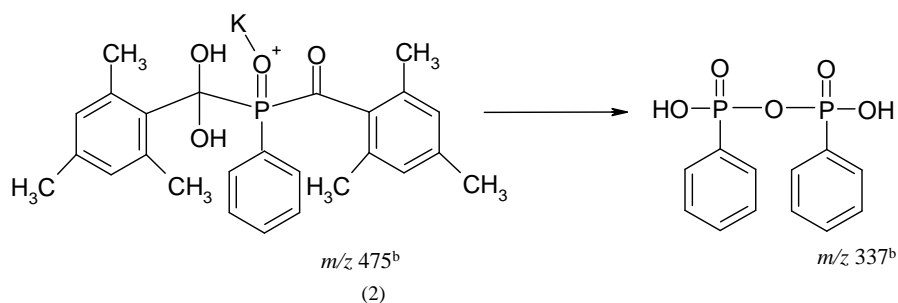
b)



c)



d)

<sup>a</sup>[M+Na]<sup>+</sup><sup>b</sup>[M+K]<sup>+</sup><sup>c</sup>[M+H]<sup>+</sup>

**Figure 3.10:** Proposed mass fragmentation of degradation product  $m/z$  475.

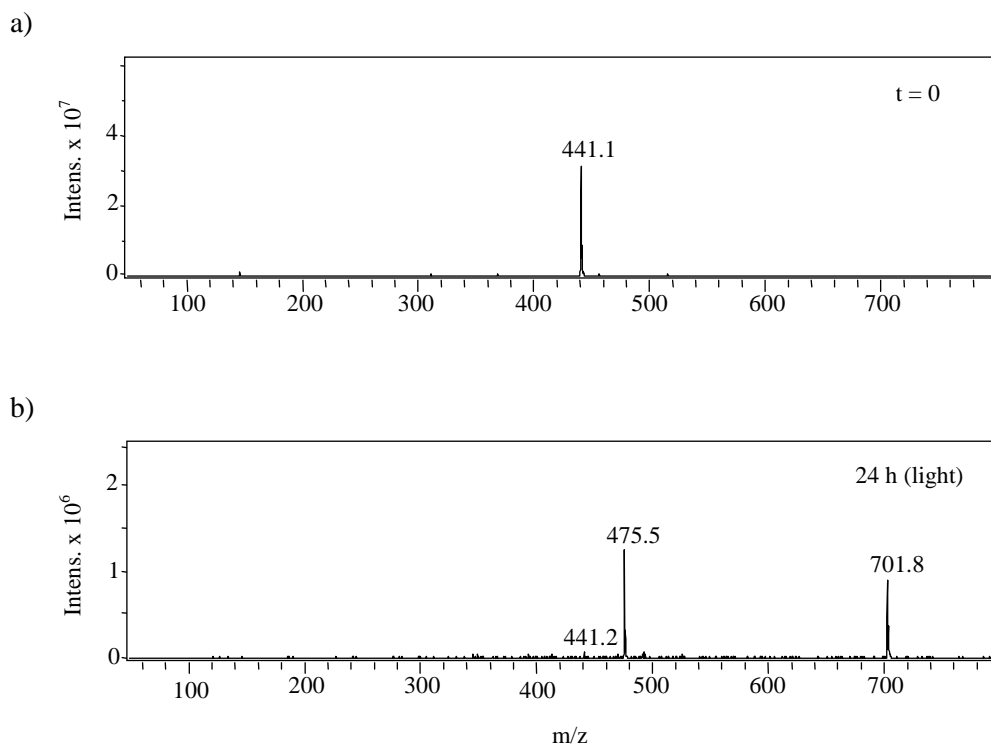
A time stability study and degradation study were also carried out and the curing mechanism of BAPO was investigated with various additives, such as protonic and Lewis acids and is discussed in section 3.4.4.

### 3.4.4 Analysis of BAPO with strong and weak acids

The effects of addition of protonic and Lewis acid to the BAPO solutions were investigated.

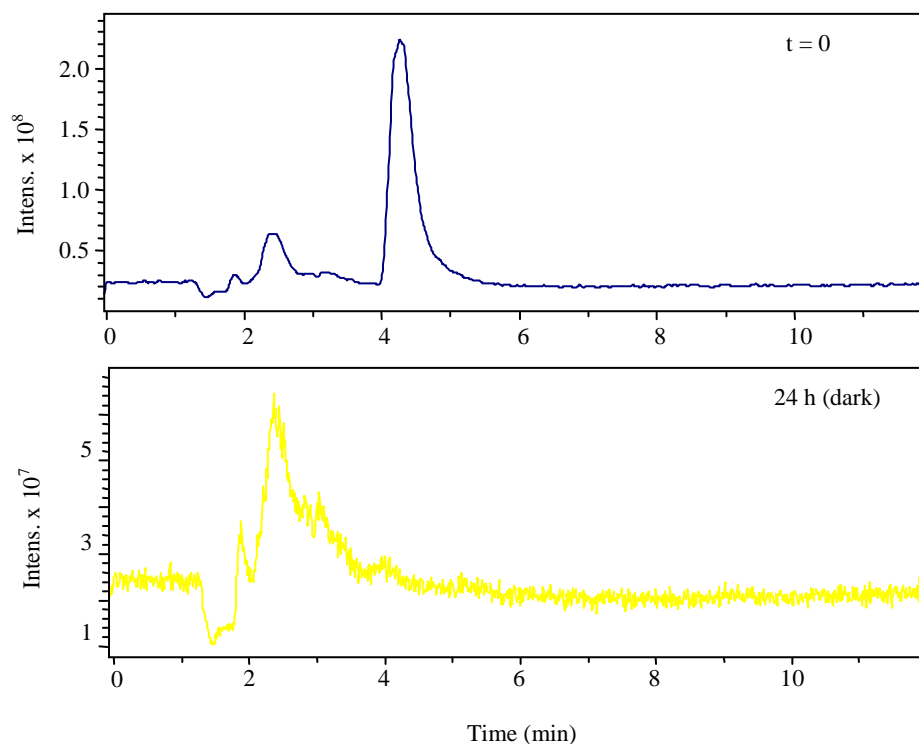
For samples protected from light, no significant difference was observed in the rate of degradation upon the addition of MSA. Analysis of the results showed that after 48 h the signal at  $m/z$  441, [M+Na]<sup>+</sup> observed for BAPO was of high intensity.

With the addition of MSA in the BAPO samples exposed to ambient light, the BAPO had almost completely degraded by 24 h with the appearance of the signals at  $m/z$  475 and  $m/z$  702, and no significant intensity of BAPO ( $m/z$  441) signal as illustrated in Figure 3.11. The signals at  $m/z$  475 may represent to the product of degradation of the BAPO, with the same trend observed for the BAPO sample with and without strong acid when exposed to ambient light.

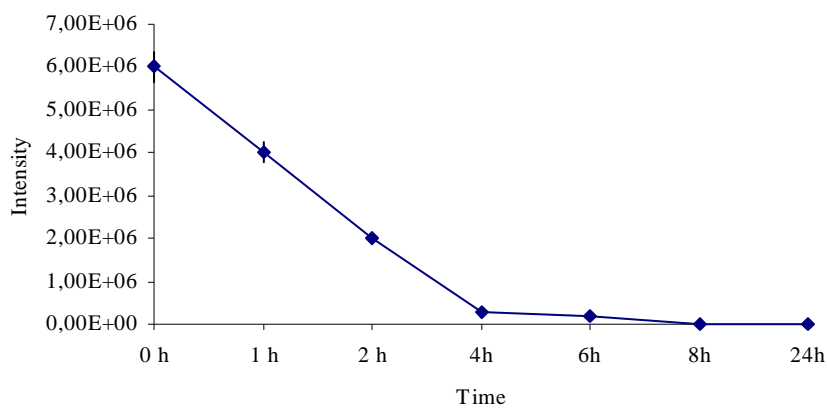


**Figure 3.11:** (+) ESI-MS mass spectra of BAPO with MSA: (a) BAPO with MSA spectrum after  $t = 0$  and (b) spectrum of degradation products in MSA after 24 h, for samples exposed to ambient light.

When the Lewis acid was added, this affected the rate of degradation differently compared with neat BAPO or BAPO/MSA. The addition of the Lewis acid  $\text{BF}_3 \cdot 2\text{H}_2\text{O}$  increased the rate of BAPO degradation for both samples exposed to ambient light and kept in the dark. Figure 3.12 illustrates the effect of the presence of the Lewis acid on the separation of BAPO monitored by ESI-MS for samples kept in the dark. It was found from the TIC that degradation of the BAPO was completed after 24 h, for samples maintained in the dark as depicted in Figure 3.13.



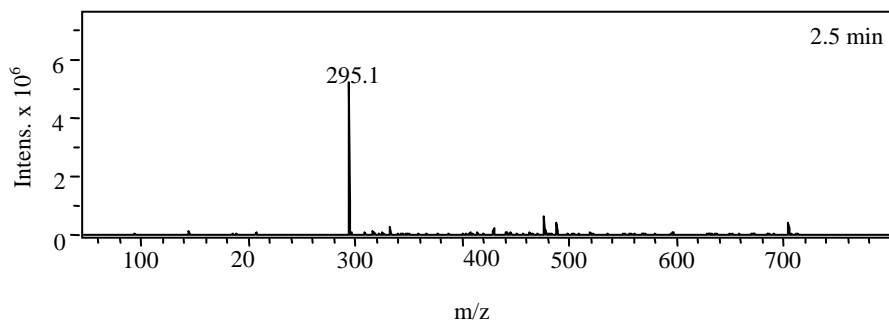
**Figure 3.12:** TIC of BAPO with  $\text{BF}_3 \cdot 2\text{H}_2\text{O}$ :  $t = 0$  and after 24 h for samples kept in the dark.



**Figure 3.13:** Graphical illustration of the time of degradation of BAPO in presence of  $\text{BF}_3 \cdot 2\text{H}_2\text{O}$  for samples kept in the dark, ( $n=3$ ).

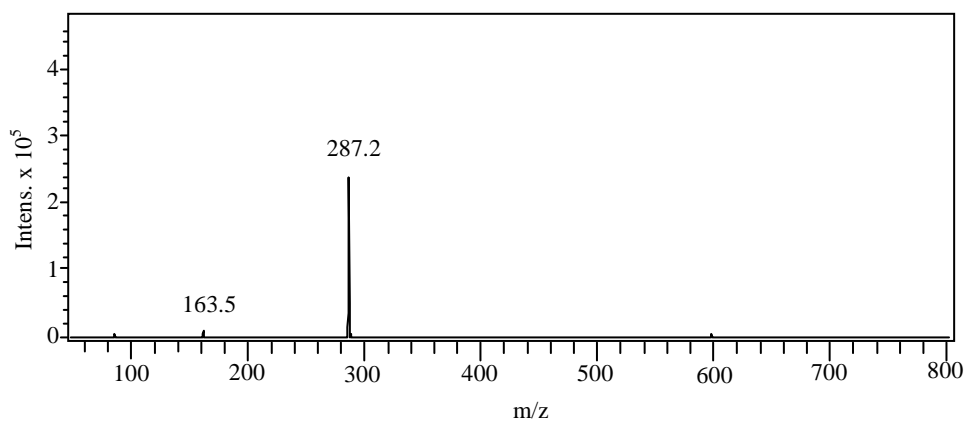
The appearance of a peak at retention time 2.5 minutes was also observed in the TIC which corresponds to the degradation product of BAPO  $m/z$  295 as illustrated in

Figure 3.14. The ion at  $m/z$  295,  $[M+Na]^+$  may represent 2,4,6-trimethylbenzoylphenylphosphine oxide and was discussed in section 3.4.2.



**Figure 3.14:** (+) ESI-MS mass spectrum of BAPO with  $BF_3 \cdot 2H_2O$  ( $t=0$ ) for samples kept in the dark.

Also for the negative mode, the LC-MS spectrum of the BAPO (Figure 3.15) showed two ions at values  $m/z$  163 and  $m/z$  287 after 24 h.



**Figure 3.15:** Mass spectrum of BAPO with  $BF_3 \cdot 2H_2O$  (after 24 h) for samples kept in the dark (negative mode)

The formation of both ions might possibly be explained by hydrolysis of BAPO. The main ion at  $m/z$  287 may arise from nucleophilic attack by water at phosphorus giving

rise to a hydrate (path 1) as illustrated in Figure 3.16a. Fragmentation of the intermediate product via deprotonation (path 2), could give an intermediate product (9) which may form a phosphinic acid by via homolytic cleavage of the C-P bond, (path 3). The phosphinic acid undergoing ionisation may lose of the proton (deprotonation) and formed the ion  $m/z$  287.

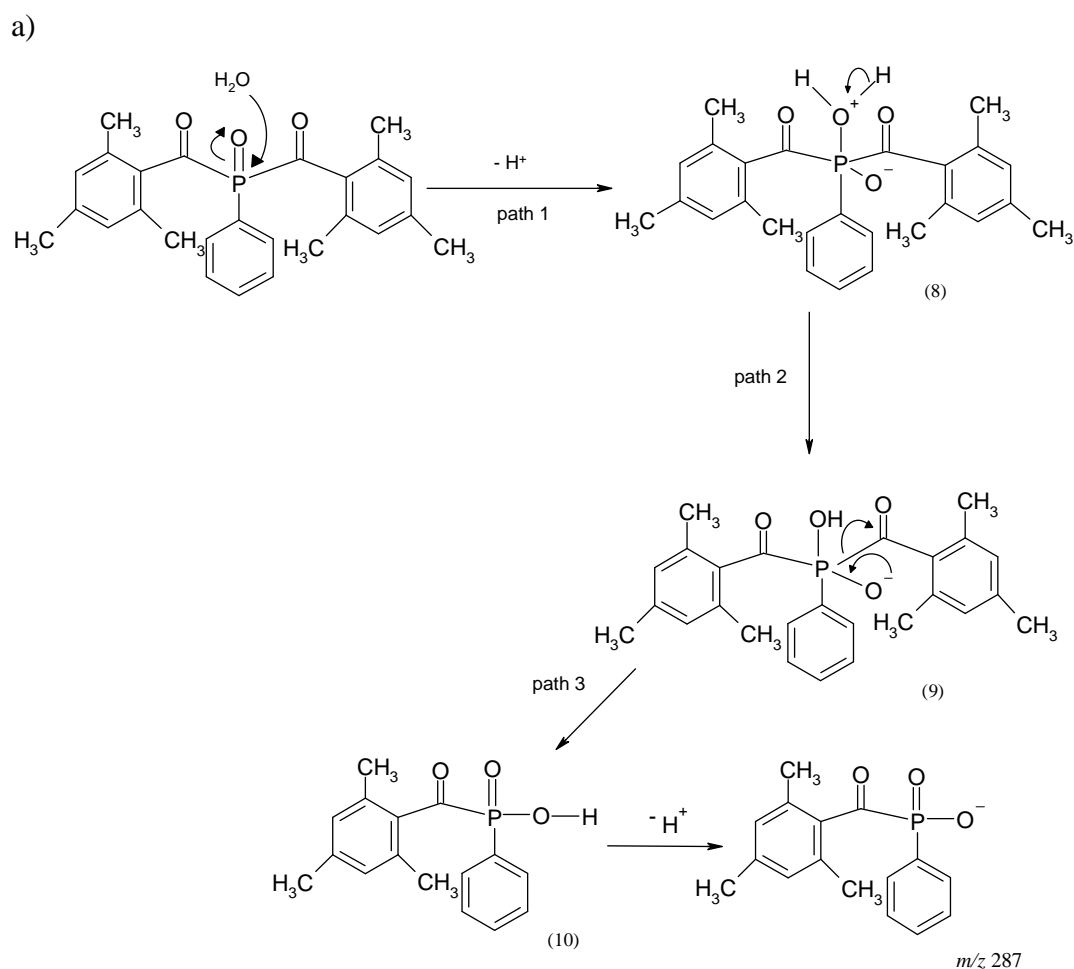


**Figure 3.16a:** Proposed photodegradation pathway of degradation product  $m/z$  287.

The peak at  $m/z$  163 might be attributed (path 1) by nucleophilic attack by water one of the carbonyl carbon group followed by elimination of 2,4,6-trimethylbenzoylphenylphosphine oxide. The formation of 2,4,6-trimethylbenzoyl acid (12) from the intermediate product (11) can be rationalised via a five-membered transition state whereby a proton is transferred from the OH group. For the third

reaction (path 3) the 2,4,6 trimethylbenzoyl acid undergoing ionisation may lose one of the proton and formed the ion  $m/z$  163, as illustrated in Figure 3.16b.

b)

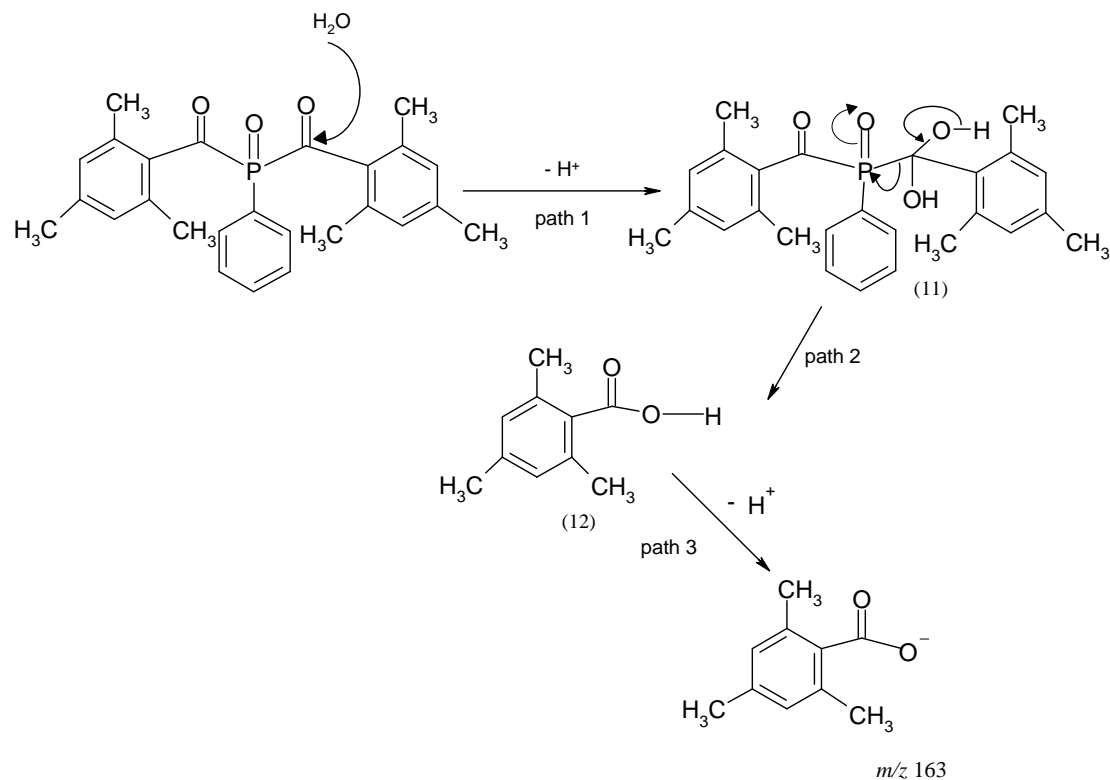


**Figure 3.16b:** Proposed photodegradation pathway of degradation product  $m/z$  163.

For the analysis of samples exposed to the ambient light after 24 h other signals were observed which might be explained by degradation of BAPO as illustrated in Figure 3.17. The ion  $m/z$  702 is an impurity corresponding to the cyclic nylon trimer sodium adducts, what was reported in literature.<sup>[49]</sup>



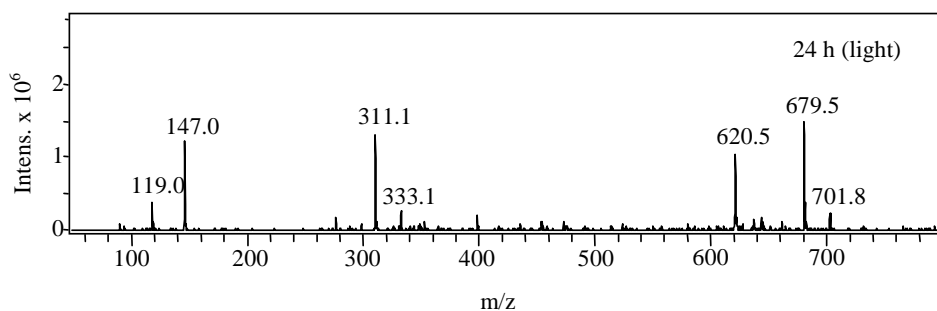
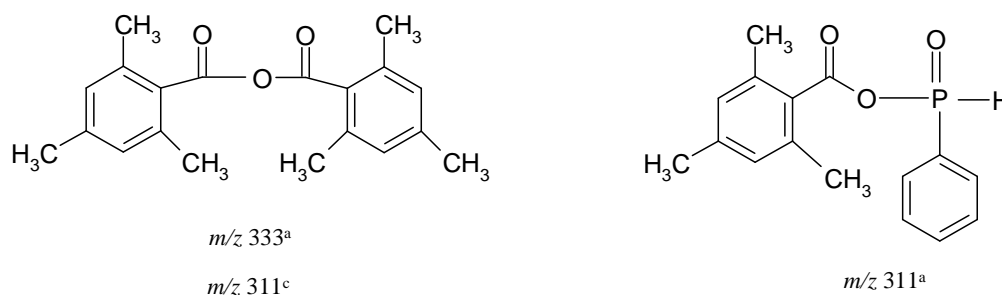


**Figure 3.17:** (+) ESI-MS mass spectra of BAPO with  $\text{BF}_3 \cdot 2\text{H}_2\text{O}$  after 24 h for samples exposed to the ambient light.

From Figure 3.17 it was found that the ion  $m/z$  147 may possibly be the result of the general “ortho effect”, (see Figure 3.3b). The ion of  $m/z$  119 may correspond to the 2,4,6 trimethylbenzoyl ion. The product ion at  $m/z$  311 was possibly formed by 2,4,6-trimethylbenzoylphenylphosphine oxide, sodium adduct or may be explain by combination of the benzoyl radical with 2,4,6-trimethylcarboxy radical,  $[\text{M}+\text{H}]^+$  as illustrated in Figure 3.18. Another product at  $m/z$  620.5 may possibly be the result of cluster ion of the type  $[\text{2M}]^+$ . The fragment ion of  $m/z$  679.5 is discussed in section 3.4.6. The proposed degradation products for BAPO in the presence of  $\text{BF}_3 \cdot 2\text{H}_2\text{O}$ , are illustrated in Figure 3.18.

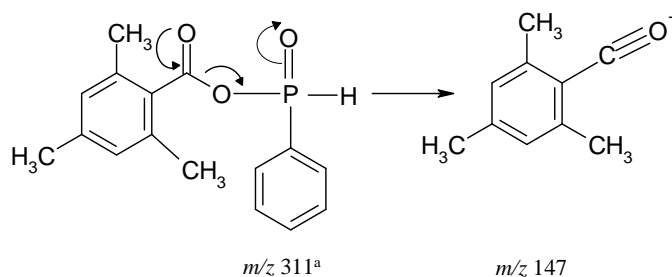


<sup>a</sup> $[\text{M}+\text{Na}]^+$

<sup>c</sup> $[\text{M}+\text{H}]^+$

**Figure 3.18:** Proposed structures of the degradation products of BAPO with  $\text{BF}_3 \cdot 2\text{H}_2\text{O}$  after 24 h for samples exposed to ambient light.

The MS<sup>2</sup> of the ion with  $m/z$  311 yielded the fragment ions at  $m/z$  147 and  $m/z$  163.5 with  $m/z$  147 as base peak. The possible mechanism of fragmentation as shown in Figure 3.19.



<sup>a</sup>[M+Na]<sup>+</sup>

**Figure 3.19:** (+) ESI-MS/MS of  $m/z$  311.

### 3.4.5 Analysis of BAPO with additives

From the LC-UV investigations, it was determined that the addition of ferrocene to the BAPO sample resulted in a slight decrease in the rate of degradation of the BAPO samples exposed to ambient light. A comparison of the  $t=0$  and 24 h samples exposed to ambient light was performed and Figure 3.20 represents the mass spectra for  $m/z$  441 for both samples. It was found from the spectrum in Figure 3.20 b) that degradation of the BAPO was not complete after 24 h. Also, from this spectrum it was found that the ion at  $m/z$  441, had decreased slightly in intensity, from  $5 \times 10^7$  to  $1.5 \times 10^7$  as shown in Figure 3.20.

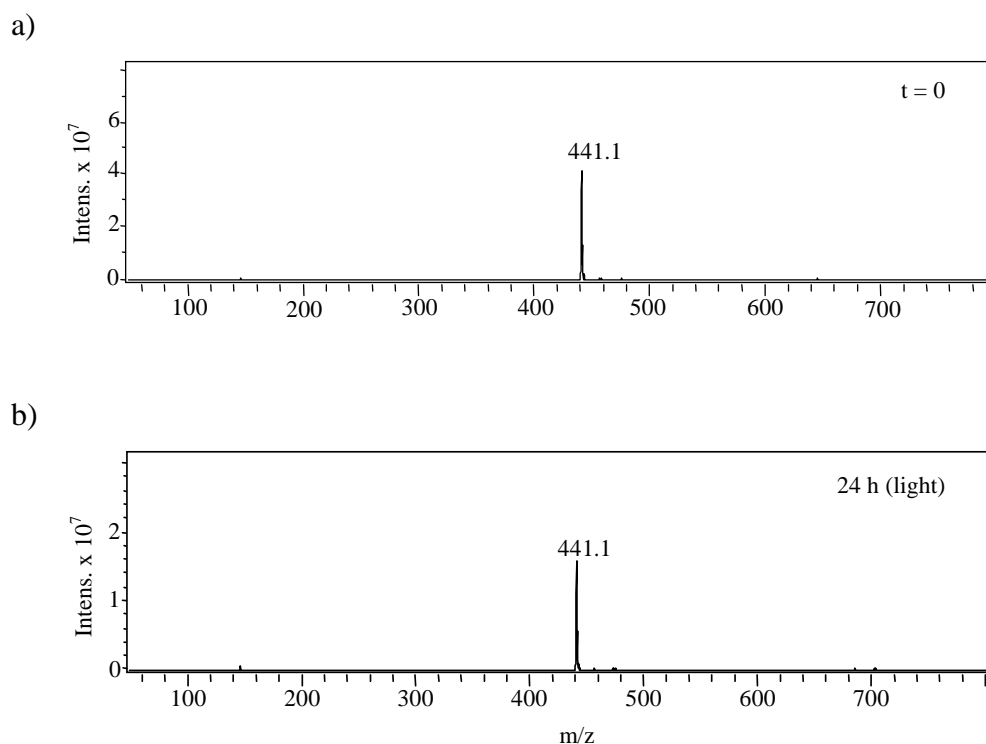


**Figure 3.20:** Mass spectra at  $m/z$  441 for BAPO with ferrocene ( $t=0$  and 24 h sample) in ACN.

For BAPO samples with addition of ferrocene, which were maintained in the dark, the degradation of BAPO was not affected. The BAPO ion at  $m/z$  441 possesses greater intensity than in the BAPO samples at  $t=0$ .

The effect of addition of protonic acid, MSA, and Lewis acid  $\text{BF}_3 \cdot 2\text{H}_2\text{O}$  in combination with ferrocene in the BAPO samples was examined for the samples after 24 h. The effect of adding  $\text{BF}_3 \cdot 2\text{H}_2\text{O}$  to the samples of BAPO/ferr resulted in a 32.1% reduction with the intensity of the BAPO peak. In contrast, the addition of protonic acid (MSA) caused only slight reduction in intensity, of about 8.5%. Again, ions of  $m/z$  147, 295, 475, 679, and 702 were acquired as shown in the ESI-MS in Figure 3.21. Both of the ions  $m/z$  147 and  $m/z$  295 were discussed in section 3.4.2. The ion at  $m/z$  475 may represent the degradation of BAPO was discussed in section 3.4.3 and the fragment ion of  $m/z$  679.5 and  $m/z$  702 as discussed in section 3.4.6.

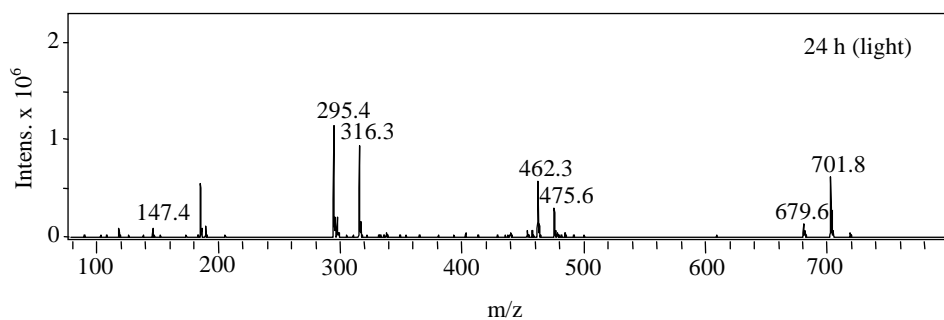
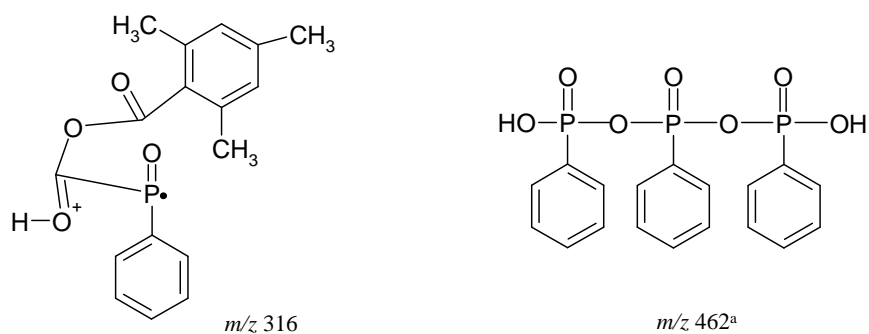


**Figure 3.21:** LC-MS spectrum of BAPO degradation products.

In this mass spectrum two new signals were observed at  $m/z$  316 and 462. The proposed structures of the new products (in presence of  $\text{BF}_3 \cdot 2\text{H}_2\text{O}$  and ferrocene) are illustrated by Figure 3.22.

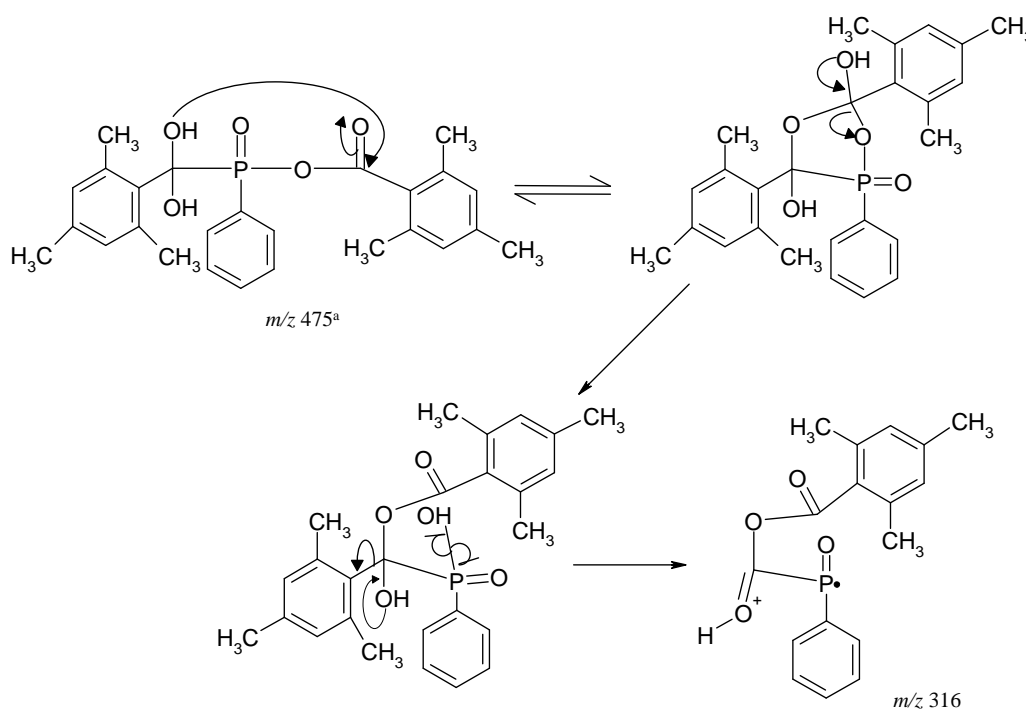


<sup>a</sup> $[\text{M}+\text{Na}]^+$

**Figure 3.22:** Proposed molecular structures of  $m/z$  316 and  $m/z$  462.

The ion at  $m/z$  316 may possibly be formed by rearrangement processes of degradation product of BAPO at  $m/z$  475,  $[\text{M}+\text{Na}]^+$ , as illustrated in Figure 3.23. The rearrangement produces five-membered transition states of intermediate product that can be further fragmented to produce  $m/z$  316. A cage recombination<sup>[29]</sup> between three phosphinoyl radicals could be formed from bisacylphosphine oxide and would

result in formation of a product at  $m/z$  462. This indicated that the fragments  $m/z$  462 existed as  $\text{Na}^+$  adducts in (+) ESI-MS mode.

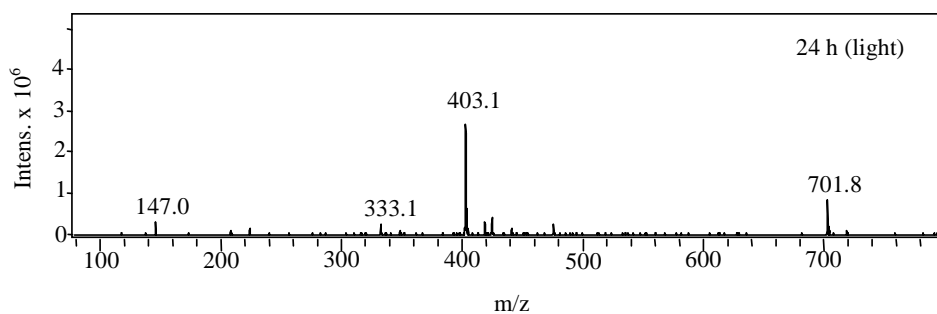


<sup>a</sup>[M+Na]<sup>+</sup>

**Figure 3.23:** Proposed photodegradation pathway of  $m/z$  316.

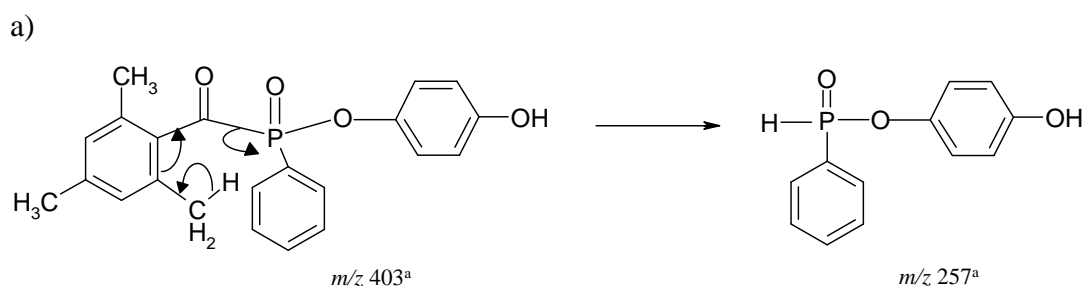
The addition of CHP and HQ to BAPO in conjunction with ferrocene was investigated for both  $t=0$  and 24 h. The addition of CHP to BAPO in conjunction with ferrocene did not significantly affect the rate of degradation of BAPO. For both sets of conditions for samples exposed to ambient light and kept in the dark the BAPO signal at  $m/z$  441 was observed.

It was found that the addition of HQ to BAPO in conjunction with ferrocene for samples exposed to ambient light significantly affected the degradation of BAPO. At a retention time around of 2.1 minutes signals at  $m/z$  147, 333, and 403 are present and are illustrated in Figure 3.24. Ions of  $m/z$  147 and 333 were also obtained, with the same trend observed as that shown in Figure 3.17 for the BAPO sample with addition of Lewis acid after 24 h.

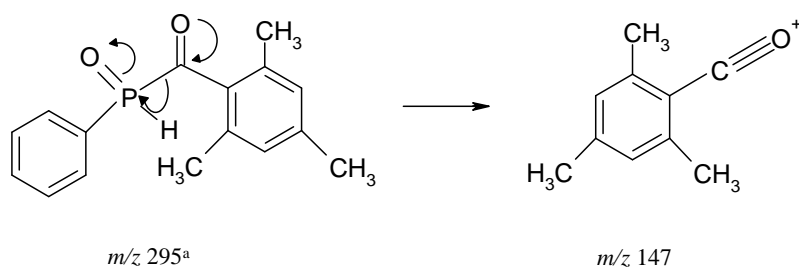


**Figure 3.24:** (+) ESI-MS mass spectrum of BAPO with HQ in conjunction with ferrocene degradation products.

The ion of  $m/z$  147 was as discussed in section 3.4.2. The ion at  $m/z$  333 which might correspond to the degradation of BAPO also was discussed in section 3.4.3. The signal at  $m/z$  403 corresponds to the structure given in Fig 3.25. The ion at  $m/z$  403 was sodium adduct  $[M+Na]^+$  most probably due to the presence of sodium in ACN solution employed in mobile phase. The MS<sup>2</sup> spectrum of the precursor ion  $m/z$  403 showed two product ions at  $m/z$  147 and  $m/z$  257. The ion at  $m/z$  257 was possibly formed by six-membered transition state whereby a proton from the *ortho* CH<sub>3</sub> group was transferred to the phosphinate group to produce a neutral molecule sodium adduct, see Figure 3.25 a. The ion at  $m/z$  147 may represent the 2,4,6-trimethylbenzoyl ion (see Figure 3.25 b) and was discussed in section 3.4.2.



b)

<sup>a</sup>[M+Na]<sup>+</sup>

**Figure 3.25:** Mechanisms of  $m/z$  403  $MS^2$  fragmentation.

### 3.4.6 Sources of contamination in LC-MS

Improvements in trace techniques combined with sensitivity of mass spectrometry offer enhanced opportunities to analyze ever lower concentrations of metabolites, drugs or pesticides. To perform HPLC and LC-MS quality of instruments, columns and eliminating contaminations of solvents<sup>[44]</sup> occupy a prominent role in the analytical process. Although it is difficult to completely eliminate contamination, it is possible to minimise the problem using the highest-purity water<sup>[45]</sup> or refraining from using improperly cleaned glassware.<sup>[46]</sup> However, minimising contamination can be very difficult.

During this work two significant signals were observed in LC-MS experiments. The first eluting peak (I) displays a protonated molecular ion at  $m/z$  453 and the second compound (II) has an  $m/z$  of 679,  $[M+H]^+$  or sodium adduct, formed the ion at  $m/z$  702. The mass spectrum corresponding to the signal at  $m/z$  679 are also shown in Fig. 3.17 and 3.21. Both of the fragment ions were identified as photodegradation products of BAPO, when samples were exposed on the light. During this study the filter was changed from Nylon 66<sup>[47, 48]</sup> to PTFE (polytetrafluoroethylene) filter and after this, the contamination signal was not observed. Also when unfiltered solvent was used, the contamination signals at  $m/z$  453 and 679 were not observed. It was deduced that the contaminations are associated with the filtration of the solvent.

The source of contamination was traced to the membrane disks that are universally employed to filter from the mobile phase. The filtration of the mobile phase is very important when preparing solvent with buffer or salts, as non-dissolved products can reduce the column lifetimes, and column performance.

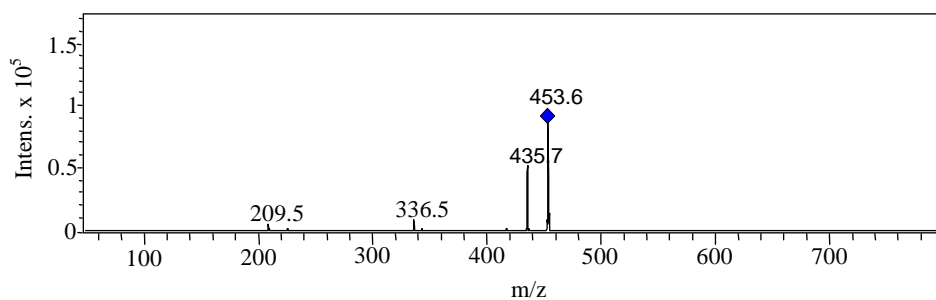
Tran and Doucette investigated the source of contamination in LC-MS testing several nylon membranes. Results of this work showed that the compounds of molecular weight at  $m/z$  453 and  $m/z$  679 are a cyclic dimer and a cyclic trimer of polyamide 66. Nylon 66 is a polymer manufactured from the condensation of adipic acid with hexamethylene diamine<sup>[49]</sup> The first reports of interfering signals at  $m/z$  453, 679 and 905 have been discussed on the Association of Biomolecular Resource Facilities forum<sup>[40]</sup>, and were recently attributed to nylon oligomers arising from filtering of solvents with usage of nylon 66 membranes.<sup>[50]</sup> It is therefore evident, that



cyclic oligomers are present in nylon membranes, and that these products will migrate into the solvents during the solvent filtration.

The MS<sup>2</sup> spectra of  $m/z$  453 and  $m/z$  679 confirm that both these compounds possess very similar structures, as illustrated in Figure 3.26.

a)



b)

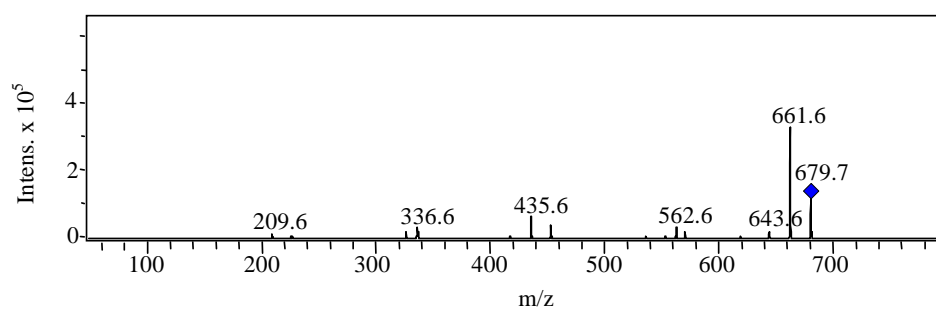


**Figure 3.26:** MS<sup>2</sup> spectra corresponding to a) compound I at  $m/z$  453 and b) compound II at  $m/z$  679.

Many of the product ions observed in the MS<sup>2</sup> spectrum of the ion at  $m/z$  679 can also be observed in the spectrum from  $m/z$  453, for example, the ions at  $m/z$  435, 336 and 209. The same results were presented in the paper by Tran and Doucette.<sup>[49]</sup> A potential reaction mechanism was proposed for the fragment ions of cyclic nylon dimer, as illustrated in Figure 3.27.

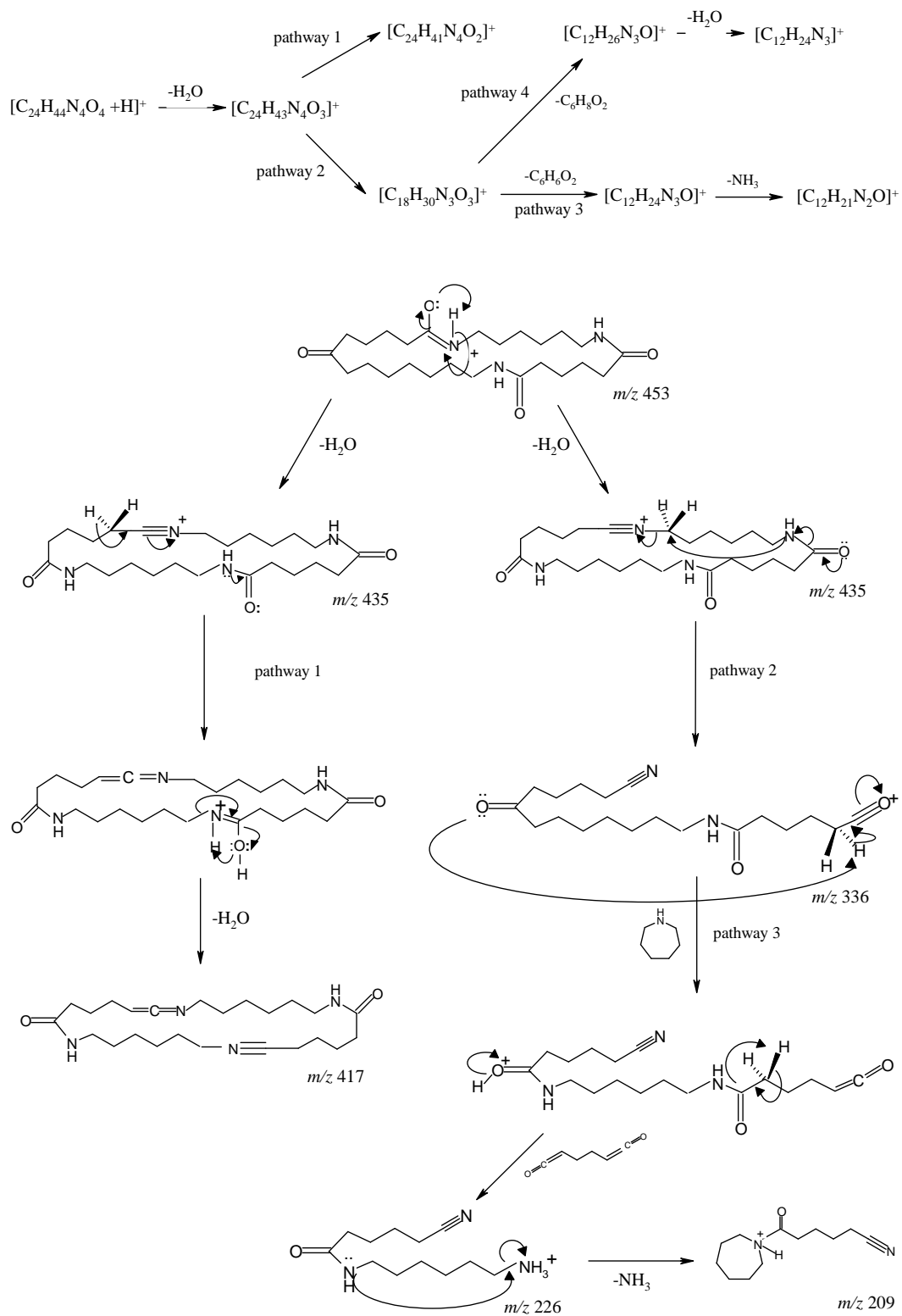


Figure 3.27: Fragment ions of cyclic nylon dimer. <sup>[33]</sup>

### 3.5 CONCLUSION

The stability of the photoinitiator, bis(2,4,6-trimethylbenzoyl)phenyl-phosphine oxide (BAPO), when stored in the dark and when exposed to the ambient light was studied. The investigation involved the assessment of bis(2,4,6-trimethylbenzoyl)phenylphosphine oxide, containing various additives, such as ferrocene, protonic and Lewis acids, using the newly developed LC-MS method.

LC-MS scans in both (+) ESI and (-) ESI modes and LC-MS/MS have proven to be powerful complementary techniques. LC-MS has been utilised in this work to characterise two important photodegradation products of a bis(2,4,6-trimethylbenzoyl)phenylphosphine oxide (BAPO), in a dosage formulation. For the neat samples of BAPO exposed to ambient light these degradation products were found to be  $m/z$  475 through reaction by 2,4,6 trimethylbenzoyl acid with phosphinoyl or phosphinoxy radicals. The second product with  $m/z$  357 is forming rationalised via a six –membered transition state for the product at  $m/z$  475 sodium adduct. It was found that addition of protonic acid (MSA) or ferrocene, to the samples protected from light did not change the rate of degradation and the signal of BAPO ( $m/z$  441) was still observed with high intensity. When Lewis acid,  $\text{BF}_3 \cdot 2\text{H}_2\text{O}$  was added to BAPO samples, the photoinitiator readily hydrolysis and gave the degradation products at  $m/z$  163 and 287. The hydrolysis of BAPO could occur by either nucleophilic attack at the carbonyl carbon or phosphorus atom. All compounds were identified based on the molecular weight and fragmentation profiles from LC-MS/MS data.

Additionally the possible source of contamination and interferences in LC-MS analysis of BAPO are describes in this Chapter. It was found that the signals of  $m/z$  453, 679 and 702 are the contamination products arising from Nylon 66 membrane filter.

**3.6 REFERENCES**

- [1] Ran, D., Ratnaswamy, G., Beierle J., Treuheit, M.J., Brems, D.N., Bondarenko, P.V., *Inter. J. of Biol. Macrom.*, **2009**, 44, 81.
- [2] Armenteros, M., Heinonen, M., Ollilainen, V., Toldra, F., Estevez, M., *Meat Sci.*, **2009**, 83, 104.
- [3] Sanz- Nebot, V., Benavente, F., Toro, I., Barbosa, J., *Anal. Chem. Acta*, **2004**, 521, 25.
- [4] Orioli, M., Aldini, G., Beretta, G., Facino, R.M., Carini, M., *J. Chromataogr. B*, **2005**, 827, 109.
- [5] Lovdahl, M., J., Prebe, S., R., *J. Pharm. Biom. Anal.*, **2000**, 23, 521.
- [6] Hernando, M.D., Petrovic, M., Fernandez- Alba, A.R., Barcelo, D., *J. Chromatogr. A*, **2004**, 1046, 133.
- [7] Fenli, S., Feng, W., Wei G., Huande, Li., *J. Chromatogr. B*, **2007**, 853, 364.
- [8] Rybak, M., E., Parker, D., L., Pfeiffer, Ch., M., *J. Chromatogr. B*, **2008**, 861, 145.
- [9] Wu, L., Hong, T.Y., Vogt, F., G., *J. Pharm. Biom. Anal.*, **2007**, 44, 763.
- [10] Pan, Ch., Liu F., Ji, Q., Wang, W. Drinkwater, D., Vivilecchia, R., *J. Pharm. Biom. Anal.*, **2006**, 40, 581.
- [11] Zwiener, Ch., Richardson, S.D., *Trends in Anal. Chem.*, **2005**, 24, 7.
- [12] Kumar Malik, A., Blasco, C., Pico, Y., *J. Chromatogr. A*, **2010**, 1217, 4018.
- [13] Jürgen, Gross, H., *Mass Spectrometry*, Springer-Verlag Berlin Heidelberg, **2004**.
- [14] de Hoffman, E., Stroobant, V., *Mass Spectrometry: principles and applications*, John Wiley & Sons Ltd., New York, **2007**.
- [15] Beu, S.C., Senko, M.W., Quiinn, J.P., McLafferty, F.W., *J. Am., Soc., Mass Spectrom*, **1995**, 4, 190.
- [16] Kelleher, N.L, Senko, M.W., Little, D, *J Am., Soc. Mass Spectrom*, **1995**, 6, 220.
- [17] European Agency for the Evaluation of Medicinal Products , (EMA), *Photostability Testing of New Active Substance and Medicinal Products*, ICH, Topic Q1B, EMA, London, **1995**.

- [18] Maquille, A., Habib Jiwan, J.L., *J. Photoch. Photobio. A*, **2009**, 205, 197.
- [19] Bansal, G., Singh, M., Jindal, K.C., Sing, S., *J. Pharm. Biom. Anal.*, **2008**, 48, 788.
- [20] Fiori, J., Gotti, R., Bertucci, C., Cavrini, V., *J. Pharm. Biom. Anal.*, **2006**, 41, 176.
- [21] Gosetii, F., Frascarolo, P., Mazzucco, E., Gianotti, V., Bottaro, M., Gennaro, M.C., Gennaro, *J. Chromatogr. A*, **2008**, 1202, 58.
- [22] Chen, T., Fu, F., Chen, Z., Li, D., Zhang, L., Chan, G., *J. Chromatogr. A*, **2009**, 1216, 3217.
- [23] Baxter, J.E., Davidson, R.S., Hageman, H.J., *Eur. Polym. J.*, **1988**, 24, 419.
- [24] Baxter, J.E., Davidson, R.S., Hageman, H.J., *Eur. Polym. J.*, **1988**, 24, 551.
- [25] Baxter, J.E., Davidson, R.S., Hageman, H.J., *Polymer*, **1988**, 29, 1569.
- [26] Baxter, J.E., Davidson, R.S., Hageman, H.J., Hakvoort, G.T.M., Overeem, T., *Polymer*, **1988**, 177, 1575.
- [27] Gatlik, I., Rzadek, P., Gescheidt, G., Rist, G., Hellrung, B., Wirz, J., Dietliker, K., Hug, G., Kunz, M., Wolf, J-P., *J. Am. Chem. Soc.*, **1999**, 121, 8332.
- [28] Sluggett, G.W., Turro, C., George, M.W., Koptuyug, I.V., Turro, N.J., *J. Am. Chem. Soc.*, **1995**, 117, 5148.
- [29] Kolczak, U., Rist, G., Dietliker, K., Wirz, J., *J. Am. Chem. Soc.*, **1996**, 118, 6477.
- [30] Ciba Specialty Chemicals Inc, *Photoinitiator for UV Curing*, **2003**.
- [31] Carl Stuart Limited, *LC-MS for Chromatographer*, Crawford Scientific, **2006**.
- [32] Bruker-HP Esquire, *LC Operations Manual*, Version 3.1.
- [33] Corrales, T., Catalina, F., Peinado, C., Allen, N.S., *J. Photoch. Photobio. A*, **2003**, 159, 103.
- [34] Pasto, D., Johnson, C., Miller, M., *Experiments and Techniques in Organic Chemistry*, Prentice-Hall, Inc., New Jersey, **1992**.
- [35] Silverstein, M.R., Webster, F.X., Kiemle, J.D., *Spectrometric Identification of Organic Compounds*, John Wiley & Sons Ltd., New York, **2005**.
- [36] Wilson, S.R., Yunhui Wu, *J. Am. Soc. Mass Spectrom.*, **1993**, 4, 596.
- [37] Dole, M., Mach, L.L., Hines, R.L., Mobley, R.C., Ferguson, L.P., Alice, M.B., *J. Chem. Phys.*, **1968**, 49, 2240.
- [38] Mach, L.L., Kralik, P., Rheude, A., Dole, M., *J. Chem. Phys.*, **1970**, 52, 4977.

- [39] Smith, M.R., Busch, L.K., *Understanding Mass Spectra A Basic Approach*, John Wiley & Sons Ltd., New York, **1999**.
- [40] Report by Ciba-Geigy Company, UK, **2009**.
- [41] Blake, S., Mayer, T., Mayer, M., Yang, J., *CHEMBIOCHEM*, Wiley-VCH Verlag GmbH & CO, Weinheim, **2006**.
- [42] Emmer, J., Plugger, M., Wahl, F., Sigma-Aldrich Company of Fluka, Switzerland, **2004**.
- [43] Buijs, J., Hagman, C., Hakansson, K., Richter, J.H., Hakansson, P., Oscarsson, S., *J Am. Soc. Mass Spectrom*, **2001**, *12*, 410.
- [44] Hart-Smith, G., Barner-Kowalik, Ch., *Polymer*, **2009**, *50*, 5175.
- [45] Williams, S., *J. of Chromatogr. A*, **2004**, *1052*, 1.
- [46] Regnault, C., Kano, I., Darbouret, D., Mabic, S., *J. of Chromatogr. A*, **2004**, *1030*, 289.
- [47] Ballistreri, A., *Encyclopedia of Polymer Science*, vol. V, John Wiley & Sons Ltd., New York, **1969**.
- [48] Carroccio, S., Concetto, P., Montaudo, G., *Macromolecules*, **2004**, *37*, 6037.
- [49] Tran, J.C., Doucette, A., *Am. Soc. of Mass Spectrom.*, **2006**, *17*, 652.
- [50] Önnerfjord, P., **2004**, [http:// www.abrf.org/index.cmf/list.msg/58765](http://www.abrf.org/index.cmf/list.msg/58765).

*Chapter Four*

*Determination of the Cure Mechanism and Stability of  
BAPO and TPO using LC-MS, NMR  
and  
Computational Calculation*

## 4.1 INTRODUCTION

### 4.1.1 Photochemistry of photoinitiators and photosensitisers

The photochemical crosslinking of coatings and inks by visible or ultraviolet light has become an established technology for many manufacturing applications<sup>[1-5]</sup>. Over the years, several types of photoinitiators have been developed to induce the polymerisation or photocrosslinking of acrylate systems.

*Photoinitiators*- cause photoinitiation by direct photoproduction of active intermediate -radicals, (and others cations or anions), see Figure 4.1<sup>[6, 7]</sup> that can interact with the acrylate group, inducing a chain growth polymerisation and eventually termination and crosslinking.

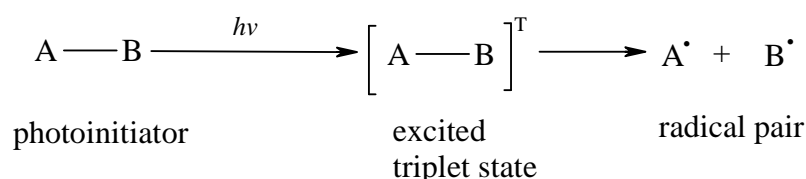
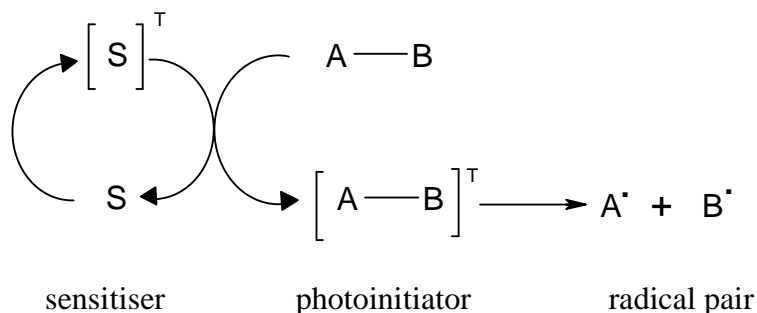


**Figure 4.1:**  $\alpha$ -cleavage of a photoinitiator via triplet state.<sup>[8, 9]</sup>

However, free radicals can not only be formed by direct irradiation of the photoinitiator [A-B], but also via triplet-triplet energy transfer reactions primarily involve triplet energy transfer from excited molecules- sensitiser (S) to the other reaction components (photoinitiator) to create triplet excited photoinitiator,<sup>[6]</sup> as illustrated in Figure 4.2. This occurs when the energy acceptor molecules [A-B], have triplet states of energy similar to that of energy of the donor molecule (sensitiser).





where:

S sensitiser, is a singlet ground state,

$[S]^T$  sensitiser, is a triplet state,

$[A-B]$  photoinitiator.

**Figure 4.2:**  $\alpha$ -cleavage of a photoinitiator via sensitiser. <sup>[8, 9]</sup>

The sensitiser cleavage of the photoinitiator is a significant issue since it allows the use of light with various wavelengths independent of the absorption spectrum of the photoinitiator. Such a shift of the absorption wavelength to a desired region could lead to an increase of the cure speed and efficiency.

#### 4.1.2 Types of photoinitiators

There are two fundamental categories of photoinitiators. In the first group, there are type I photoinitiators, that undergo a direct photo fragmentation process ( $\alpha$ - or less common  $\beta$ -cleavage) upon absorption of light yielding radicals capable of inducing the polymerisation. The second group is known as type II photoinitiators and the main process they undergo is a hydrogen atom abstraction from the environment, which may be the resin itself or solvent. <sup>[10, 11]</sup>

#### 4.1.2.1 Type I photoinitiators

$\alpha$ -cleavage photoinitiators are the most important type I photoinitiators due to their high reactivity and stability and the most recognised members in this group are shortly described below.

##### *Benzil ketals*

Benzil ketals represent a versatile family of photoinitiators. 2,2-dimethoxy-2-phenylacetophenone (DMPA or BDK) is one of the most important commercial photoinitiators in the  $\alpha$ -cleavage group. However, the major disadvantage of this compound is its considerable yellowing. BDK found its first commercial application in unsaturated polyester resin for wood coatings.

##### *$\alpha,\alpha$ -Dialkoxyacetophenones (DEAP)*

$\alpha,\alpha$ -Dialkoxyacetophenones are structurally similar to benzil ketals and DEAP is the most frequently used photoinitiator of this class. The excited state undergoes two competitive reactions<sup>[11]</sup> (Norrish types I and II). The type II reactions do not initiate the polymerisation process.

##### *Acylphosphine oxide*

Acylphosphine oxides were introduced some years ago as a new class of  $\alpha$ -cleavage photoinitiators, derived from DEAP by replacing C-H by P=O and alkoxy by aryl groups.

Acylphosphine oxides have the clear advantage of undergoing a fast photolysis which generates very reactive free radicals. They have proved to be more efficient in a number of systems where conservative photoinitiators lag behind, for example the photocuring of pigment coatings. Considering their enhanced performance (illustrated in Figure 4.3) it is expected that acylphosphine oxides will be increasingly

used in UV-curable formulations in a growing number of industrial applications of this advanced technology.

The photochemistry and properties of acylphosphine oxide were discussed in Chapter 2, in sections 2.1.1 and 2.1.2.

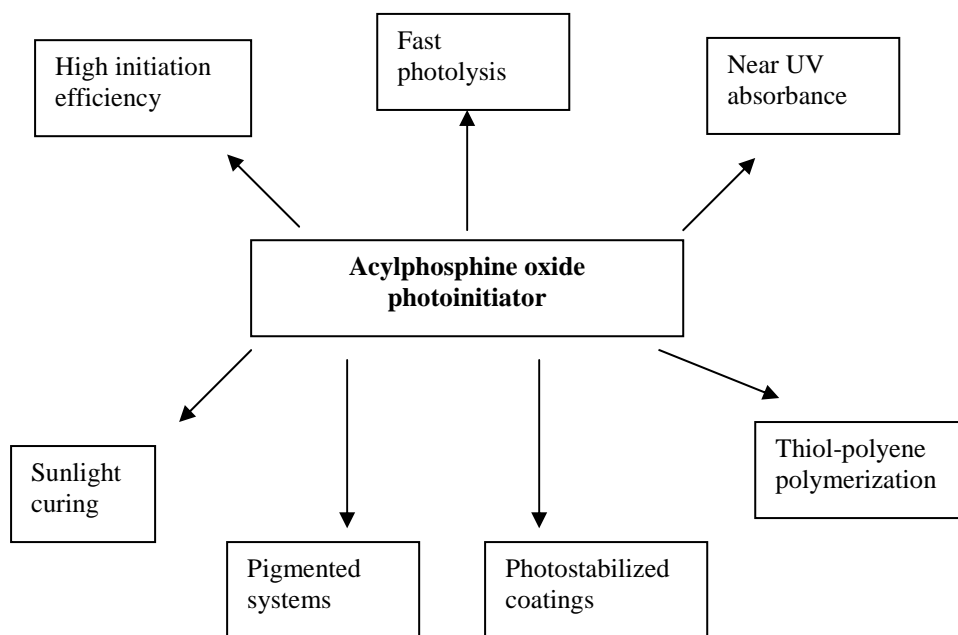


**Figure 4.3:** Performance of acylphosphine oxide photoinitiators in UV –radiation curing. <sup>[12]</sup>

#### 4.1.2.2 Type II photoinitiators

A diverse range of bimolecular photoinitiators has been used in the curing of pigmented and clear systems. Tertiary amines are typically used as coinitiators, since they react as oxygen scavengers and thus help to overcome oxygen inhibition.

*Benzophenones (BP)*

Benzophenone and its derivatives are bimolecular photoinitiators mainly used in manufacturing due to their low cost and regardless of their relatively low reactivity and stability of cured films. BP combined with tertiary amines is universally used in blends with other photoinitiators.

## **4.2 SCOPE OF RESEARCH**

In this Chapter ESI-MS and NMR spectroscopy are used as the main analytical techniques for the analysis of stability and photodegradation products of two photoinitiators: BAPO and TPO. The results are acquired at different conditions of light exposure. The potential cure mechanism of photoinitiators is investigated by computational studies.

## 4.3 MATERIALS AND METHODS

### 4.3.1. Instrumentation and conditions

#### 4.3.1.1 *Liquid chromatography-Mass spectrometry*

The MS and LC-MS system is described in Chapter 3 in section 3.3.1.1. The HPLC system for LC-UV analysis consisted of a binary pump Varian Pro Star 210, a photodiode array (PDA) detector and an autosampler (Varian Pro Star 410). The MS and LC-MS studies were carried out using positive as well as negative electrospray ionisation ((+) ESI and (-) ESI) modes on a Varian 500 MS ion trap. The operating conditions for the MS scan of cyanoacrylate in (+) ESI mode was optimised as follows: capillary exit offset: 55.0 V, collision cell RF 55%, nebuliser pressure 30 psi, dry gas 8.01 L min<sup>-1</sup>, and dry temperature 365° C. The operating conditions for MS of cyanoacrylate in (-) ESI mode were the same as in (+) ESI mode except the drying temperature was set at 325° C. The MS/MS scans of cyanoacrylate and LC-MS scans of all products were recorded in the range 100–1300 *m/z*.

#### 4.3.1.2 *Nuclear magnetic resonance*

NMR experiments were recorded at 400 MHz on Bruker ACF-400 series spectrometer. Typical proton NMR experiments were performed over the spectral range 0-8 parts per million (ppm) by acquiring 16384 total points using quadrature detection. Eight to thirty two scans were sufficient to give adequate signal to noise ratio for proton experiments. Carbon experiments were performed over the range 0-240 ppm with proton decoupling employed. Phosphorus

experiments were performed over the spectral range -200-200 ppm with proton and carbon decoupling employed and 85% phosphoric acid used as an internal standard. Gradient correlation spectroscopy (COSY) experiments were acquired with 2 scans per increment and 512 increments using the same 0-8 ppm spectral width as that used for proton experiments. Heteronuclear multiple-quantum coherence experiments (HMQC) were run gradient enhanced employing 8 scans per increment and 512 increments.

#### ***4.3.1.3 Computational calculations***

The computational calculation was performed using the Gaussian 03W software package. The structures of both photoinitiators and radicals were generated with the help of *GaussView* software.

#### **4.3.2 Chemicals**

Bis(2,4,6-trimethylbenzoyl)phenylphosphine oxide (Irgacure 819 or BAPO) and (2,4,6-trimethylbenzoyl)diphenylphosphine oxide (TPO or Darocur) photoinitiator samples were all obtained from Henkel Technologies (Irl). All other chemicals were of reagent grade and prepared as described in Chapter 3 in section 3.3.2.

### 4.3.3 Procedures

#### 4.3.3.1 Preparation of mobile phase

The preparation of mobile phase was performed as described in Chapter 3 in section 3.3.3.1.

#### 4.3.3.2 Preparation of standard solution for LC-MS

A stock (0.5% BAPO or TPO) solution of each analyte was prepared using acetonitrile as a solvent. Standards of known concentration were prepared in volumetric flasks by dilution of the stock with acetonitrile and making the volume to 100 mL. One set of samples was prepared in amber volumetric flasks and stored in a dark room; the other set was prepared in clear volumetric flasks and exposed to the ambient light at room temperature. The samples were injected directly into the LC-MS system.

#### 4.3.3.3 Preparation of standard solution for NMR

Typical experiments involved dissolving 3-5 mg of BAPO or TPO in acetonitrile- $d_3$  and obtaining the NMR spectrum.



## 4.4 RESULTS AND DISCUSSION

### 4.4.1 Mass fragmentation of TPO

The parent ion of TPO (MW= 348) provided a signal at  $m/z$  371 was the sodium adduct  $[M+ Na]^+$ , owing to the presence of sodium ion in ACN solution employed as the mobile phase.

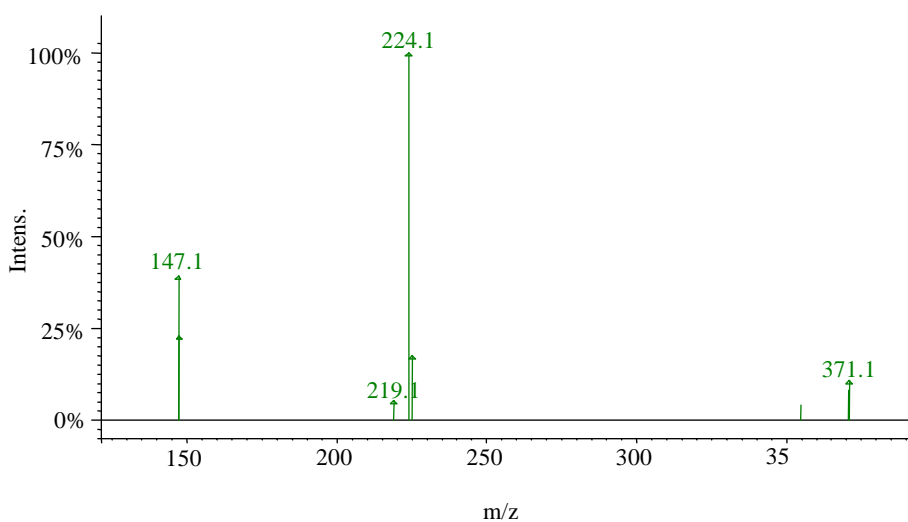
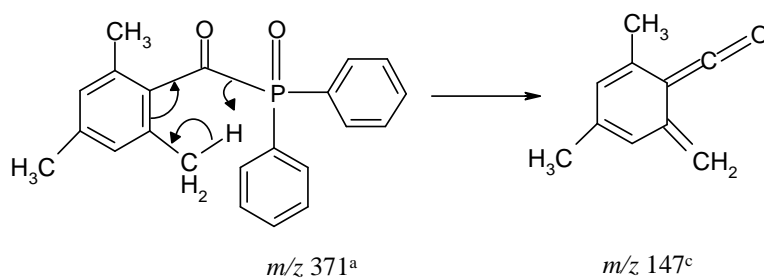


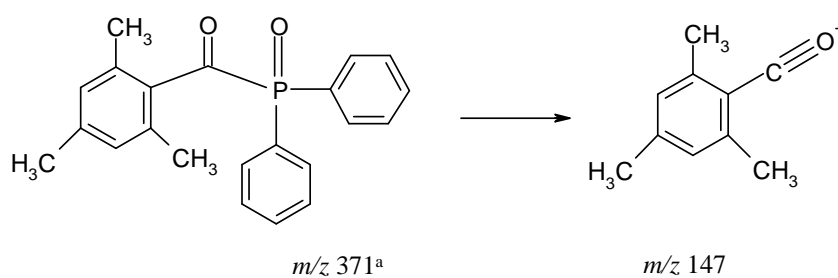
**Figure 4.4:**  $MS^2$  spectrum of TPO from  $m/z$  371.

The  $MS^2$  spectrum of TPO reveals product ions at  $m/z$  values of 147 and 224, see Figure 4.4. Taking the potential reaction schemes supplied by Henkel (Irl.) the following mechanism is proposed for the TPO as illustrated in Figure 4.5.

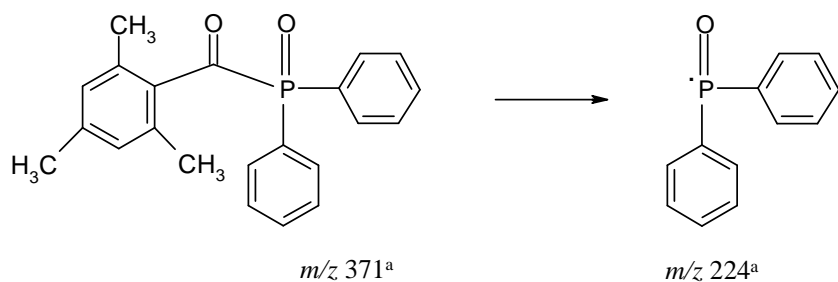
a)



b)



c)

<sup>a</sup>[M+Na]<sup>+</sup><sup>c</sup>[M+H]<sup>+</sup>**Figure 4.5:** Mechanisms of TPO fragmentation.

The formation of  $m/z$  147 from TPO can be rationalised via a six-membered transition state (see Figure 4.5a) or by another possible mechanism shown in Figure 4.5 b which generated easily the 2,4,6-trimethylbenzoyl ion. The base peak at  $m/z$  224 in the MS<sup>2</sup> spectrum of TPO might possibly be formed by loss of 147 Da from the precursor ion

at  $m/z$  371. The  $MS^2$  of product ion  $m/z$  224 reveals a product ion  $m/z$  143 which could not be rationalised.

#### 4.4.2 TPO degradation product determination by LC-MS

The (-) LC-MS spectrum of TPO (Figure 4.6) showed one ion at  $m/z$  217 after 24h for samples exposed to ambient light.

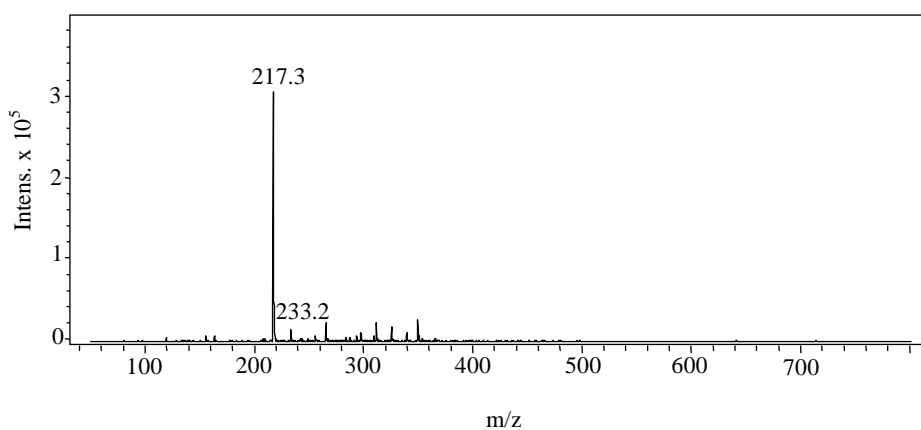


**Figure 4.6:** Mass spectrum of TPO after 24 h (negative mode).

The formation of the degradation product ( $m/z$  217) could be explained by the reaction between two phosphinoyl radicals which generated an intermediate product (path 1). For the second step: the nucleophilic attack at the phosphorus atom (path 2) formed the diphenylphosphinic acid which deprotonated and formed the ion at  $m/z$  217 as illustrated in Figure 4.7.

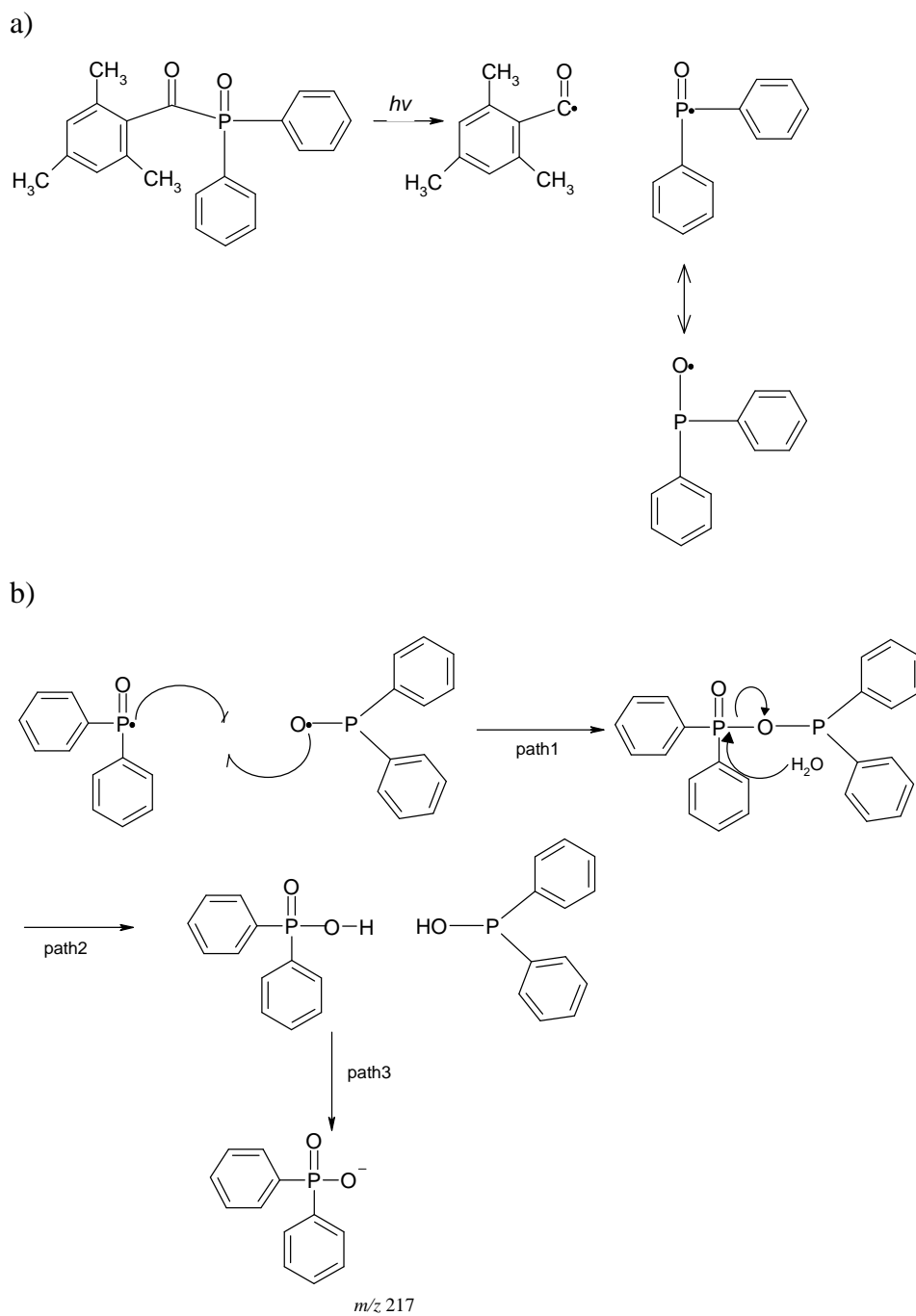


**Figure 4.7:** a) resonance structures of diphenylphosphinoyl radicals; b) proposed degradation pathway of degradation product  $m/z$  217.

#### 4.4.3 BAPO and TPO degradation products determination by LC-MS

The stability study for both photoinitiators BAPO and TPO was performed from  $t = 0$  to 24 h and a comparison was made between samples maintained in the dark and ambient light. From the ESI-MS study it was determined that photodegradation of BAPO and TPO did not occur for samples kept in dark as shown in Figure 3.6 (TIC in BAPO for samples kept in dark).

When both photoinitiators were exposed to ambient light after 24 h, five signals were clearly observed for BAPO (illustrated in Figure 4.8). The ions at  $m/z$  295, 333, 357 and 475 were identified as photodegradation products of BAPO and were reported in section 3.4.3.

For TPO samples after the same time two signals were observed. One of these signals at  $m/z$  441 with very low intensity, was identified as a photodegradation product as shown in Figure 4.9. Another signal at  $m/z$  371 was (2,4,6-trimethylbenzoyl)diphenylphosphine oxide, suggesting that TPO is a more stable photoinitiator than BAPO and even when exposed to ambient light did not degrade completely after 24 h.

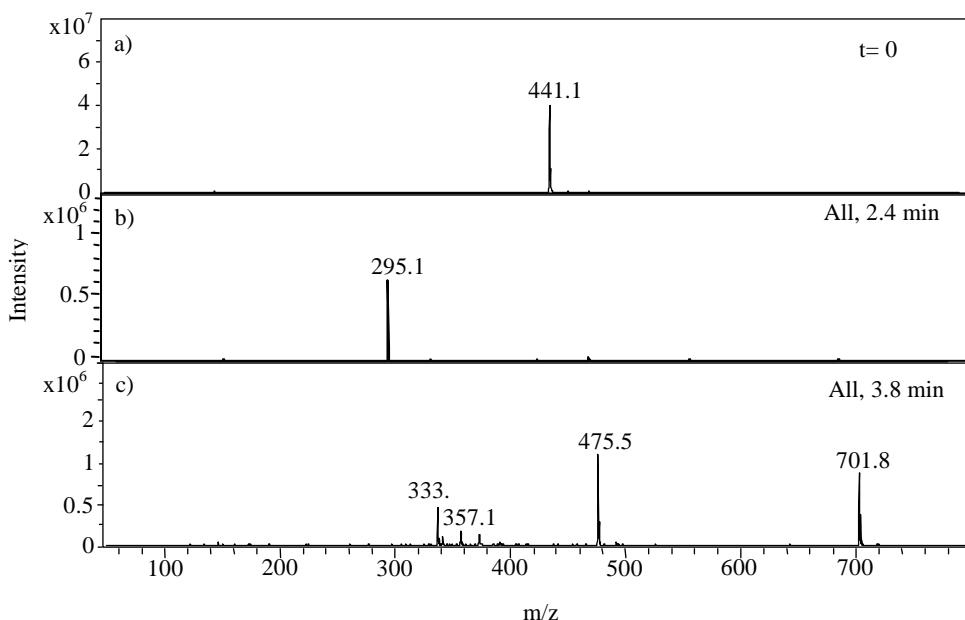


**Figure 4.8:** (+) ESI-MS mass spectrum of BAPO, a)  $t = 0$ , b) and c) spectrum of degradation products of BAPO after 24 h for samples exposed to ambient light.

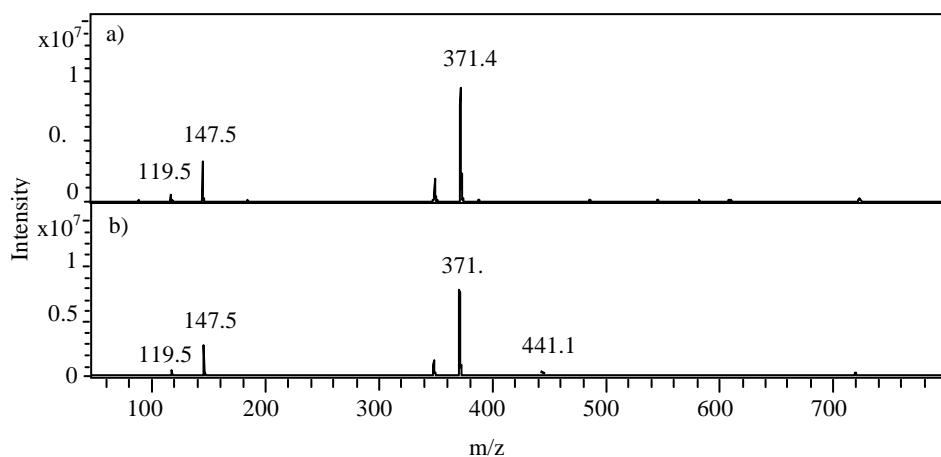
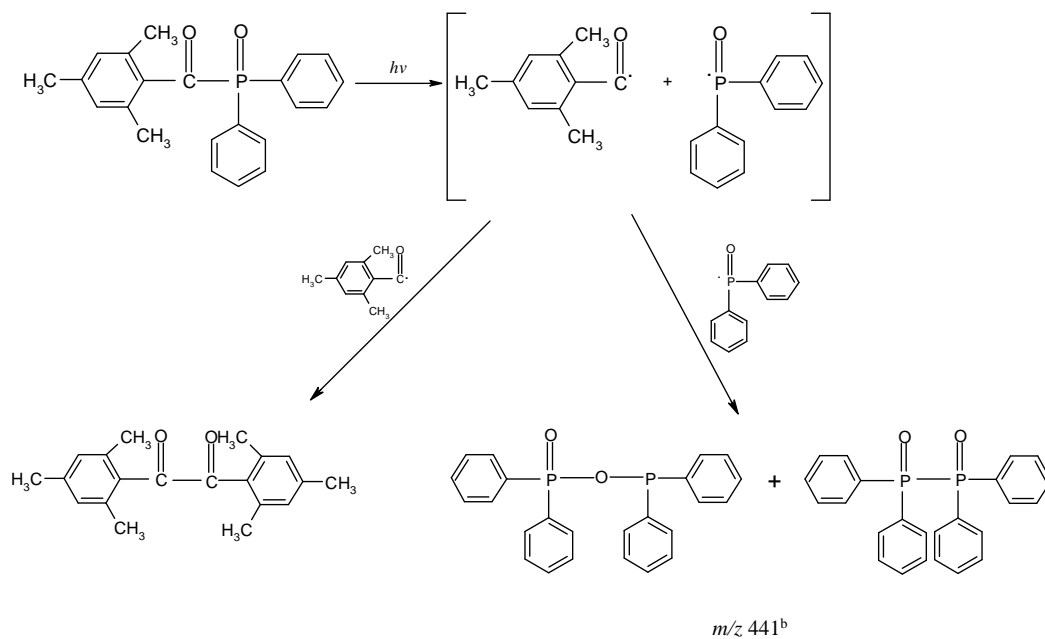


**Figure 4.9:** (+) ESI- MS mass spectrum of TPO, a)  $t= 0$  and b) TPO spectrum after 24 h for samples exposed to ambient light.

The photodegradation product of TPO at  $m/z$  441 suggested that two possible types of products could be obtained by recombination of these radicals and they are compounds that possess a P-P or P-O bond as illustrated in Figure 4.10.



<sup>b</sup>[M+K]<sup>+</sup>

**Figure 4.10:** Proposed photodegradation products of TPO.

A comparison between the stabilities of TPO and BAPO was done and as it is presented in Figure 4.11, it was found that TPO samples degraded just partially after 24 h, whereas the BAPO samples were decomposed completely during the same period of time as illustrated in Figure 4.11. This indicates that TPO photoinitiators are more stable than BAPO, also the pathway of the photodegradation products formed are different for both photoinitiators.

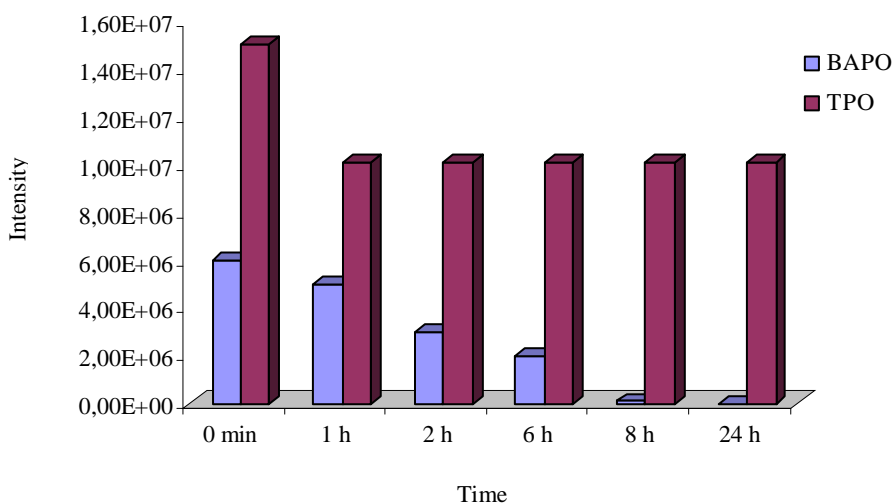


**Figure 4.11:** Graphical illustration of degradation for BAPO and TPO photoinitiators for samples exposed to ambient light.

#### 4.4.4 NMR analysis

The ESI-MS results indicated that degradation of BAPO and TPO only occurred in the samples exposed to ambient light but for the same time period TPO was more stable than BAPO. It was also found that for both photoinitiators the complete degradation was not observed after 24 h in dark conditions. In this section the NMR technique was used to further confirm degradation products of BAPO and TPO samples stored in ambient light conditions.

##### 4.4.4.1 $^1\text{H}$ and $^{13}\text{C}$ NMR study of stability of BAPO and TPO

Following ESI-MS studies, studies were carried out to confirm the stability of BAPO and TPO using NMR experiments.

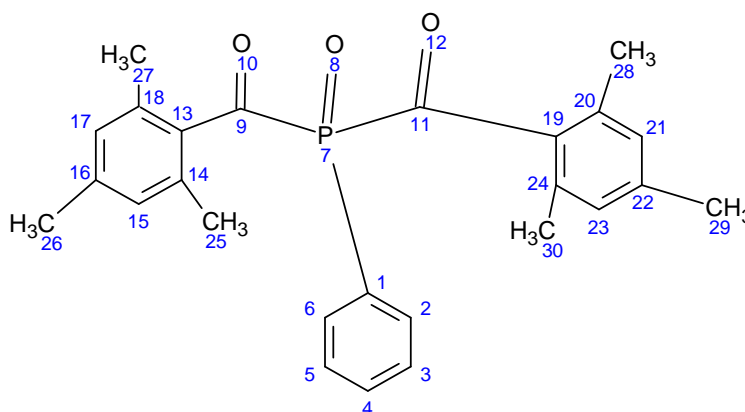


Initially, complete  $^1\text{H}$  and  $^{13}\text{C}$  NMR was investigated after 24h. The NMR spectrum for both photoinitiators did not occur for samples kept in dark but for samples exposed to ambient light after the same time the  $^1\text{H}$  and  $^{13}\text{C}$  NMR spectrum was unsuccessful to interpretation (see Figure 4.12 and 4.13) Secondly, to help interpret the  $^1\text{H}$  and  $^{13}\text{C}$  NMR spectrum, the proton-proton connectivities were established using combination of COSY, HMQC (Heteronuclear Multiple Quantum Correlation) and HMBC (Heteronuclear Multiple Bond Correlation).

The individual proton-proton connectivities were recorded in a gradient-enhanced COSY experiment; the identity of carbon directly attached to each proton is read from the HMQC map, and HMBC data gives information about carbon –proton couplings and longer range couplings (2- 3 bond coupling).

Finally, it was found that only the  $^{31}\text{P}$  NMR proved useful for investigating the stability of BAPO and TPO.

The  $^1\text{H}$  NMR spectrum of BAPO,  $t= 0$ , (see Figure 4.12) and after 24h (see Figure 4.13) could be divided into four main different domains.



Atom number	$^1\text{H}$	
1		
<b>2,6</b>	7.52 (td, $J=7.71, 3.28$ Hz, 2 H)	phenyl protons
<b>3,5</b>	7.80 - 7.92 (m, 2 H)	phenyl protons
<b>4</b>	7.61 - 7.71 (m, 1 H)	phenyl protons
9,11		
13,19		
14,18,20,24		
<b>15,17,21,23</b>	6.90 (s, 4H)	benzoyl protons
16,22		
<b>25,27,28,30</b>	2.12 (s, 4xCH <sub>3</sub> )	three methyl proton in <i>ortho</i> position
<b>26,29</b>	2.28(s, 2xCH <sub>3</sub> )	three methyl proton in <i>para</i> position

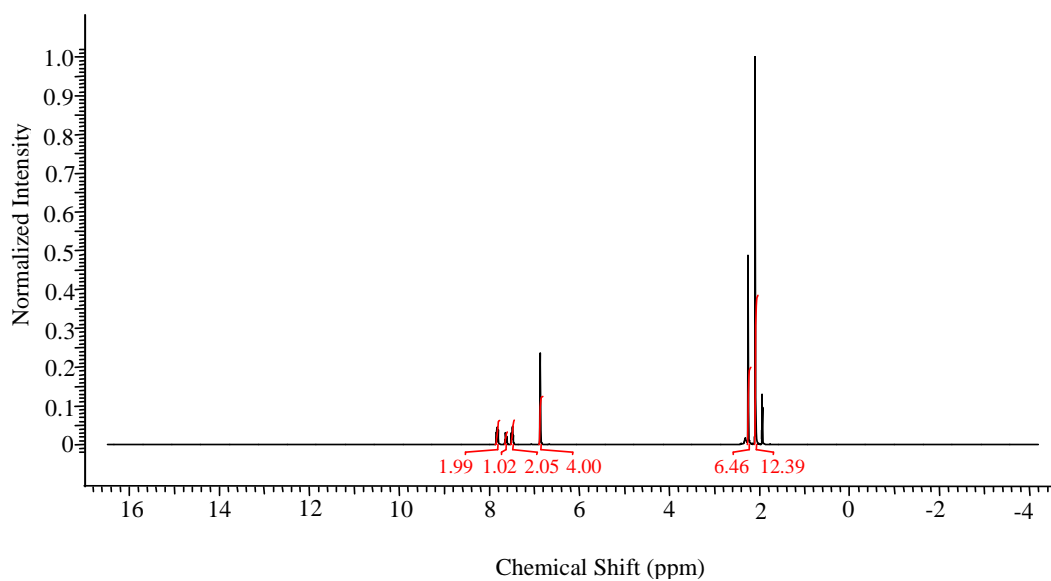


**Figure 4.12:**  $^1\text{H}$  NMR spectrum of BAPO in  $\text{acetonitrile-}d^3$ .

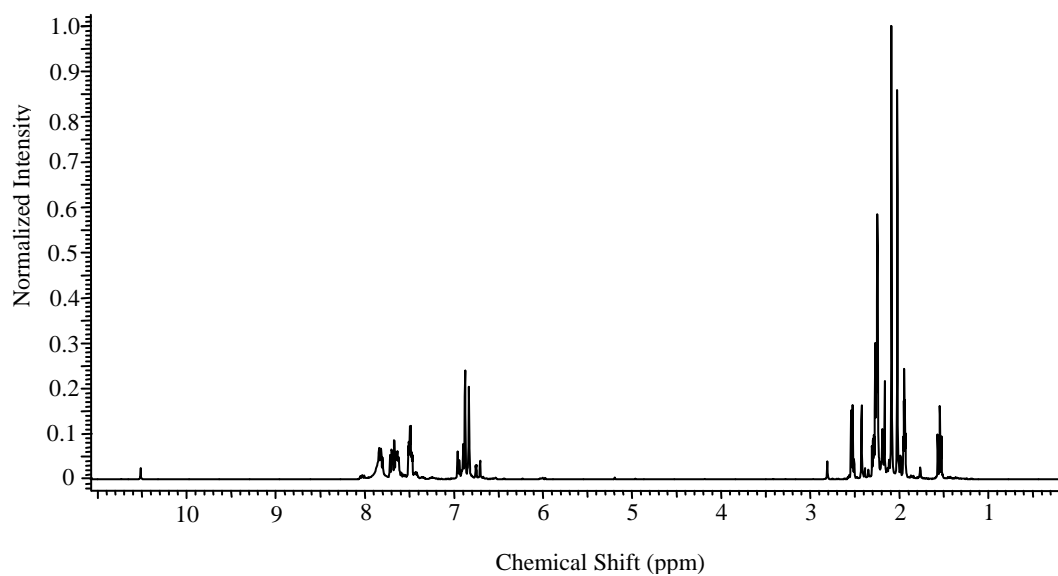
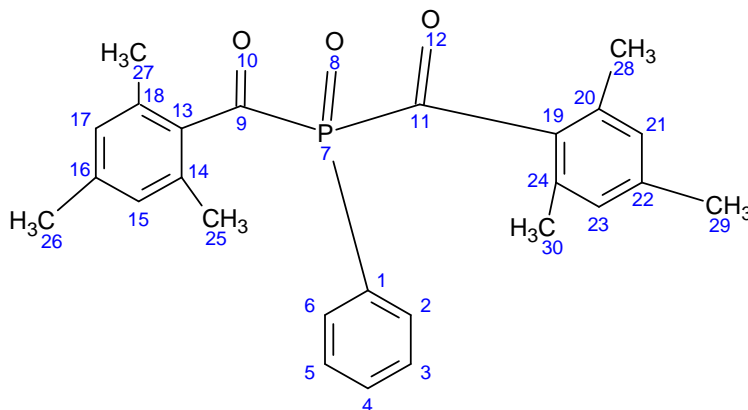
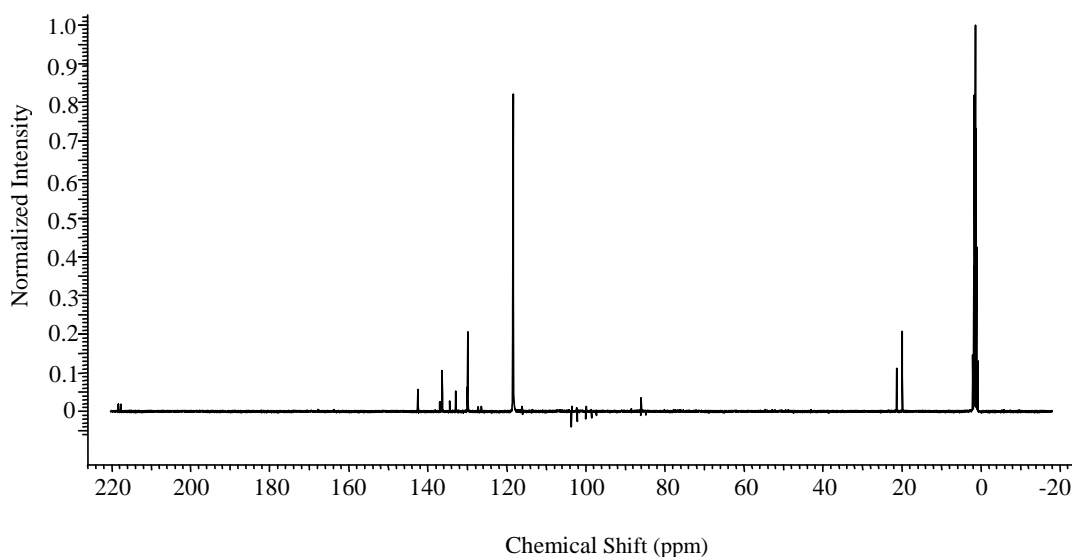


**Figure 4.13:**  $^1\text{H}$  NMR spectrum of BAPO in  $\text{acetonitrile-}d^3$  for samples exposed to ambient light after 24 h.

The  $^{13}\text{C}$  NMR spectrum (Figure 4.14) was complementary to the  $^1\text{H}$  NMR spectrum and could be divided into five main different domains.

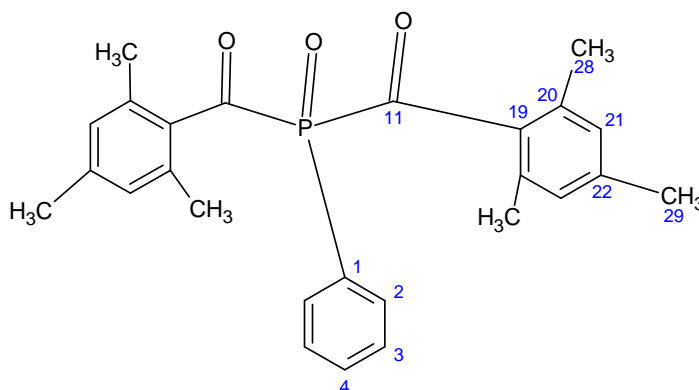


Atom number	$^{13}\text{C}$	
<b>1</b>	126.90 (d, $^1J_{\text{C,P}}=76.1$ Hz)	phenyl carbons
<b>2,6</b>	129.91 (d, $^2J_{\text{C,P}}=10.8$ Hz)	phenyl carbons
<b>3,5</b>	132.74 (d, $^3J_{\text{C,P}}=8.8$ Hz)	phenyl carbons
<b>4</b>	134.50 (d, $^4J_{\text{C,P}}=2.9$ Hz)	phenyl carbons
<b>9,11</b>	215.89 (d, $^1J_{\text{C,P}}=60$ Hz)	carbonyl carbon
<b>13,19</b>	136.85 (d, $^2J_{\text{C,P}}=41.7$ Hz)	benzoyl carbon
<b>14,18,20,24</b>	142.55	benzoyl carbon
<b>15,17,21,23</b>	129.91	benzoyl carbon
<b>16,22</b>	136.20	benzoyl carbon
<b>25,27,28,30</b>	19.65	methyl proton in <i>ortho</i> position
<b>26,29</b>	21.49	methyl proton in <i>para</i> position



**Figure 4.14:**  $^{13}\text{C}$  NMR spectrum of BAPO in acetonitrile- $d^3$ .

The HMBC spectrum (Figure 4.15) was used to study the two or three bond coupling correlations, where the HMQC spectrum (see Figure 4.16) gives information's about proton- carbon couplings, proton was directly bonded to the carbon.



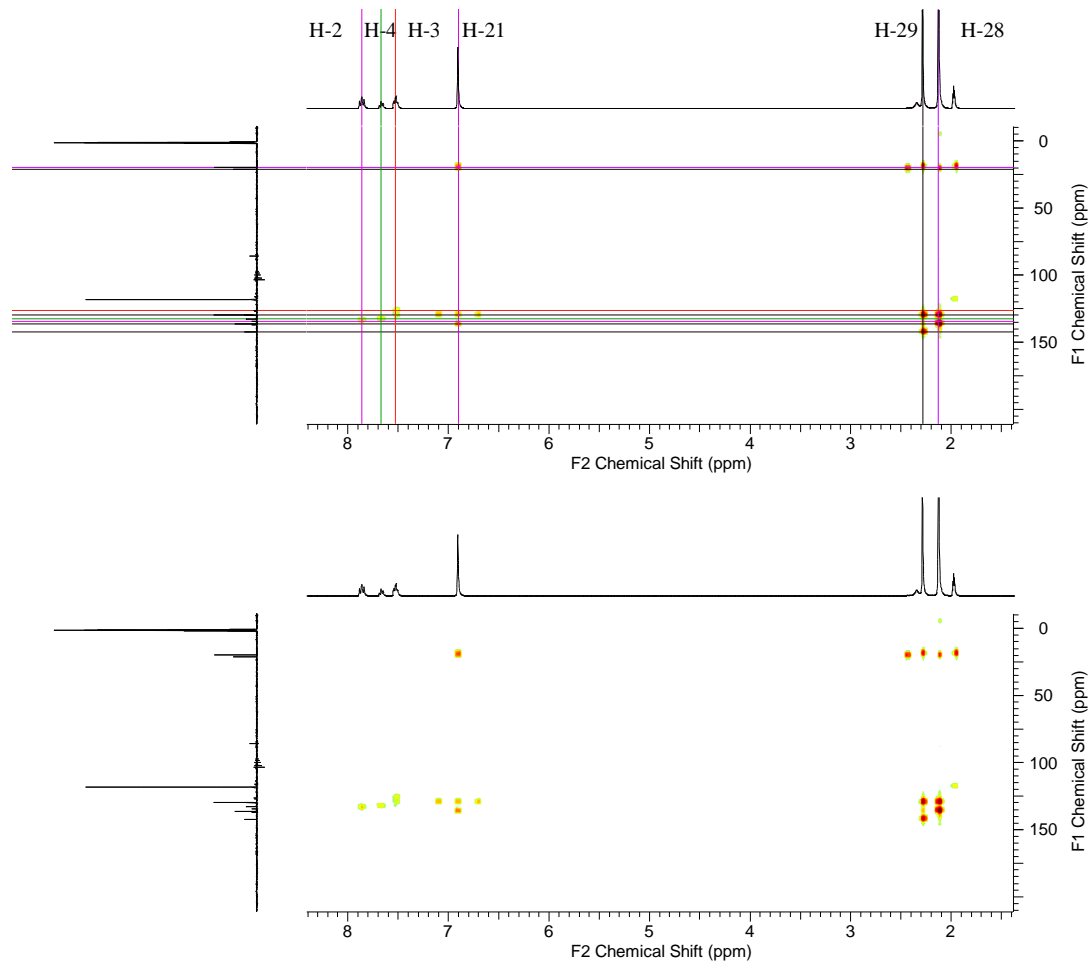


**Figure 4.15:** HMBC spectrum of BAPO in acetonitrile- $d^3$ .

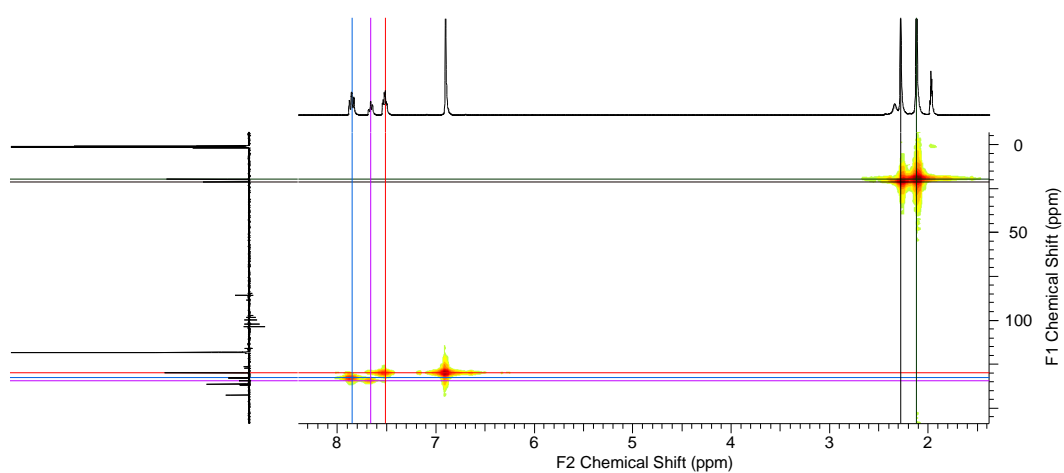


**Figure 4.16:** HMQC spectrum of BAPO in acetonitrile- $d^3$ .

#### 4.4.4.2 $^{31}\text{P}$ NMR stability study of BAPO and TPO

Following the results of early investigations (see section 4.4.2) into the stability of BAPO and TPO involving  $^1\text{H}$  and  $^{13}\text{C}$  NMR, further analysis was based on information obtained from  $^{31}\text{P}$  NMR experiments. Assuming that each product of degradation contains one phosphorus atom in the molecule the LC-MS results suggested three plausible photodegradation products containing one phosphorus atom. The  $^{31}\text{P}$  NMR spectra of BAPO for authentic samples and samples exposed to ambient light after two, six and 24 h are depicted in Figure 4.17.

A comparison of the spectra for authentic samples of BAPO and TPO reveal that both photoinitiators exhibit resonances in the same range (0-50 ppm) in  $^{31}\text{P}$  NMR typical of pentavalent phosphorus. Only one phosphorus resonance was observed at 7.03 ppm in the authentic sample of BAPO as illustrated in Figure 4.17. Similar only one signal at 13.10 ppm was observed in the  $^{31}\text{P}$  NMR spectrum of authentic TPO as shown in Figure 4.18.

For BAPO the resonance at 7.03 ppm is representative of pentavalent phosphorus (P=O) covalently bonded to carbon with no (P-O) single bonds. <sup>[13]</sup> After 2h for BAPO samples exposed to ambient light another two signals with very low intensity were observed in the  $^{31}\text{P}$  NMR spectrum. These two resonances at 16.10 ppm and 19.45 ppm probably arise from phosphorus atoms of two different photodegradation products. From inspection of the  $^{31}\text{P}$  NMR spectrum of BAPO it was apparent that the signal at 16.10 ppm became much more intense after each 2h interval compared with the signal at 19.45 ppm. This could explain the possible structure of the photodegradation products. The resonance at 16.10 ppm may correspond to one of the photodegradation products of BAPO at  $m/z$  475 which contains a pentavalent phosphorus with a P=O double bond and a P-O single bond related to a BAPO photodegradation product reported in the literature  $^{31}\text{P}$  NMR (15.78 ppm). <sup>[13]</sup> The resonance at 19.45 ppm may correspond to another pentavalent phosphorus species, ion  $m/z$  357, similar to an unstable photoproduct of BAPO reported by Kolczak and co-workers ( $^{31}\text{P}$  NMR, 20 ppm). <sup>[13]</sup> Also it was found that two new phosphorus resonances (16.10 and 19.45 ppm), after 24 h were much more intense than after two and six hours. However for the same time frame the signal at 7.03 ppm was not

observed, so it was postulated that the BAPO samples exposed to ambient light degraded completely after 24 h. Analogous observations was made analysing by ESI-MS spectra after 24 h for samples exposed to ambient light. The best verification of the photodegradation product of BAPO would be to isolate the products with retention time 2.4 minutes and 3.4 minutes, (see Figure 3.6) and analyse them by  $^{31}\text{P}$  NMR.

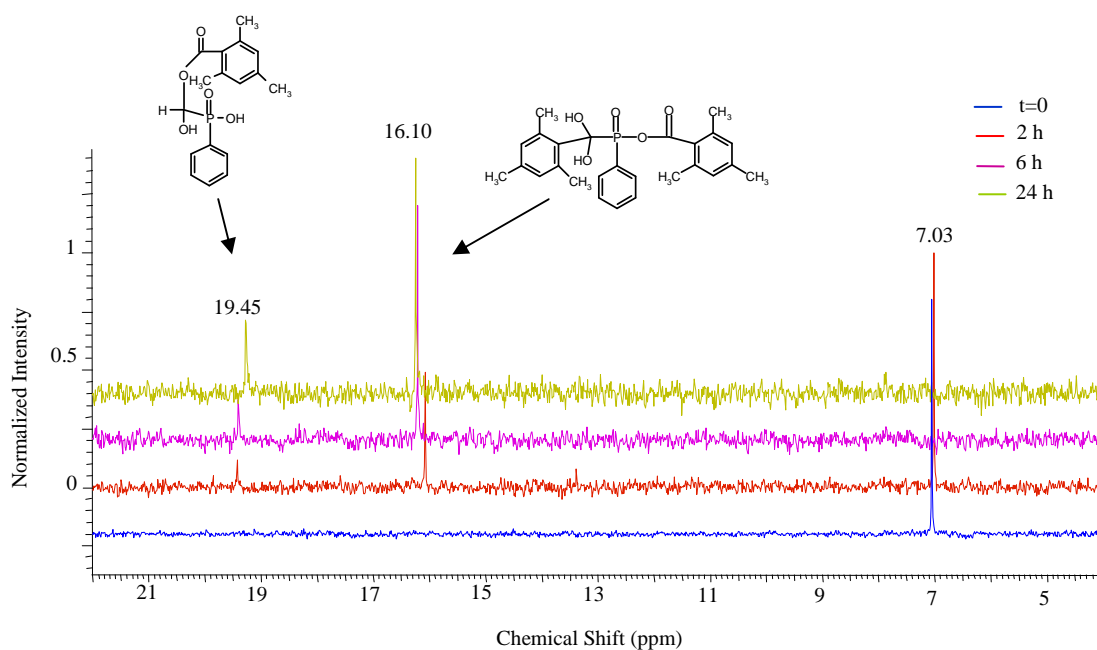


**Figure 4.17:**  $^{31}\text{P}$  NMR of BAPO in acetonitrile- $d_3$  for samples exposed to ambient light after  $t=0$ , 2 h, 6 h and 24 h.

In contrast in the  $^{31}\text{P}$  NMR spectrum of TPO after 2 and 6 h only one phosphorus resonance at 13.95 ppm was observed. Lastly, after 24 h, a new phosphorus resonance in TPO spectrum at 29.70 ppm was observed which possibly corresponds to photodegradation product. Also a signal at 13.10 ppm characteristic for the starting materials was observed. It means that TPO didn't degrade completely during this time. The  $^{31}\text{P}$  NMR results were thus consistent with ESI-MS experiments. ESI-MS experiments suggested that two types of degradation products at  $m/z$  441 are possible.

One of these products possesses a P-P bond and the second one P-O bond as illustrated in Figure 4.10. The two symmetric phosphorus atoms in this structure give rise to one resonance signal. For the structure with P atoms bridged by an oxygen atom two likely resonance signals could be observed, one from the trivalent phosphorus between at 100-130 ppm and another resonance between 0-50 ppm could be observed. The comparison of the information for both methods showed a more probable structure of degradation product of TPO containing P-P bond.

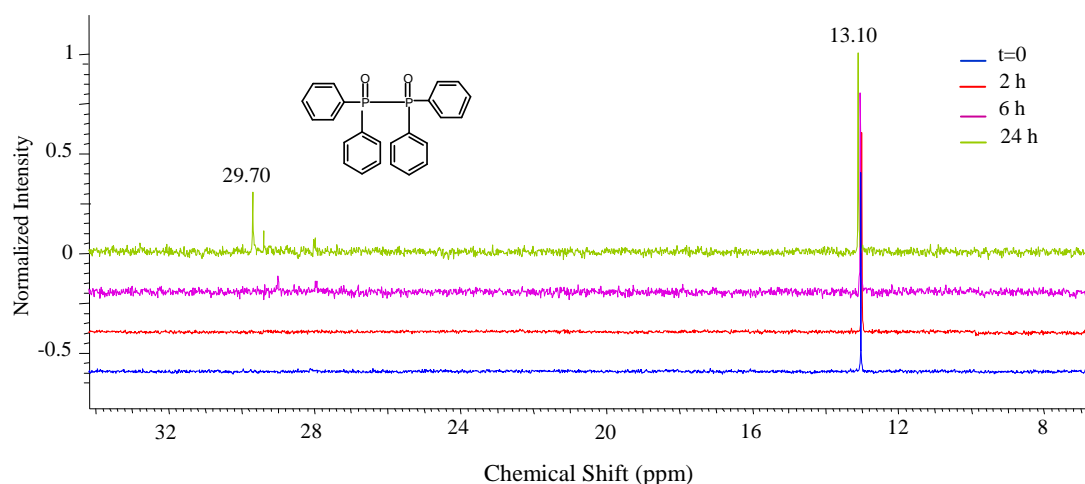


**Figure 4.18:**  $^{31}\text{P}$  NMR of TPO in acetonitrile- $\text{d}_3$  for samples exposed to ambient light after  $t=0$ , 2 h, 6 h and 24 h.

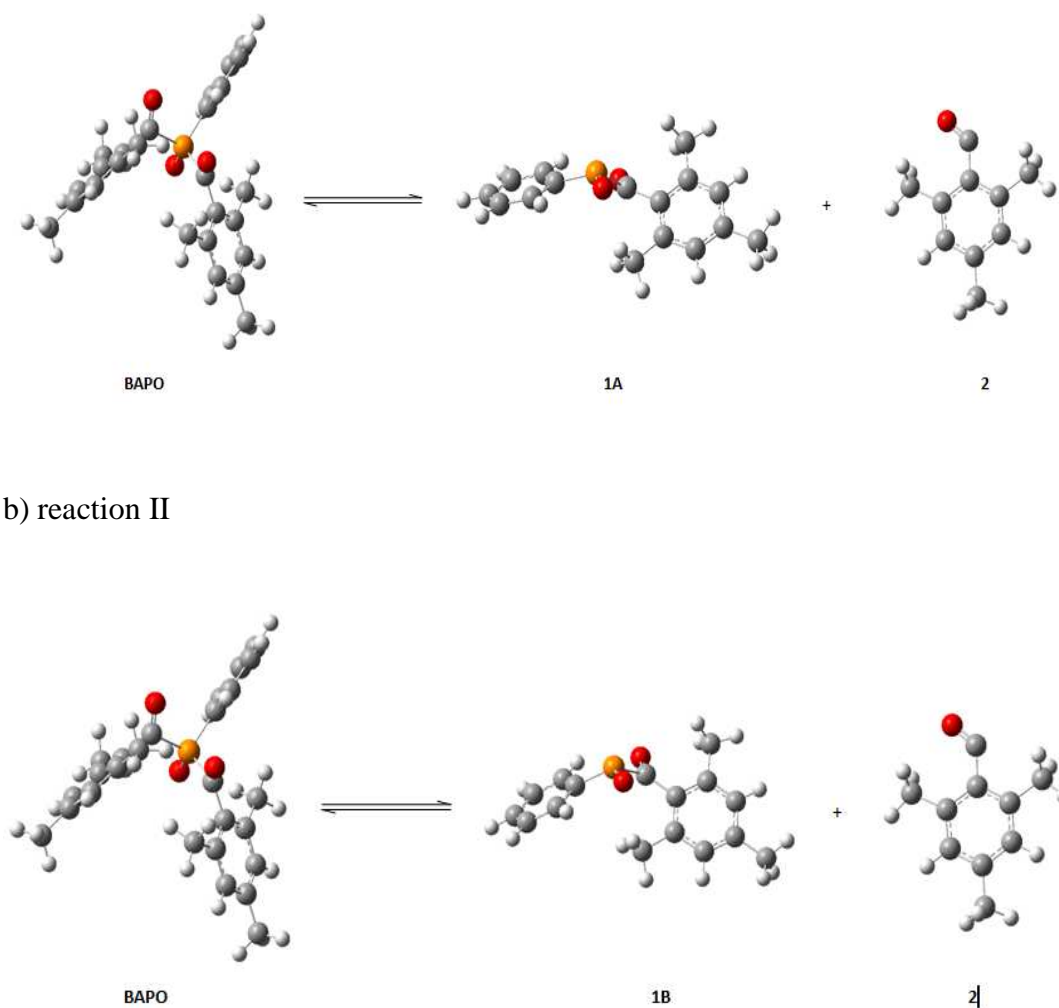
#### 4.4.5 Computational studies

From the previous studies two possible pathways for cure mechanism of BAPO and one for TPO were postulated. For the first reaction of BAPO it was suggested that two species, benzoyl radical and phosphinoyl diradical, were formed as shown in Figure 3.2a. The second reaction generated one benzoyl radical and the 2,4,6-trimethylbenzoylphenylphosphine oxide radical as illustrated in Figure 3.2 b. For both reactions the same products were observed- the benzoyl radical and two different of phosphinoyl radicals for each reaction.



Furthermore, study of the BAPO and TPO cure mechanism was modelled with Gaussian 03 using the B3LYP functional. The optimised equilibrium geometry of BAPO, TPO and radicals were obtained at the B3LYP/6-31G+ (d) level using the default convergence criteria. To ensure that the geometry optimised conformations are at local minima, vibrational frequencies were calculated using an analytical Hessian, which provided zero point vibrational energies, enthalpies, and entropies. Based on the results a three pathway reaction of cure mechanism of BAPO was proposed. The first and second reactions generated the same benzoyl radicals and 2,4,6-trimethylbenzoylphenylphosphine oxide radical as illustrated in Figure 4.19 (a) and (b), but the reaction energies for both reactions are insignificantly different as listed in Table 4.1. The  $\Delta G$  for the first reaction is highest a 1.73 kcal/mol compared to the reaction second, suggesting two different configurations of the 2,4,6-trimethylbenzoylphenylphosphine oxide radicals which has also been reported in the literature.<sup>[14]</sup> In 2001 Spichty and Turro, published a paper with calculated rational profiles for the C(O)-P(O) bond for acylphosphine oxide, in the ground ( $S_0$ ) and excited states ( $S_1$  and  $T_1$ ) of the model system using B3LYP and RCIS functional.<sup>[14]</sup>

a) reaction I



b) reaction II

**Figure 4.19:** Proposed cure mechanism of BAPO at the B3LYP/6-31G+ (d) level: a) and b) to produce (1A) (1B)- 2,4,6-trimethylbenzoylphenylphosphine oxide radical and (2) benzoyl radical.

On the other hand, the third reaction of cure mechanism which generated the phosphinoyl radical (see Figure 4.20) possesses over three times higher energy in comparison with the first and second reaction as illustrated in Table 4.1.

a) reaction III

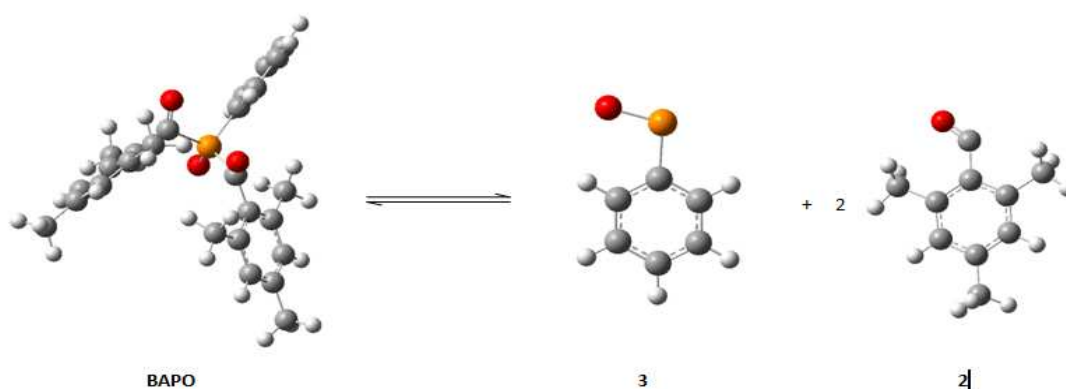


**Figure 4.20:** Proposed of cure mechanism of BAPO at the B3LYP/6-31G+ (d) level, to produce (3)-phosphinoyl radical and (2)-benzoyl radical.

**Table 4.1:** Reaction energies of BAPO at the B3LYP/6-31G+ (d) level.

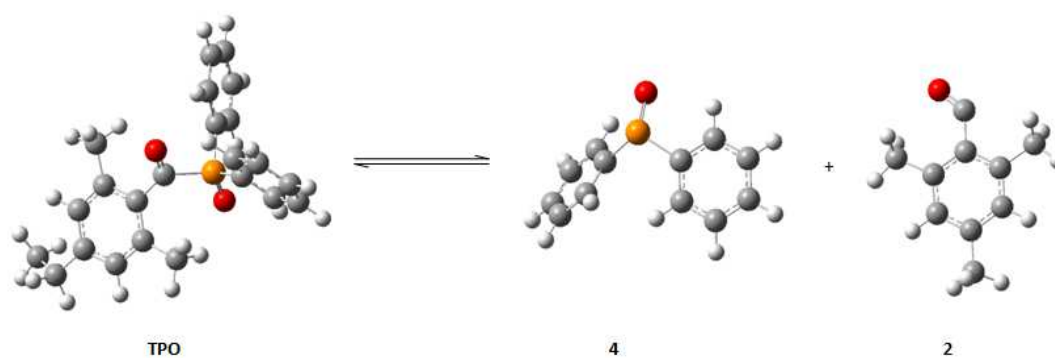
	$\Delta H$ (kcal/mol)	$\Delta G$ (kcal/mol)
BAPO (reaction I)	47.57	32.83
BAPO (reaction II)	47.13	31.10
BAPO (reaction III)	178.75	147.15

The results suggest that the most probable pathway for the cure mechanism of BAPO is reaction I or II, which corresponds well with the reaction observed in the experimental part for ESI-MS.

The computational studies of TPO showed two possible pathways for cure mechanism. The IV reaction generated the benzoyl radicals and diphenylphosphinoyl radical as illustrated in Figure 4.21 (a).

The fifth reaction produced three radicals as shown in Figure 4.21 (b) but the reaction energies for this process are four times higher than for reaction IV which is illustrated in Table 4.2.

a).reaction IV



b).reaction V

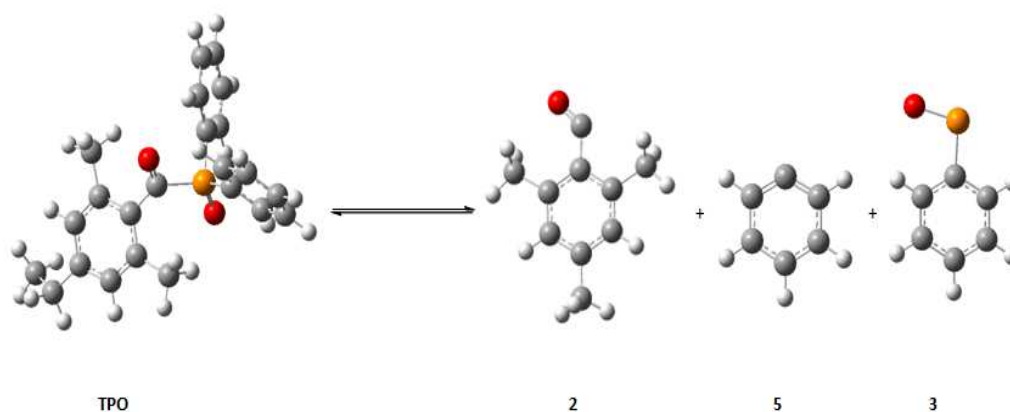


**Figure 4.21:** Proposed cure mechanism of TPO at the B3LYP/6-31G+ (d) level: to produce: a) (2) benzoyl radical and (4) diphenylphosphinoyl radical, b), (2)- benzoyl radical, (3)-phosphinoyl radical and (5) phenyl radical.

**Table 4.2:** Reaction energies of TPO at the B3LYP/6-31G+ (d) level.

	$\Delta H$ (kcal/mol)	$\Delta G$ (kcal/mol)
TPO (reaction IV)	51.11	36.21
TPO (reaction V)	210.94	181.55

The theoretical results for reaction IV correspond well with the experimental part of this work, in which ESI-MS results showed evidence of two signals at  $m/z$  147 and  $m/z$  224.

The calculation of activation energy for both photoinitiators was attempted and performed with use of a computational method, to confirm the stability of BAPO and TPO and correlation to experimental results. A number of trials of this calculation over four weeks using 4-CPU computer were not successful.

## 4.5 CONCLUSION

The stability study for both photoinitiators, BAPO and TPO, was carried out using two techniques -ESI-MS and  $^{31}\text{P}$  NMR. The use of these two different analytical methods allowed complementary information to be obtained. For both methods it was observed that TPO is a more stable photoinitiator than BAPO. Also the  $^{31}\text{P}$  NMR data confirmed the possible structures of degradation products of TPO and BAPO.

The theoretical results correspond well with the experimental data. By means of *Gaussian 03W* calculations and experimental evidence the most probable pathway of the cure mechanism of BAPO was demonstrated in which the benzoyl and 2,4,6-trimethylbenzoylphenylphosphine oxide radical and for TPO benzoyl radical and (2,4,6-trimethylbenzoyl)diphenyl-phosphine oxide radical formed. This information is valuable for further study about the polymerisation reaction and products of photoinitiator/-monomer system and is discussed in Chapter 5. The use of computational calculation was found to reinforce the conclusions obtained by the other analytical methods.

**4.6 REFERENCES**

- [1] Eichler, J., Herz C.P., Natio I., Schnabel W., *J. Photochem.*, **1980**, *12*, 225.
- [2] Decker, C., Biry S., *Prog. in Org. Coat.*, **1996**, *29*, 81.
- [3] Tasdelen, M. A., Levent Demirel, A., Yagci, Y., *Eur. Polym. J.*, **2007**, *43*, 4423.
- [4] Decker, C., *Prog. Polym. Sci*, **1996**, *21*, 593.
- [5] Studer, K., Decker C., Beck, E., Schwalm, R., *Prog. in Org. Coat.*, **2003**, *48*, 101.
- [6] Roffey, C.G., *Photopolymerisation of Surface Coatings*, Wiley, New York, **1982**.
- [7] Allen, N.S., Rabek, J.F., *New Trends in the Photochemistry of Polymers*, Elsevier Sciences, New York, **1986**.
- [8] Turro, N.J., Ramamurthy, V., Scaiano, J., C., *Modern Moelecular Photochemistry of Organic Molecules*, Copyright, US, **2010**.
- [9] Turro, N., J., Ramamurthy, V., Scaiano, J., C., *Principles of Molecular Photochemistry*, Copyright, US, **2009**.
- [10] Rabek, J.F., *Mechanisms of Photophysical Processes and Photochemical Reactions in Polymers*, John Wiley & Sons, **1987**.
- [11] Segurola, J., Allen, N., Edge, M., Roberts, I., *Polym. Degrad. Stabil.*, **1999**, *65*, 153.
- [12] Decker, C., Zahouily, K., Decker, D., Nguyen, T., Viet, T., *Polymer*, **2001**, *42*, 7551.
- [13] Kolczak, U., Rist, G., Dietliker, K., Wirz, J., *J. Am. Chem.Soc.*, **1996**, *118*, 6477.
- [14] Spichty, M., Turro, N.J., Rist, G., Birbaum, J-L., Dietliker, K., Wolf, J-P., Gescheidt, G., *J. Photoch. Photob. A*, **2001**, *142*, 209.

*Chapter Five*

*An Investigation of the Cure mechanism and Polymer  
products of Ethyl Cyanoacrylate samples using  
LC-MS*



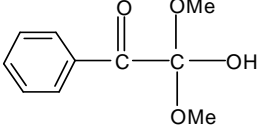
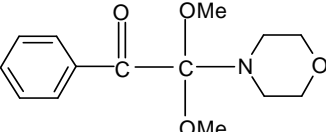
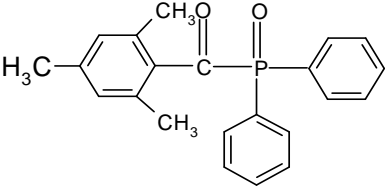
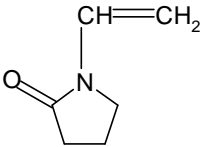
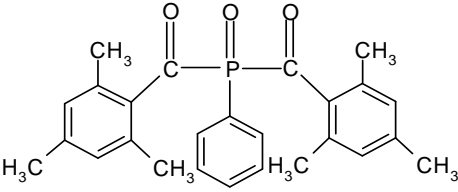
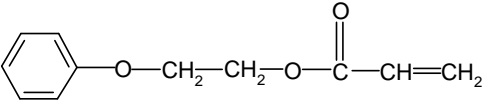
## 5.1 INTRODUCTION

The photoinitiated polymerisation of multiacrylate monomers and reactive oligomers is a powerful method to obtain a solid crosslinked polymer material. Photopolymerisation reactions are extensively used in the coating industry for the surface protection of many materials, including different metals, plastics, glasses, paper, wood coatings, screen printing, pigmented coatings for textile application <sup>[1]</sup>, coatings exhibiting a stereoscopic pattern <sup>[2]</sup>, pigmented primary <sup>[3]</sup> and secondary optical fiber coatings <sup>[4]</sup>.

Over the years, several types of photoinitiator have been developed to induce the photopolymerisation or photocrosslinking of acrylated systems. Free radical photoinitiators induce a free radical chain process in which low molecular weight monomers and prepolymers are converted by the absorption of UV-vis light into the highly crosslinked films. The basic mechanism for any photocurable free radical system involves the formation of free radical species through the absorption of light by the photoinitiator. The active radical will then attack the monomer, inducing a chain growth polymerisation. The most important commercial photoinitiators and monomers employed for industrial applications are shown in Table 5.1. The photophysical and photochemical properties of the photoinitiators are extremely important in controlling the reactivity and they should possess the following properties: <sup>[5]</sup>

- a) High absorptivity in the region of activation
- b) High quantum yield for free radical formation
- c) Solubility
- d) No- yellowing
- e) No- odour
- f) Low volatility
- g) No toxicity
- h) Low migration
- i) Cost effectiveness. <sup>[5]</sup>

**Table 5.1:** The most important photoinitiators and monomers used in the industry. <sup>[6]</sup>

photoinitiators	monomers
 <p><b>Darocure 1173- Ciba Geigy</b></p>	$\text{CH}_2=\text{CH}-\overset{\text{O}}{\parallel}{\text{C}}-\text{O}-\text{C}_2\text{H}_5$ <p>ethyl acrylate</p>
 <p><b>Irgacure 651- Ciba Geigy</b></p>	$\text{CH}_2=\text{CH}-\overset{\text{O}}{\parallel}{\text{C}}-\text{O}-\text{CH}_2-\text{N}(\text{CH}_3)_2$ <p>methyl 2-(dimethylamino) acrylate</p>
 <p><b>MAPO- Ciba Geigy</b></p>	 <p><i>N</i>- Vinyl- pyrrolidone</p>
 <p><b>BAPO 2- Ciba Geigy</b></p>	 <p>2-phenoxyethyl acrylate</p>

### 5.1.1. Characteristics of Cyanoacrylate Adhesives

Cyanoacrylate adhesives, commonly known as Superglues, are defined as compounds which are capable of forming and maintaining a bond between two surfaces. They are single component, instant bonding adhesives that cure at room temperature by addition polymerisation initiated by adsorbed water.<sup>[7]</sup> Cyanoacrylate was first invented by Harry Coover, at Eastman Chemical Company in the 1949s, with ethyl cyanoacrylate being one of the monomers under investigation. In 1958, Eastman Kodak produced its first commercially available cyanoacrylate adhesive under the name Eastman 910<sup>[8]</sup>.

Several methods are used to synthesise cyanoacrylate monomers, among which the most important industrial process is: base-catalysed Knoevenagel reaction followed by thermal depolymerisation under acidic conditions to regenerate the monomer.

The synthesis of cyanoacrylate is based on the Knoevenagel reaction<sup>[9]</sup> as shown in Figure 5.1. It involves the condensation of formaldehyde (methanal) and an alkyl cyanoacetate. In the first step an enolate is formed from the alkyl cyanide. The resulting enolate anion acts as a nucleophile and attacks the electrophilic carbon on the formaldehyde. Then the condensation reaction occurs where the hydroxyl group leaves, thus forming methyl 2- cyanoacrylate.

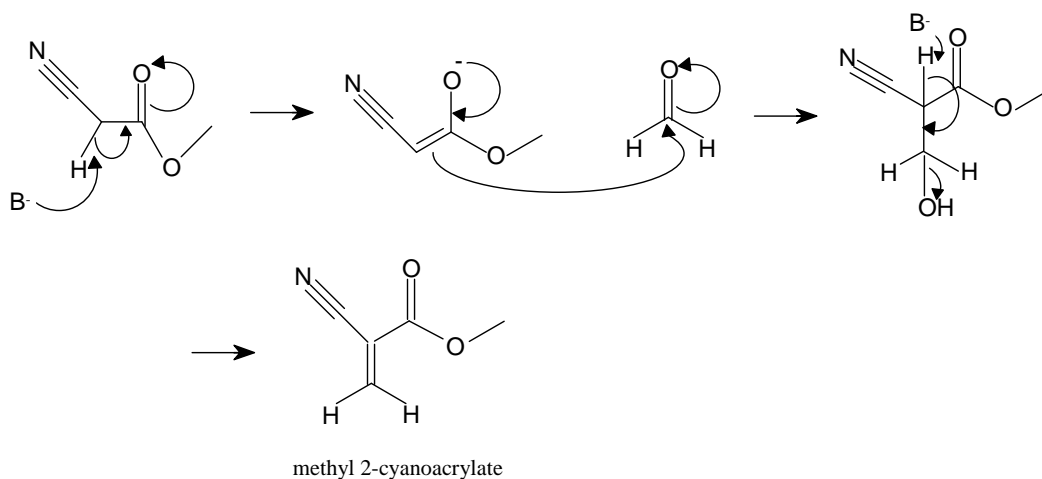


**Figure 5.1:** Knoevenagel reaction showing the synthesis of methyl 2-cyanoacrylate.

The second step in the industrial method is depolymerisation of the polymer. A cyanoacrylate polymer readily depolymerises into the liquid monomer (crude monomer) because of the heating of prepolymer. The depolymerisation process is carried out at high temperatures ( $-150^\circ$   $-190^\circ$ ). The crude monomer undergoes a purification process (distillation) where impurities are removed. This distillation process generates a pure monomer which will form strong bonds between surfaces by addition polymerisation initiated by adsorbed water. Additionally, a free radical inhibitor, such as hydroquinone, prevents the monomer undergoing a free radical polymerisation during storage. A by-product of the depolymerisation is a 2,4-dicyanoglutarate as shown in Figure 5.2.

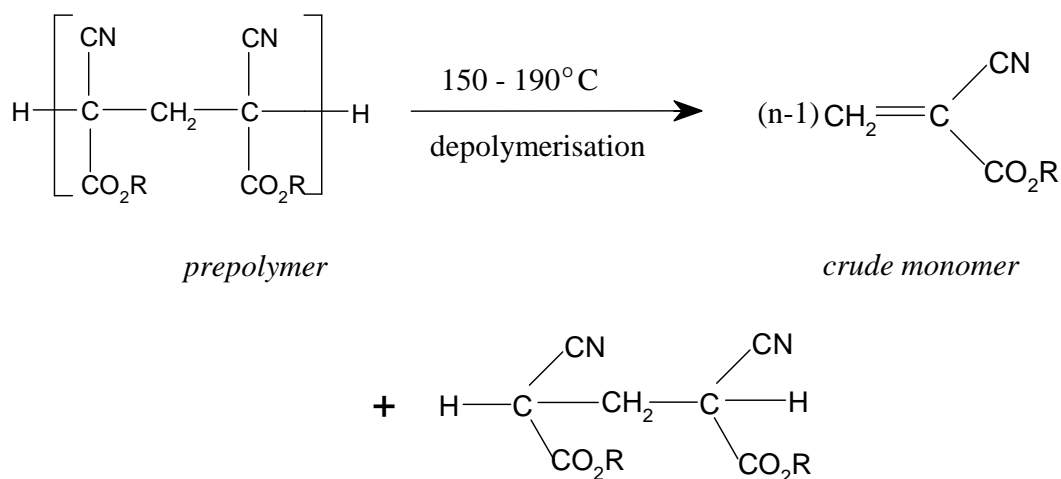


**Figure 5.2:** Depolymerisation of the polymer based on cyanoacrylate esters. <sup>[10]</sup>

Initially, the cyanoacrylate adhesives were slow to develop market acceptance. Firstly, they were unstable during manufacturing and storage. Secondly, consumers were slow to recognise the advantages of these adhesives. These problems were addressed in the 1970s with the introduction of new manufacturers into the market and rapid growth resulted. <sup>[11]</sup> Due to their properties, cyanoacrylates may be used in a wide range of industries. They are now used in areas such as electronics (component bonding, circuit boards), the motor industry, the plastics industry and jewellery bonding. Cyanoacrylates also have applications in medicine and dentistry. The purpose of these medical adhesives is to replace sutures after surgery, whereby the skin can be glued together until the wound heals.

### 5.1.2 Chemistry of Cyanoacrylate Adhesives

Cyanoacrylate adhesives consist of mixtures of the following common components: monomers, initiators, accelerators and inhibitors/stabiliser. The monomer is normally the principal component in the mixture and forms the backbone of the resulting polymer. Accelerators and inhibitors are used to control the curing

rate. An accelerator speeds up the curing reaction, while an inhibitor will stop the curing process completely.

Monomers in cyanoacrylate adhesive formulations are classified according to their odour and are divided into two classes: high odour or low odour. High odor monomers are the more volatile of the two classes and these include methyl- or ethyl cyanoacrylates. Low odour monomers include cyanoacrylates such as  $\beta$ -methoxyethyl cyanoacrylate and  $\beta$ -ethoxyethyl cyanoacrylate hydroxyethyl which are less volatile but more expensive. Due to overall cost considerations, availability and performance, high odor methacrylates are most widely used.<sup>[12]</sup>

The reactivity of cyanoacrylate adhesives is directly related to their basic chemical structure which consists of two electron-withdrawing groups: CN and COOR<sup>[13]</sup>, (Figure 5.3)

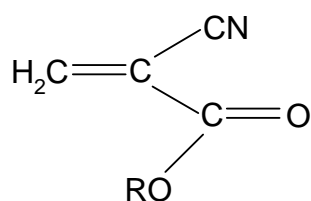


**Figure 5.3:** The structure of a cyanoacrylate monomer, where *R* is the alkyl group, for example: methyl, ethyl or butyl.<sup>[11]</sup>

The presence of the two electron withdrawing groups make the double bond extremely vulnerable to nucleophilic attack by a weak base such as H<sub>2</sub>O or an alcohol. Also, it makes the resulting anion extremely stable because the negative charge was pulled across the entire molecule. The cure process for anionic polymerisation of cyanoacrylates consists of three steps: initiation, propagation and termination as shown in Figure 5.4.

***Initiation Step***

The nucleophile ( $B^-$ ) initiates the reaction (they are frequently Lewis bases *e.g.*  $OH^-$ , amino acid, etc.) by attacking the  $C=C$  double bond, which breaks and forms a new bond with the nucleophile on one side of the double bond. It also forms the anion on the other side.

***Propagation Step***

The anion formed in the initiation step attacks another cyanoacrylate monomer at the  $C=C$  double bond. The bond forms between the anion generated in the initiation step and the new cyanoacrylate monomer. The reaction forms another anion, which can then attack another cyanoacrylate monomer. The process continues until it is terminated.

***Termination Step***

The reaction is terminated by the presence of  $H_2O$ , and particularly by acidic protons because they react with the growing anion effectively quenching the reaction. The cyanoacrylate responds to strong and weak acids in different ways. The addition of weak acids inhibits and slows down the polymerisation whereas strong acids stop polymerisation completely as shown in Figure 5.4.

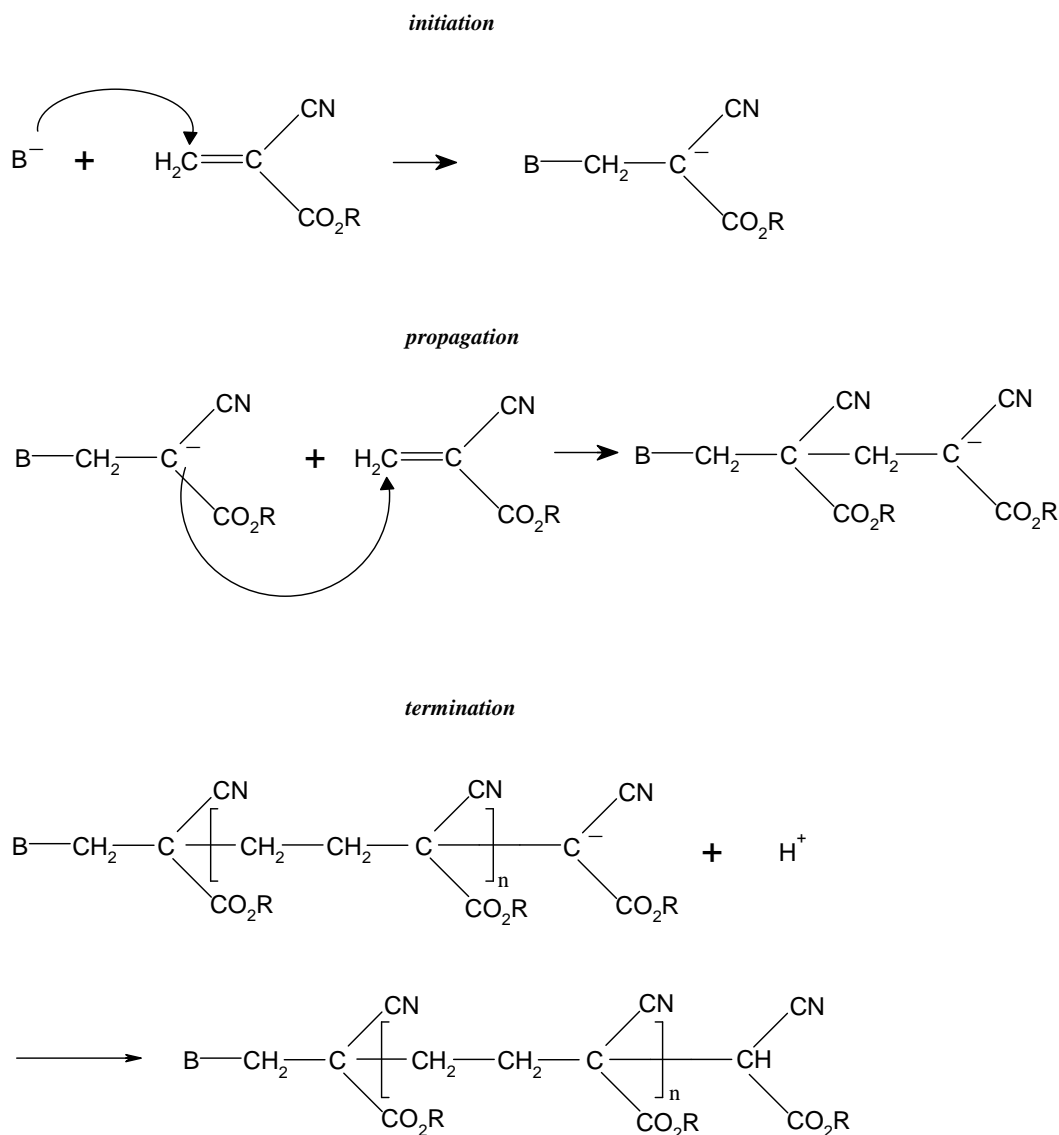


**Figure 5.4:** The cure mechanism of cyanoacrylate adhesives.

Other components present in cyanoacrylates include modifiers, which are added to adhesives in order to obtain desired physical properties and the required appearance. Modifiers include tougheners which enhance the impact resistance and the peel strength of the adhesives. A rubbery compound such as chlorosulphonated polyethylene is sometimes added to achieve this. Plasticisers, such as aliphatic diesters and alkyl phthalates are added to improve the heat resistance of adhesives and reduce brittleness. <sup>[15]</sup>



## **5.2 SCOPE OF RESEARCH**

In this chapter the formulation of photoinitiator/ monomer is prepared and the resultant compounds are characterised using LC-MS. The pathways of the cure mechanism of the both photoinitiators (BAPO and TPO)/- ethyl cyanoacrylate (CA) monomer are investigated. Analytical experiments were performed using an ESI-MS system. The products of polymerisation for ethyl CA and the photoinitiator/ - ethyl CA system were studied, and a comparison of samples, kept in dark in room temperature and exposed to sun light and ambient light was made. Additionally, the effect of the elevated temperatures, 55° C and 82° C on the polymerisation products of photoinitiator/- ethyl CA kept in dark and light conditions were assessed.

## 5.3 MATERIALS AND METHODS

### 5.3.1 Instrumentation

#### 5.3.1.1 *Liquid chromatography-Mass spectrometry*

The MS and LC-MS experiments were performed as described in Chapter 4 in section 4.3.1.1

#### 5.3.1.2 *UV Power Meter*

Light intensity was measured using a UV Power Meter, QAI's Model 306. Calibration accuracy was within +/-3% and was NIST traceable. Measurement repeatability was within +/-1%. It was auto ranging from 0.1 to 1999 mW/cm<sup>2</sup> full scale and has 15 linearity in this range.

### 5.3.2 Chemicals

Bis-(2,4,6- trimethylbenzoyl)phenylphosphine oxide (Irgacure 819 or BAPO) photoinitiator, (2,4,6-trimethylbenzoyl)diphenylphosphine oxide (TPO or Darocur) photoinitiators, ferrocene, and ethyl cyanoacrylate (Ethyl CA) samples were all obtained from Henkel Technologies Center (Irl). Acetonitrile (Romil-SpS Super Purity Solvent) and water were purchased from Lennox (Irl.)

### 5.3.3 Procedures

#### 5.3.3.1 Preparation of mobile phase

The mobile phase for LC-MS was a mixture of water-acetonitrile [90/10, v/v] and was filtered using PTFE filter under vacuum and sonicated for 20 to 30 min to remove dissolved gases.

#### 5.3.3.2 Preparation of formulation of ethyl cyanoacrylate (ethyl CA)

##### Formulation of ethyl CA:

Compound	Value (g)
ethyl cyanoacrylate (ethyl CA)-	48.835
stabiliser	0.91
ferrocene	0.005
BAPO or TPO	0.25

The formulation was stirred for 15 min to completely dissolve the components, and then transferred to clear or amber tubes. Clear tubes were exposed to the sunlight and ambient light. Amber tubes were protected from light stored at room temperature and at 55° C and 82 ° C temperatures in a heated up oven.

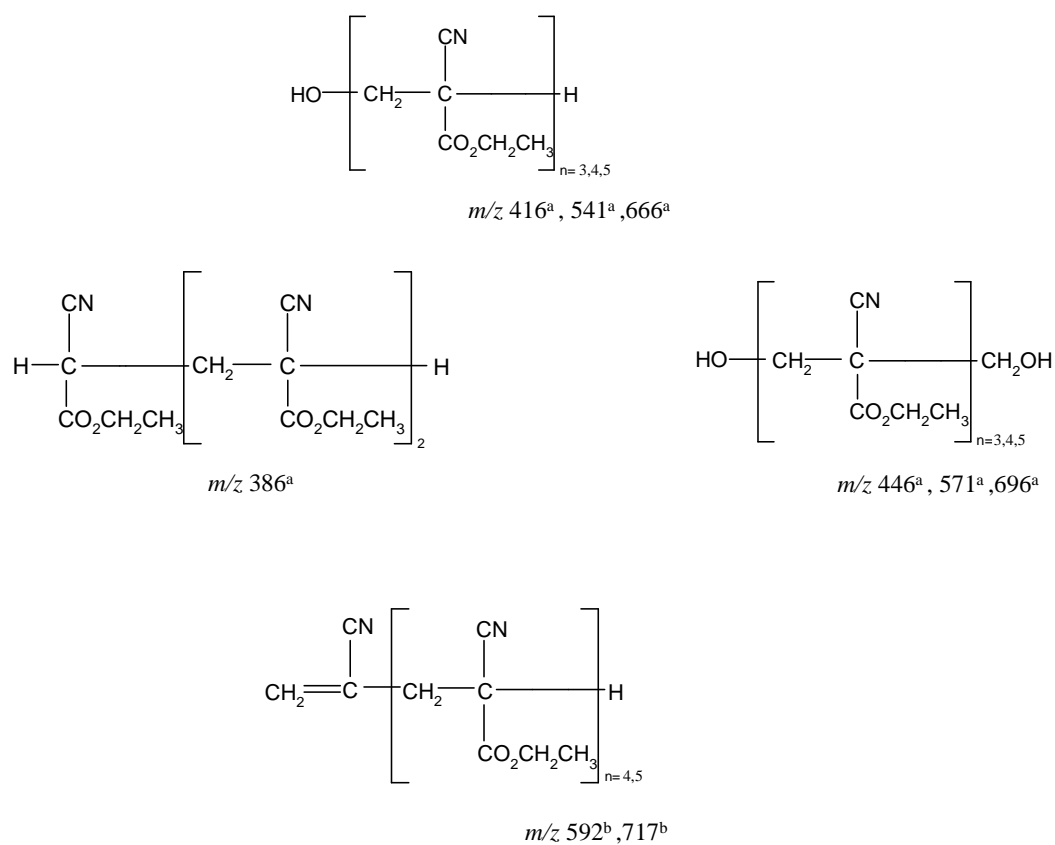
### ***5.3.3.3 Preparation of formulation of ethyl cyanoacrylate (ethyl CA) for LC-MS analysis***

The polymerisation procedure was as follows: 5 mL of CH<sub>3</sub>CN was transferred into a 25 mL volumetric flask, than 0.25g of ethyl CA formulation was added to the flask followed by 2.5 mL of deionised water. The mixture was stirred for 15 min to polymerise the ethyl cyanoacrylate. The mixture was made up to the mark with CH<sub>3</sub>CN. The solution was stirred for 15 min to dissolve the polymer completely. The samples were then injected directly onto the LC-MS system.

## 5.4 RESULTS AND DISCUSSION

### 5.4.1 Cure mechanism of ethyl CA oligomers

To aid in assigning the mixture of BAPO/ ethyl CA the analogous experiment was carried out for only ethyl CA without photoinitiator for dark conditions at room temperature, see section 5.3.3.3. A possible combination of oligomer products from ethyl CA are depicted in Figure 5.5.



<sup>a</sup>[M+Na]<sup>+</sup>

<sup>b</sup>[M+K]<sup>+</sup>

**Figure 5.5:** Proposed structures of ethyl CA oligomers, for samples kept in dark at room temperature.

Focusing on the (+) ESI-MS results for three different ions (three different types of oligomers), three series are clearly present and gave evidence for the range of oligomeric products from the polymerisation of ethyl CA (see (+) ESI-MS mass spectrum in Figure 5.6 and 5.7). The mass difference of 125 amu is common in the (+) ESI-MS spectrum and corresponds to the repeat unit of ethyl CA (ethyl cyanoacrylate, MW 125). In the (+) ESI-MS spectrum (Figures 5.6 and 5.7) the most intense peaks were the sodium adducts.

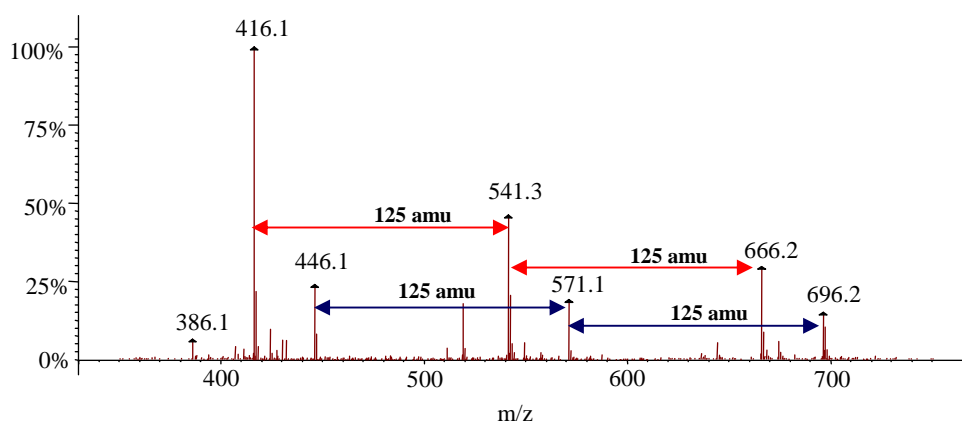


**Figure 5.6:** (+) ESI-MS mass spectrum of two series of oligomers.

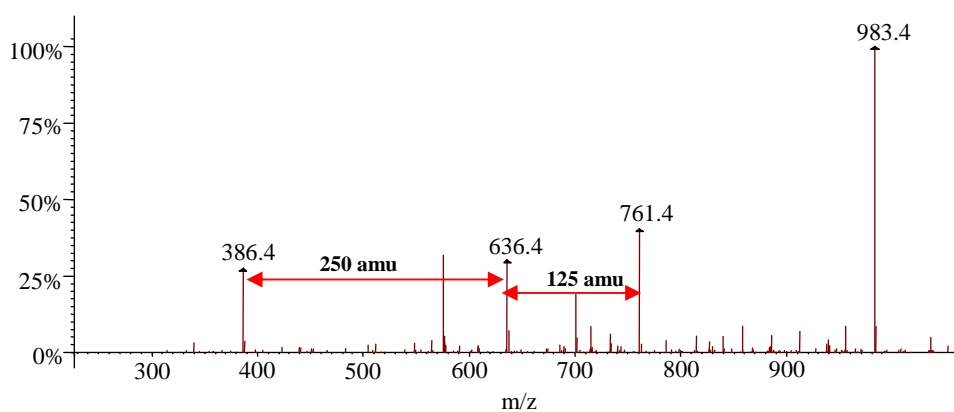
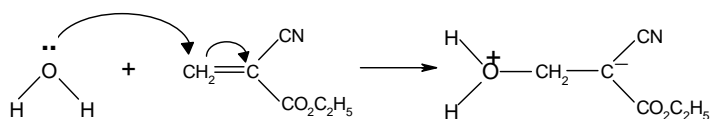


**Figure 5.7:** (+) ESI-MS mass spectrum of oligomers.

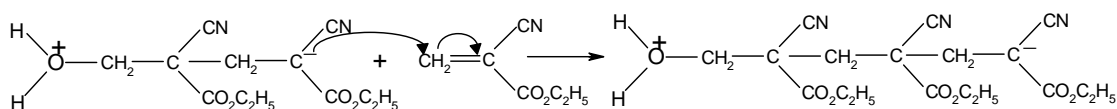
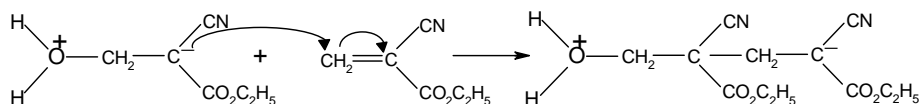
Polymerisation reactions of all three types of oligomers were initiated by water molecules as illustrated in Figures 5.8, 5.9, 5.10 and 5.11. Interestingly, two steps of the cure mechanism, initiation and propagation were the same for the three oligomers and only the last step-termination was different. In the first step the molecules of water attack the C=C double bond, which breaks and forms a new bond with the nucleophile on one side of the double bond and the anion on the other side. The anion formed in the initiation step attacks another ethyl CA monomer to produce a longer chain. The repeat mass of 125 is present in the structure of every type of oligomer.

In the termination step for the oligomer at  $m/z$  416 (see Figure 5.8) the anion which formed in the propagation step reacts with the proton which completely stops the polymerisation process, as shown in Figure 5.8. The pathway of another oligomer at  $m/z$  386 is illustrated in Figure 5.9. It was postulated that the oligomer could be formed by elimination of the  $\text{CH}_2\text{O}$ . In 2008, Henkel Loctite Technology Center analysed of formaldehyde in cyanoacrylate ester using pulse polarography. The results suggested that  $\text{CH}_2\text{O}$  is released after polymerisation possibly due to some degradation of the monomer.<sup>[16]</sup> This is in contrast to the termination step of the next oligomer, when the  $\text{CH}_2\text{O}$  and proton was added to generate the new oligomer as shown in Figure 5.10. The pathway of the last oligomer with  $m/z$  592, 717 is illustrated in Figure 5.11. This oligomer is possibly formed by elimination of  $\text{CH}_3\text{CH}_2\text{OH}$  for the first reaction and  $\text{CO}_2$  and  $\text{H}_2\text{O}$  for the second reaction (see Figure 5.11 (b)).

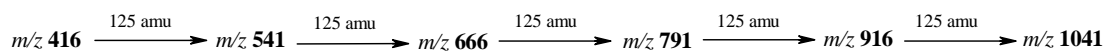
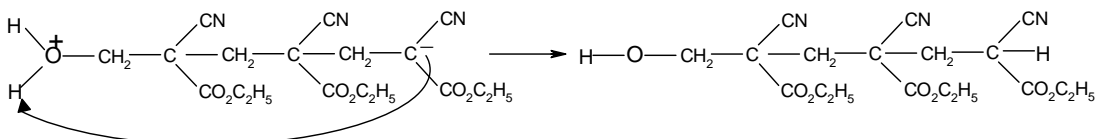
## I. INITIATION



## II. PROPAGATION

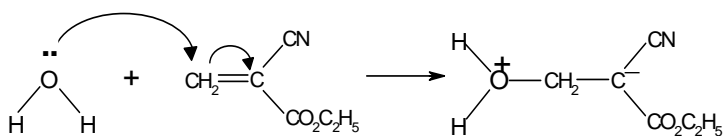
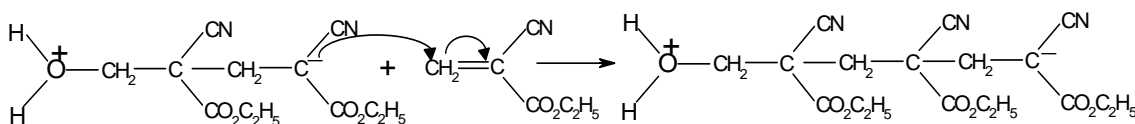
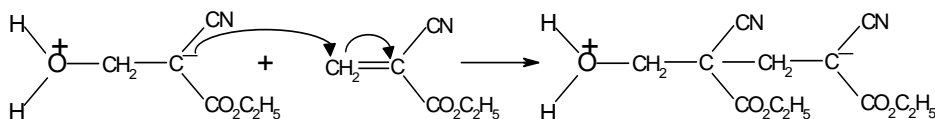
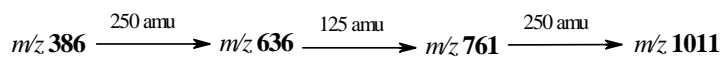
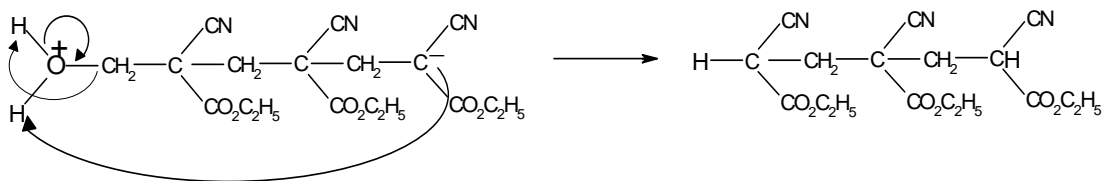


## III. TERMINATION



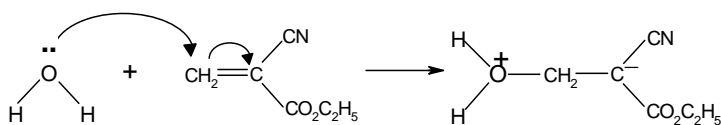
**Figure 5.8:** Proposed cure mechanism for oligomers at  $m/z$  416, 541 and 666,  $[M+Na]^+$  for samples kept in dark.



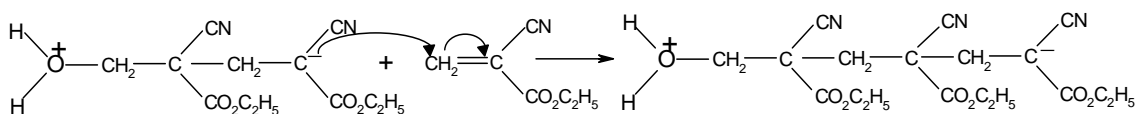
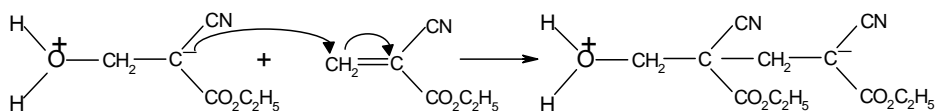
**I INITIATION****II PROPAGATION****III TERMINATION**

**Figure 5.9:** Proposed cure mechanism for oligomers at  $m/z$  386, 636, 761 and 1011,  $[M+Na]^+$  for samples kept in dark.

## I. INITIATION



## II. PROPAGATION



## III. TERMINATION

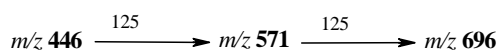
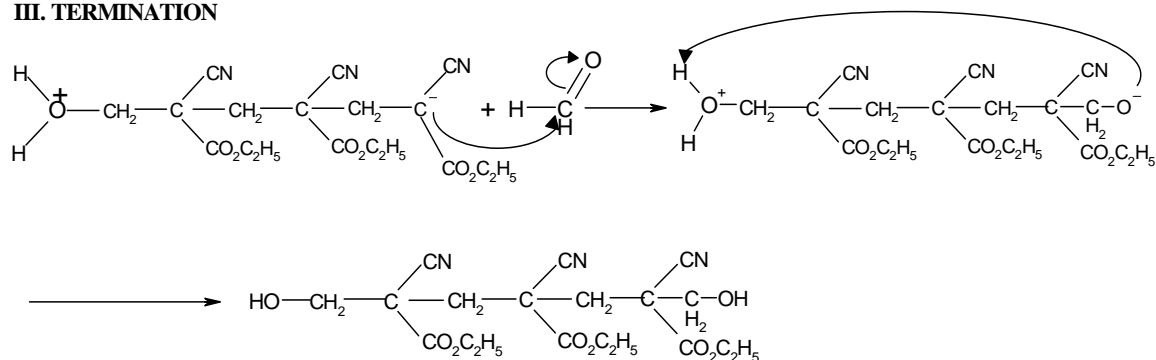
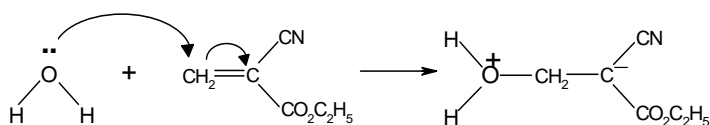
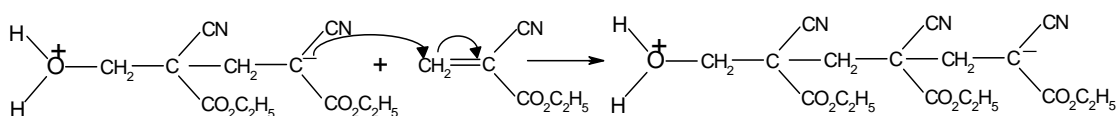
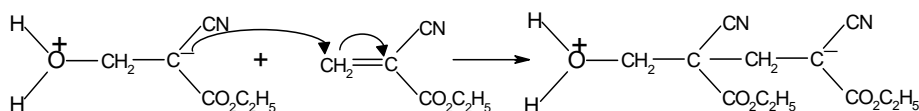


**Figure 5.10:** Proposed cure mechanism for oligomers at  $m/z$  446, 571 and 696,  $[M+Na]^+$  for samples kept in dark.

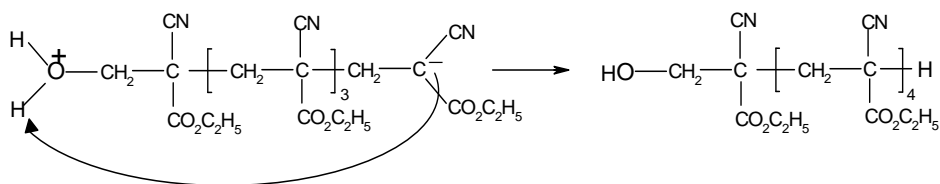
## I. INITIATION



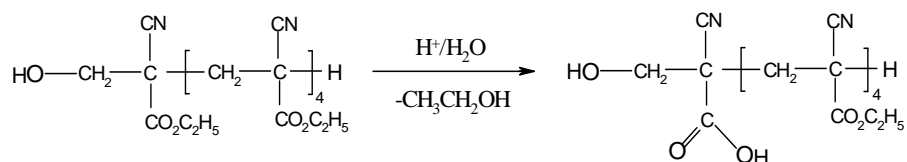
## II. PROPAGATION



## III. TERMINATION



A.



B.

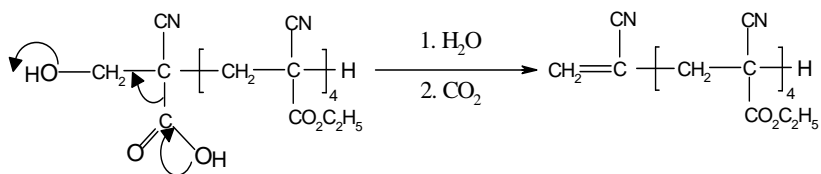
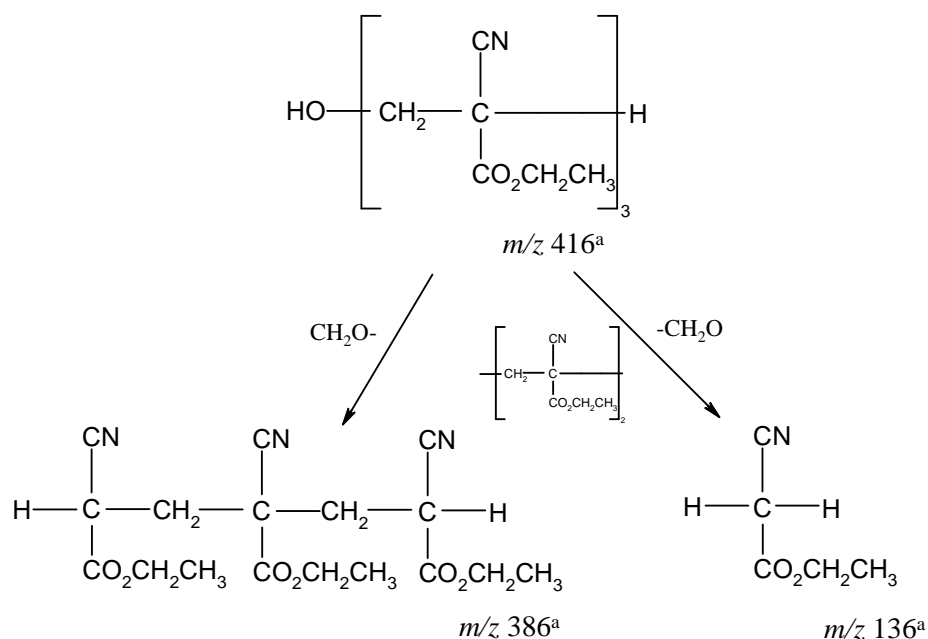


**Figure 5.11:** Proposed cure mechanism for oligomers at  $m/z$  592 and 717 for samples kept in dark.

The major peaks of ethyl CA oligomers were assigned based on tandem mass spectrometry (MS/MS) dissociation patterns to give a consistent explanation of the observed spectrum. The MS<sup>2</sup> of the oligomer at  $m/z$  386,  $[M+Na]^+$  showed fragmentation corresponding to the loss of one ethyl CA monomer (to give  $m/z$  261,  $[M+Na]^+$ ). From the (+) ESI-MS/MS of  $m/z$  261 another product ion of  $m/z$  148 was detected, which was identified as ethyl CA monomer, as the sodium adduct. The (+) ESI-MS/MS for the oligomer at  $m/z$  416 formed product ions at  $m/z$  386 and  $m/z$  136 which is shown in Figure 5.12. The product ion at  $m/z$  386 was formed most likely by loss of CH<sub>2</sub>O from the precursor ion at  $m/z$  416. The ion at  $m/z$  136 corresponds to the loss of two molecules of ethyl CA monomer and CH<sub>2</sub>O.



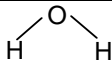
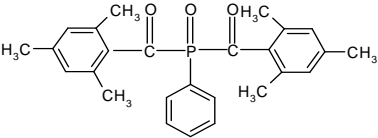
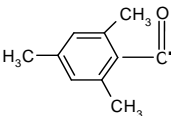
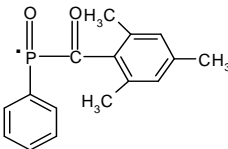
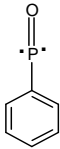
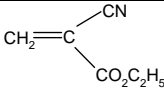
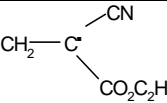
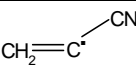
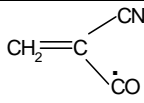
<sup>a</sup> $[M+Na]^+$

**Figure 5.12:** Proposed mass fragmentation of product at  $m/z$  416.

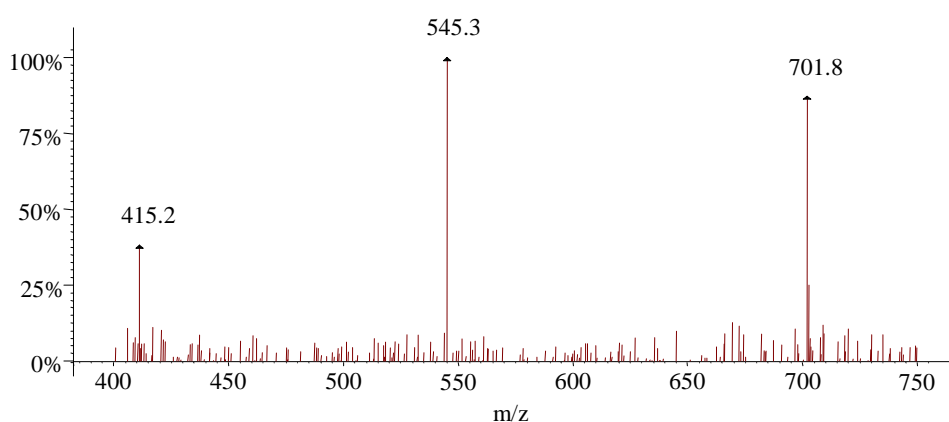
### 5.4.2 BAPO /ethyl CA system in samples kept in dark and exposed to the light

The photolysis products of bis(2,4,6-trimethylbenzoyl)phenylphosphine oxide (BAPO) are of special interest for several reasons. First, BAPO is a widely used commercially available photoinitiator. <sup>[17]</sup> This photoinitiator may fragment to yield a phosphorus centered radical species which initiates polymerisation (see Table 5.2). While it is likely that a radical will form during photodissociation of the BAPO, a bond cleavage to either side of the phosphorus atom may occur throughout the reaction. Furthermore, acylphosphine oxide has been shown to be highly reactive toward acrylates with the high reactivity ascribed to the phosphinoyl radicals generated during photodissociation. <sup>[18]</sup>

**Table 5.2:** Radicals considered as potential initiating species. <sup>[19]</sup>

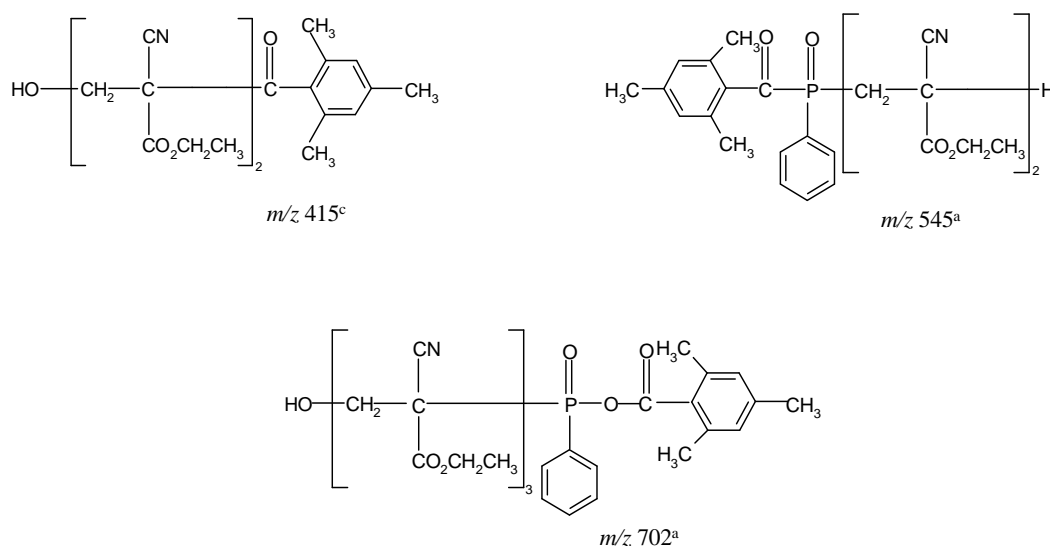
Parent compound	Potential Initiating Radical Species		
 water	$\cdot\text{OH}$ A	$\cdot\text{H}$ B	$\cdot\text{O}-\text{OH}$ C
 Irgacure 819	 D	 E	 F
 Ethyl CA	 G	 H	 I

Initially, ESI mass spectrometry (in positive as well as negative mode) was used to investigate the spectrum of polymer products of the complex BAPO mediated bulk ethyl CA polymerisation initiated by light (sunlight and ambient light) and dark condition at room temperature. Additionally, spectra of polymerisation products for samples kept in the dark at temperatures of both 55° C and 82° C were also analysed. Figure 5.13 clearly shows the mass spectrum of three reaction products for samples kept in dark for 24 h at 82° C. Polymerisation to a solid polymer did not occur for the samples maintained for 24 h at 82° C nor for the samples kept at 55° C.



**Figure 5.13:** (+) LC-MS mass spectrum of reaction products of BAPO/ ethyl CA for samples kept in dark, after 24 h at 82°C.

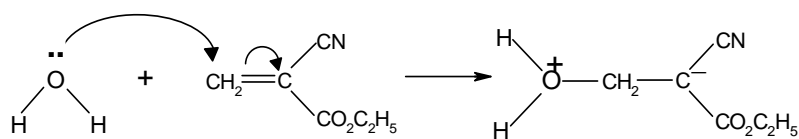
Possible combination products generated as a result of the reaction of ethyl CA and BAPO are given in Figure 5.14.

<sup>a</sup>[M+Na]<sup>+</sup><sup>c</sup>[M+H]<sup>+</sup>

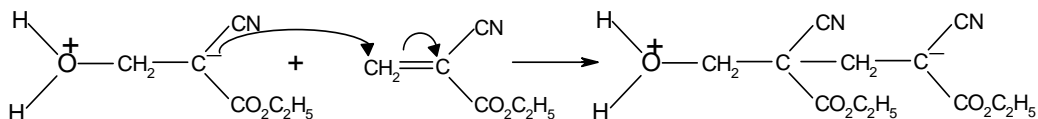
**Figure 5.14:** Probable structure derived from (+) ESI- MS distributions for the oligomer sample prepared by reaction at 82° C for samples kept in dark after 24 h

For all these ions of  $m/z$  415,  $m/z$  545 and  $m/z$  702, both the initial photolysis product fragments of BAPO (*i.e.* D and E refer to Table 5.2) initiated or completely stopped polymerisation. The first oligomer product at  $m/z$  415 might possibly be formed by a chain reaction that consisted of the sequential steps of initiation, propagation and termination, as illustrated in Figure 5.15. The polymerisation reaction was initiated by water. The initiating groups in water are the basic hydroxide ions (OH<sup>-</sup>) which starts the reaction by attacking the monomer molecule– ethyl CA, (C=C double bond) and also form the anion on the another side, see the initiation reaction. In the propagation step another ethyl CA monomer is added to produce a longer-chain. In the next step, the anion formed in the propagation reaction attacks only one of the carbonyl groups of the photoinitiator (BAPO) and stops polymerisation completely, forming a oligomer product at  $m/z$  415 and 2,4,6-trimethylphenylphosphine oxide, as illustrated in Figure 5.15 (termination step).

## I. INITIATION



## II. PROPAGATION



## III. TERMINATION

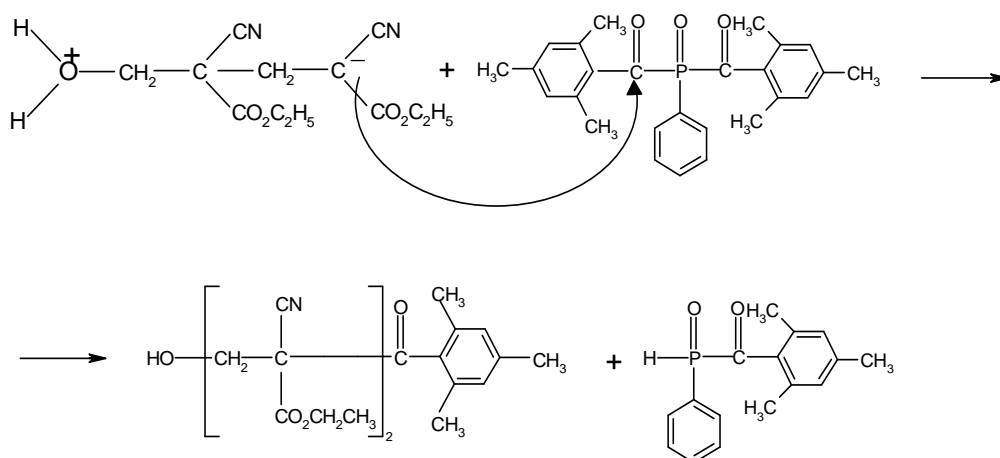


**Figure 5.15:** Proposed cure mechanism for reaction product at  $m/z$  415.



The positive mode ESI-MS/MS spectrum of the ion at  $m/z$  415 shows three main product ions at  $m/z$  290, 399 and  $m/z$  147. The most intense peak, observed at  $m/z$  290,  $[M+H]^+$ , indicates the elimination of ethyl CA monomer molecule from the precursor ion, as described in Figure 5.16. The product ion at  $m/z$  399 could not be rationalised. The formation of  $m/z$  147 from the precursor ion can be rationalised via a six-membered transition state, where a proton was transferred from a  $CH_3$  group.

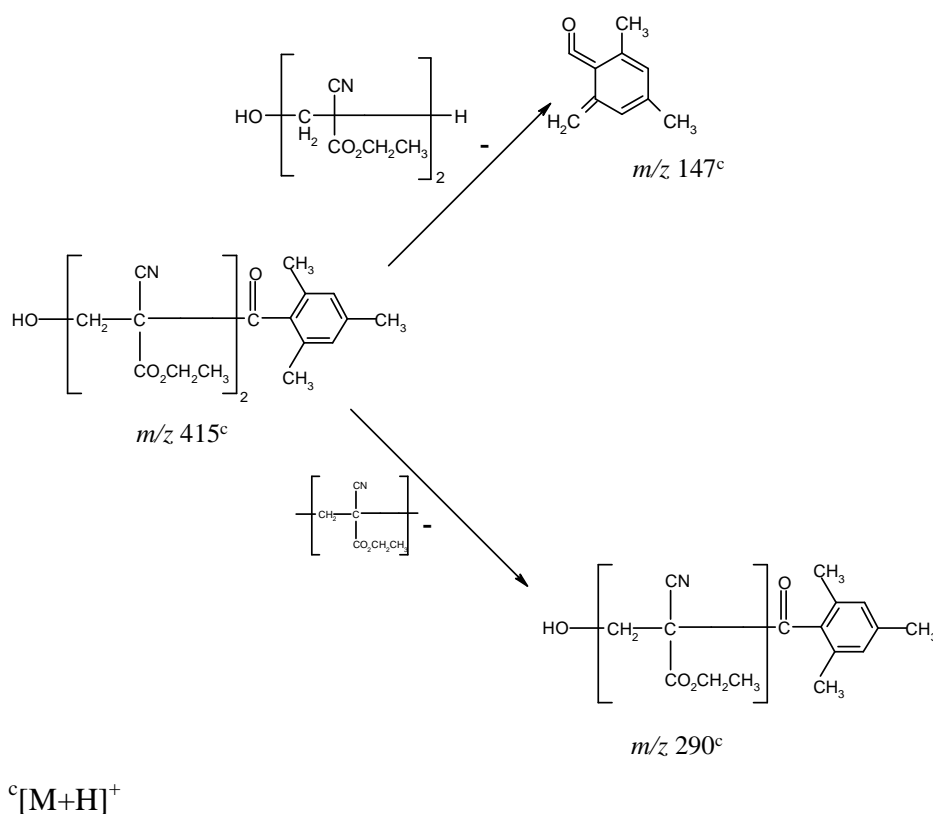
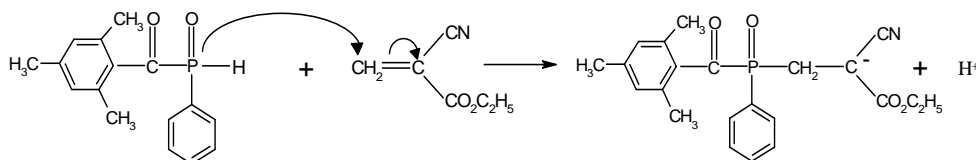


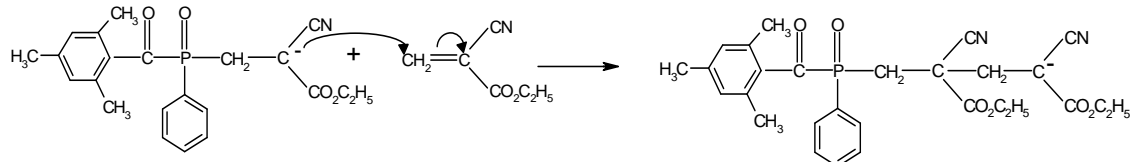
**Figure 5.16:** Proposed mass fragmentation of reaction product  $m/z$  415.

The other product of oligomerisation at  $m/z$  545 was formed possibly by nucleophilic oligomerisation. In the first step– the initiation step–the product of the hydrolytic reaction of BAPO, the 2,4,6-trimethylbenzoylphenylphosphinic oxide initiates the reaction by attacking the C=C double bond, which breaks and forms a new bond with the nucleophile on one side of the double bond. It also forms the anion on the other side. The anion formed in the initiation step attacks another ethyl CA monomer at the C=C double bond, and in result forms another anion. The addition of acidic proton in the termination step stopped polymerisation completely as illustrated in Figure 5.17.

### I. INITIATION



### II. PROPAGATION



### III. TERMINATION

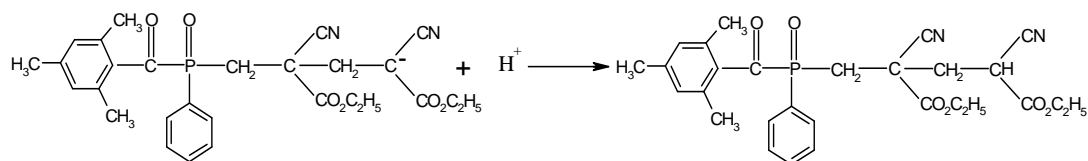
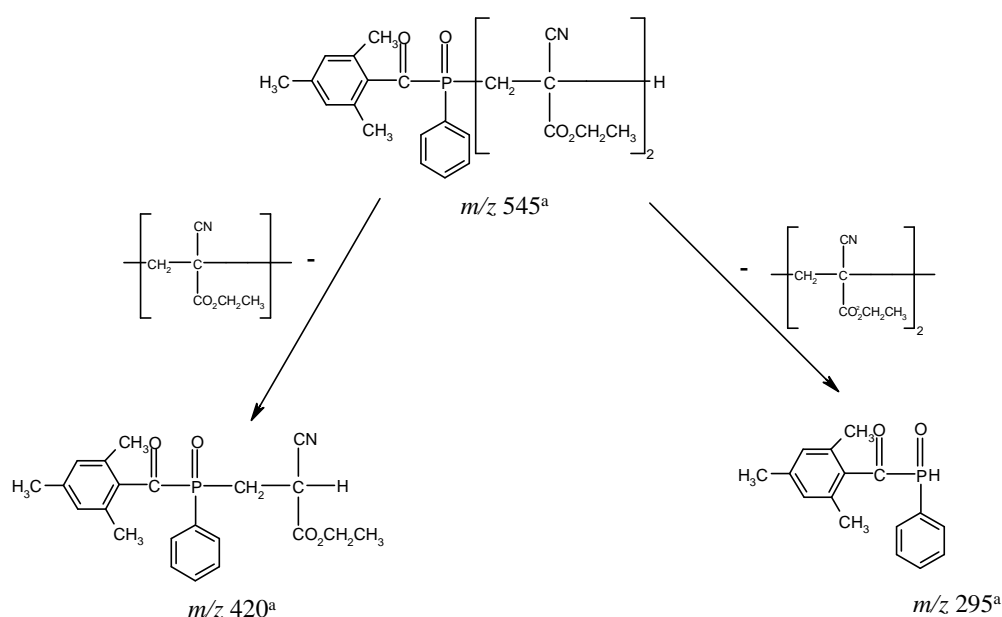


**Figure 5.17:** Proposed cure mechanism for reaction product at  $m/z$  545.

The (+) ESI MS/MS of the ion  $m/z$  545 yielded the product ions at  $m/z$  420 and  $m/z$  295 (see Figure 5.18). The ion at  $m/z$  420 exhibiting a loss of 125 amu is proposed to be formed by elimination of one monomer molecule of ethyl CA from the precursor ion. The other product ion at  $m/z$  295 was formed possibly by the loss of two monomer molecules of the ethyl CA. This ion was identified as 2,4,6-trimethylbenzoylphenylphosphine oxide. All the fragment ions  $m/z$  545,  $m/z$  420 and  $m/z$  295 were analysed as to be sodium adducts, (owing to the presence of sodium ion in solution employed as the mobile phase).



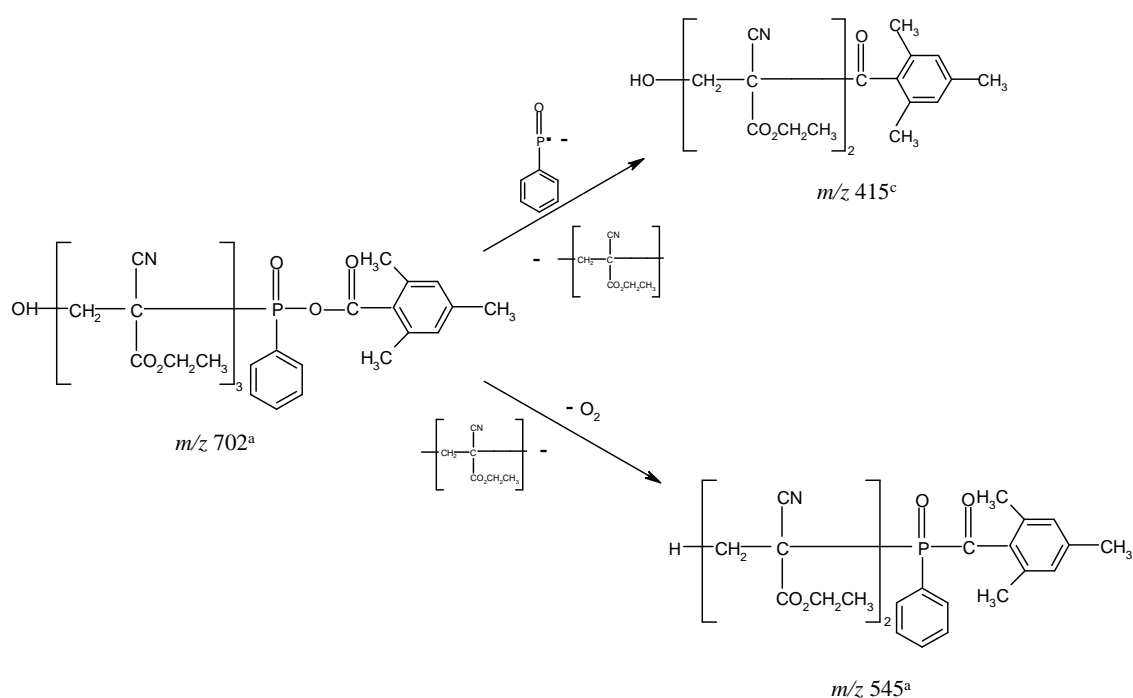
<sup>a</sup>[M+Na]<sup>+</sup>

**Figure 5.18:** Proposed mass fragmentation ((+) ESI-MS/MS) of reaction product at  $m/z$  545

The last reaction product at  $m/z$  702 for samples kept in the dark was possibly formed by the same pathway as for the product of  $m/z$  415. The oligomerisation reaction is also initiated by water attack on the ethyl CA monomer and formation of the anion on the other side. In the propagation step for the oligomerisation product at  $m/z$  702 one more monomer (ethyl CA) was added in comparison to the reaction pathway of

product at  $m/z$  415. Only the termination step was different. This time the anion which was formed in the propagation step attacked the phosphorous atom of the photoinitiator (BAPO) and formed an oligomerisation product at  $m/z$  702 and 2,4,6-trimethylbenzoic acid, and stopped completely the polymerisation process.

The (+) ESI MS/MS of the ion at  $m/z$  702 yielded the product ions corresponding to  $m/z$  545 and at  $m/z$  415, as shown in Figure 5.19. The product ion at  $m/z$  545 is formed by elimination of the one monomer molecule of ethyl CA from the precursor ion and oxygen molecule. The other product ion at  $m/z$  415 was possibly formed by a loss of 249 Da which is proposed to be elimination of one ethyl CA monomer molecule and phosphinoyl radical from the precursor ion.



<sup>a</sup>[M+Na]<sup>+</sup>

<sup>c</sup>[M+H]<sup>+</sup>

**Figure 5.19:** Proposed mass fragmentation of reaction product at  $m/z$  702.

The negative mode ESI-MS spectrum of the reaction products, obtained at temperature of 325°C, showed one main fragment ion at  $m/z$  406. The ion at  $m/z$  406 was also possibly formed by nucleophilic attack of the 2,4,6-

trimethylbenzoylphenylphosphineoxide, but this time only one-two step addition across the double bond was involved. In the first step, the 2,4,6-trimethylbenzoylphenylphosphine oxide initiates the reaction with ethyl CA, by attacking the C=C double bond of this monomer. The new product is attacked by one molecule of water at the phosphorous atom and generates a new reaction product at  $m/z$  267 and 2,4,6-trimethylbenzaldehyde which easily oxidises giving a 2,4,6-trimethylbenzoic acid as illustrated in Figure 5.20 (C). In the next step, phenylphosphonic acid reacted with product at  $m/z$  267 (see Figure 5.20 D) forming the reaction product at  $m/z$  406 with elimination one molecule of water.

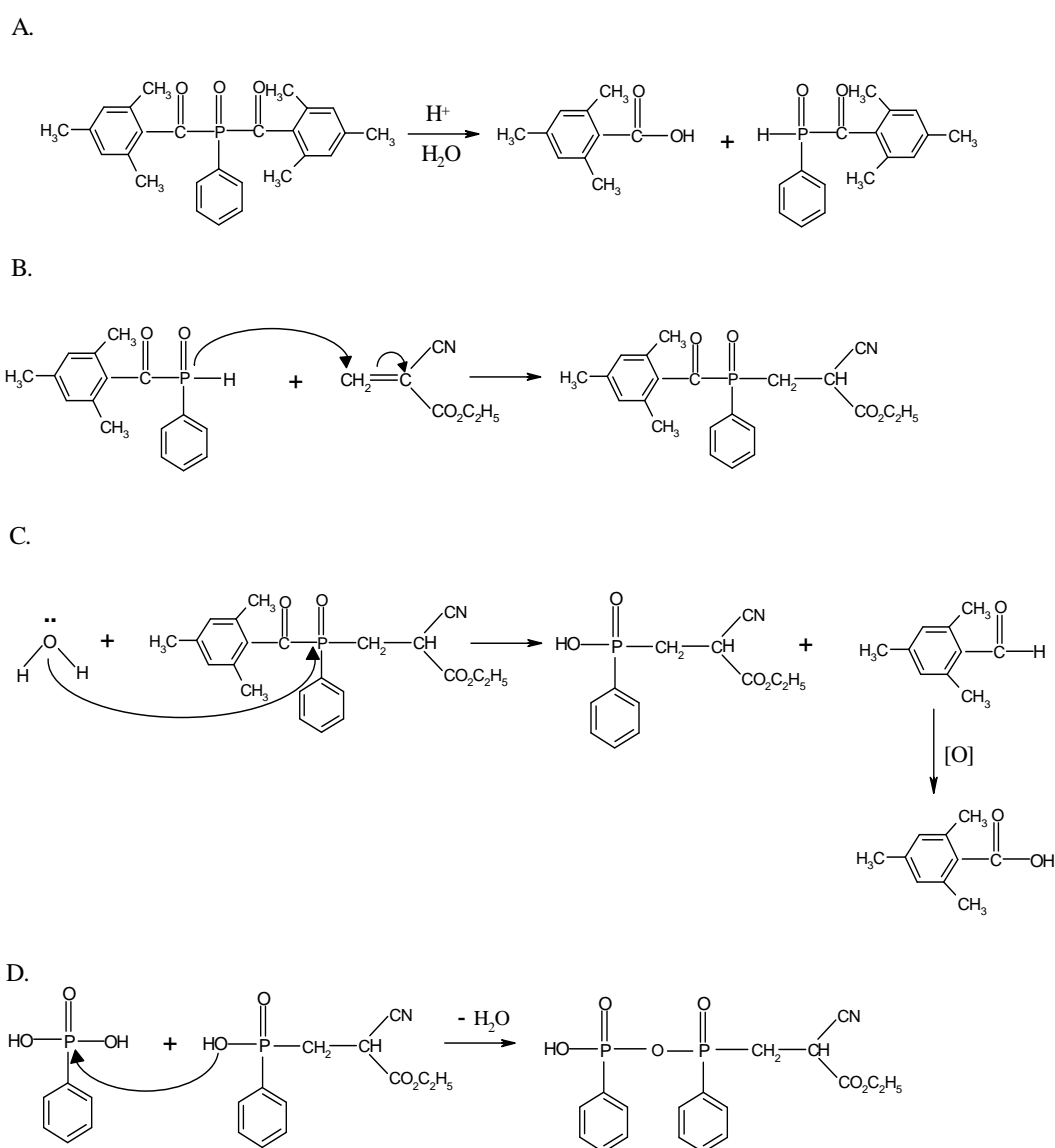
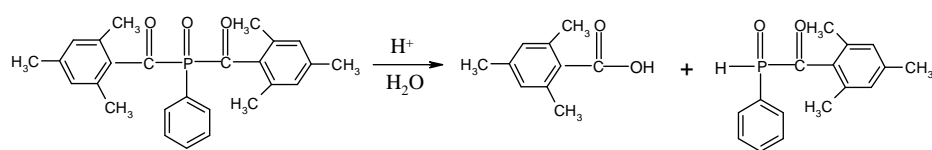


**Figure 5.20:** Proposed cure mechanism for reaction product at  $m/z$  406.

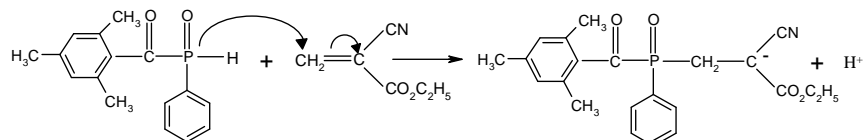
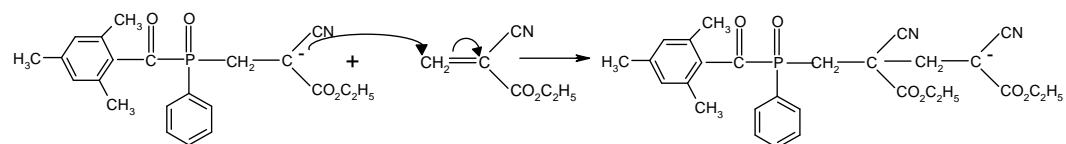
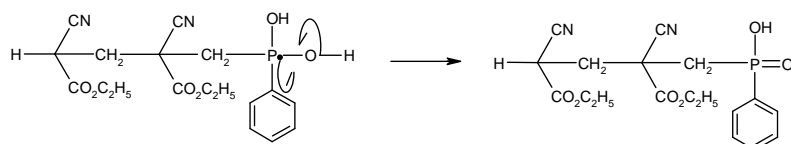
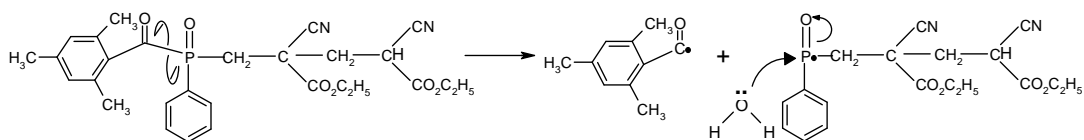
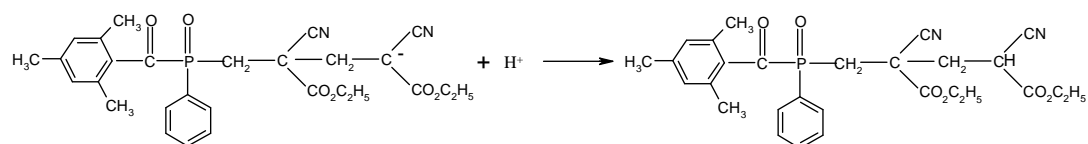
On the other hand, for samples exposed to light the polymerisation process is much faster. The polymerisation products of BAPO/ ethyl CA were monitored over 24 h, and a comparison was made between samples exposed in the ambient light and sunlight. When the mixture of BAPO/ ethyl CA was exposed to laboratory light after 5 h one new peak at  $m/z$  410 was clearly observed.

The reaction product was probably formed by a chain reaction: initiation, propagation and termination as illustrated in Figure 5.21. In the first step, the 2,4,6-trimethylbenzoylphenylphosphine oxide initiates the nucleophilic polymerisation reaction of ethyl CA monomer as illustrated in Figure 5.21 (B). The last reaction, termination, the phosphorous radical is attacked by one molecule of water and generates a new polymer product at  $m/z$  410, as illustrated in Figure 5.21.

A.



B.

**I. INITIATION****II. PROPAGATION****III. TERMINATION**

**Figure 5.21:** Proposed cure mechanism for polymerisation product at  $m/z$  410.

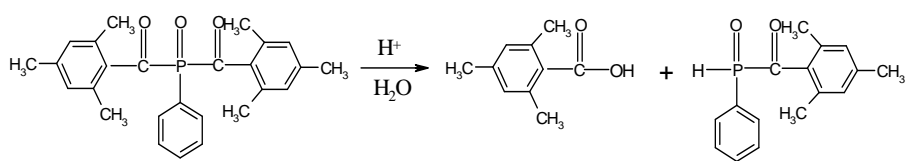
In the (+) ESI MS/MS spectrum of the polymerisation product of  $m/z$  410, product ion of  $m/z$  336 was observed. This product ion was possibly formed by a loss of 74 Da from the precursor ion. The (+) ESI- MS/MS of  $m/z$  336 gave rise to two different charge-induced mechanisms: elimination of 44 Da generates fragment ion  $m/z$  292 whereas elimination of 74 Da gave  $m/z$  262.

Interestingly, it was found that the polymerisation process of BAPO/ ethyl CA system exposed to sunlight was much more rapid when compared to the same system photoinitiator/ monomer under ambient light conditions. For samples in sunlight a new polymer product at  $m/z$  691 was detected after one hour. Polymerisation reaction was also initiated by the nucleophile 2,4,6-trimethylbenzoylphenylphosphine oxide which attacks the monomer ethyl CA, as illustrated in Figure 5.22 (B). The second step of the polymerisation process, involved another ethyl CA monomer being added to produce a longer chain. In the termination step, the anion formed in the propagation reaction attacked only one of the carbonyl atoms of photoinitiator (BAPO) and stopped polymerisation completely, forming polymerisation product at  $m/z$  691 and 2,4,6-trimethylbenzoylphenylphosphine oxide.

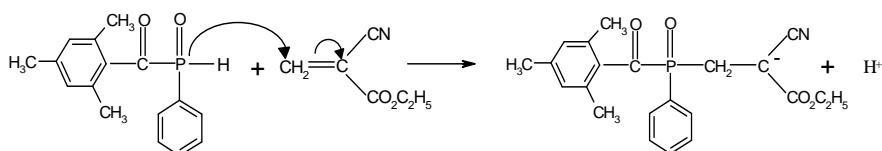
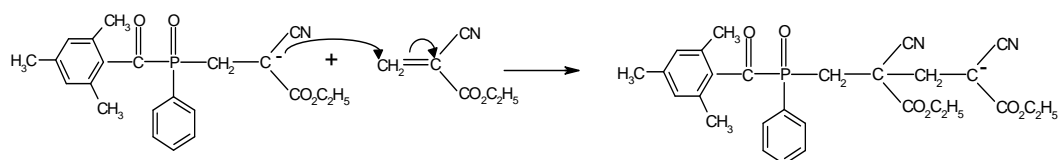
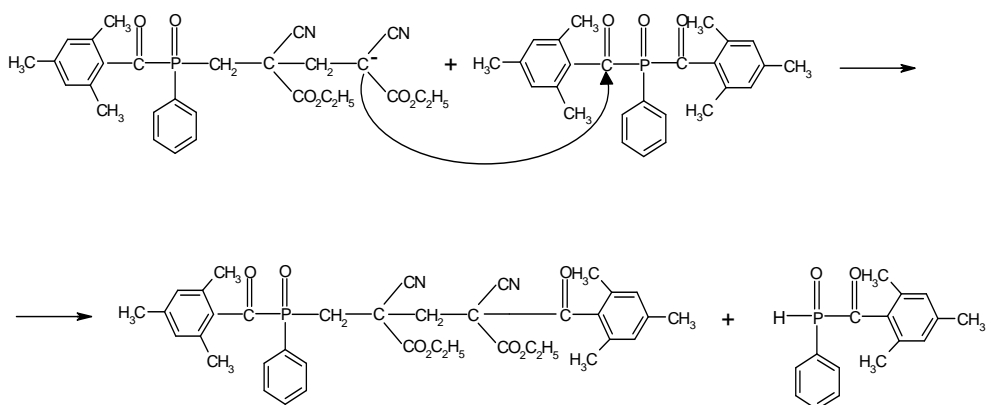
The termination reaction, when the polymer anion attacked the photoinitiator was similar to the one observed for curing mechanism of polymer products at  $m/z$  415.



A.



B.

**I. INITIATION****II. PROPAGATION****III. TERMINATION**

**Figure 5.22:** Proposed cure mechanism for polymerisation product at  $m/z$  691.

The positive mode ESI-MS/MS spectrum of the polymer product at  $m/z$  691 resulted in three main products ion at  $m/z$  645, 520 and 294. The product ion at  $m/z$  645 can be formed by loss of 46 Da from the precursor ion. The product ion at  $m/z$  520 might be formed by losing 171 Da from the ion at  $m/z$  691 and the product ion at  $m/z$  294 was possibly formed by losing 397 Da from the precursor ion as illustrated in Figure 5.23. The product ion at  $m/z$  294 may correspond to the 2,4,6-trimethylbenzoylphenylphosphine oxide radical, sodium adduct.

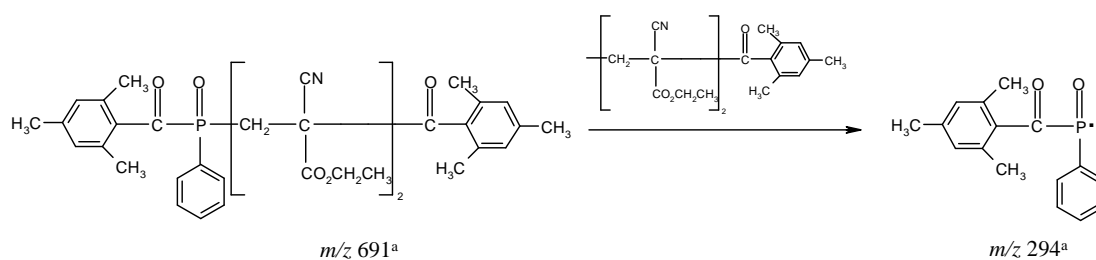


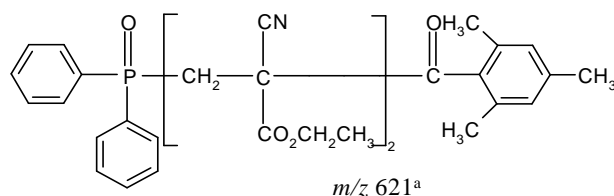
**Figure 5.23:** Proposed dissociation of polymerisation product at  $m/z$  691.

### 5.4.3. TPO /ethyl CA system in samples kept in dark and exposed to light

The cure mechanism study and polymerisation products of BAPO/ ethyl CA system was investigated over 48 h and a comparison of samples kept in the dark at room temperature, 55°C and 82° to samples exposed to light (sunlight and ambient light) was performed. The same experimental set- up was employed to investigate TPO/ ethyl CA system.

As mentioned previously, TPO is a much more stable photoinitiator than BAPO.

The ESI-MS analysis of the TPO/ethyl CA system showed that after 48 h the signal at  $m/z$  371 was still observed in dark (for all temperatures) and also under ambient light conditions, which meant that this reaction is not obtained easily for TPO and ethyl CA monomer, even at a temperature of 82° C. However, under sunlight conditions after 3 h the polymerisation product of TPO/ethyl CA monomer is observed as shown in Figure 5.24.



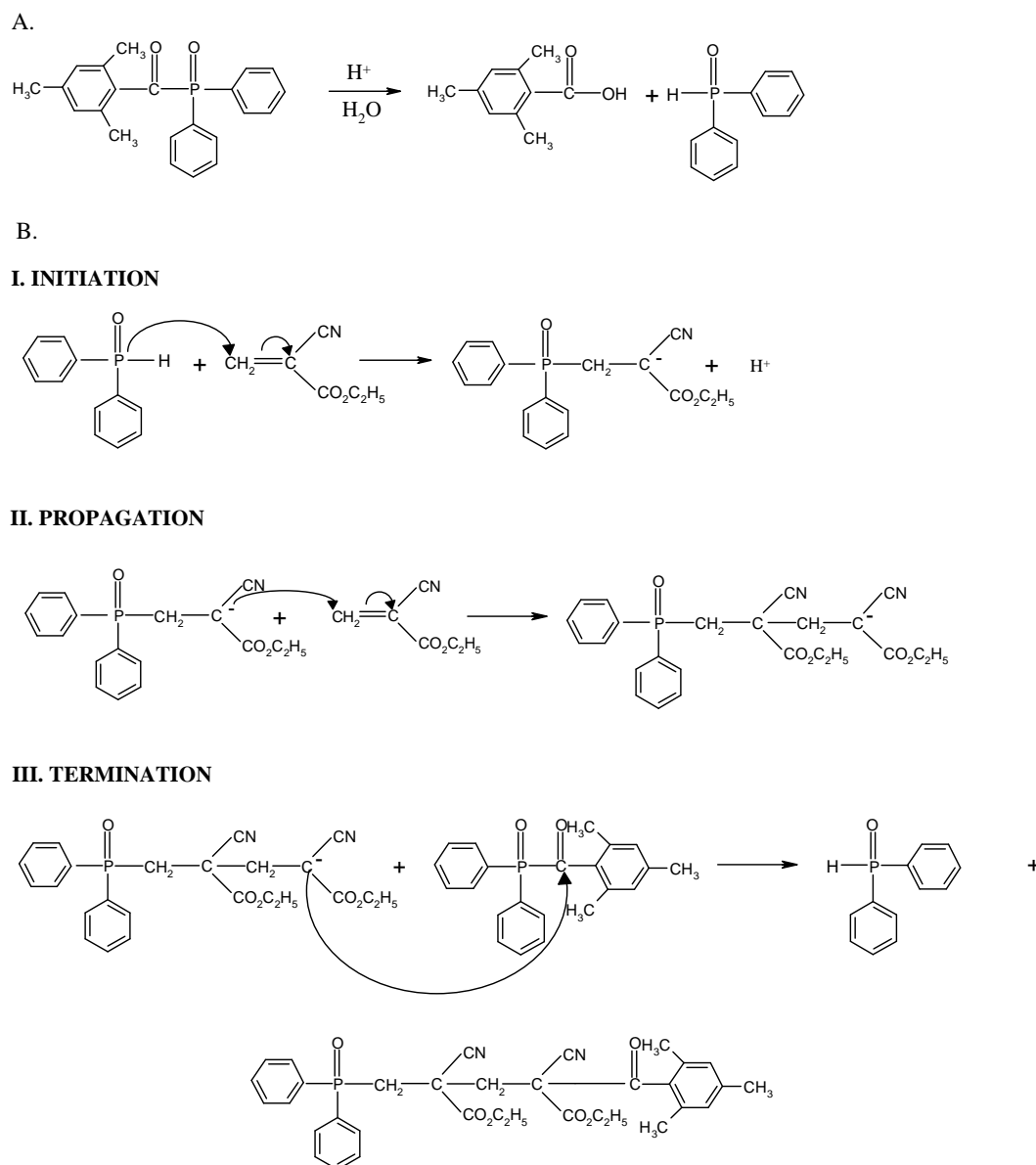
<sup>a</sup>[M+Na]<sup>+</sup>

**Figure 5.24:** Proposed structure of polymer products of TPO/ethyl CA monomer for samples exposed to sunlight after 3 h.

The structure of this product is very similar to the polymerisation product of BAPO/ ethyl CA ( $m/z$  691) under sunlight conditions, see Figure 5.22. Also the pathway of the cure mechanism is similar to that depicted in Figure 5.25. The only difference is the speed of polymerisation which for the TPO/ethyl CA system needed three hours

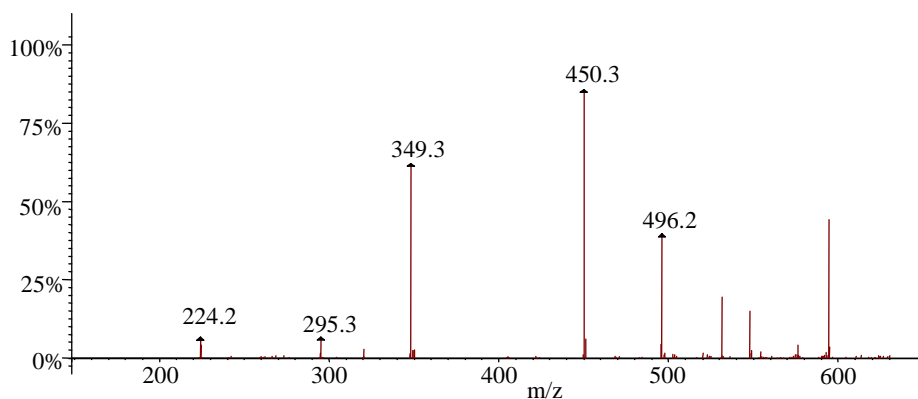
to form the product, whereas for of the BAPO/ monomer system the reaction took only one hour.

Figure 5.25 show that the diphenylphospine oxide nucleophile attacks the C=C double bond of ethyl CA monomer and forms the anion on the other side of molecule. The second step of-propagation and the last step of termination, both have the same pathway as for the polymer product of BAPO/ ethyl CA under sunlight conditions. In the propagation step another ethyl CA monomer is added to form longer chain product. In the last step, the anion formed in the propagation reaction attacks the carbonyl atom of photoinitiator (TPO) and stops the polymerisation process completely, generating a polymer product of  $m/z$  621 and diphenylphosphine oxide.



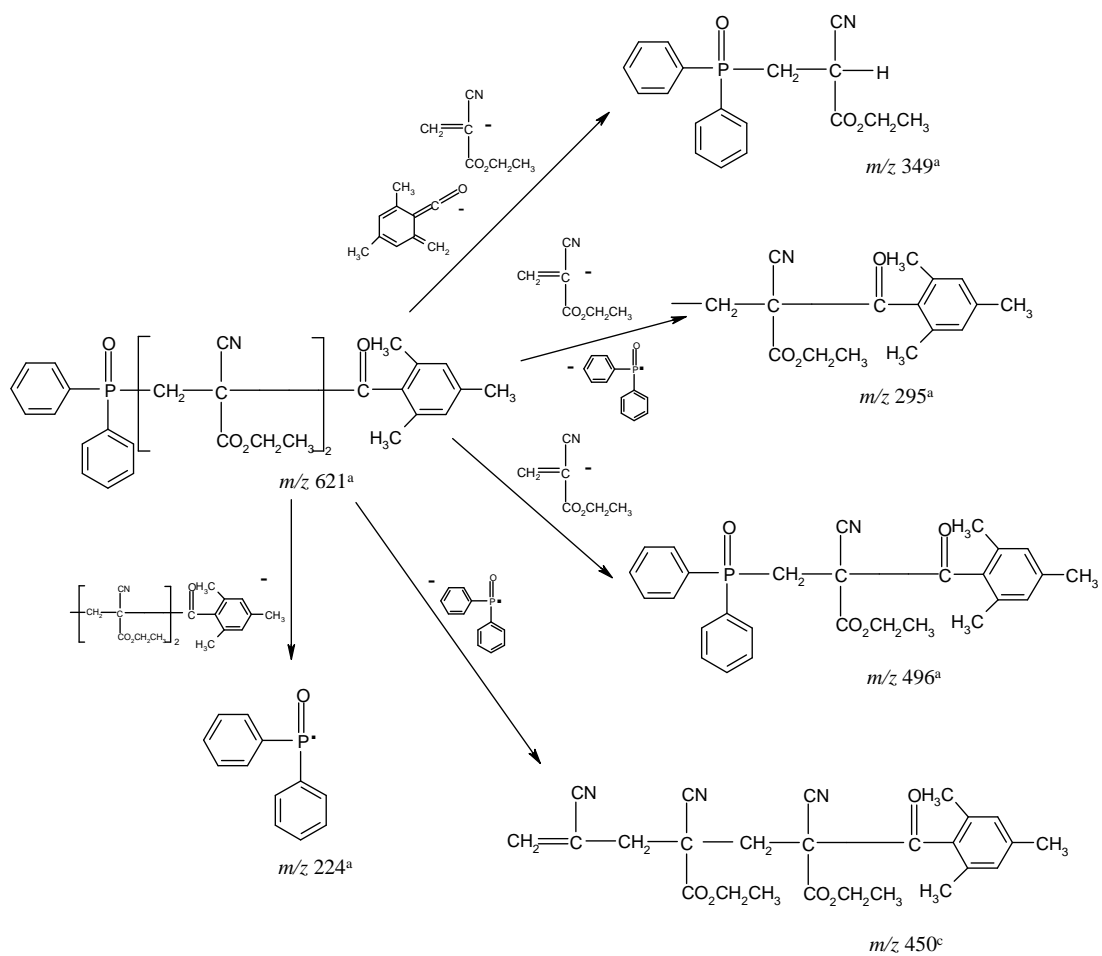
**Figure 5.25:** Proposed cure mechanism for polymerisation product at  $m/z$  621.

The resulting (+) ESI-MS/MS mass spectrum of polymer product at  $m/z$  621 in the mass range 200-600  $m/z$  is presented in Figure 5.26.



**Figure 5.26:** Mass spectrum of polymer product at  $m/z$  621 in sunlight after 3 h.

The (+) ESI-MS/MS mass spectrum of precursor ion  $m/z$  621 showed five main product ions at  $m/z$  224, 295, 348, 450 and 496. The most intense peak, observed at  $m/z$  450, indicates the elimination of diphenylphosphine oxide from the precursor ion. Also, the product ion at  $m/z$  295,  $[M+Na]^+$ , was formed by elimination of diphenylphosphine oxide and one of the ethyl CA monomer molecule. Another product ion at  $m/z$  496 may possibly be the result reaction of photoinitiator with the product of initiation step. The product ion of  $m/z$  349 could possibly be generated by a loss of 2,4,6-trimethylbenzoyl radical and ethyl CA monomer. This ion is a sodium adduct like the fragment ion at  $m/z$  224,  $[M+Na]^+$ , which probably was formed by a loss of two monomer molecules and 2,4,6-trimethylbenzoyl radical from the precursor ion. This fragment ion at  $m/z$  224,  $[M+Na]^+$  was discussed in Chapter 4. Possible structures of all fragment ions are illustrated in Figure 5.27.


<sup>a</sup>[M+Na]<sup>+</sup>
<sup>c</sup>[M+H]<sup>+</sup>

**Figure 5.27:** Proposed mass fragmentation of polymerisation product at  $m/z$  621.

#### 5.4.4 Effect of photoinitiators concentration and presence of stabiliser

Electrospray ionisation was employed to identify and characterise the polymerisation products of ethyl CA monomer with two photoinitiators: BAPO and TPO. The speed of the cure reaction in relation to the intensity of the sunlight was also investigated.

The speed of the cure mechanism was measured at room temperature for samples of BAPO/ethyl CA, TPO/ethyl CA and with addition of ferrocene. The samples were exposed to the sunlight. The intensity of the sunlight was controlled and kept between  $1.0 - 1.2 \text{ mW/cm}^2$  for all experiments. The amount of photoinitiator used affected the speed of the polymerisation reaction. The highest BAPO concentration was associated with the shortest curing time. Figure 5.28 reveals the longest cure time for the lowest concentration of BAPO. However the fastest curing process was achieved for 0.5% BAPO in conjunction with ferrocene.

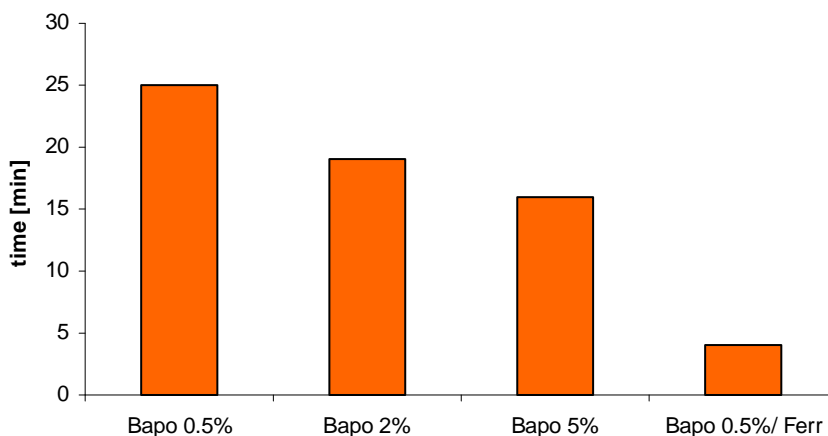


**Figure 5.28** Graphic representation of the speed of the polymerisation over time in samples with different concentration (0.5%, 2% and 5%) of BAPO and with addition of ferrocene (0.01%) under sunlight conditions.



This counterintuitive behaviour can be rationalised as follows: cure speed is much faster in the lowest concentration (0.5%) of photoinitiator in presence of ferrocene (stabiliser), this means that the ferrocene increases the ratio of reaction in the following way:

a) by functioning as a reducing agent to convert phosphinoyl radical to a 2,4,6-trimethylbenzoylphenylphosphine oxide (see Figure 5.29 (C)) which then causes nucleophilic polymerisation of the cyanoacrylate,

b) the ferrocene radical cation can then react with the trimethyl benzoyl radical to form the monobenzoylferrocene (see Figure 5.29 (D)).

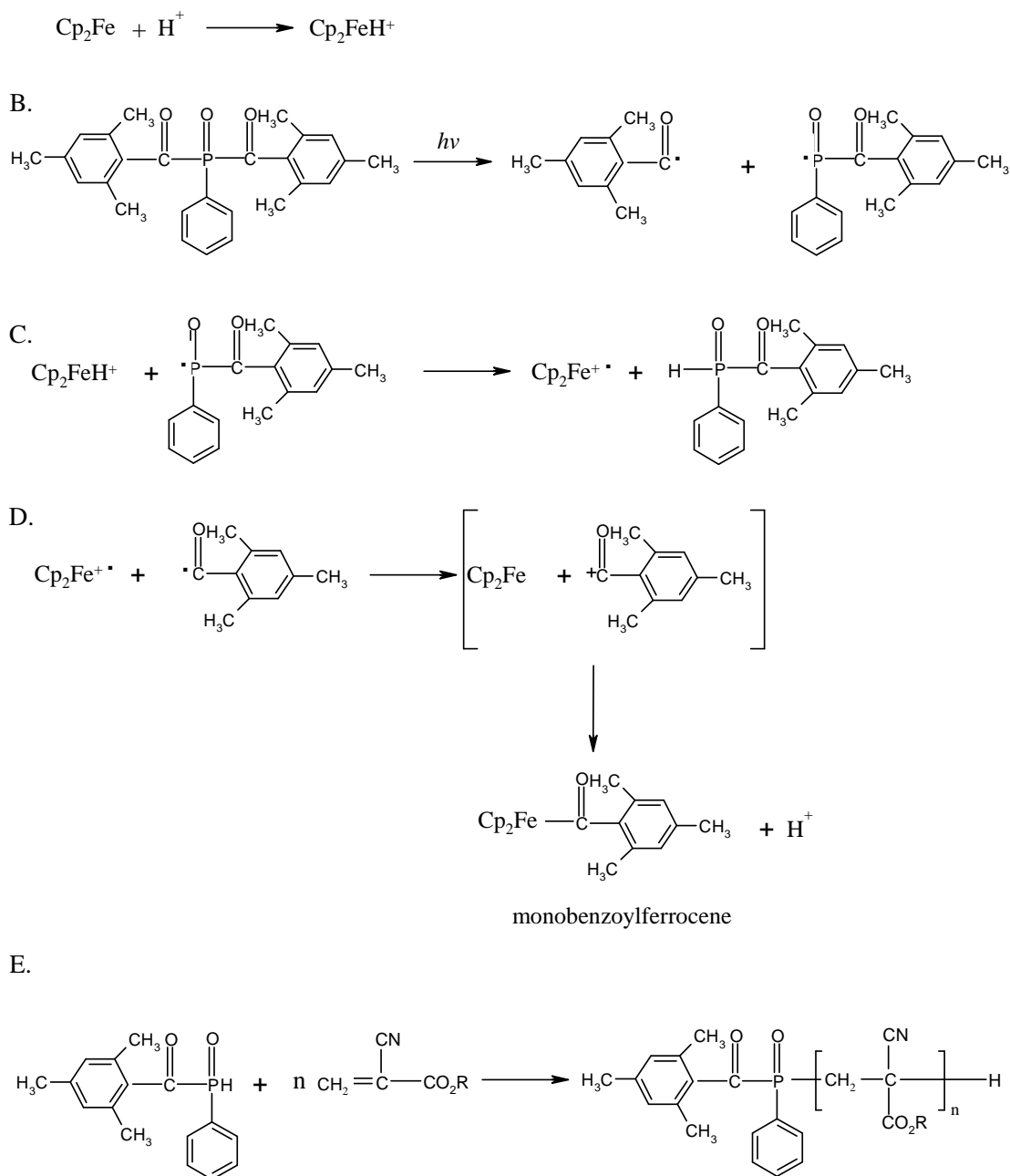


**Figure 5.29:** Proposed reaction between photoinitiator–BAPO and ferrocene.

Figure 5.30 shows the effect of both photoinitiators, with and without stabiliser, on the curing speed. The concentration of both photoinitiators was the same (0.5%). The shortest curing time was observed for BAPO with ferrocene and the longest curing time was noted for TPO without ferrocene. These results confirmed the

findings of a previous study of the stability and reactivity of both photoinitiators and were discussed in Chapter 4.

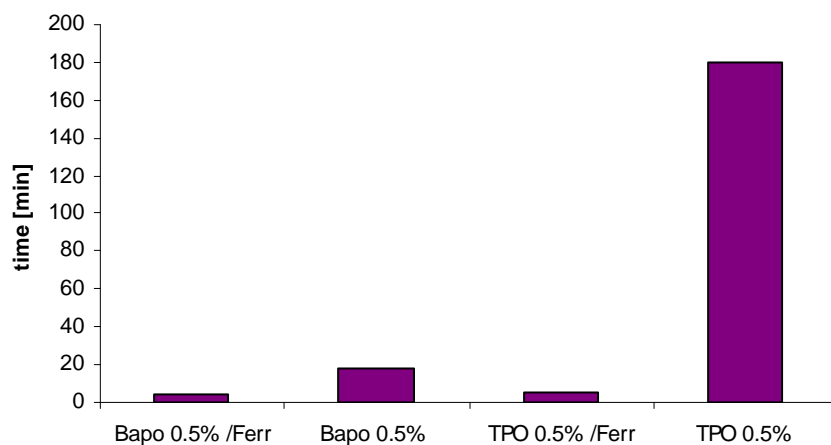


**Figure 5.30:** Graphic representation of the speed of the polymerisation versus time in BAPO, (0.5%) and TPO (0.5%), BAPO and TPO with ferrocene (0.01%). Samples exposed to sunlight.

## 5.5 CONCLUSION

An LC-MS method was successfully developed for the investigation of the photoinitiator/-monomer system. Using mass spectrometry, products of the polymerisation of photoinitiator/ethyl CA mixture were identified. Firstly, the nature of reaction products originating from hydrolysis of the BAPO photoinitiator and subsequent nucleophilic reactions involving the cyanoacrylate ester were identified. The reactions occur in the dark and progress with time until all hydrolysable BAPO functions have been consumed. Secondly, a mechanism for the light activated polymerisation of the cyanoacrylate ester in the presence of BAPO and ferrocene was proposed. The key aspect of this mechanism is the role of the ferrocene as a reductant facilitating the formation of the phosphine oxide which in turn imitates nucleophilic polymerisation of the cyanoacrylate ester.

Positive mode electrospray ionisation mass spectrometry has also been shown to be an efficient tool to determine the number of repeat units in ethyl CA oligomers.

An investigation of the speed of the curing reaction of both photoinitiators/monomer systems with and without the addition of ferrocene was performed using a UV Power Meter and it was determined that the fastest cure mechanism was achieved for the BAPO/ ethyl CA system in the presence of ferrocene.

**5.6 REFERENCES**

- [1] Marsman, M., Luiken, A., Holweg RBM., *Proceedings Conference Radtech Europe*, **1991**, p. 440.
- [2] Yoshiyuki, K., Kayuzuki, M., Toshio S., Mitsuhiro, M., Hiromi M., *US Patent 5013768*, **1989**.
- [3] Borzel, P., Haring E., *German Patent Application 3304524*, **1983**.
- [4] Murry, K.P., Bishop TE., *Int. Patent Application WO 90/13579*, **1989**.
- [5] Segurola, J., Allen, S., N., Edge, M., McMahon, A., Wilson, S., *Polym. Degrad. Stabil.*, **1999**, 64, 39.
- [6] J. Pączkowski, *Fotochemia Polimerów Teoria I Zastosowanie*, Nicolaus Copernicus University, **2003**.
- [7] Cymon, J., *Int. J. of Adhesion and Adhesives*, **1998**, 18, 247.
- [8] Coover, H.W., Dreifus, D., W., O'Connor, J.T., *Handbook of Adhesives*, Reinhold, New York, **1977**.
- [9] Clyden, J., Greeves, N., Warren, S., Wothers, P., *Organic Chemistry*, 1 st Edn, Oxford University, **2001**.
- [10] Amstock, J.S., *Hanbook of Adhesives and Sealants in Construction*, McGraw-Hill, New York, **2001**.
- [11] McManus, M.G., *MSc. Thesis*, Dublin City University, **1995**.
- [12] Kincaid, B., *PhD, Thesis*, Dublin City University, **1999**.
- [13] Comyn, J., *Adhesion Science*, RSC, Cambridge, **1997**.
- [14] Kinoch, A., J., *Structural Adhesives*, Elsevier Science Publishing, New York, **1986**.
- [15] Whitaker, G., *PhD Thesis*, Dublin City University, **2006**.
- [16] *Internal Report from Henkel Company*, **2008**.
- [17] Ciba Speciality Chemicals Website; [http://www.cibasc.com/irgacure\\_819-dw.htm](http://www.cibasc.com/irgacure_819-dw.htm).
- [18] Baxter, J. E., Davidson, S., *Macromol. Chem.*, **1988**, 189, 2780.
- [19] Hart- Smith, G., Lovestead, T., M., Davis, T.P., Stenzel, M.H., Barner-Kowalik, C., *Biomacromolecules*, **2007**, 8, 2404.

*Chapter Six*

*Conclusions*

## 6.1 OVERALL CONCLUSIONS

The aim of this work was to determine the chemical pathways of photoinitiators and study how these pathways affect the curing mechanism. The work described in this thesis provides novel insights to the understanding of the mechanisms and behavior of photoinitiators used in the curing process.

A selection of analytical methods was used in this work to characterise the  $\alpha$ -cleavable photoinitiators, BAPO and TPO. The analytical methods facilitated the understanding of the chemistry and photochemistry of these two photoinitiators.

The separation principles of capillary electrophoresis and liquid chromatography are very different. However, these two analytical separation methods were used as complementary tools for the determination of the stability of BAPO under different formulation conditions. It was found that BAPO readily hydrolysis in presence of a Lewis acid and does not undergo significant hydrolysis in the presence of a protonic acid. The effect of a stabiliser (ferrocene) served to minimise the hydrolysis of BAPO by complexing with a Lewis acid and thereby reducing its hydrolytic influence. The CE method was shown to have thirty six times the separation efficiency of HPLC and the runtime reduced to 4 min when CE was used. In order to characterise the photoinitiators, their reactions and the cure mechanism LC-MS was used. It was chosen because of the suitable LC separation and MS detection capability.

Mass spectrometry, is an essential analytical tool in elucidation of the chemical mechanisms associated with the photoinitiators under study. The photodegradation of products and degradation reactions for both photoinitiators was studied. For BAPO the results showed two possible degradation reactions: light catalysed degradation and hydrolytic degradation. From this work it is clear that the hydrolysis of BAPO can occur by either nucleophilic attack at the carbon or at the phosphorus atom. The presence of the carbonyl carbon serves to increase the electrophilic nature of the phosphorus atom. Hence BAPO, with two such functional groups, is more prone to hydrolysis at the phosphorus atom when compared to TPO.

The results obtained from LC-MS were found to be in good agreement with nuclear magnetic resonance spectroscopy (NMR) and computational studies. ESI-MS together with NMR provided a useful combination of data for monitoring photodegradation products and stability of the photoinitiators under study. Both methods confirmed that TPO was more stable photoinitiator than BAPO.

The theoretical results presented some possible pathways for the cure mechanism for both photoinitiators. The scheme suggested for BAPO was via benzoyl and 2,4,6-trimethylbenzoylphenylphosphine oxide radicals and for TPO that the benzoyl radical and (2,4,6-trimethylbenzoyl) diphenyl-phosphine oxide radical were formed.

Every piece of information about the chemistry of these photoinitiators such as their stability, cure mechanism (degradation pathways) and reactivity of radicals was crucial for the understanding and improvement of the polymerisation of the monomer/photoinitiator system. ESI-MS results proved very useful for elucidating the reaction process between monomer/ photoinitiator and monomer-monomer. Using MS, the products of the polymerisation of photoinitiator/ethyl CA mixture were identified. Based on these results, two important conclusions were arrived at. Firstly, the potential loss of photolytic activity in BAPO- initiated light curing cyanoacrylate adhesives was explained by progressive hydrolytic degeneration of the BAPO photoinitiator during storage in the dark. Secondly, a plausible mechanism for the photolytic cure of BAPO based cyanoacrylate adhesives was proposed based on nucleophilic polymerisation of the cyanoacrylate ester. The function of the ferrocene in this reaction is to reduce the phosphinoyl radical to the phosphine oxide which then initiates a nucleophilic attack on the cyanoacrylate ester.

In addition, by collating all experimental data for the photoinitiators (BAPO and TPO) with ethyl CA monomer, two key points of information were assessed- the reactivity of the photoinitiators and the reactivity of the individual fragments of photoinitiators.

Arising from the successful outcomes of this research there are a number of further research paths that can be undertaken. It would be of value to investigate different types of acid stabiliser and different concentrations of both acids and ferrocene to study the stability of these photoinitiators. The use of a combination of the mono- and bis-acylphosphine oxide for the ethyl CA formulation to investigate



the new polymerisation products would form a valuable study. Arising from the theoretical calculations carried out it is clear that molecular modelling concepts can be used to determine the optimum photoinitiator type for use with ethyl CA monomer.

## *Appendix*

**Publications**

*“The use of HPLC to characterise an Acylphosphine oxide photoinitiator under different stability conditions”*

*J. of Chromatography B*, Manuscript in preparation

Agnieszka Ciechacka, Gillian McMahon, Raymond G. Leonard, Fiona Regan

*“Study of Photodegradation of Bis(2,4,6-trimethylbenzoyl)phenylphosphine oxide using LC-MS technique”*

*Rapid Commun. Mass Spectrom.*, Manuscript in preparation

Agnieszka Ciechacka, Gillian McMahon, Paul O’Donohue, Raymond G. Leonard, Fiona Regan

*Stability study of BAPO and TPO photoinitiators using LC-MS, NMR spectroscopy and molecular modeling*

*Polymer*, Manuscript in preparation

Agnieszka Ciechacka, Gillian McMahon, Paul O’Donohue, Raymond G. Leonard, Damian Plazuk, Fiona Regan

## **Oral Presentations**

### **Irish Mass Spectrometry Society, May 13, 2009, Dublin Ireland**

*“Characterisation of an Acylphosphine Oxide Photoinitiator using LC-MS”*

Agnieszka Ciechacka, Gillian McMahon, Paul O’Donohue, Raymond G. Leonard,  
Fiona Regan

### **PITTCON, February 27- March 5, 2010, Orlando, United States**

*“Multiple Analytical Approaches to the Characterization of Acylphosphine Oxide  
Photoinitiator”*

Agnieszka Ciechacka, Gillian McMahon, Paul O’Donohue, Raymond G. Leonard,  
Fiona Regan

**Poster Presentations****Analytical Research Forum, July 21-23, 2008, University of Hull, United Kingdom**

*“Characterisation of an Acylphosphine Oxide Photoinitiator using HPLC and CE methods”*

Agnieszka Ciechacka, Gillian McMahon, Raymond G. Leonard, Fiona Regan

**34 th International Symposium on High Performance Liquid Phase Separations and Related Techniques, Jun 28-July 2, 2009, Dresden, Germany**

*“Stability study of an Acylphosphine Oxide Photoinitiator using LC and LC-MS methods”*

Agnieszka Ciechacka, Gillian McMahon, Raymond G. Leonard, Fiona Regan

**Analytical Research Forum, July 13-15, 2009, University of Kent, United Kingdom**

*“Stability study of an Acylphosphine Oxide Photoinitiator using LC and LC-MS methods”*

Agnieszka Ciechacka, Gillian McMahon, Raymond G. Leonard, Fiona Regan

**35 th International Symposium on High Performance Liquid Phase Separations and Related Techniques, Jun 19-24, 2010, Boston, United States**

*“Stability study of BAPO and TPO photoinitiators using LC-MS method”*

Agnieszka Ciechacka, Gillian McMahon, Paul O’Donohue, Raymond G. Leonard, Fiona Regan